LIPID NANOCARRIERS: A NOVEL APPROACH TO DELIVERING OPHTHALMIC CLARITHROMYCIN

A Thesis Submitted to Rhodes University in
Fulfillment of the Requirements for the Degree of

DOCTOR OF PHILOSOPHY (PHARMACY)

by

Pedzisai Anotida Makoni

ORCID: 0000-0002-8475-447X

December 2020

Faculty of Pharmacy
RHODES UNIVERSITY
Grahamstown/Makhanda
South Africa

ABSTRACT

The feasibility of incorporating clarithromycin (CLA) into innovative solid lipid nanoparticles (SLN) and nanostructured lipid carriers (NLC) using hot emulsification ultrasonication (HEUS) was investigated. This approach was investigated in an attempt to address the shortcomings associated with the use of lyophilized parenteral formulations administered *via* the ocular route such as toxic reactions, intolerance and patient discomfort due to frequent instillation of topical solutions of CLA. In particular, sustained release approaches to delivery may enhance precorneal retention, increase ocular availability and permit dose reduction or use of a longer dosing frequency when treating ocular non-tuberculous mycobacterial (NTM) keratitis infections. This approach may potentially improve the delivery of CLA to the eye, thereby addressing some or all of the unmet clinical needs described *vide infra*.

Prior to initiating pre-formulation, formulation development and optimization studies of CLA-loaded SLN and/or NLC, Design of Experiments (DoE), specifically a Central Composite Design (CCD) was used in conjunction with Response Surface Methodology (RSM) to develop and optimize a suitable method for the quantitative determination of CLA in pharmaceutical formulations and for monitoring CLA release from SLN and/or NLC *in vitro*. A simple, accurate, precise, sensitive and stability-indicating reversed phase-high performance liquid chromatography (RP-HPLC) method with electrochemical (EC) detection was developed, validated and optimized for the *in vitro* analysis of CLA loaded SLN and/or NLC formulations.

Pre-formulation studies were undertaken to investigate the thermal stability of CLA and bulk lipids to facilitate the selection of lipid excipients for the manufacture of nanocarriers in addition to establishing compatibility of CLA with the excipients. It was established that CLA was thermostable up to a temperature of approximately 300 °C thereby indicating that HEUS could be used for the manufacture of CLA-loaded SLN and/or NLC. Lipid screening revealed that CLA is, in general, poorly soluble in solid and liquid lipids however a combination of stearic acid (SA) and Transcutol® HP (THP) exhibited the best dissolution potential for CLA of all lipids tested. Stearic acid appears to exist as polymorphic form B prior to exposure to heat however occurs as the form C polymorph following heating at 85 °C for one hour. The best ratio for the mixture of SA and THP for the manufacture of CLA-NLC

was an 80:20 (*w/w*) ratio of SA: THP as the two lipids are miscible in this ratio and exhibited the greatest dissolution potential for CLA. Furthermore, an investigation of binary mixtures of CLA/SA and SA/Transcutol® HP, in addition to eutectic mixtures of CLA, SA and Transcutol® HP, revealed no obvious interaction between CLA and the lipids selected for the production of the nanocarriers.

Due to the relatively high solubility of CLA in THP in comparison to SA, NLC are likely to exhibit a higher loading capacity (LC) and encapsulation efficiency (EE) for CLA than SLN. Consequently the feasibility of incorporating CLA (10% *w/w*) into NLC was investigated and evaluation of the production of SLN was not undertaken as the production of these might not result in the manufacture of a delivery technology with a high EE and LC for CLA.

Tween®20 was used as the surfactant as it is readily available, exhibits little or no cytotoxicity and is relatively cheap. Polyethylene glycol (PEG) was used as a coating polymer to impart muco-adhesive properties the formulated CLA-NLC. Response surface methodology (RSM) in conjunction with DoE, specifically a Box-Behnken Design (BBD) used as a screening design was used to identify a formulation composition which would produce a product that would meet the pre-defined target critical quality attributes (CQA) for the nanoparticles *viz.* particle size (PS) in the nano-range, polydispersity index (PDI) < 0.5, Zeta Potential (ZP) ≥ ± 30 mV, and EE > 80%. The formulation composition identified was subsequently used for the optimization of the manufacturing parameters *viz.* sonication time and amplitude, using a Central Composite Design (CCD). The LC and EE, *in vitro* CLA release, cytotoxicity, osmolarity, pH, degree of crystallinity and lipid modification, elemental analysis and surface morphology of the optimized batch was investigated and monitored to ensure that CLA-loaded NLC, of the desirable quality, had been produced.

On the day of manufacture the mean PS and PDI of the optimized CLA-loaded NLC formulation adjusted to physiological osmolarity (250–450 mOsm/kg) was 461.9 ± 40.16 nm and 0.523 ± 0.104, respectively. The ZP for the optimized NLC generated on the day of manufacture using HPLC grade water as the dispersion medium was -20.5 ± 4.82 mV. The pH and osmolarity of the optimized CLA-loaded NLC formulation was 7.76 ± 0.01 and 316 ±

2 mOsm/Kg, respectively and the EE was 88.62 ± 0.23 %. The optimized NLC exhibited a decreased crystallinity in comparison to the bulk lipid materials. DSC, WAXS and FT-IR revealed that CLA was molecularly dispersed in the nanocarriers. The optimized CLA-loaded NLC exhibited muco-adhesive properties, when tested under stationary conditions using laser doppler anemometry (LDA). The optimized formulation also exhibited sustained release of CLA over 24 hours during *in vitro* release testing and CLA release was best described using the Baker-Lonsdale model. The cumulative % CLA released over 24 hours was 56.13 ± 0.23% and mass balance analysis revealed 41.38 ± 0.02% CLA had been retained in the NLC. *In vitro* cytotoxicity testing revealed that the optimized CLA-NLC were less cytotoxic to HeLa cells when compared to CLA alone and further confirmed that the lipids and excipients used in these studies were of GRAS status.

Stability studies revealed that the EE reduced over 28 days by 14.42% and 5.14% when stored at 4 °C and 22 °C, respectively. In addition, the particle size increased from the nm to µm range for samples stored at 22 °C. The findings are a good starting point but require further optimization to ensure prolongation of stability. In addition, the technology requires additional developmental studies and a powder for reconstitution for use as a single-dose considered as single dose packaging may be a solution to the compromised formulation stability observed in these studies.

The CLA-NLC produced in these studies exhibit sound product attributes which serve as a useful foundation for the novel delivery of antibiotics to the eye. The results suggest that the optimized NLC have the potential to enhance precorneal retention and increase ocular availability of CLA, which in turn may be useful to reduce the required dose and dosing frequency when administering CLA as a reconstituted solution to treat susceptible organisms that infect ocular tissues.

ACKNOWLEDGEMENTS

Firstly, I would like to thank the Lord Almighty for giving me protection, strength and determination to succeed throughout my life and for allowing me to carry out and complete this work in a timely manner.

I would like to express my sincere gratitude to the following people and organizations:

My supervisor, Professor R.B Walker for his expert guidance, encouragement, continuous support and patience during the research and the writing of this thesis.

My co-supervisor, Professor S.M. Khamanga for his availability and assistance during the research and the writing of this thesis.

The Dean and Head, Professor S.M. Khamanga and the staff of the Faculty of Pharmacy for allowing me to use the facilities in the Faculty at Rhodes University.

Dr. S Abboo for providing technical support and Mr. N Borland for his administrative assistance and continuous help throughout the duration of this project.

My colleagues and friends in the Department of Pharmacy for their academic assistance, objectiveness, honesty, and pleasant company for the duration of my project. Special thanks to Dr. Bwalya Witika, Dr. Mellisa Chikukwa and Mr. Siyabonga Melamane for listening to all my research anguishes and providing continuous intellectual support during this project.

My parents, Mr. E.J. and Mrs. S Makoni for giving me a life that I have come to love and treasure. My family members and my in laws for their encouragement, love, support and understanding throughout my studies. Special thanks to my aunt Mrs. V Matangaidze for her encouragement, love and support. My late uncle, Mr H.T. Matangaidze for having played a major role in my upbringing and grooming me into the man I have become. My sister, Nyaradzo, my brother Mauru and my mother in law Mrs Mangoma for their unceasing encouragement and support, during my studies.

My lovely wife, Yemurai. I thank you for the sacrifices you made to support me while doing my doctoral studies. You provided unwavering support in hard times and showed the true love that you have always had for me. Thank you for listening to all my research anguishes and for the encouragement. In addition, thank you for always showing interest in my research work. Thanks babe!

STUDY OBJECTIVES

Non-tuberculous precipitating *mycobacteria* are ecological pathogens which are a significant cause of a number of different human diseases. *Mycobacterium fortuitum* and *Mycobacterium chelonae* are examples of such *mycobacteria* and are a leading cause of infectious keratitis. The development of ocular non-tuberculous mycobacterial (NTM) keratitis has been attributed to trauma following penetration of the corneal epithelium. Outbreaks of NTM keratitis following laser-assisted *in situ* keratomileusis (LASIK) has been reported in Brazil, USA and Japan and are due to improper sterilization of surgical fluids and instruments subsequently leading to the introduction of pathogens to the corneal stroma during surgery. NTM is a common pathogen causing post-LASIK keratitis (47%) however causative agents of infectious keratitis vary by region with the highest rates being observed in developing countries. Clarithromycin (CLA) exhibits inhibitory activity against > 275 NTM clinical isolates. The treatment of NTM keratitis with topical CLA has been successful however, toxic reactions, intolerance and patient discomfort due to frequent instillation of topical solutions of CLA is of concern. Commercially available CLA dosage forms for ocular use are not readily available and the *in vivo* efficacy of CLA for the treatment of NTM keratitis has, to date, been determined by reconstitution and use of lyophilized parenteral formulations administered *via* the ocular route. Innovative lipid carriers such as muco-adhesive nanostructured lipid carriers (NLC) have the potential to enhance precorneal retention, increase ocular availability and permit dose reduction or permit use of a longer dosing frequency. This may potentially improve the delivery of CLA to the eye thereby addressing some or all of the aforementioned unmet clinical needs.

The objectives of this research were:

1. To obtain data pertaining to the physicochemical properties of CLA that would assist in the development of quality delivery systems using experimental studies and the literature.
2. To develop, optimize and validate using response surface methodology (RSM), a simple, sensitive, precise, accurate and linear RP-HPLC method, with electrochemical detection, suitable for the quantitative analysis of CLA for use during formulation development and optimization studies of CLA-loaded nanocarriers.
3. To establish the thermal stability of CLA, select and characterize lipidic excipients for the manufacture of CLA-loaded nanocarriers.
4. To design, develop and optimize polyethylene glycol (PEG) coated CLA-loaded nanocarriers using a minimum number of experimental runs using RSM and to evaluate the critical quality attributes (CQA) of the formulations.
5. To investigate and identify an optimum and stable nanoparticulate delivery system for CLA with the appropriate loading capacity (LC) and encapsulating efficiency (EE), that is muco-adhesive, biocompatible and that sustains CLA release over 24 hours.
6. To determine the short term stability attributes of the optimum nanoparticulate delivery systems based on their CQA.

TABLE OF CONTENTS

LIST OF TABLES

LIST OF FIGURES

LIST OF ACRONYMS

3D	Three dimensional
ACN	Acetonitrile
AIC	Akaike Information Criterion
AIDS	Acquired Immune Deficiency Syndrome
ANOVA	Analysis of Variance
API	Active Pharmaceutical Ingredients
AUC	Area Under the Curve
BCS	Biopharmaceutical Classification System
CED	Cohesive Energy Density
CLA	Clarithromycin
CNS	Central Nervous System
CQA	Critical Quality Attributes
CY	Cytochrome
DC	Direct Current
DoE	Design of Experiments
DSC	Differential Scanning Calorimetry
DTA	Differential Thermal Analysis
ECD	Electrochemical Detection
EE	Encapsulation Efficiency
ERY	Erythromycin
FDA	Food and Drug Administration
FTIR	Fourier Transform Infrared
GIT	Gastrointestinal
GRAS	Generally Regarded As Safe
HDV	Hydrodynamic Voltammetry
HEUS	Hot Emulsification Ultrasonication
HHPH	Hot High-Pressure Homogenization
HIV	Human Immunodeficiency Virus
HMDS	Hexamethyldisilazane
HPH	High Pressure Homogenization
HPLC	High Performance Liquid Chromatography
HSP	Hansen Solubility Parameters

ICH	International Conference of Harmonization
INR	International Normalized Ratio
IR	Infrared
IS	Internal Standard
Ka	Dissociation Constant
KOH	Potassium Hydroxide
LASIK	Laser-Assisted *In* Situ Keratomileusis
LC	Loading Capacity
Log $Po_{/w}$	Partition Coefficient
MAC	Mycobacterium Avium Complex
MIC	Minimum Inhibitory Concentration
MSC	Model Selection Criterion
NLC	Nanostructured Lipid Carriers
NMR	Nuclear Magnetic Resonance
NTM	Non-Tuberculous Mycobacterial
PCS	Photon Correlation Spectroscopy
PDI	Polydispersity Index
PEG	Polyethylene Glycol
PHR	Peak Height Ratio
PS	Particle Size
RSD	Relative Standard Deviation
Rsqr_adj	Adjusted Coefficient of Determination
SA	Stearic Acid
SLN	Solid Lipid Nanoparticles
TGA	Thermogravimetric Analysis
THP	Transcutol® HP
USA	United States of America
USP	United States Pharmacopeia
UV	Ultraviolet
UV/Vis	Ultraviolet and Visible
Vd	Volume of Distribution
WP	Width of the Peak
ZP	Zeta Potential

CHAPTER 1

CLARITHROMYCIN

1.1 INTRODUCTION

Macrolides are a group of antibiotic molecules that exhibit activity originating from the presence of a macrolide ring which is a large macrocyclic lactone ring to which one or more deoxy sugars may be attached. These compounds are a product of the Streptomyces bacterial species and are used primarily to treat gram-positive bacterial infections [1]. In clinical practice, the most commonly used macrolides exhibit a macrocyclic lactone ring containing 14, 15 or 16 atoms with sugars linked *via* glycosidic bonds. These clinically useful macrolide antibiotics are assigned to one of three groups stemming from the number of atoms in the lactone nucleus [2]. The 14-membered macrolide group includes erythromycin A, B, C, D, E and F, oleandomycin, roxithromycin, dirithromycin, clarithromycin (CLA) and flurithromycin. Azithromycin is a 15-membered molecule and 16-membered macrolides include josamycin, rosaramicin, rokitamycin, kitasamycin, mirosamicin, spiramycin and tylosin. Spiramycin and tylosin are mainly used in veterinary medicine [2,3]. The pharmacodynamic properties of macrolide antibiotics are very similar and these compounds generally exhibit low toxicity while displaying a comparable spectrum of antimicrobial activity with evidence of cross-resistance between specific members of a group [1,4]. Macrolides are either bacteriostatic or bactericidal, depending on the concentration used and type of microorganism targeted. They act through interfering with bacterial protein synthesis, *via* binding to the 50S ribosomal subunit of bacteria at the peptidyl transferase centre formed by 23S rRNA [4–6]. Macrolides are particularly useful for the treatment of *Legionella pneumophilia*, *Mycoplasma pneumonia* and some *Rickettisial* and *Chlamydial infections*. Their spectrum of antimicrobial activity is broader than that of the penicillins and is comparable to many late-generation cephalosporins. Consequently, macrolide antibiotics have been successfully used as substitutes when treating patients with known penicillin allergy [1,2,7].

Erythromycin A, the first macrolide antibiotic discovered, has been used since the early 1950s for the treatment of upper respiratory tract, skin and soft tissue infections caused by susceptible organisms, particularly in patients allergic to penicillin [8,9]. Owing to several

drawbacks including frequent gastrointestinal (GIT) intolerance and a short serum half-life when using erythromycin, advanced macrolide antimicrobials were synthesized by altering the erythromycin base resulting in compounds with broader activity, more favourable pharmacokinetics and pharmacodynamics, and better tolerability. In 1991 and 1992, the United States Food and Drug Administration (FDA) approved CLA and azithromycin for clinical use. Since their inception, these compounds have been extensively used for the treatment of respiratory tract infections, sexually transmitted diseases and infections caused by *Helicobacter pylori* and *Mycobacterium avium* complex (MAC) [8].

CLA is a structural analogue of erythromycin A that differs in the chemical structure due to methylation of the hydroxyl group at position 6 on the lactone ring (Figure 1.1) [10].The substitution results in a more acid stable antibiotic and prevents the degradation of the erythromycin base to form a hemiketal intermediate. The enhanced acid stability in turn results in improved oral bioavailability and decreased GIT intolerance. In South Africa, CLA is mainly indicated, in combination therapy, for the treatment of MAC and *Helicobacter pylori* [11]. However, Wenjuan *et al.,* [12] reported CLA exhibited inhibition activity against > 275 clinical non-tuberculosis mycobacterium isolates. In a study comparing the activity of four macrolides, *viz*. azithromycin, erythromycin, CLA and roxithromycin against *Mycobacterium fortuitum and Mycobacterium chelonae,* CLA demonstrated the highest potency against these strains [13]. The two strains of non-tuberculous *Mycobacteria* are the most commonly implicated species in cases that involve non-tuberculous mycobacterial (NTM) keratitis [14,15].

The development of NTM keratitis has been attributed primarily to the trauma of penetration of the corneal epithelium. In addition, topical corticosteroid use has been shown to suppress granulomatous inflammation facilitating the growth of non-tuberculous mycobacteria in the eye [15,16]. Outbreaks of NTM keratitis following laser-assisted *in situ* keratomileusis (LASIK) has been reported in Brazil, USA and Japan. These outbreaks were attributed to improper sterilization of surgical fluids and instruments leading to the introduction of pathogens to the corneal stroma during surgical procedures [17–19]. NTM has been reported to be some of the most common pathogens (47%) causing post-LASIK keratitis [20]. The causative agents of infectious keratitis vary by region and the incidence of infections ranges between 0.0063% and 0.71% with higher rates observed in developing countries [15,21].

The cornea (Chapter 5 *vide infra*) is approximately 500-µm-thick, is a transparent and collagenous structure that is the primary barrier to topical drug absorption in the eye [22]. The layers of the cornea, from anterior to posterior include the corneal epithelium, stroma, and endothelium. An area of concern in ocular drug delivery is that only moderately-charged small molecules are likely to penetrate through the corneal epithelium [23,24]. The passage of hydrophilic molecules is limited due to the tight junctions of the corneal epithelium while the charged collagen fibres of the corneal stroma limit passage of hydrophobic molecules. In addition, the collagen fibres of the stroma are highly organized and act as sieves to large molecules [25,26] The treatment of NTM keratitis is frequently substandard due to late diagnosis, inadequate penetration of drugs and a delayed therapeutic response. Antimicrobial resistance to most conventional therapies and the occurrence of resistant strains during long-term treatment is also a reason for poor therapeutic results [27–29]. NTM is sensitive to aminoglycoside, macrolide and fluoroquinolone therapy [28,30]. Of the macrolides, CLA has been shown to exhibit good *in vitro* sensitivity and favourable corneal penetration in addition to a bactericidal effect when administered in high doses resulting in high concentrations [13,31]. The treatment of NTM keratitis with topical CLA has also been reported to be successful [28]. However, toxic reactions, intolerance and patient discomfort from frequently instilling topical CLA solutions have been reported [32]. Of particular concern is that a commercially available CLA dosage form for ocular use is not readily available. The *in vivo* efficacy of CLA for the treatment of NTM keratitis has to date been determined by reconstitution and use of lyophilized parenteral formulations [28,31,33].

CLA is available as immediate-release (250 or 500 mg) and extended-release tablets (500 mg), intravenous solution (500 mg/vial) and granules for an oral suspension (125 or 250 mg/5 mL) [11]. The ophthalmic formulary in the United Kingdom lists 1% CLA eye drops for the treatment of bacterial keratitis [34].

Commercially available products containing CLA in South Africa include Klacid®, Klaryvid®, Klarizon®, Klaribin®, Clacee®, ClariHexal®, Simayla Clarithromycin®, Klarithran® and Mylan-Clarithromycin® [11].

The primary objective of this research was to investigate and optimize the development of potential innovative formulations that could be used as carriers for the ocular administration of CLA for the treatment of NTM keratitis.

1.2 PHYSICO-CHEMICAL PROPERTIES

1.2.1 Description

CLA is 3R,4S,5S,6R,7R,9R,11S,12R,13S,14S)-6-{[(2S,3R,4S,6R)-4-dimethylamino)-3-hydroxy-6-methyloxan-2-yl] oxy}-14-ethyl-12,13-dihydroxy-4-[(2R,4S,5S,6S)-5-hydroxy-4-methoxy-4,6-di-methyloxan-2-yl]oxy}-7-methoxy-3,5,7,9,11,13-hexamethyl-1-oxacyclotetrade-cane-2,10-dione or 6-*O*-Methylerythromycin [35,36]. It is a white to off-white crystalline powder with the empirical formula $C_{38}H_{69}NO_{13}$ and a molecular weight of 747.96 g/mol [35–37]. The chemical structure of CLA is depicted in Figure 1.1 [35,36].

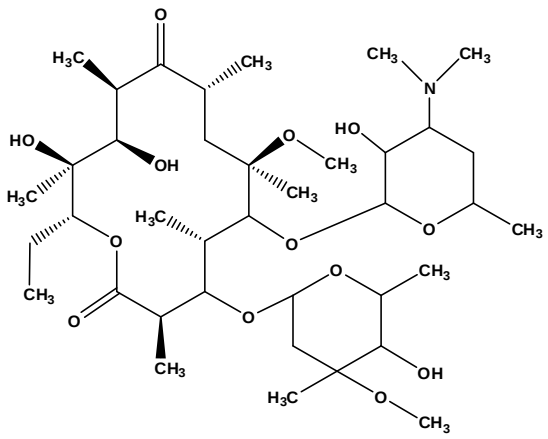

Figure 1.1 Chemical structure of CLA (MW = 747.96 g/mol)

1.2.2 Solubility

The pH-solubility profile of CLA at 37 °C in addition to the solubility of CLA in water at different temperatures was investigated by Nakagawa *et al.,* [38]. The authors reported that the solubility of CLA decreased with an increase in pH and was constant at pH > 9.00. At these pH CLA which is a basic molecule, forms an undissociated structure that is less likely to dissolve in aqueous solutions [38,39]. At low temperatures, water molecules are ordered regularly around the hydrophobic regions of CLA. These hydrophobic regions are destroyed as the temperature of the system increases, resulting in a decrease in the solubility of CLA [38]. Shinoda *et al.,* [40] postulated that hydrophobic compounds such as benzene and toluene dissolve due to hydrophobic hydration in water. CLA is soluble in acetone, slightly soluble in methanol, ethanol, acetonitrile and is practically insoluble in water [41]. The aqueous solubility of CLA is approximately 0.342 µg/mL at 25 °C and neutral pH [41,42].

1.2.3 Biopharmaceutical Classification System (BCS)

CLA is a biopharmaceutical classification system (BCS) class II molecule that exhibits poor aqueous solubility and high intestinal permeability [42]. The poor aqueous solubility not only limits the biological application of the molecule but also poses challenges in pharmaceutical development.

1.2.4 Dissociation constant

The ionization state of most active pharmaceutical ingredients (API) is a consequence of the pH of solution in which the molecule is dissolved and the acid dissociation constant (K_a) stemming from the presence of acidic and/or basic functionalities located on the compound. The K_a is usually expressed as a negative logarithm or pK_a [43]. Acid–base properties of an API are an important parameter for drug product development as these impact solubility, absorption, distribution, metabolism and elimination. Weakly acidic drugs ionize as the pH of a solution increases and conversely weak bases ionize with decreasing pH. In general, macrolide antibiotics contain a basic dimethylamine [–$N(CH_3)_2$] functional group, which is able to gain a proton. According to the chemical structure macrolides possess a single pK_a value of approximately 9.00 [38,43] and the pK_a of CLA is 8.99 [41].

1.2.5 Partition Coefficient (Log $P_{o/w}$)

The Log $P_{o/w}$ value is used to describe the distribution of a solute between two immiscible solvents, usually octanol and water. These values are used in drug design as a measure of the hydrophobicity of an API, from which membrane permeability is inferred [44,45]. The Log $P_{o/w}$ of CLA is 2.69 [41] at an unspecified pH in one study and 1.70 at pH 7.40 in another [46]. Furthermore, a Log $P_{o/w}$ of 3.24 [47] and a Log $P_{octanol/buffer}$ of 4.89 at pH 4.00 [38] has also been reported thus inferring the molecule is lipophilic.

1.2.6 Ultraviolet (UV) Absorption Spectrum

The wavelength of maximum absorption (λ_{max}) of CLA dissolved in water and methanol was 210 nm [48] and 211 nm [49], respectively. In chloroform, the λ_{max} of CLA was 240 nm [49]. The absorption spectrum of CLA was determined using a 100 µg/mL solution in acetonitrile over the wavelength range 190-700 nm at a scan speed of 600 nm/min. The spectrum was generated using a double beam Model GBC 916 UV-VIS spectrophotometer (GBC Scientific

Equipment Pty Ltd, Melbourne, Australia). The UV absorption spectrum of CLA is depicted in Figure 1.2 and reveals a λ_{max} for CLA of 192.11 nm.

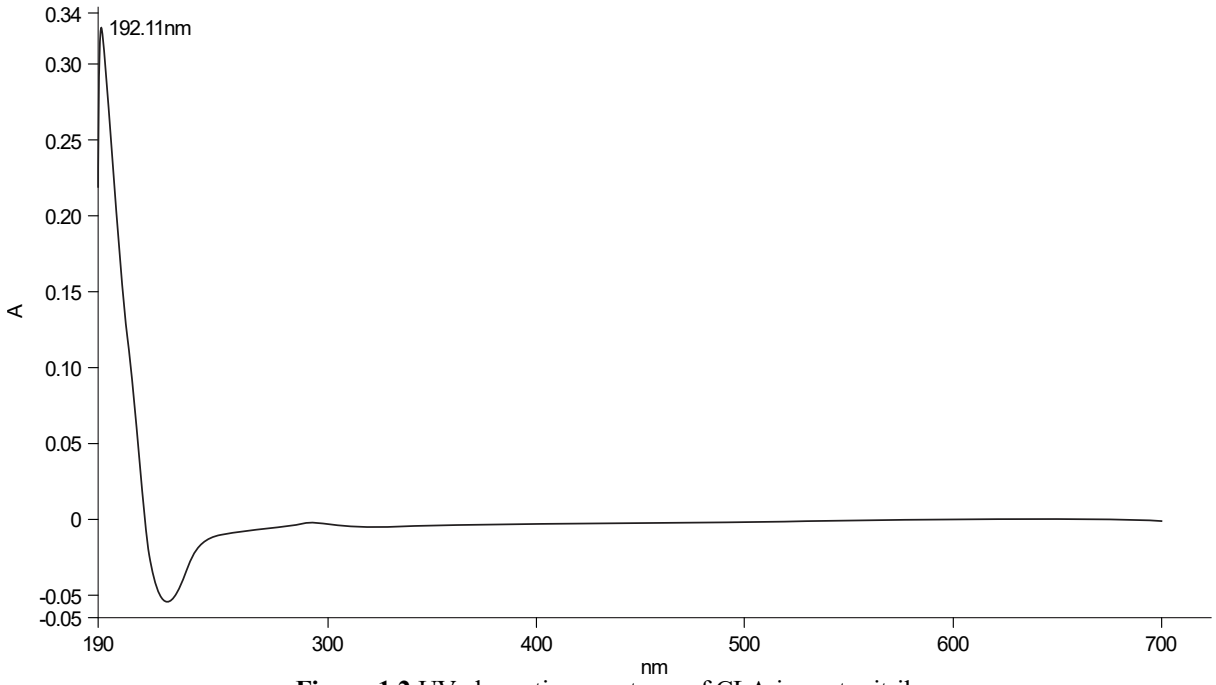

Figure 1.2 UV absorption spectrum of CLA in acetonitrile

CLA lacks a chromophore as there is no conjugated double bond in the lactone ring therefore, significant UV absorbance is only observed at wavelengths < 210 nm [1]. Detection at these wavelengths is suitable for the analysis of most *in vitro* samples but lacks the necessary sensitivity for the quantitation of low concentrations of CLA, such as those observed when characterizing nanoparticles [50]. CLA has a tertiary amino group which is a potential reactive site for oxidation and may therefore be suitable for electrochemical detection [51]. Electrochemical detection (ECD) is therefore a potentially useful tool for ensuring the accurate determination of CLA in dosage forms. Consequently, ECD was used for the *in vitro* analysis of CLA during formulation development and optimization studies.

1.2.7 Melting point range

The melting point range of CLA is 217 – 220 °C [1,41]. Differential scanning calorimetry (DSC) studies conducted by Tozuka *et al.,* [52] revealed that CLA melts at 228 °C. Sharma *et al.,* [50] reported a melting point of 227 °C for CLA during formulation studies with nanoparticles. The melting point of the CLA (Skyrun Industrial Co. Limited Taizhou, China) used in these studies was investigated using DSC and the data revealed a melting point of 229.25 °C (§ 4.3.2). Lipid based nanocarriers depending on the lipid matrix used are usually manufactured at temperatures of between 60-80 °C. Therefore, it is possible to formulate and

manufacture CLA-loaded lipidic formulations at these temperatures since CLA would not melt and/or decompose during the manufacturing process. However, thermogravimetric analysis (TGA) characterizations of the API should be conducted to ascertain the feasibility of exposing CLA to high temperatures.

1.2.8 Optical rotation

CLA is laevorotatory with an optical rotation of −90.4 ° at 25 °C determined using a 1 mg/mL solution in chloroform [1,49].

1.2.9 Hygroscopicity

CLA is commercially available in the anhydrous form and does not form hydrates [53] therefore eliminating manufacturing challenges involving water based processes.

1.2.10 Stereochemistry and Polymorphism

Polymorphism of a compound is a solid crystalline phase that emanates from the possibility of at least two different arrangements of the molecules of that compound in the solid state [54]. CLA is known to exist in at least five crystalline polymorphic forms. Polymorphism of CLA has been reported in patents with Form 0, Form I, Form II, Form III and Form IV crystal modifications having been characterized. Commercially available CLA dosage forms are formulated with the thermodynamically stable Form II polymorph [54–57].

1.2.11 Infrared Absorption Spectrum (IR)

The use of Fourier transform infrared (FTIR) spectroscopy facilitates identification of variations in the total composition of compounds through the identification of unique functional groups in the compounds. FTIR measures the vibration and rotation of molecules following infrared radiation at specific wavelengths [58]. The infrared absorption spectrum is a unique property of the sample as a whole and the technique is applicable to analysis of discrete samples or mixtures. The spectrum is representative of the different functional species that are present in mixtures, and is practically, the summation of the contributions of the individual components in a spectrum [59]. The IR spectrum of CLA was generated using a Perkin-Elmer® Precisely FT-IR Spectrum 100 spectrophotometer (Perkin-Elmer® Pty Ltd, Beaconsfield, England). Scans were performed in the 4000-650 cm^{-1} wavelength range and data analyzed using version 4.00 Peak® Spectroscopy software (Operant LLC, Burke, VA, USA). The resultant absorption spectrum of CLA is depicted in Figure 1.3. The principal

bands observed at 3461 cm^{-1} (hydrogen bonds between –OH groups), 2972 cm^{-1} (alkane stretching peaks), 1729 cm^{-1} (lactone carbonyl), 1687 cm^{-1} (ketone carbonyl), 1419 cm^{-1} (N-CH_3) and 1374 cm^{-1} (-CH2 groups) are consistent with those reported in literature for CLA [49,60].

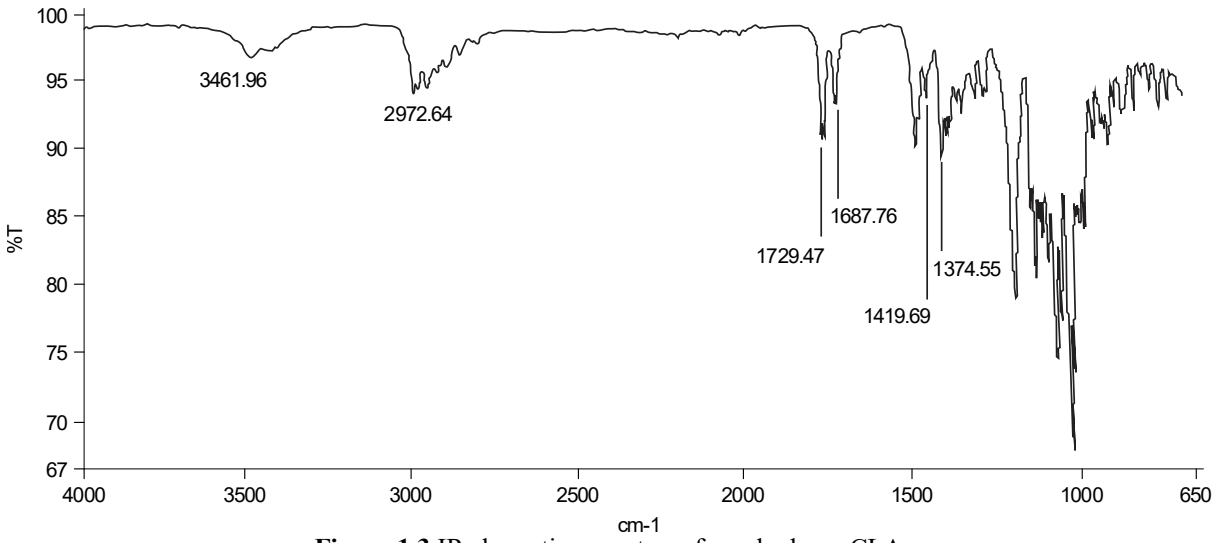

Figure 1.3 IR absorption spectrum for anhydrous CLA

1.2.12 Nuclear Magnetic Resonance (NMR) Spectroscopy

Nuclear magnetic resonance (NMR) studies were conducted in an attempt to evaluate the purity of CLA, prior to its use in formulation development studies. One-dimensional NMR data were acquired using a Bruker Avance® 400 MHz spectrometer (Bruker Avance®, Rheinstetten, Germany) used in the ^{2}H lock mode. Chemical shifts were analyzed using MestRe Nova® software (Bruker, Avance® Rheinstetten, Germany) and were recorded in parts per million (ppm) in reference to residual deuterated $CDCl_3$ δ_H 7.26, δ_C 77.0. All coupling constants are reported in Hz. Samples of CLA were transferred to 178 mm glass ultra-precision ASTM Type 1 Class A borosilicate thin-walled NMR tubes (Norell® Inc. Mays Landing, NJ). The design of the glass tubes permits use in high resolution NMR studies and in chemical structure determination, low and high temperature applications and sample storage at low temperature [61]. The ^{1}H NMR and ^{13}C NMR spectra of CLA are depicted in Figures 1.4 and 1.5, respectively.

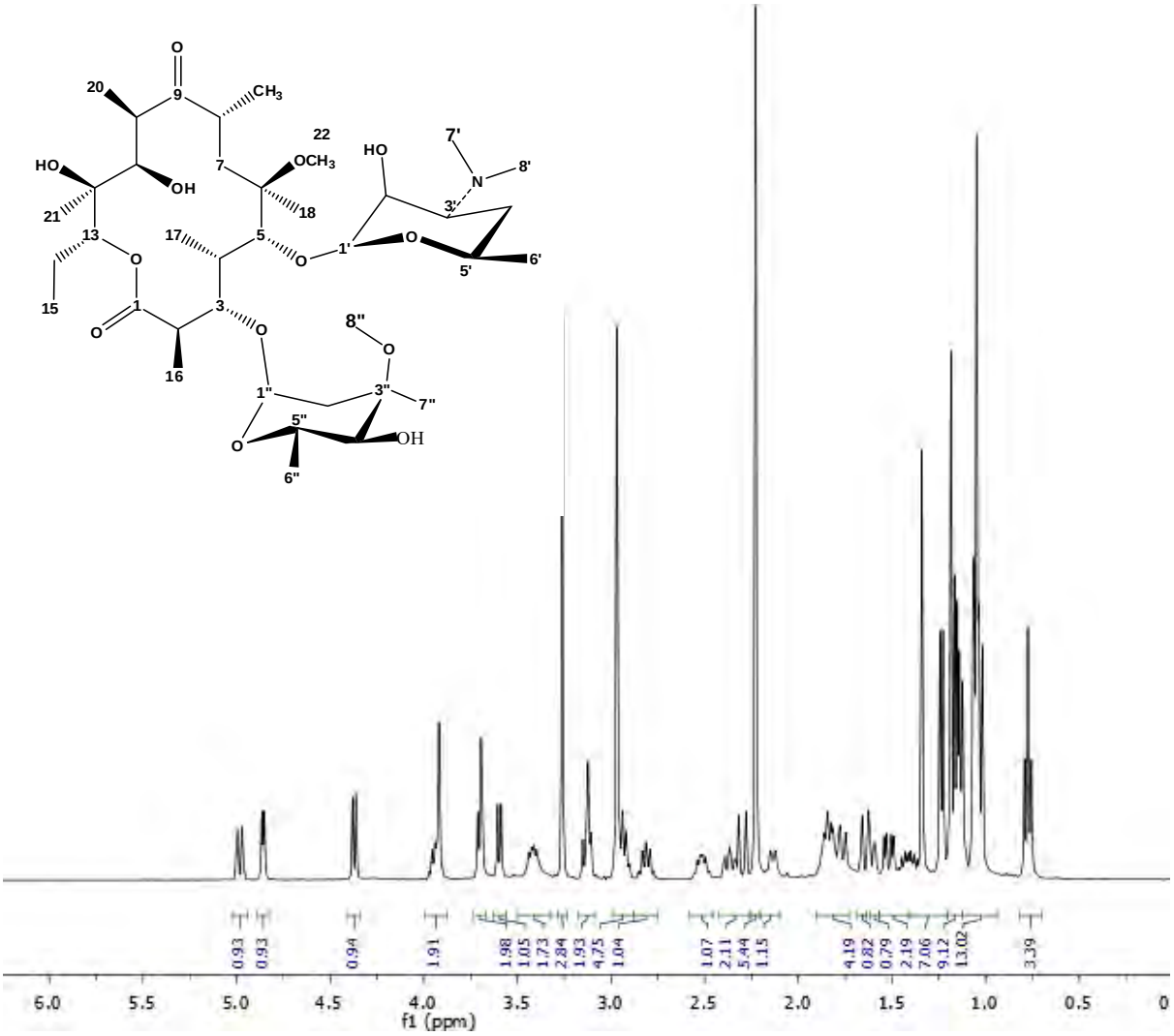

Figure 1.4 ^{1}H NMR (400 MHz; $CDCl_3$) spectrum of CLA

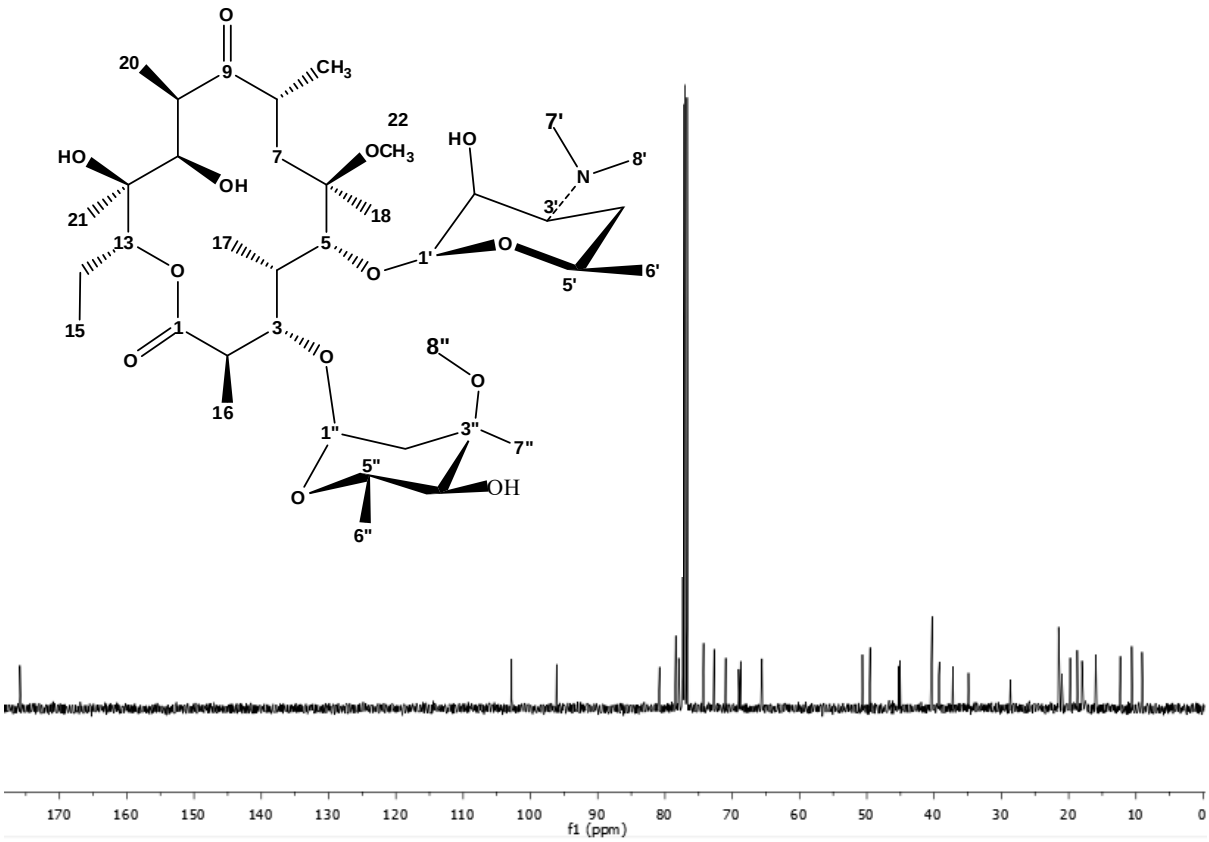

Figure 1.5 ^{13}C NMR (400 MHz; $CDCl_3$) spectrum of CLA

The NMR spectra of CLA reveal no signs of peak doubling and the high frequency ^{13}C signal C-1 (δ 175.83) can be assigned by inspection. This assignment is indicative of the existence of CLA in the 9-ketone form in $CDCl_3$ [62]. The low frequency triplet at δ 0.84 in the ^{1}H spectrum can be assigned to H_3-15. The highest frequency signal at δ 5.06 in ^{1}H spectrum can be attributed to H-13 double doublet while the broad doublet at δ 4.92 is due to H-1" and the signals at δ 2.36 and 1.58 are a result of H_2-2" [49,62]. The high frequency narrow doublet at δ 4.44 is indicative of H-1'. The double quartet at δ 4.03 is indicative of H-5". The broader doublet at δ 3.79 is due to H-3 while the δ 1.92 can be assigned to H-4 and δ 3.70 to H-5 [49,62]. Positions 7',8'-$(CH_3)_2$ can be assigned as δ 40.24 and 2.29 using ^{13}C and ^{1}H NMR, respectively. The assignment of 8"-CH_3 is possible at δ 50.58 using ^{13}C NMR while the other methoxy group at position 22 *viz.* 22-CH_3 is attributed to δ 3.06 using ^{1}H NMR. At δ 3.04 the 2'-OH exists [49,62]. The signals identified in the spectra correspond accurately to those reported in literature [49,62] indicating that CLA of high purity is available for use in the formulation studies intended in this research.

1.3 STABILITY

1.3.1 Solid State Stability

CLA is stable under storage conditions at 25 °C and the compound should be protected from light and stored in air-tight containers [49].

1.3.2 Solution Stability

CLA gradually loses antibacterial activity in dilute hydrochloric acid (HCI) solutions. The stability of CLA in aqueous and hydroalcoholic solutions has been monitored at 4 °C for 20 days with no degradation products observed in the samples [49]. Nakagawa *et al.,* [38] reported the degradation of CLA in HCI solutions of pH between 1.22 and 3.00 at 37 °C follows pseudo first-order kinetics with a maximum stability observed at pH 3.00. In addition the solution stability of CLA subjected to different stress conditions *viz*. 0.1 M HCI, 0.1 M NaOH, 4% H_2O_2 at 80 °C and 500W/m^2 for 12 hours showed that CLA was stable to heat, ultra-violet light and acidic conditions but degraded when exposed to alkaline and oxidative conditions using the degradation parameters set in those studies [63].

1.4 SYNTHETIC PATHWAY

The synthesis of CLA is depicted in Figure 1.6. CLA is synthesized from erythromycin thiocyanate. Initially erythromycin thiocyanate (**I**) is reacted with ammonia in dichloromethane to form erythromycin base (A) (**II**) [64]. The C-9 position of erythromycin is oximated by reacting the base with hydroxylamine HCI and triethylamine. Erythromycin oxime (**III**) is then treated with 2-methoxypropene and hexamethyldisilazane (HMDS) to silylate the hydroxyl groups at the oxime functional group and positions 2' and 4**"** forming the silylated derivative (**IV**) [64]. The isolated silyl derivative is converted to 6-O-methyl-2', 4**'**-bis(trimethylsilyl)-erythromycin A 9-O-(2-methoxyprop-2-yl)oxime (SMOP) (**V**) in a biphasic system of methyl iodide and KOH [64]. Subsequent deoximation of SMOP in aqueous ethanol, in the presence of formic acid yields crude CLA (**VI**) which is then further purified with ethanol resulting in pure CLA [64].

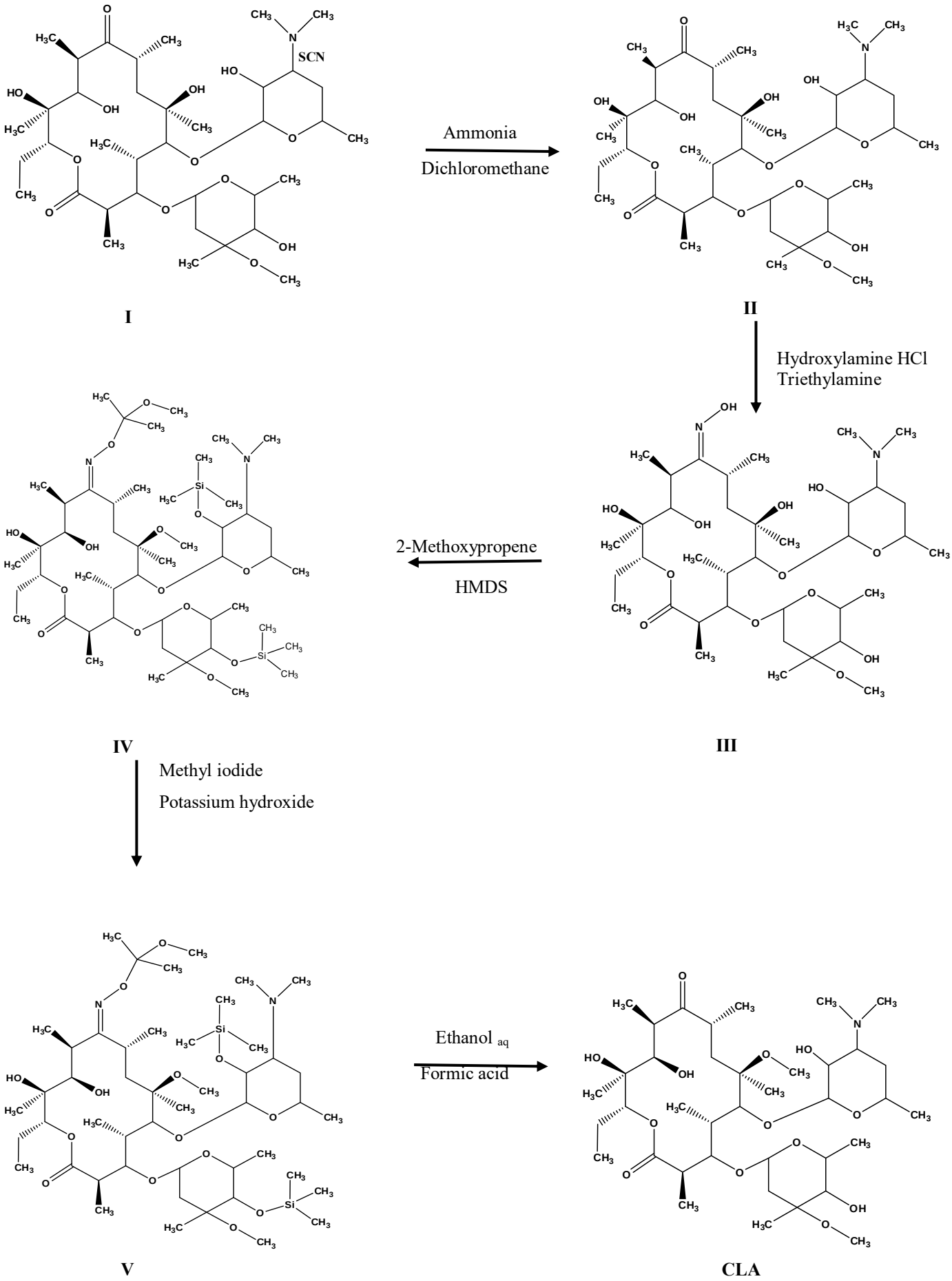

Figure 1.6 Synthesis of CLA

1.5 STRUCTURE ACTIVITY RELATIONSHIPS

CLA is a semi-synthetic derivative of erythromycin exhibiting a methoxy group at position C6 of the lactone ring (Figure 1.1) [65]. CLA is an active inhibitor of protein biosynthesis in bacterial cells [66]. In a study conducted by Mabe *et al.,* [65] the effects of CLA, flurithromycin and roxithromycin on cellular processes in *Haemophilus influenzae* revealed that CLA did not significantly affect the 30S subunit formation whereas cells treated with roxithromycin and flurithromycin exhibited an apparent decline in the amounts of both the 30S and 50S subunits. In addition, Schlunzen *et al.,* [67] and Hansen *et al.,* [68] revealed a common binding site in the peptide exit tunnel of the large 50S subunit for CLA, erythromycin, roxithromycin and azithromycin. Macrolide binding has been shown to be a consequence of hydrogen bond formation between the 23S rRNA and functional groups on the desoamine sugar in addition to the lactone ring [69]. The 2-OH functional group of the desoamine sugar forms three hydrogen bonds at position N6 and N1 of A2058Ec using the *E. coli* numbering system. The position for hydrogen bonding suggests elucidation of resistance by methylation of A2058Ec [65,67]. Adenine residue methylation at domain V of the 23S rRNA, interceded by erythromycin ribosome methylase genes, inhibits the binding of macrolides to domain V resulting in high level resistance to macrolides [8]. In addition, ribosome methylation has been postulated to provide more definitive evidence in comparison to macrolide efflux and/or modification in the innate resistance of *Mycobacterium tuberculosis* to second generation macrolide antibiotics such as CLA [69].

1.6 CLINICAL PHARMACOLOGY

1.6.1 Mechanism of Action

CLA possesses species specific bacteriostatic antimicrobial properties *in vivo* [70]. However, concentration dependent bactericidal activity has been demonstrated against certain strains of *Streptococcus pyogenes* and *Streptococcus pneumonia in vitro* in addition to demonstration of *in vivo* bactericidal activity against *Haemophilus influenzae* [71]. CLA acts by reversibly binding to domain V of 23S ribosomal RNA (rRNA) of the 50s subunit of the bacterial ribosome of susceptible organisms, inhibiting protein synthesis through translocation of aminoacyl transfer-RNA [8,49]. CLA is a poor inducer of mRNA and does not trigger activation of the methylase enzyme, thereby retaining activity against inducible bacteria in the absence of a strong inducer. CLA produces an active metabolite (14-hydroxy CLA) *in*

vivo resulting in a synergistic effect of the two compounds in respect of activity against bacteria [49,72]. In comparison to the penicillins and cephalosporins, the uptake of CLA by human neutrophils is high, resulting in higher concentrations of CLA in human macrophages, lymphocytes and polymorphonuclear leukocytes. In addition, CLA has been demonstrated to inhibit production of interleukin-1 by murine peritoneal macrophages, lymphocyte proliferation and lymphocyte transformation of murine spleen cells at low concentrations, thereby also exhibiting anti-inflammatory effects [49,73].

1.6.2 Spectrum of Activity

Brown *et al.,*[13] demonstrated that CLA has fairly poor activity against *Mycobacterium tuberculosis in vitro* but exhibits better activity against *Mycobacteriun avium* (MIC_{90} 8 µg/ml), and *Mycobacterium kansasii* ($MIC_{90} \leq 0.5$ µg/ml). The study concluded that CLA could be useful for treatment of the slowly growing nontuberculous mycobacteria with the exception of *Mycobaterium simiae* [13]. CLA is active against a range of aerobic and anaerobic Gram-positive and Gram-negative bacteria *in vitro*, including most MAC microorganisms [41]. The 14-hydroxy metabolite of CLA has antimicrobial activity of a different spectrum to CLA as shown by the reduction in activity by 4-7 times of the metabolite when targeting *Mycobactrium avium* isolates. CLA exhibits clinical and *in vitro* activity against *Staphylococcus aureus, Streptococcus pneumoniae, Streptococcus pyogenes, Haemophilus influenzae, Haemophilus. parainfluenzae, Moraxella catarrhalis, Mycoplasma pneumoniae, Chlamydia pneumoniae, Mycobacterum avium and Mycobacterium intracellulare* [41]. In addition, CLA exhibits *in vitro* but has untested clinical activity against the *Streptococci, Bordetella pertussis, Legionella pneumophila, Pasteurella multocida, Clostridium perfringens and Propionibacterium acnes* [41]. However the *in vitro* susceptibility testing fails to account for the antimicrobial activity of the active 14-hydroxy metabolite of CLA, thereby potentially underestimating the actual activity of CLA [8,74]. CLA is also effective against *Helicobacter pylori* in combination with a proton pump inhibitor and amoxicillin or metronidazole [75,76].

1.6.3 Clinical Indications

CLA is indicated for use in adults and children older than 12 years for the treatment of mild to moderately severe infections caused by susceptible strains of microorganisms that cause acute streptococcal pharyngitis, community acquired pneumonia due to *Chlamydia pneumoniae*, *Mycoplasma pneumoniae*, *Legionella pneumophila* and *Streptococcus*

pneumonia, uncomplicated skin and skin structure infections due to *Staphylococcus aureus or Streptococcus pyogenes* amongst others [37]. CLA should be used in combination with other antimicrobial agents for the treatment of disseminated or localized mycobacterial infections due to *Mycobacterium avium or Mycobacterium intracellulare,* skin and skin structure infections due to *Mycobacterium chelonae* [37]. CLA is also indicated for the prevention of disseminated MAC infection in human immunodeficiency virus (HIV)-infected adults with CD4 lymphocyte counts < 75 cells/mm^3 [11,37]. In addition, CLA is also indicated for the treatment of acute bacterial exacerbation of chronic bronchitis due to *Haemophilus influenzae*, *Moraxella catarrhalis* or *Streptococcus pneumonia* including its use in combination therapy for the treatment of peptic ulcer disease due to *Helicobacter pylori* infection [11,37].

In children < 12 years of age, CLA is indicated for the treatment of mild to moderately severe infections caused by susceptible strains of microorganisms for acute otitis media, acute streptococcal pharyngitis and tonsillitis caused by *Streptococcus pyogenes*, community acquired pneumonia including infections due to *Chlamydia pneumoniae*, *Mycoplasma pneumoniae* and *Legionella pneumophila*, skin and skin structure infections such as impetigo, disseminated or localized infections resulting from *Mycobacterium avium* or *Mycobacterium intracellulare* in immunocompromised children, including those with HIV infection or acquired immune deficiency syndrome (AIDS) [37].

1.6.4 Dosage and Administration

1.6.4.1 Non mycobacterial infections

The recommended dose of CLA is 250 mg administered twice daily. In more severe infections, the dose can be increased to 500 mg administered twice daily with a duration of therapy of 7 to 14 days. In patients suffering with haemolytic streptococcal infections, treatment should be administered for a minimum of 10 days. For the treatment of *Legionella pneumophila* infections, the dose should be adjusted to 500 mg administered twice daily for 4 weeks [37].

In patients with renal impairment and a creatinine clearance of < 30 mL/min, the dose of CLA should be reduced by one-half, with the treatment capped at 14 days in these patients [11,37].

The recommended dosing regimen for the treatment of *Helicobacter pylori* eradication is 500 mg CLA administered twice daily in combination with 1000 mg amoxicillin twice daily and 20 mg omeprazole twice daily or 400 mg metronidazole twice daily for 7-10 days [11,37].

1.6.4.2 Mycobacterial Infections

The recommended dose for adults and children older than 12 years with disseminated or localised mycobacterial infections is 500 mg twice daily in conjunction with other anti-mycobacterial agents [11,37]. The dose may be increased to 1000 mg twice daily if no clinical or bacteriological response is observed after 3-4 weeks of therapy. Elderly patients > 65 years of age with a calculated creatinine clearance > 30 mL/min are recommended a dose of 500 mg twice daily [37]. A reduction of the initial dose and dose titration is recommended in patients with renal impairment (§ 1.6.4.1) [11,37]. An oral dosing regimen of 7.5-15 mg/kg/dose administered 12 hourly, with a maximum dose of 500 mg, is recommended for paediatric patients [11].

In HIV-infected adults with CD4 lymphocyte counts < 75 cells/mm^3, the recommended dose of CLA for prophylaxis of disseminated MAC infections is 500 mg twice daily [37].

1.6.4.3 Overdose

Overdoses with CLA are reported to produce pronounced GIT symptoms such as nausea, diarrhoea, abdominal pain, taste perversion and include headache. In addition, severe liver toxicity, including cholestatic jaundice may occur [37,77]. Treatment of overdose should promote elimination of unabsorbed CLA and includes general supportive measures such as monitoring vital signs. CLA is highly protein bound therefore serum levels are not expected to be appreciably affected by haemo- or peritoneal dialysis [37,78].

1.6.5 Contraindications

CLA is contraindicated in patients with known hypersensitivity to macrolide antibiotics. In addition, CLA is contraindicated when used concurrently with cisapride, pimozide, terfenadine, ergotamine or dihydroergotamine [37]. Concomitant therapy of CLA with cisapride, pimozide, terfenadine has been reported to result in QT interval prolongation and cardiac arrhythmias including ventricular tachycardia, ventricular fibrillation and torsades de pointes [79]. Co-administration of CLA with ergotamine or dihydroergotamine has been

associated with acute ergot toxicity characterized by vasospasm and ischaemia of the extremities and other tissues, including the central nervous system (CNS) [37,80,81].

1.6.6 Use in Special Patient Populations

1.6.6.1 Geriatric Patients

The pharmacokinetics of CLA have not been studied in patients older than 65 years of age. However, dosage adjustments are recommended in those patients who present with severe renal impairment (§ 1.6.4.1) [37].

1.6.6.2 Breastfeeding Mothers

CLA is excreted in human breast milk and its safety for use during breast-feeding of infants has not yet been established [37]. However Kawada *et al.,*[82] investigated *Staphylococcus aureus* transmission between healthy, lactating mothers without mastitis and their infants by breastfeeding using bacteriological and molecular-epidemiological methods and concluded that methicillin-resistant or methicillin-sensitive *Staphylococcus aureus* may be transmitted between healthy, lactating mothers without mastitis and their infants through breastfeeding. Therefore, CLA use during breastfeeding is likely to reduce transmission of the aforementioned bacterial strains.

1.6.6.3 Pregnancy

The safety of CLA use in pregnancy has not yet been established. In animal studies, while some rats exposed to CLA in the first trimester did reveal teratogenicity, other rats presented with a low occurrence of cardiac abnormalities, post CLA exposure [83]. In a cohort and post marketing surveillance study conducted following the use of CLA in early pregnancy, it was reported that there is an increased likelihood of miscarriage without an increased prevalence of malformations in offspring in women who filled a prescription for CLA use during early pregnancy [84,85]. Therefore, the use of CLA in pregnancy should only be considered with extreme caution and implemented only if the benefits outweigh the risks [83,86].

1.6.6.4 Renal Impairment

Approximately 18% CLA is excreted as the parent drug in urine and therefore a progressive increase in serum concentrations of CLA and the 14-hydroxy metabolite in patients with

renal impairment may occur. [87]. The dose of CLA may need to be reduced in patients with severe renal impairment (§ 1.6.4.1).

1.6.6.5 Hepatic Impairment

The bioavailability of CLA following oral administration is approximately 50% However, additional CLA is absorbed in the liver and is converted to the 14-hydroxy CLA metabolite prior to entering the systemic circulation [87]. Theoretically, severe hepatic impairment could potentially alter the pharmacokinetics of CLA and the metabolite resulting in a lower conversion of the parent molecule to the metabolite which in turn results in an increase in the renal clearance of the parent compound. However, steady-state levels of unchanged CLA in hepatically impaired patients were similar to those in patients with healthy and normal functional livers. Therefore, if renal function is normal, CLA can be administered without any dose adjustment in patients with hepatic impairment [78,88].

1.6.7 Drug Interactions

Macrolide antibiotics have the potential to induce hepatic microsomal enzymes and studies in rats in the presence of troleandomycin and erythromycin showed that inactive cytochrome P450 (CYP 450) complexes are formed [89,90]. Many drugs are extensively metabolized in the liver *via* CYP 450 isoenzymes and the most common mechanism by which CLA interacts with drugs when used concomitantly, involves inhibition of subclasses of the CYP 450 enzyme system, particularly CYP 3A4, through formation of an inactive complex, thereby decreasing clearance [11,71,91]. The list of drugs reported in Table 1.1 are known to exhibit interactions of clinical importance when used with CLA.

Table 1.1 Drug-drug interactions for CLA

Drug	Interaction effects during co-administration	Recommendations	Reference
Alfentanil	Plasma clearance may be decreased leading to prolonged duration of action of alfentanil	Avoid concomitant use of the drugs wherever possible	[11,92]
Carbamazepine	Elevated carbamazepine concentrations leading to toxicity	Carbamazepine dosage should be decreased by 25–50%, and drug concentrations should be monitored frequently during concurrent use of the drugs	[91,93]
Cimetidine*	Cimetidine prolongs the absorption of CLA, thus decreasing peak concentrations of CLA and its 14-hydroxy metabolite. This may ultimately decrease the effectiveness of CLA against *Haemophilus influenzae*		[94]
Cisapride	CLA inhibits the CYP 3A4 isoenzyme resulting in the accumulation of cisapride, causing torsade de pointes arrhythmias	The use of these agents simultaneously is contraindicated	[95,96]
Colchicine	Increased risk of colchicine–induced toxic effects	Reduce colchicine dose by 50%	[11]
Cyclosporine	CLA inhibits the hepatic and intestinal metabolism of cyclosporine leading to an increase in whole blood cyclosporine levels	Caution should be used when administering these agents simultaneously, including considering appropriate dose reductions	[97–99]
Digoxin	Increased bioavailability of oral digoxin is induced by increased gastric emptying caused by CLA	Patients should be closely monitored for clinical signs and symptoms of digoxin toxicity and digoxin concentrations should be measured to avoid it	[100,101]
Ebastine	Increased risk of cardiotoxicity from increased ebastine serum levels		[11,102]
Ergot alkaloids	Increased risk of clinical ergotism (hypertension, lingual ischemia, and peripheral cyanosis)	Ergot preparations should be avoided in patients who are taking CLA	[11,81]
Midazolam	CLA significantly raises midazolam serum concentrations,	Midazolam dose should be reduced by 50%, or even 75%, if	[91,103]

	increasing the duration of the patient's sleep thus decreasing patient alertness	concurrent CLA therapy is required. Co-administration is not advisable in the elderly or those patients sensitive to the effects of benzodiazepines	
Oral contraceptives	Efficacy of oral contraceptives may be reduced	Additional contraception use is advisable	[11]
Pimozide	CLA inhibits the metabolism of pimozide in human liver microsomal preparations. Pimozide in turn prolongs QT intervals in a dose-dependent manner. Torsade de pointes may occur	Concomitant administration of the agents is contraindicated	[104,105]
Rifabutin*	Rifabutin, a highly effective enzyme inducer, may significantly decrease serum concentrations of CLA. Rifabutin and its metabolite show elevated serum concentrations when given with CLA	This combination should be avoided, with careful monitoring for rifabutin toxicity (neutropenia) if concomitant use is necessary	[91,106]
Ritonavir*	Ritonavir leads to a marked inhibition of the metabolism of CLA leading to the complete inhibition of the formation of 14-hydroxy metabolite. CLA increases ritonavir area under the curve (AUC) by 12%	No dosage adjustments are necessary for ritonavir or CLA (in patients with normal renal function) during concomitant use For patients with creatinine clearance of 30-60 mL/min, the dose of CLA should be reduced by 50%. For patients with creatinine clearance of < 30 mL/min, the dose of CLA should be decreased by 75%. Doses of CLA greater than 1000 mg/day should not be co-administered with ritonavir. No dosage adjustment of ritonavir is recommended	[37,91]
Saquinavir*	Both CLA and saquinavir are substrates and inhibitors of CYP3A, and there is evidence of a bidirectional drug interaction	Patients receiving this combination should be monitored carefully, as there is an increased risk for adverse effects with both agents Patients with *Haemophilus influenzae* should probably have an additional agent added to their regimen	[37,91]

Simvastatin	Rhabdomyolysis after concomitant therapy was reported in two women. Rapid recovery was observed after simvastatin withdrawal.		[107]
Terfenadine	Unmetabolized terfenadine serum levels have been associated with altered cardiac repolarization	CLA must not be given in combination with terfenadine in patients with a history of ischaemic heart	[37,91]
Theophylline	Increased serum theophylline concentrations may result from concomitant use	Monitoring of serum theophylline concentrations should be considered for patients receiving high doses of theophylline Theophylline dosage may need to be reduced.	[37,91]
Warfarin	Increases in International Normalized Ratio (INR) have been detected in patients who have previously been stabilized on warfarin when they were simultaneously given a macrolides	Close monitoring of INR is recommended and warfarin dose adjustment may be necessary	[108,109]
Zidovudine	CLA decreases zidovudine's absorption leading to decreased steady-state zidovudine concentrations	Zidovudine and CLA should not be given at the same time and should be staggered by at least 2 hours This interaction does not appear to occur in paediatric HIV-infected patients taking CLA suspensions with zidovudine	[37,91,110]

* The drug also has an effect on CLA

1.6.8 Adverse Effects

Dose related GIT upset is the most common adverse event associated with macrolide therapy. CLA stimulates motilin receptors in the GIT thus acting as a gastric prokinetic agent [71]. The incidence of significant GIT effects such as nausea, diarrhoea, abdominal pain and vomiting following the use of CLA occur in 10-15% of patients [8,37,71]. Adverse effects reported during clinical trials with a frequency of ≤ 2% include headache, hepatic dysfunction, changes in neutrophil or leukocyte counts, skin rash and taste perversion [37,71]. In addition, visual hallucinations associated with CLA have been reported in two children who took CLA in therapeutic dosages with symptoms gradually disappearing following withdrawal of the macrolide [107].

1.6.9 Resistance

Resistance of microbial organisms to macrolide antibiotics may either be intrinsic or acquired in nature. The intrinsic resistance of the vast majority of Gram-negative bacilli and enterococci to the hydrophobic macrolides is believed to be due to the barrier properties of the Gram-negative cell outer membrane envelope [111]. Induction of enzymes causing ribosomal methylation, target site modification or active drug efflux have mostly been shown to be the cause of acquired resistance [71]. Ribosomal target site modification occurs *via* modification of the ribosome through methylation of a specific adenine residue in a conserved region of the 23S ribosome that interacts with macrolide antibiotics, resulting in high levels of resistance to all macrolides [112]. Resistance to 14- and 15-membered macrolides, such as CLA, has been shown to be a result of efflux of the antibiotic from the cell, encoded by the gene, mefE, in *S pneumonia* [112]. Furthermore, active efflux of macrolides has been demonstrated in both *staphylococci* and *streptococci*, conferring low level resistance to these drugs [71].

1.7 CLINICAL PHARMACOKINETICS

There is a dearth of information relating to ocular pharmacology and pharmacokinetics of CLA. However, a study that evaluated the ocular pharmacokinetics of CLA eye drops topically applied to the corneas of rabbits concluded that therapeutic levels of CLA can be achieved in rabbit corneas after topically applying the drug as eye drops [113]. Nonetheless, Al-Sibai *et al.,* [114] conducted a study on the ocular penetration of oral CLA in humans. The authors concluded that CLA widely penetrates and adequately concentrates in the aqueous

humor, vitreous humor, and iris tissue after oral administration and therefore is effective in the management of many infectious ocular conditions. To date, innovative CLA-loaded chitosan nanoparticles have been optimized for the effective management of bacterial conjunctivitis by increasing the precorneal residence time of the carriers [115].

1.7.1 Absorption

CLA is stable in gastric acid, and is rapidly absorbed from the GIT with peak concentrations reached within two hours of dosing and a bioavailability of approximately 55% [49,71,116]. The time to peak serum concentrations of CLA is delayed following administration with food and the formation of the 14-hydroxy metabolite is slightly retarded, however the extent of absorption of CLA is not affected. Conversely, plasma concentrations of the14-hydroxy metabolite are higher following oral dosing than after intravenous dosing [49,71,87] which can be attributed to the hepatic first pass effect.

1.7.2 Distribution

CLA and the 14-hydroxy metabolite are widely distributed into most body tissues, reaching high concentrations in the lung that have been shown to be in excess of those observed in plasma by at least six-fold. Two-to-six fold tissue to plasma CLA concentrations have also been observed in the nasal mucosa and tonsils [49,71]. Because of high CLA intracellular concentrations, negligible accumulation of CLA has been observed [49]. At clinically achieved concentrations, CLA was found to be 42% to 70% bound to human plasma proteins [87,116]. The apparent volume of distribution (Vd) of CLA in 'Western' volunteers was approximately 226-266 L, implying that CLA is widely distributed in the body [116].

1.7.3 Metabolism

CLA undergoes extensive hepatic metabolism producing at least eight (8) metabolites. Hydroxylation and oxidative N-demethylation are the two (2) major pathways that have been identified for the metabolism of CLA with hydrolysis of the cladinose sugar only being a minor contributor[10,78,117]. Therefore, the metabolic process of CLA is primarily a consequence of CYP 450 (CYP) 3A isozyme activity. Of the eight metabolites, 14-hydroxy CLA only exhibits therapeutic activity and contributes synergistically to the activity of the parent compound, as the pharmacological activity is comparable to or greater than that of the parent compound [10,78,117].

1.7.4 Elimination

The serum half-life of CLA is 4.9 hours and steady-state amounts of CLA and the 14-hydroxy metabolite are reached after 2-3 days post administering a 250 mg dose every 12 hours [10]. The elimination half-live of CLA is 4 hours following administration of a single 500 mg oral dose [71]. CLA and its principal metabolites are excreted in the faeces *via* bile, in urine by renal and non-renal mechanisms. Between 20-30% of the dose is excreted in this manner as unchanged drug [49,117]. CLA metabolism is dose dependent and the compound exhibits non-linear pharmacokinetics due to saturable metabolic processes. Increased doses of CLA therefore result in an increase in the half-life and decrease in metabolic clearance rates [49,78,117].

1.8 CONCLUSIONS

CLA is a semisynthetic macrolide derivative of erythromycin which differs from erythromycin in respect of a methyl substitution at the position 6 of the macrolide ring. In comparison to erythromycin, CLA is more stable in acid and requires less frequent dosing whilst exhibiting a lower incidence of the GIT side effects [118].

CLA has been shown to have remarkable potency against strains of *Mycobacterium fortuitum and Mycobacterium chelonae* which are known causes of majority of cases involving NTM keratitis [14,15]. Treatment of NTM keratitis with topical CLA has been successful [28]. However, toxic reactions, intolerance and patient discomfort due to frequent instillation of topical CLA solutions have been reported [32]. Furthermore, commercially available CLA dosage forms for ocular use are not readily available. The *in vivo* efficacy of CLA for the treatment of NTM keratitis has to date been determined by reconstitution and use of lyophilized parenteral formulations administered *via* the ocular route [28,31,33].

An area of concern in ocular drug delivery is that only moderately-charged small molecules are likely to penetrate through the corneal epithelium [23,24]. The passage of hydrophilic molecules is limited due to the tight junctions of the corneal epithelium while the charged collagen fibres of the corneal stroma limit passage of hydrophobic molecules. In addition, the collagen fibres of the stroma are highly organized and act to sieve large molecules [25,26] such as CLA. Furthermore, there is a constant flow of tear films across the outer surfaces of the cornea, naso-lachrimal drainage and blinking that contribute to a reduction in the

availability of drugs to the anterior segment of the eye [25,119,120]. Nanoparticulate formulations have been investigated as potential ocular delivery systems to enhance corneal permeation thereby improving API availability to the eye whilst ensuring safe, non-invasive treatments that facilitate patient adherence. The mucoadhesive nature of some lipid based nanocarriers has been shown to improve interaction with ocular membrane resulting in a prolonged residence time, enhanced availability and fewer local and systemic side effects [121].

There is clearly a need to improve the delivery of CLA to the eye. Less-frequent dosing, controlled delivery and improved targeting to the cornea to increase efficacy and reduce side effects are important technology characteristics and overcoming these challenges by formulating CLA into mucoadhesive nanocarriers was undertaken, in an attempt to address the unmet clinical needs described *vide infra* and are reported in rest of this thesis.

CHAPTER 2

HPLC WITH ELECTROCHEMICAL DETECTION FOR THE ANALYSIS OF CLARITHROMYCIN

2.1 INTRODUCTION

The analysis of pharmaceutical compounds can be achieved using a variety of techniques. However, high performance liquid chromatography (HPLC) is the principal analytical technique used for pharmaceutical analysis and is predominantly applied to a large assortment of sample types in the pharmaceutical industry [122]. A key instrumentation requirement for HPLC is the need for a sensitive detector for quantitation of components in the column effluent. A variety of detectors used for HPLC analysis have been developed over the years based on differential measurement of a bulk or general property of a sample and solvent, measurement of a sample property that is non-existent in the mobile phase or detection following elimination of the mobile phase [123].

The use of electrochemistry in liquid chromatography has been rapidly growing since the 1980s with > 500% increase between the 1980s and 1990s [124,125]. The use of electroanalytical techniques with HPLC provides an approach for the specific determination of trace quantities of electrochemically active molecules [126]. In comparison to other detection methods such as ultraviolet or fluorescence, electrochemical detection does not exploit the physical properties of an analyte but rather an induced chemical change resulting from an electrochemical reaction in an electrically conductive HPLC mobile phase [124,127]. For oxidizable and/or reducible compounds, the electrochemical detector is one of the most sensitive and selective HPLC detectors available for use [127].

Electrochemical detectors for HPLC usually contain three separate electrodes *viz*. a working, a counter (auxiliary) and a reference electrode. Materials commonly used to manufacture the electrodes include carbon, gold, silver or platinum [126,127]. A predetermined potential difference, usually between -1.2 V and +1.3 V is applied across the working and reference electrodes to drive an electrochemical reaction at the surface of the working electrode. As

compounds are oxidized or reduced, a current is produced from the electrochemical reaction, which is balanced by a current flowing in the opposite direction to the counter electrode. The detector response output is a consequence of the amplified current resulting from the electrochemical reaction at the surface of the working electrode [126,127]. A schematic representation of the principle behind the operation of an EC detector is depicted in Figure 2.1.

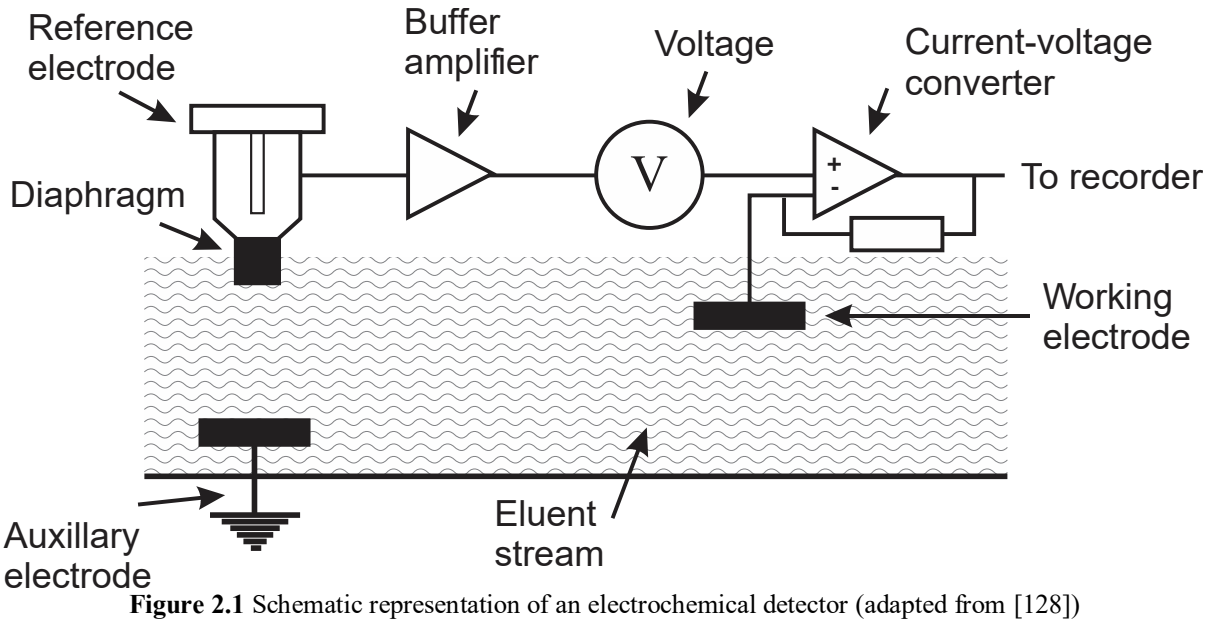

Figure 2.1 Schematic representation of an electrochemical detector (adapted from [128])

Electrochemical detection in HPLC follows Faraday's Law which states that "the amount of substance consumed or produced at one of the electrodes in an electrolytic cell is directly proportional to the amount of electricity that passes through the cell" [124]. The response of a molecule or ion reacting at the surface of the electrode is therefore directly proportional to the concentration of that compound. When all the analyte in a solution is electrolyzed at an electrode, the quantifiable response or output is directly related to the molar amount of the analyte present and can be mathematically represented using Equation 2.1. Measurement of current therefore implies measurement of the rate of a chemical reaction [124].

$$Q = nFN \qquad \textbf{Equation 2.1}$$

Where,

Q = the total charge transferred in coulombs
n = the number of electrons transferred or equivalents per mole
F = the Faraday constant
N = the number of chemical equivalents of the analyte

Commonly used EC detectors include amperometric and coulometric detectors. Amperometric detectors are either disk type thin-layer electrodes and coulometric detectors are flow-through "frit" type porous graphite working electrodes [125,127,129]. When using coulometric EC detection, 100% EC conversion of the analyte occurs while partial electrolysis of between 1-10% is achieved with amperometric detectors. Amperometric EC detectors can be operated in the direct current, pulsed or scan modes. As a result of their higher conversion efficiency, coulometric EC detectors are more sensitive and robust than their amperometric counterparts, while still exhibiting the flexibility to operate in an amperometric, pulsed amperometric or cyclic voltammetric modes in addition to the coulometric mode. However, in spite of the low conversion efficiencies, amperometric EC detectors are quite sensitive and commonly used [124,127,128,130].

Although EC detectors are widely used for many essential applications, their use is limited as the performance of EC detectors is strongly influenced by factors such as sample solubility properties, mobile phase, sample and detector compatibility, mobile phase viscosity in addition to system efficiency [125]. Furthermore, detector performance is strongly influenced by the nature of the working electrode, specifically the material used to manufacture the electrodes. The selection of a working electrode depends primarily on the redox behaviour of target analytes and the background current likely to be observed over the region of the applied potential [124,125]. Finally, fouling of the working electrode surface by the products of the electrochemical reaction may affect chromatographic analysis when conventional electrode materials are used in the detector. To maintain the sensitivity of an electrochemical detector the products of the electrochemical reaction that form a residue on the active surface of the working electrode must be frequently removed by mechanical polishing [125,130–132]. In spite of the limitations of using EC detectors for HPLC analyses, this system offers distinct advantages over other detectors commonly used with HPLC. Specifically EC detection with HPLC only requires simple sample pre-treatment prior to immediate analysis, offers remarkable sensitivity, is independent of optical path length, is not compromised by miniaturization, and associated instrumentation is relatively inexpensive and simple compared to optical or mass spectrometric detectors [125,130].

The use of EC detectors results in sensitive detection at the nanogram and picogram level for oxidizable compounds such as catecholamines, neurotransmitters, reducing sugars and glycoproteins amongst others [128,132]. Due to the presence of dissolved oxygen, and electrode instability, the limit of detection for reducible compounds is approximately ten times less favourable than that for oxidizable compounds [133,134]. EC detection with HPLC has been applied to the determination of analgesics [135,136], antibiotics [137–139], alkaloids [140,141], antidepressants [142,143], antiretrovirals [144,145] and many other compounds in pharmaceutical dosage forms [146] and biological fluids [147,148].

CLA has a tertiary amino functional group which is suitably reactive for electrochemical oxidation [51], suggesting ECD as a potentially useful tool for ensuring the accurate determination of CLA in the development and characterization of dosage forms. Quantitative analysis of CLA has been achieved in biological samples using HPLC with ECD [149–151], UV [152,153], LCMS [154] and fluorescence detection [155]. Published HPLC-ECD methods have reported limits of detection of 10.03 µg/mL [156], 0.5 µg/mL [157], 0.03 µg/mL [149], 0.1 µg/mL [158], 0.01 µg/mL [137], 0.15 µg/mL [159] and 0.02 µg/mL [160]. The objectives of this study were to develop an HPLC-ECD method for the quantitation of CLA with the aid of experimental design. The validated method will be applied to the analysis of CLA in commercially available dosage forms and CLA-loaded lipid nanocarriers.

2.2 METHOD DEVELOPMENT AND OPTIMIZATION

2.2.1 Design of Experiments and Statistical Analysis

HPLC method development should only be initiated subsequent to a thorough understanding of the following factors *viz*. the nature of the sample including molecular weight, solubility and ionization behavior, the required selectivity of the separation, experimental convenience and experience of the analyst with the method amongst other considerations [123,132]. Rigid guidelines for the development of experimental conditions for a particular separation are difficult to establish as different experimental approaches are required to optimize each chromatographic separation [123]. Furthermore, optimization of HPLC methods are complex processes, since, several variables including mobile phase composition, pH, buffer concentration, flow rate, stationary phase, column temperature and detector wavelength must

be concurrently controlled to achieve a separation [161]. Although chromatography is a useful technique for many sample analyses, it remains a challenge to master the technique due to the fact that a variety of constraints affect the performance of a separation [162].

The traditional approaches to HPLC method development have been to change a single parameter at a time while keeping all other variables constant. These approaches are time consuming, rely on analyst experience, serendipity and instinct while conducting a large number of experiments using extensive resources to successfully acquire limited information about the processes used and/or sample behavior [163,164]. Consequently, experts have introduced chemometric strategies to liquid chromatography thereby enabling a more detailed understanding of the system under investigation with less effort. These approaches facilitate the development of mathematical models, adding valuable scientific information in support of the ability of the model to assess the statistical significance of the influence of input variables on the chromatographic responses monitored [162,165]. The significance of chemometry has been espoused in the publication of countless research articles in recent years, in addition to the publication of several books, book chapters and review articles about various applications in analytical chemistry. These reports emphasise the fact that chemometric approaches are becoming an essential tool in pharmaceutical analysis.

Design of Experiments (DoE) is a chemometric approach that ensures that the information about a separation can be gained using a reduced number of experiments associated with lower reagent consumption and less intensive laboratory work [165]. The primary objective of applying experimental design to analytical processes is the ultimate acquisition of optimized valid results with minimum effort, time and resources. When using an experimental design, one or several predetermined factors are intentionally manipulated to identify the impact of that change on the experimental outcome(s) [165].

All designs for DoE can be classified into two broad categories *viz*. screening or response surface designs based on the experimental objectives and these are depicted in Figure 2.2.

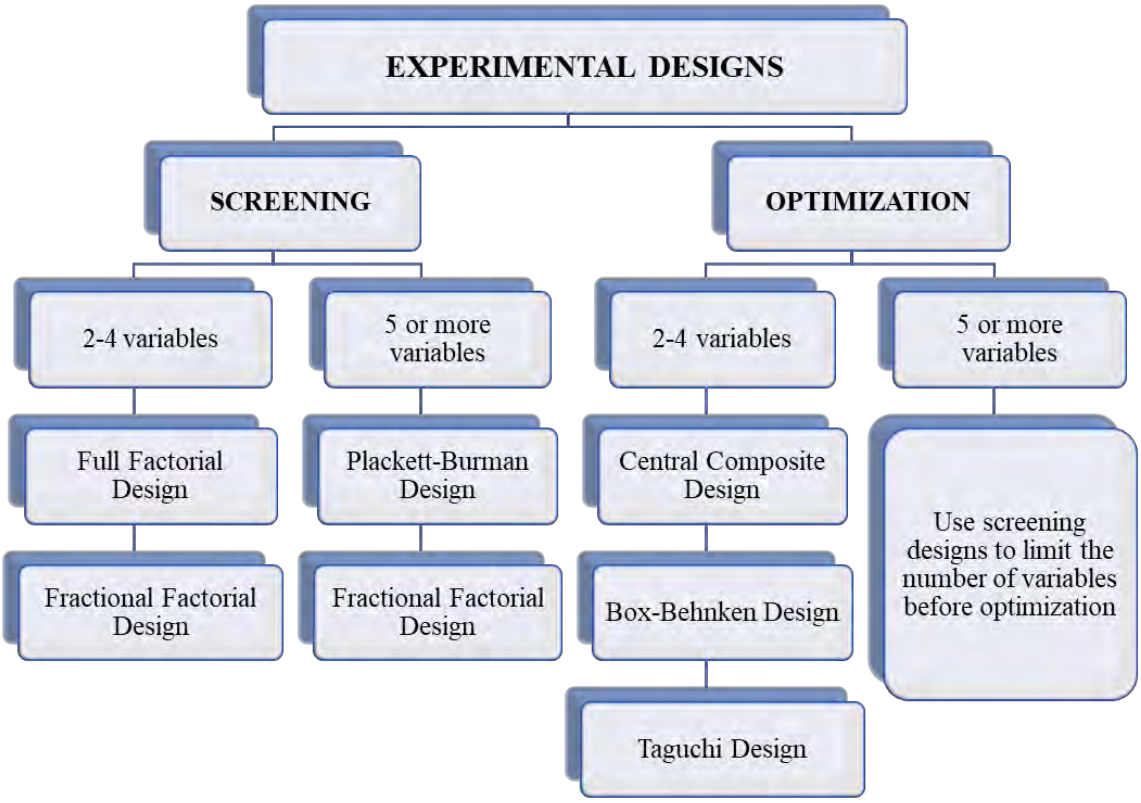

Figure 2.2 Classification of experimental designs (adapted from [165])

Optimization practices of chemometrics validate the optimal condition(s) or settings of a process. These approaches usually follow the use of a screening design or procedure that facilitates the selection of potential factors that may affect the outcomes of a process [165,166]. Response surface designs are of two types *viz.* symmetrical or asymmetrical designs. Three-level Full Factorial, Central Composite (CCD), Box-Behnken (BBD), Taguchi and Doehlert designs cover the symmetrical domain with use of a centre point to estimate experimental error. Asymmetrical designs include the D-optimal design that form an asymmetrical shape when an asymmetrical experimental domain is examined. Such designs can also form a symmetrical shape when used with a symmetrical domain. Mixed designs are applied to study a mixture of variables so as to optimize the composition of mixtures [165,166]. The productive application of experimental design in HPLC can be accomplished through application of four main stages, *viz.* selection of an appropriate design, use of appropriate software, experimental trials and finally undertaking data analysis including interpretation of the data [165].

In these studies, a CCD was used to identify the optimum conditions for the HPLC-ECD method of analysis for CLA. The CCD is a three-level full factorial design covering a

symmetrical domain with a centre point used to estimate experimental error [167]. A CCD may include a two-level full factorial design (2^f experiments), a star design ($2f$ experiments) and a centre point, requiring $N = 2^f + 2f + 1$ experiments to examine f factors [168,169]. The points of the full factorial design are located at factor levels -1 and +1 and for the star design at factor levels 0, $-\alpha$ and $+\alpha$, whereas for the centre point at a factor level 0 [170]. An in depth and more detailed literature review of the principles of HPLC as well as CCD and BBD response surfaces has previously been reported [171].

All experiments undertaken during optimization studies for CLA were performed in a randomized order to minimize bias of uncontrolled factors. A computer-generated rotatable CCD design consisting of 13 experiments with five (5) centre points and eight (8) axial points was generated using Design Expert® version 8.0.2 statistical software (Stat-Ease Inc., Minneapolis, MN, USA) which is summarized in Table 2.1. The experimental levels investigated and responses monitored are listed in Table 2.2. The minimum and maximum values for phosphate buffer molarity (X_1) were 10 mM and 50 mM, with the lower and upper axial points were set at 1.72 mM and 58.28 mM, respectively. Similarly, ACN concentration (X_2) was used at a minimum and maximum level of 40% *v/v* and 50% *v/v* of the mobile phase composition, with lower and upper axial levels of 37.9% *v/v* and 52.1% *v/v*, respectively. The independent input variables and ranges were selected following preliminary studies, and the retention time (Y_1) of the last peak eluted, peak asymmetry (Y_2) and peak resolution (Y_3) were the responses monitored. Data generated were analyzed using Design Expert® version 8.0.2 statistical software (Stat-Ease Inc., Minneapolis, MN, USA). The significance of relevant factors was determined using Fisher's statistical test for Analysis of Variance (ANOVA). Models were established and used to compare first-order interaction terms. ANOVA for linear regression, partitions the total variation of a sample into components that are used to compute an F-ratio which is interrogated to evaluate the effectiveness of the model. If the probability associated with the F-ratio is low, the model is considered to better fit the data from a statistical perspective. In these calculations, the higher-order interaction terms are assumed not to contribute to the behaviour of the statistical model to any great extent [61,165].

Table 2.1 Randomized coded experimental runs for method optimization using CCD

		Factor 1	Factor 2
Std	**Run**	**Buffer Molarity (X_1) mM**	**ACN (X_2) % v/v**
7	1	0	-1.414
11	2	0	0
1	3	-1	-1
12	4	0	0
9	5	0	0
10	6	0	0
13	7	0	0
6	8	1.414	0
4	9	1	1
5	10	-1.414	0
8	11	0	1.414
3	12	-1	1
2	13	1	-1

Table 2.2 Actual design values used CCD experiments

Variable	**Level**			
Input	**-α**	**-1**	**1**	**+α**
Mobile phase mM (X_1)	1.72	10	50	58.28
ACN content % v/v (X_2)	37.9	40	50	52.1
Output	**Constraints**			
Retention time	$Y_1 \leq 10$ minutes			
Peak asymmetry	Y_2 = minimize			
Peak resolution	Y_3 = maximize			

2.2.2 Literature Review and Preliminary Studies

Prior to developing a method for the analysis of CLA using DoE, preliminary studies were undertaken on the basis of published literature. A summary of methods using RP-HPLC with EC detection that have been published and used for the quantitative determination of CLA in pharmaceutical formulations and biological samples is listed in Table 2.3.

The data summarized in Table 2.3 reveals that the analysis of CLA in pharmaceutical dosage forms and biological fluids has been achieved using both coulometric and amperometric detection approaches. The methods make use of binary mobile phases consisting of

acetonitrile and phosphate buffer or ternary mobile phases in which methanol is used. It has been established that step-by-step optimization procedures for any reliable HPLC method requires good peak resolution with acceptable retention time(s), the absence of 'ghost' peaks and stable sensitivity with minimal peak tailing [172]. The initial aim of these studies was to screen for factors that would hinder the achievement of an appropriate chromatographic separation with the requisite performance, with the ultimate goal of developing a rapid, simple, selective and sensitive analytical method using a minimum number of experimental runs. The data in the published manuscripts were used to establish the preliminary RP-HPLC conditions for the development of an analytical method for the separation and accurate quantitation of CLA.

Table 2.3 Summary of published HPLC-ECD methods of analysis for CLA

Column	Mobile Phase	Flow Rate	Detector Settings	Retention Time	Reference
Spherisob® Nucleosil C_8,5 µm, 250x4.6 mm	acetonitrile-methanol-buffer (39:9:52, *v/v/v*), 0.04 M NaH_2PO_4 (pH = 6.8)	1.2 mL/min	Coulometric screening electrode +0.5 V working electrode +0.78 V	21.0 mins	[156]
YMC-Pack™ ODS-AP, 5 µm, 250x6.0 mm	acetonitrile and 0.05 *M* phosphate buffer (pH 7.2) (43:57, *v/v*)	1.7 mL/min	Amperometric +950 mV	13.3 mins	[149]
Zorbax® SB CN 5µm, 150x4.6 mm	50 mM sodium phosphate–acetonitrile–methanol (450:300:50, *v/v/v*), pH 7.5.	1.0 mL/min	Coulometric guard cell +1.0 V screening cell +0.50 V analytical cell +0.80 V	16.1 mins	[137]
Kromasil® ODS 5µm,4.6x75 mm	acetonitrile–aqueous phosphate buffer (pH 7.0, 0.086 M) (45:55 *v/v*)	1.0 mL/min	Coulometric guard cell +1.0 V screening cell +0.60 V analytical cell +0.85 V	5.9 mins	[159]
Phenomenex® Luna C_{18}, 5 µm,150x4 mm	acetonitrile–methanol–0.05 M potassium phosphate buffer (pH 7.0) (41:6:53, *v/v*)	0.8 mL/min	Amperometric +0.87 V	15.3 mins	[158]
Nucleosil® C_{18},5 µm, 150x4.6 mm	acetonitrile–acetate buffer (pH 6.6, 0.1 M) (40:60 *v/v*)	1.7 mL/min	Coulometric	7.0 mins	[173]
Spheri-5 cyano 5 µm, 100x4.6 mm	acetonitrile/methanol/0.0 4M phosphate buffer (pH 6.9) (52:9:39, *v/v/v*)	1.0 mL/min	Amperometric +1000 mV	9.2 mins	[174]
Symmetry® C_8 3.5 µm, 100x4.6 mm	acetonitrile and 0.045 M H_3PO_4 (37:63, *v/v*), pH 6.7	1.2 ml/min	Amperometric +0.85 V	12.26 mins	[150]
Hypersil™ BDS C_{18} 3 µm, 100 × 4.6 mm	Acetonitrile-0.025 M sodium phosphate buffer 54:46, *v/v*) pH 7.0	1.0 ml/min	Coulometric Upstream +0.65 V Downstream +0.85 V	-	[157]
MZ- C_8 125×4.0 mm	acetonitrile-methanol-potassium dihydrogen phosphate buffer (40:6:54, *v/v/v*), pH 7.5	1.5 ml/min	Amperometric +1.25 V 100 nA	-	[160]
Alltech® C_8, 3 µm;53x 7.0 mm	Acetonitrile-methanol-acetate buffer (50:10:40), pH 7.5.	1.3 ml/min	Coulometric guard cell +850 mV screening cell +500 mV analytical cell +780 mV	-	[151]

2.2.2.1 Column Selection

During the development of the analytical method, a Phenomenex® Luna C_{18} 150 mm x 2 mm, i.d 5 µm column, and a Beckman® Ultrashere C_8 150 mm x 4.0 mm, i.d 4 µm column were tested. In all instances, columns were equilibrated for approximately 60 minutes with a mobile phase containing acetonitrile and a 50 mM phosphate buffer (pH 7.00) in a 45:55 *v/v* ratio delivered at a flow rate of 1.0 mL/min. Column efficiency was quantitatively determined using Equations 2.2 and 2.3.

$$N=16\left(\frac{t_r}{w_b}\right)^2 \qquad \textbf{Equation 2.2}$$

$$N=5.54\left(\frac{t_r}{w_{1/2}}\right)^2 \qquad \textbf{Equation 2.3}$$

Where,
N = number of theoretical plates of a column
t_r = the retention time of the probe molecule
w_b = the width of the peak at the baseline
$w_{½}$ = the width of the peak at one half the maximum height

The theoretical plate number is dependent on elution time and should generally be > 2000 [175]. The Phenomenex® column produced a plate count number of approximately 2500 while the plate number for the Beckman® column was approximately 4500. In addition, the Beckman® column produced a better peak shape on inspection than the Phenomenex® column. Decreasing the particle size while keeping the column length constant, increases column efficiency and peak resolution [132]. Although C_{18} and C_8 columns have similar selectivity, C_8 columns are much less likely to retain compounds due to the presence of shorter alkyl chains, resulting in improved peak shape [132] as observed with the Beckman® column. The Beckman® column was therefore selected as the initial column of choice for the analysis of CLA.

2.2.2.2 Internal standard selection

Internal standard use in analytical methods is common for analysis of drugs in biological and physiological fluids or complex samples that would require compensation for any potential loss during sample preparation [132]. The addition of a known compound of fixed concentration allows for compensation of the effect(s) of minor variations in responses and

separation parameters on peak size, including sample size fluctuations. The internal standard (IS) should ideally have a similar structure to the analyte(s) of interest and should be completely resolved from the analytes to avoid interference [123,132,176].

The selection of an IS was based on evaluating structurally similar molecules to CLA in addition to known compounds that possess oxidizable moieties. Consequently, the macrolide antibiotics erythromycin (ERY), josamycin base and josamycin proprionate were tested. In addition, ketoconazole, labetalol, efavirenz and caffeine were also evaluated as potential candidates using the preliminary mobile phase described in § 2.2.2.1. The results are summarized in Table 2.4, and reveal that ERY is an ideal IS for this separation.

Table 2.4 Internal standard selection

Internal Standard	Retention Time(mins)	Comments
CLA	8.3	
Erythromycin	4.2	Ideal to be IS
Ketoconazole	-	No elution within 10 mins
Labetalol	2.64	Too close to solvent front
Efavirenz	-	No elution within 10 mins
Caffeine	-	No elution within 10 mins
Josamycin base	-	No elution within 10 mins
Josamycin proprionate	-	No elution within 10 mins

2.2.2.3 Hydrodynamic Voltammetric studies

Hydrodynamic voltammetry (HDV) is a steady state technique in which the electrode potential of the system is altered prior to the injection of an analyte and following injection, the resultant current observed is plotted as a function of the applied potential [61]. Detection limits are therefore resolved by optimizing the working potential using a current-potential curve or voltammogram. Establishing the correct working potential is necessary to optimize the signal produced during electrolysis of samples whilst minimizing the noise due to electrolysis of the solvent and contaminants in the sample. HDV studies were undertaken to identify the optimum working electrode potential for the analysis of CLA. The HDV of CLA and ERY generated in direct current (DC) mode at applied potential settings between +900 mV and +1300 mV at a scan background current of 100 nA are depicted in Figure 2.3.

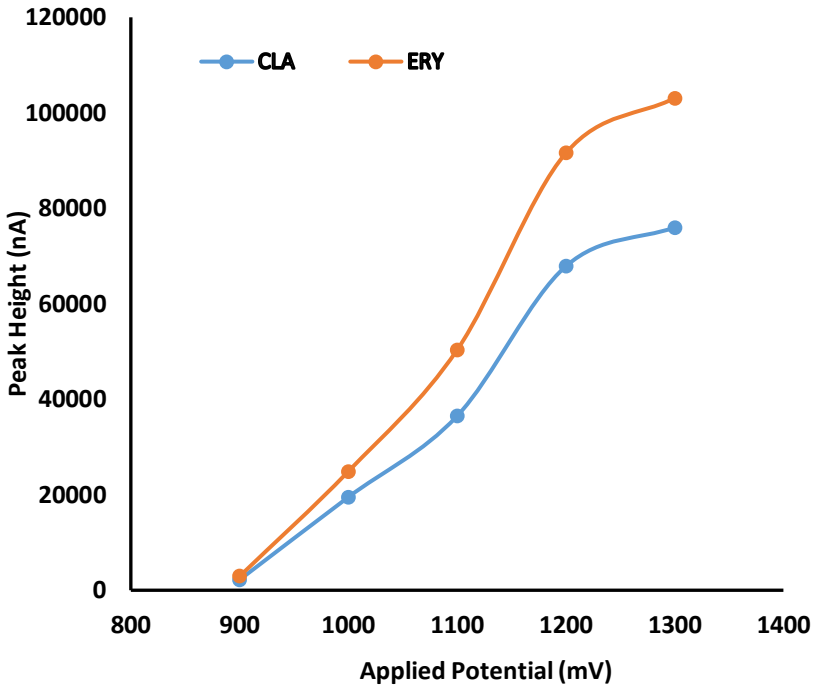

Figure 2.3 Hydrodynamic voltammogram (HDV) for CLA and erythromycin (ERY) generated in direct current (DC) mode at a sensitivity of 100 nA

These data reveal that a limiting current plateau commences at a potential of +1200 mV for both CLA and ERY. The response of both macrolides was sigmoidal and can be explained mathematically as a logistic function voltammogram [146]. The background current that exhibited the best signal to noise ratio compromise occurred at 100 nA and was selected for use.

Preliminary screening chromatographic experiments were performed to identify potential factors for the optimization studies. The inclusion of methanol (MeOH) in the mobile phase improved the chromatographic behaviour of CLA and ERY and influenced the detector signal positively. However, the use of MeOH resulted in a longer retention time due to low solvent strength established using the Hildebrand's elution strength scale for reversed-phase liquid chromatography [132]. Consequently, MeOH content was limited to and maintained at 5% *v/v* of the organic phase composition for the optimization studies. An increase in column temperature resulted in longer retention times and an increase in baseline noise, possibly due to an increase in the oxidation of mobile phase impurities at these higher temperatures. However, the drift in baseline was reduced at temperatures above ambient (22 °C) conditions. Consequently, a temperature of 30 °C was selected as a compromise and used for the optimization studies. Buffer pH was maintained at 7.00 since ERY is stable between pH 7.00

and 8.00 [137,177,178] and the life of silica-based stationary phases is significantly reduced when used under alkaline conditions [179].

2.2.3 Experimental

2.2.3.1 Chemicals and Reagents

All reagents were at least of analytical reagent grade and used without further purification. CLA was purchased from Skyrun Industrial Co. Limited (Taizhou, China) and ERY was purchased from Sigma Aldrich Chemical Co. (Milwaukee, WI, USA). HPLC-grade water was prepared by reverse osmosis using a RephiLe® Direct-Pure UP ultrapure and RO water system (Microsep®, Johannesburg, South Africa), consisting of a deionization RephiDuO® H PAK cartridge and a polishing RephiDuO® PAK cartridge. The water was filtered through a 0.22 µm PES high-flux capsule filter (Microsep®, Johannesburg, South Africa) and used to prepare all buffer solutions. Honeywell Burdick and Jackson HPLC far UV-grade acetonitrile (ACN) and methanol (MeOH) was purchased from Anatech® Instruments Pty, Ltd. (Randburg, Johannesburg, South Africa). Potassium dihydrogen orthophosphate, sodium chloride and sodium hydroxide pellets were purchased from Merck® Laboratories (Merck®, Wadeville, South Africa).

2.2.3.2 Instrumentation and Analytical Conditions

The HPLC system was a Waters® Alliance Model 2695 separation module equipped with a solvent delivery module, an autosampler, an online degasser and a Model 2465 Electrochemical Detector (Waters®, Milford, MA, USA). Data acquisition, processing and reporting were achieved using Waters® Empower 3 software (Waters®, Milford, MA, USA). The separation was achieved under isocratic conditions using a Beckman® C_8 150 × 4.0 mm i.d 4 µm (Beckman Instruments, Inc., San Ramon, CA, USA) cartridge column with a mobile phase consisting of 50 mM phosphate buffer (pH 7.00), ACN and MeOH in a 58.5:36.5:5.0 *v/v/v* ratio. The flow rate of the mobile phase and the injection volume were 1.0 mL/min and 10 µL, respectively. The analytical column was maintained at 30 °C using an integral column heater (Waters®, Milford, MA, USA).

2.2.3.3 Preparation of Stock Solutions and Calibration Standards

Standard stock solutions of CLA (100 µg/mL) and ERY (50 µg/mL) were prepared by accurately weighing approximately 10 mg and 5 mg of each API using a Model AE 163 Mettler® analytical balance (Mettler® Inc., Zurich, Switzerland) directly into 100 mL A-grade volumetric flasks and dissolving in a small volume of ACN. The stock solutions were sonicated using an ultrasonic bath (Ultrasonic Manufacturing Company (Pty), Ltd., Kenware, Krugersdorp, South Africa) until a clear solution formed, after which the solutions were made up to volume with ACN. Calibration standards of CLA over the concentration range 5–50 µg/mL specifically 5, 8, 10, 12, 20, 30 and 50 µg/mL were prepared by serial dilution of the standard stock solution on the day of analysis, using ACN as a diluent. A 0.75 mL aliquot of the 50 µg/mL ERY stock solution was added to all calibration standards and test samples prior to analysis.

2.2.3.4 Preparation of Buffer and Mobile Phase

Phosphate buffer solutions (50 mM) were prepared by accurately weighing 6.0845 g potassium dihydrogen orthophosphate and quantitatively transferring into a 1 L A-grade volumetric flask and making up to volume with HPLC grade water. A 0.11 g aliquot of sodium chloride was added to the buffer solution to produce a final concentration equivalent to 2 mM chloride ions. The pH of the buffers was monitored at 22 °C using a Model Basic 20+ Crison pH-meter (Crison Instruments, Barcelona, Spain) and was adjusted to 7.00 using sodium hydroxide pellets. The buffer was degassed under vacuum with the aid of a Model A-2S Eyela Aspirator degasser (Rikakikai Co., Ltd., Tokyo, Japan) and filtered through a 0.22 µm cellulose membrane filter (Sartorius Stedim Biotech GmbH, Goettingen, Germany) prior to being transferred into a 1 L Schott® Duran bottle (Schott Duran GmbH, Wertheim, Germany).

2.3 RESULTS AND DISCUSSION

Following application of DoE using CCD for the optimization of chromatographic conditions for CLA, the overall design summary consisted of three quadratic mathematical models for two independent factors. Optimization of significant model variables was undertaken to identify the best combination of factors that would yield the desired responses to effect an optimized separation.

2.3.1 Retention Time

The retention time (Y_1) is the most critical response as it has an effect on the length of the analytical run and cost of using an analytical method routinely. ACN concentration and buffer molarity were found to be statistically significant factors that affected retention time (Table 2.5). The influence of ACN concentration and buffer molarity on retention time is depicted graphically in the contour plot in Figure 2.4.

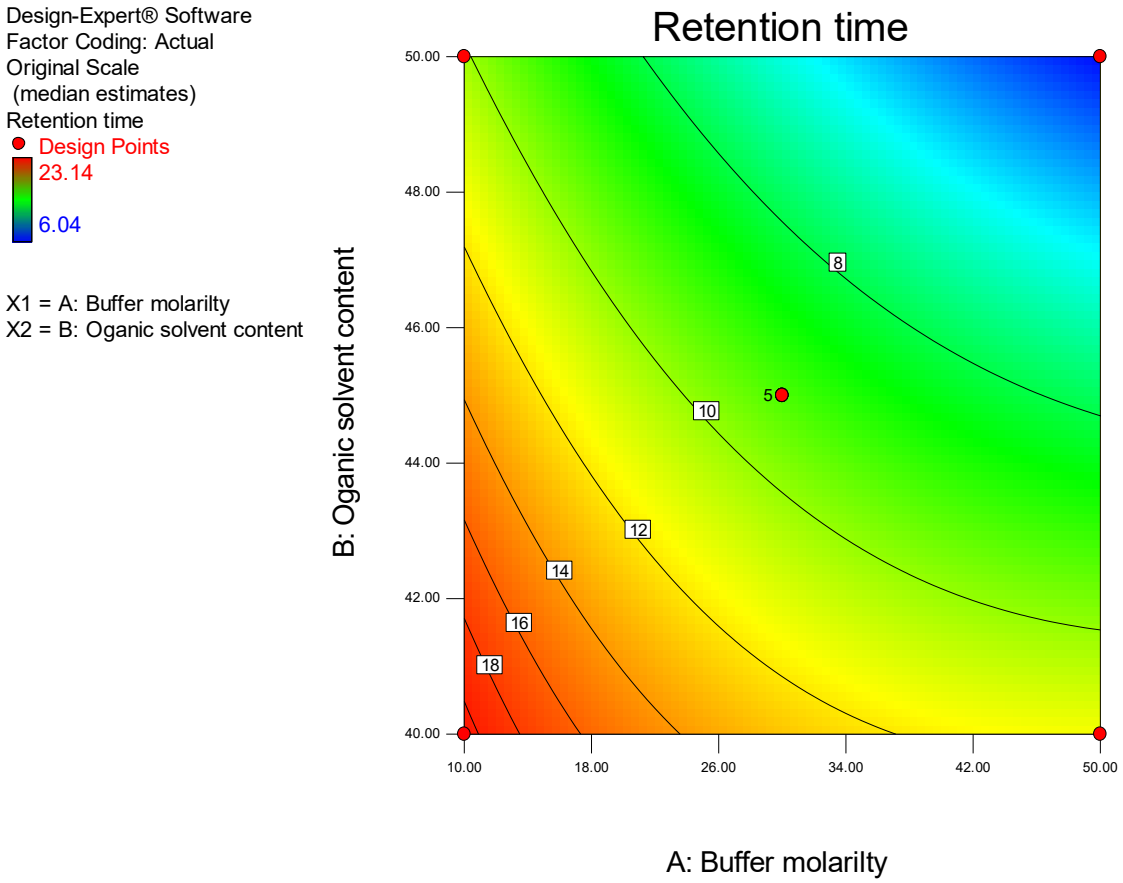

Figure 2.4 Contour plot depicting the impact of ACN content and buffer molarity on retention time

These data reveal that a decrease in retention time of CLA occurs when the ACN content is increased from 40–50% *v/v* and the buffer molarity is increased from 10–50 mM. ACN is a strong solvent according to Hildebrand's elution strength scale, thereby reducing mobile phase polarity when ACN concentrations are increased [132], leading to preferential partitioning of CLA into the mobile phase resulting in rapid elution and shorter retention times. The decrease in retention time observed with increased buffer molarity can be

attributed to increased competition of buffer cations for active silanol sites within the stationary phase, leading to preferential partitioning of CLA into the mobile phase [146].

Examination of the model Box-Cox plot (Figure 2.5) inferred the need to transform the model. The plot reveals that the blue line falls outside the 95% confidence interval, indicating that the model was not located in the optimum region of the parabola. Consequently, a power transformation of the model was undertaken using model reduction by backward elimination in order to improve the fit of the data to the model, thereby permitting navigation of the design space [144].

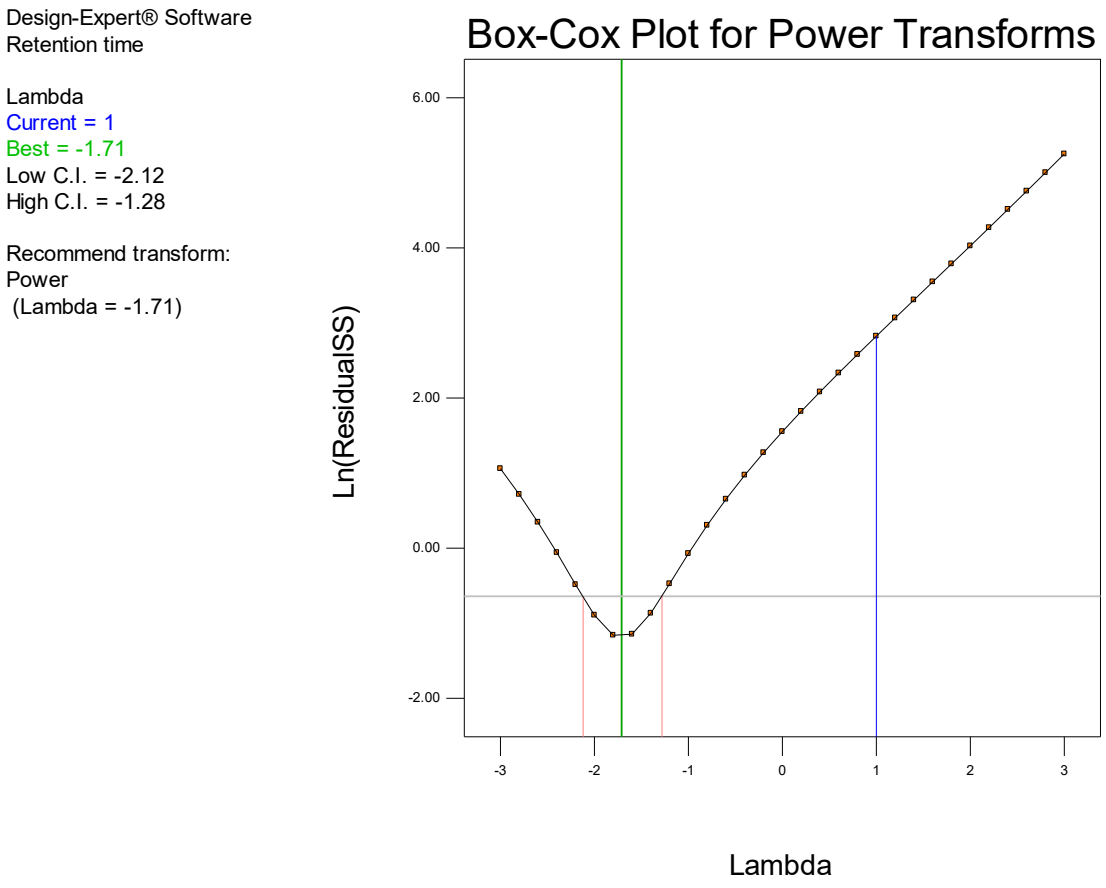

Figure 2.5 Box-Cox plot for power transformation for retention time prior to transformation

The Box-Cox plot (Figure 2.6) generated following power transformation of the data using backward elimination reveals the blue line falls within the confidence interval, confirming that the data falls in the optimum region of the parabola thereby indicating model adequacy had been achieved.

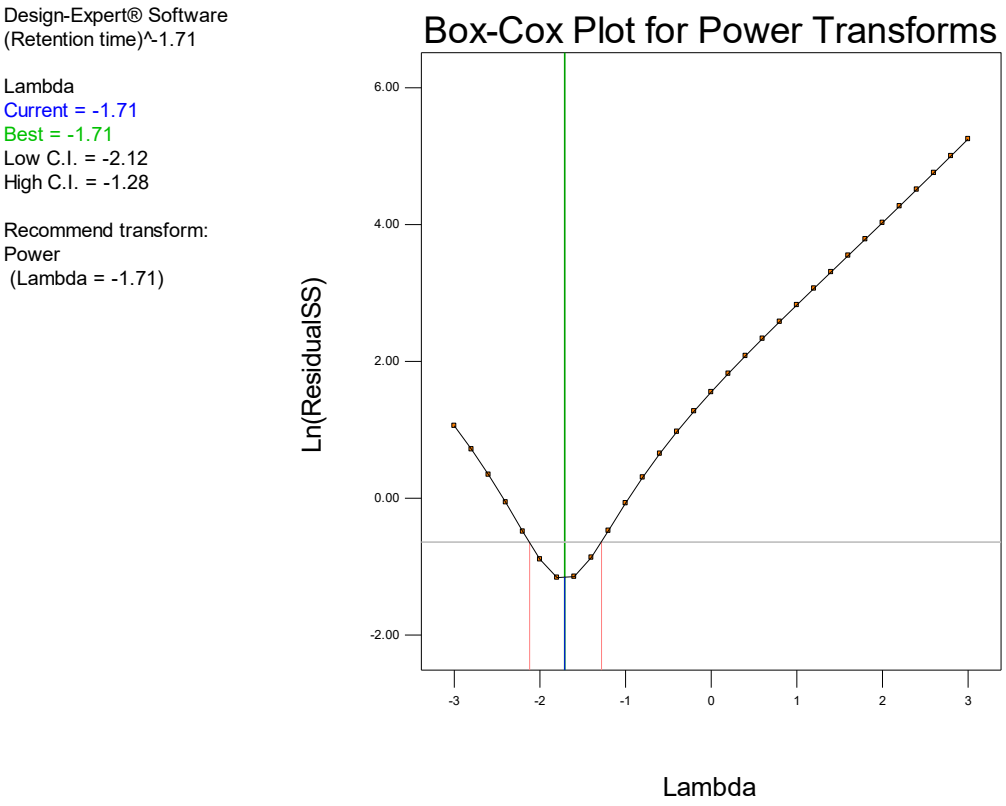

Figure 2.6 Box-Cox plot for power transformation for retention time following transformation

ANOVA was used to evaluate the quadratic model for retention time and Fisher's F-ratio was calculated to identify significant terms in the model, with the error term set at $p = 0.05$. Values of Prob > F < 0.0500 indicate model terms that are significant however, values > 0.1000 indicate that the model terms are not significant. The overall contribution of model factors to retention time were statistically significant and are summarized in Table 2.5.

Table 2.5 ANOVA table for response surface quadratic model for retention time

Source	Sum of Squares	df	Mean Square	F Value	p-value Prob>F	
Model	1.78×10^{-3}	5	3.56×10^{-4}	902.59	< 0.0001	significant
A-Buffer molarity	6.78×10^{-4}	1	6.78×10^{-4}	1719.85	< 0.0001	
B-Organic solvent	9.75×10^{-4}	1	9.75×10^{-4}	2472.06	< 0.0001	
AB	7.22×10^{-5}	1	7.22×10^{-5}	183.05	< 0.0001	
A^2	3.68×10^{-5}	1	3.68×10^{-5}	93.42	< 0.0001	
B^2	1.13×10^{-5}	1	1.13×10^{-5}	28.74	0.0011	
Residual	2.76×10^{-6}	7	3.94×10^{-7}			
Lack of Fit	2.70×10^{-6}	3	9.00×10^{-7}	57.93	0.0009	significant
Pure Error	6.21×10^{-8}	4	1.55×10^{-8}			
Cor Total	1.78×10^{-3}	12				
Std. Dev.	6.28×10^{-4}					
Mean	0.022					
C.V. %	2.86					
PRESS	1.93×10^{-5}					
R-Squared	0.9985					
Adj R-Squared	0.9973					
Pred R-Squared	0.9892					
Adeq Precision	96.322					

The Model F-value of 902.59 implies the model is significant and there is only a 0.01% chance that a Model F-value this large could occur due to noise. The Pred R-Squared of 0.9892 is in reasonable agreement with the Adj R-Squared of 0.9973. Adeq Precision measures the signal to noise ratio. A ratio > 4 is desirable and the ratio of 96.322 indicates an adequate signal. This model can thus be used to navigate the design space and, therefore, the method developed was able to be applied to predict the retention time of CLA within the limits of the identified design space. The equation for retention time (Y_1) is reported in Equation 2.4.

$$Y_1^{-1.71} = +0.023 + 9.208E-003A + 0.011B + 4.248E-003AB - 2.301E-003A^2 + 1.276E-003B^2 \quad \textbf{Equation 2.4}$$

2.3.2 Peak Symmetry

The asymmetry factor was used to evaluate the peak symmetry (Y_2) response. Excellent chromatographic columns have been reported to produce asymmetry factor values of between 0.95 and 1.1 [180]. Due to the molecular mass and the basic nature of CLA, interaction with silica-based reversed-phase columns results in marked tailing of peaks due to interaction with residual silanols of the stationary phase [181] causing poor peak symmetry.

ANOVA analysis reveals that the model for peak symmetry was significant (p = 0.0149) and the significant model term identified was ACN content (p = 0.0011) as summarized in Table 2.6. The influence of ACN concentration on CLA peak symmetry is depicted graphically in the contour plot in Figure 2.7.

Table 2.6 ANOVA table for response surface quadratic model for peak symmetry

Source	Sum of Squares	df	Mean Square	F Value	p-value Prob>F	
Model	3.80×10^{-3}	5	7.60×10^{-4}	6.45	0.0149	significant
A-Buffer molarity	2.46×10^{-4}	1	2.46×10^{-4}	2.09	0.1918	
B-Organic solvent	1.88×10^{-4}	1	1.88×10^{-4}	1.59	0.2472	
AB	5.45×10^{-5}	1	5.45×10^{-5}	0.46	0.5185	
A^2	5.35×10^{-5}	1	5.35×10^{-5}	0.45	0.5222	
B^2	3.31×10^{-3}	1	3.31×10^{-3}	28.08	0.0011	
Residual	8.25×10^{-4}	7	1.18×10^{-4}			
Lack of Fit	4.96×10^{-4}	3	1.65×10^{-4}	2.01	0.2553	not significant
Pure Error	3.29×10^{-4}	4	8.23×10^{-5}			
Cor Total	4.62×10^{-3}	12				
Std. Dev.	0.011					
Mean	0.12					
C.V. %	9.41					
PRESS	4.04×10^{-3}					
R-Squared	0.8215					
Adj R-Squared	0.6941					
Pred R-Squared	0.1261					
Adeq Precision	7.155					

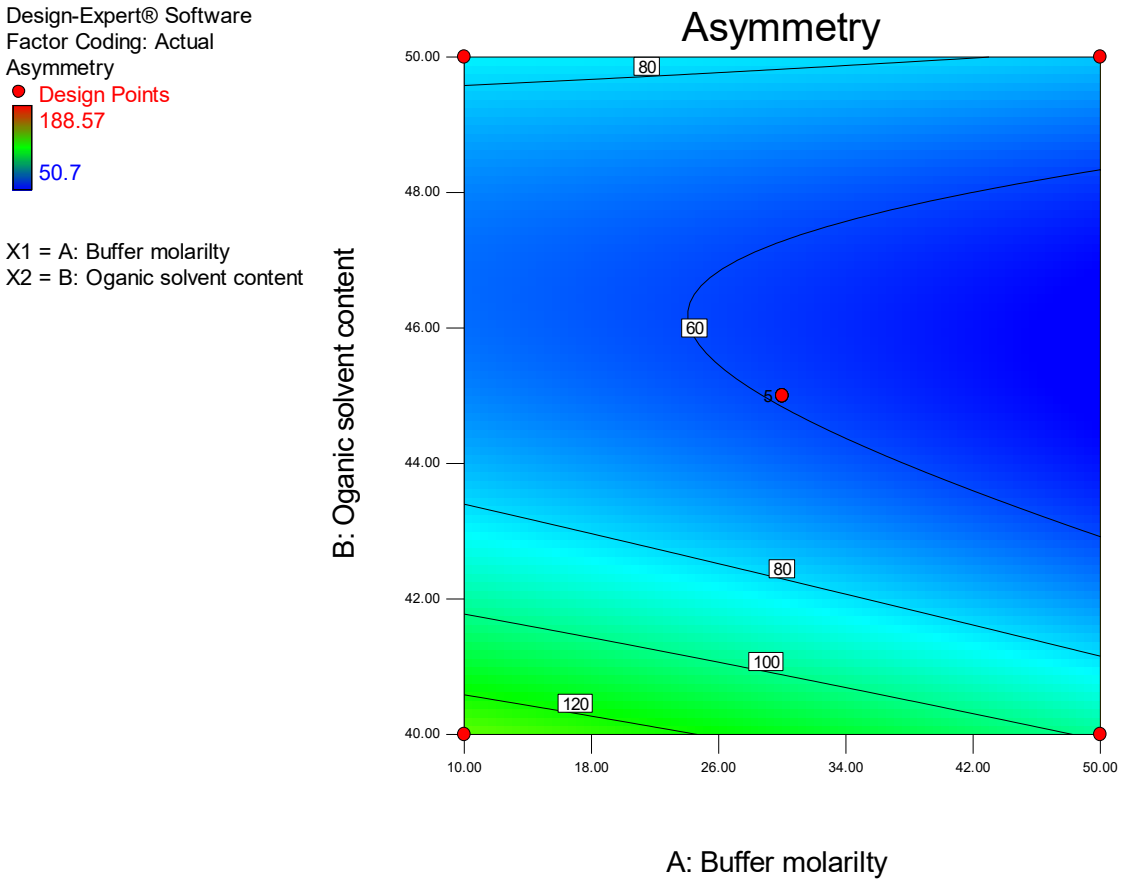

Figure 2.7 Contour plot depicting the impact of ACN content and buffer molarity on peak asymmetry

The significance of the model is implied by the F-value of 6.45. The Pred R-Squared of 0.1261 is not as close to the Adj R-Squared of 0.6941 as one might expect which may indicate a large block effect or a possible problem with the model used and/or data. In order to evaluate further, model reduction, response transformation and/or outlier analysis can be considered. However, the term Adeq Precision measures the signal to noise ratio and ratios > 4 are desirable. The ratio of 7.155 indicates an adequate signal was achieved. This model can therefore be used to navigate the design space and was therefore applied to predict the asymmetry of the CLA peak. The best peak shape with minimal tailing can be obtained at an ACN concentration of approximately 46% *v/v*. Due to peak tailing, the experimental run time was increased to 20 mins to ensure that the chromatographic signal returned to baseline. The equation for peak symmetry (Y_2) is reported in Equation 2.5.

$$1/\text{Sqrt (Asymmetry)} = + 0.13 + 5.545E - 003A + 4.846E - 003B - 3.690E - 003AB - 2.773E - 003A^2 - 0.022B^2 \quad \textbf{Equation 2.5}$$

2.3.3 Peak Resolution

The goal of this HPLC separation as with other analyses was to separate CLA from all other components that may be present in a sample. Resolution is a measure of the degree of separation of two analytes [132]. Ideally, most HPLC methods should achieve a baseline separation with resolution values of between 1.5 and 2.0 for all analytes of interest [123].

ANOVA analysis reveals that the model for peak resolution was significant ($p < 0.0001$) and the significant model terms were buffer molarity and ACN content with p values of 0.0028 and <0.0001, respectively as summarized in Table 2.7. The two-dimensional contour plot showing the influence of the two factors on peak resolution is depicted in Figure 2.8.

Table 2.7 ANOVA table for response surface quadratic model for peak resolution

Source	Sum of Squares	df	Mean Square	F Value	p-value Prob>F	
Model	4.70×10^{-1}	5	9.30×10^{-2}	34.01	< 0.0001	significant
A-Buffer molarity	5.60×10^{-2}	1	5.60×10^{-2}	20.28	0.0028	
B-Organic solvent	2.80×10^{-1}	1	2.80×10^{-1}	102.2	< 0.0001	
AB	1.60×10^{-3}	1	1.60×10^{-3}	0.58	0.4703	
A^2	2.90×10^{-2}	1	2.90×10^{-2}	10.45	0.0144	
B^2	8.50×10^{-2}	1	8.50×10^{-2}	31.05	0.0008	
Residual	1.90×10^{-2}	7	2.75×10^{-3}			
Lack of Fit	3.11×10^{-3}	3	1.04×10^{-3}	0.26	0.8529	not significant
Pure Error	1.60×10^{-2}	4	4.03×10^{-3}			
Cor Total	4.90×10^{-1}	12				
Std. Dev.	0.052					
Mean	2.39					
C.V. %	2.19					
PRESS	4.70×10^{-2}					
R-Squared	0.9605					
Adj R-Squared	0.9322					
Pred R-Squared	0.9027					
Adeq Precision	20.583					

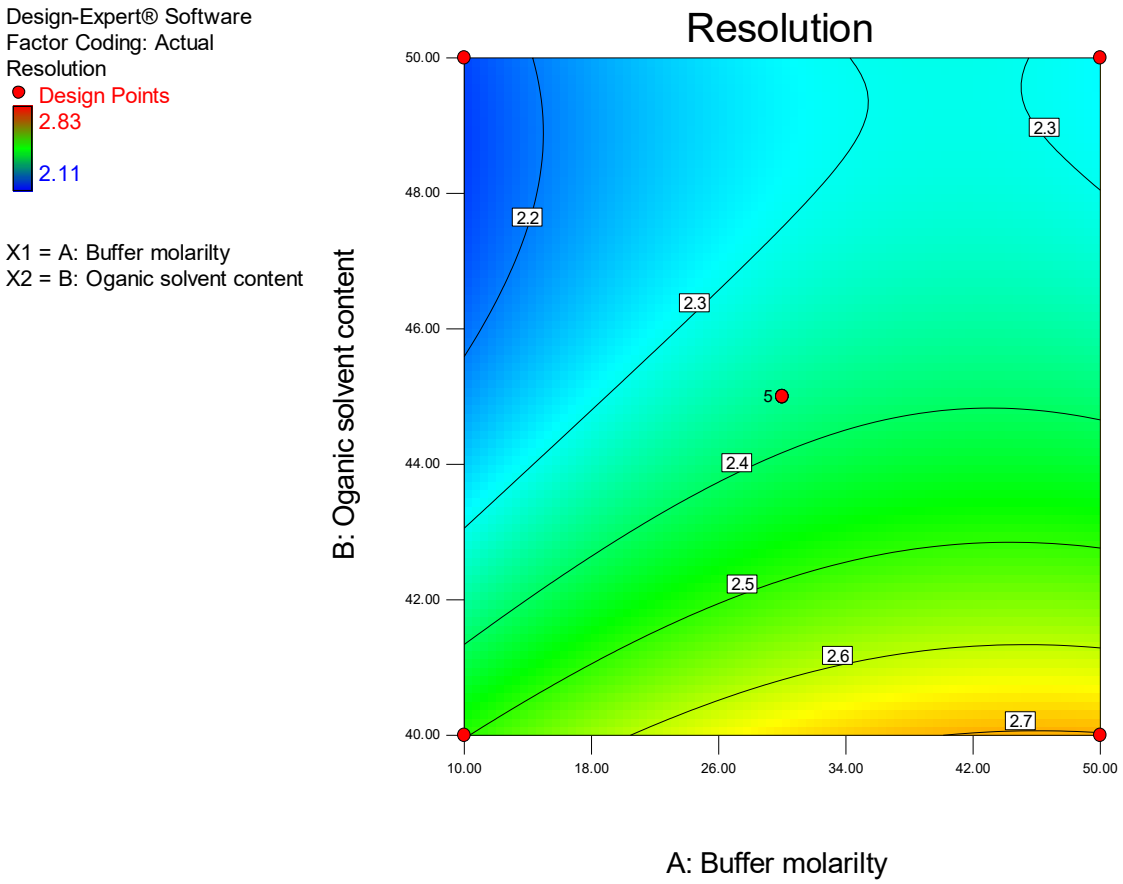

Figure 2.8 Contour plot depicting the impact of ACN content and buffer molarity on peak resolution

The Model F-value of 34.01 implies the model is significant. The Pred R-Squared of 0.9027 is in reasonable agreement with the Adj R-Squared of 0.9322. The Adeq Precision ratio of 20.583 is > 4, indicating an adequate signal therefore the model was used to navigate the design space and applied to predict the resolution factor between CLA and ERY. ACN content and buffer molarity can be manipulated to improve peak resolution. The contour plot suggests that increased peak resolution will be observed when a buffer molarity of 50 mM and ACN content of approximately 40% *v/v* is used. The equation for peak resolution (Y_3) is reported in Equation 2.6.

$$\text{Resolution} = +2.37 + 0.083A - 0.19B - 0.020AB - 0.064A^2 + 0.11B^2 \qquad \textbf{Equation 2.6}$$

2.3.4 Optimized Chromatographic Conditions

The overall solutions for chromatographic analysis of CLA and ERY were identified by optimization of the quadratic models using Design Expert statistical software Version 8.0.2 Design Expert® statistical software (Stat-Ease Inc., Minneapolis, MN, USA). A series of compromises is required when evaluating outputs from Design Expert®. For example, for a

retention time of ≤ 10 minutes, minimum peak asymmetry and maximum resolution between CLA and ERY, the impact of MeOH content was largely avoided by using a constant mobile phase content of 5.0% *v/v* which ensured the benefits of using this solvent were achieved without a major impact on the separation. Elegant multi-criteria statistical solutions are possible however, they should only be considered when this pragmatic approach to optimization is not adequate. Solutions to quadratic models have been generated by matrix calculation using Cramer's rule, Eigen values and Eigen functions, for the optimized conditions of chromatography for captopril [146] but were not considered necessary for this separation. The optimized conditions for the overall separation are summarized in Table 2.8.

Table 2.8 Optimized chromatographic conditions for the overall separation of CLA and ERY

Parameter	Results
Buffer molarity	50 mM
Organic phase content	41.5% *v/v*
Flow rate	1.00 mL/min
Column temperature	30 °C
Mode	Isocratic
Detection voltage	+1200 mV
Injection volume	10 µL

The optimized chromatographic separation was applied to the quantitative analysis of CLA and the final separation produced well resolved peaks for CLA and ERY as depicted in Figure 2.9. The % prediction error for retention time of CLA using the optimized conditions in relation to the predicted retention time was −6.19%. The % prediction errors for resolution and asymmetry were −2.38% and −10.13%, respectively. The low values for the calculated percentage prediction errors indicate the robustness of the mathematical models used. In addition, the high predictive ability of DoE is also demonstrated, suggesting the efficiency of DoE, for process optimization [182].

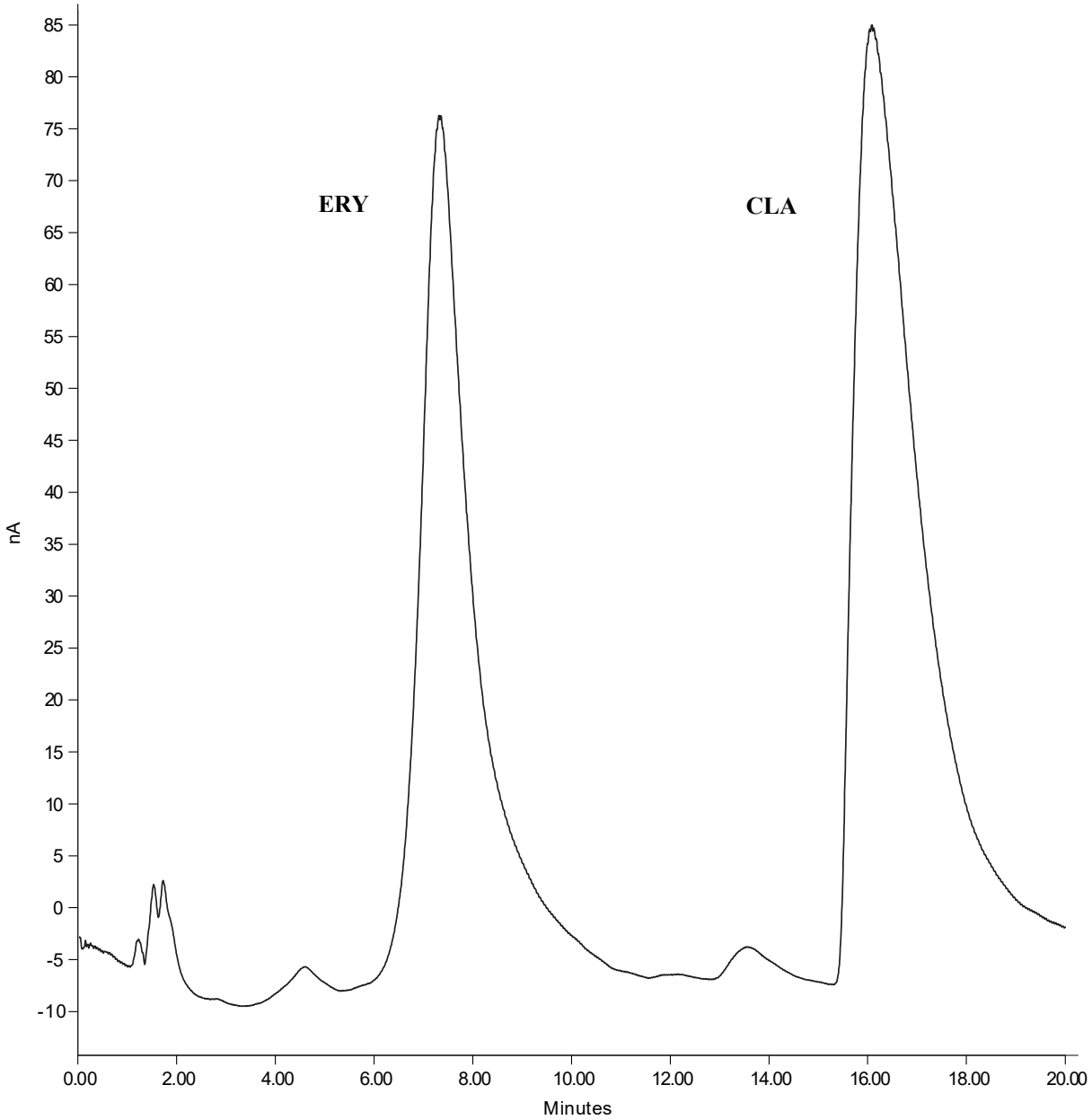

Figure 2.9 Typical chromatograms depicting the separation of CLA (45 µg/mL) and ERY (50 µg/mL) obtained using the optimized chromatographic conditions

2.4 CONCLUSIONS

Ultraviolet and visible (UV/Vis) spectroscopic modes of detection have withstood the test of time as the mainstay for sample analysis in the pharmaceutical laboratory since these detectors are inexpensive, easy to use, and are more widely distributed than other detectors. However, in many instances, largely when the analytes of interest do not possess a strong UV/Vis chromophore, alternate modes of detection are essential.

CLA is a molecule that lacks a suitable chromophore and exhibits weak UV absorbance in the low wavelength range < 220 nm making it difficult to develop specific, selective and sensitive UV/Vis methods for the compound due to substantial UV absorption in this region, particularly when analysing complex matrices such as biological fluids [153,183] and low analyte concentrations in formulations such as those used to produce nanoparticles. Chemical derivatization has been shown to increase sensitivity of detection and improve selectivity by means of pre-column or post-column HPLC [184,185].

Quantitation of CLA using pre-column derivatization with UV/Vis detection methods has been achieved at sensitivities of 0.1 µg/mL [153], 0.025 µg/mL [183] in biological matrices including 0.034 µg/mL [186] in pharmaceutical dosage forms. However, pre-column derivatization methods possess several disadvantages in comparison to EC detection methods of detection. These disadvantages include the use of complex analytical systems and equipment such as fluorescence detectors, tedious preparatory requirements to produce reaction products, toxicology concerns relating to the derivatizing agents and/or the reaction conditions. In addition, there exists a possibility of chromatographic interference if excess reagent is present in addition to artefact formation that may well reduce the selectivity of the separation [61,186].

The use of HPLC-ECD requires simple sample pre-treatment prior to immediate analysis and offers remarkable sensitivity, is independent of optical path length effects and is not compromised by miniaturization. Furthermore, the associated instrumentation is relatively inexpensive and simple compared to some optical or mass spectrometric detectors.

The application of DoE in combination with CCD to the development and optimization of the performance of an HPLC-ECD method has been discussed. CCD was used to design an experimental program for modelling the effects of mobile phase molarity and concentration of organic solvent on the retention time, peak asymmetry and resolution of CLA. Thirteen experiments including centre points were conducted. Equations for the mathematical model were derived for the response factors by using the experimental data and the statistical software package Design Expert 8.0.2.

The results of statistical analysis for the model reveal that it can be adequately used to navigate the design space. Contour plots were used to explain the interactive effects of factors on the responses. Statistical analysis of the models revealed that both buffer molarity and ACN concentration had a significant effect on the retention time of CLA. Furthermore, the responses observed for the method were closely related to the predicted values generated using the optimized method. The analytical method was developed and optimized using a small number of experimental runs further echoing that DoE is an important and efficient tool for extracting the maximum amount of information in a short period of time therefore minimizing the wastage of materials and personnel time.

An investigation into validation of the analytical method will be conducted using the optimized mobile phase conditions suggested by the model with an organic phase content of 36.5 % *v/v* ACN and 5 % *v/v* MeOH, a 50 mM (58.5% *v/v*) buffer at pH = 7.00 at a flow rate of 1.0 ml/min. Detector conditions will be maintained at a voltage of + 1200 mV, a background current of 100 nA and the integral column temperature at 30 °C.

CHAPTER 3

VALIDATION AND SCALING OF A STABILITY-INDICATING HPLC-ECD METHOD FOR THE QUANTITATION OF CLARITHROMYCIN

3.1 INTRODUCTION

Due to high accuracy and precision, HPLC is the analytical tool of choice in the pharmaceutical, food product and other industries for which sample analyses are conducted under regulatory constraints to ensure the health and safety of the general public. Validation of an analytical method is therefore of utmost importance and is a process that demonstrates the ultimate success of a method in meeting or exceeding the minimum standards recommended by relevant regulatory authorities, specifically for accuracy, precision, linearity and range, selectivity, sensitivity, reproducibility, robustness and stability [132,187,188]. However, method robustness is rarely reported in manuscripts reported in literature [188] Despite regulatory authorities requiring validation for all analytical methods, the actual implementation thereof, is to some extent open to interpretation and might significantly differ between organizations. The analytical method developed and used in these studies was validated in terms of accuracy, precision, robustness, specificity, detection limit, quantitation limit, linearity and range as per the International Conference of Harmonization (ICH) guidelines [189].

As of 2017, the United States Pharmacopeia (USP) proposed the use of USP <621> guidelines for this purpose [36]. In these guidelines, the USP suggests the possibility of scaling an analytical method without the need for method re-validation provided certain parameters are considered and constraints are met. Method scaling entails adjustment of a method, where certain parameters are changed within allowable limits so as to preserve the integrity of the chromatographic separation. Specific parameters that may need adjustment during scaling of methods include alteration of the dimensions of an analytical column, specifically the particle size and column length. In addition, when changes are made to the analytical column, method flow rates may also require adjustment so as to maintain and

ensure that the original chromatographic performance is achieved [36]. Chapter <621> in the USP [36] defines the method adjustments that are permitted in order to scale that method without the need for re-validation. These adjustments are permissible provided system suitability requirements, as described in the relevant monograph for the method, are met when the changes to the method are implemented [36,190]. The permitted adjustments are summarized in Table 3.1.

Table 3.1 USP <621> guidelines for method scaling

Variable	HPLC method	
	Isocratic	**Gradient**
Stationary phase	No change of the physio-chemical characteristics of the stationary phase (same L designation)	
Particle size/column length	*Constant L/dp or -25% to +50%	No changes permitted
Flow rate	Based on particle size and ± 50%	No changes permitted
Injection volume	Flexible	
Column temperature	±10 °C	
Mobile phase pH	±2 pH units	
Concentration of buffer salts	±10%	
Detector wavelength	No adjustment permitted	

*ratio of the column length (L) to the particle size (dp) or L/dp remains constant or within the limits of -25% to +50%

When the particle size is changed, the flow rate may require adjustment and the new flow rate can be calculated using Equation 3.1. In addition, the USP [36] also specifies and explains permitted adjustments to the changes of ratio of the components in the mobile phase.

$$F_2 = F_1 \times [(dc_2^2 \times dp_1)/(dc_1^2 \times dp_2)] \qquad \textbf{Equation 3.1}$$

Where,
F_1 and F_2 = flow rates used for the original and modified conditions
dc_1 and dc_2 = the respective column diameters
dp_1 and dp_2 = particle sizes of the stationary phases

Forced degradation studies of new API and drug products are conducted as a requirement to demonstrate specificity for stability indicating methods in addition to providing insight into the degradation pathways and formation of the degradation products of a substance. These studies are performed under more rigorous conditions than those used for accelerated stability testing (40 °C/75% RH). Structural elucidation of degradation products is also possible through these studies. Ultimately, forced degradation studies provide an indication of the

chemical behaviour of the molecule in question, which in turn aids further development of the formulation(s) and relevant packaging requirements [191].

An HPLC method with EC detection developed for the quantitative determination of CLA in pharmaceutical formulations and monitoring the incorporation of CLA into lipid nano-carrier technologies was validated in accordance to ICH guidelines [189]. Method re-validation in addition to modified method scaling was conducted per the USP [36] in order to assess and assure the performance of the method when changing analytical columns to that of a different L-designation. The method was also evaluated for specificity by conducting forced degradation studies in addition to assaying commercially available dosage forms.

3.2 METHOD VALIDATION

Prior to validation of the analytical method, an attempt was made to improve peak shape and detector sensitivity by investigating the impact of methanol (MeOH) as a component of the mobile phase. The inclusion of MeOH in the mobile phase exhibited a positive effect on peak shape and other chromatographic responses during method development. MeOH inclusion in the mobile phase was investigated over the 2 to 10% *v/v* range and well resolved chromatographic responses were achieved for all concentrations of MeOH investigated. The average peak height ratio of CLA and ERY over the concentration range investigated are summarized in Table 3.2.

Table 3.2 Chromatographic response of CLA and ERY with changes in mobile phase content (n=3)

MeOH % *v/v*	Peak height ratio (CLA/ERY)	%RSD	Run time (mins)
2	0.1272±0.0034	2.698	15
5	0.1424±0.0023	1.627	20
10	0.1605±0.0025	1.533	30

The increase in MeOH content in the mobile phase resulted in a longer retention time for CLA and ERY. The % RSD of the peak response decreased with the increase in MeOH content. Consequently, 5% *v/v* MeOH was used in the mobile phase for all validation studies as a run time of 20 minutes was deemed suitable for this analysis.

3.2.1 Calibration, linearity and range

The linearity of a method reflects the suitability of that method to produce test results that are directly proportional to the sample concentration over a specified range. For HPLC analysis, the relationship between detector response *viz*. peak area or height and sample concentration is used to determine the linearity of the method [132]. The range of an analytical method is the interval between the upper and lower concentrations of samples that have demonstrated acceptable levels of accuracy, precision and linearity. The range is therefore the concentration range over which linearity of the method is determined [132,192].

Linearity of the method was determined using a minimum of five standards injected five times as per the ICH guidelines [189]. The linearity of the method was evaluated over the concentration range 5–50 µg/mL, specifically 5, 8, 10, 12, 20, 30 and 50 µg/mL and least squares linear regression analysis of the peak height ratio (PHR) of CLA to ERY *versus* concentration data was used to establish the linearity of the method. The calibration curve was found to be linear with an R^2 of 0.9997, a slope of 0.0233 and a y-intercept of 0.0439, yielding a regression equation of y = 0.0233x + 0.0439. The calibration curve for CLA over the concentration range 0.5-50 µg/mL is depicted in Figure 3.1. Correlation coefficients of >0.990 are generally considered as evidence of acceptable linearity for the regression line [193]. Consequently, the HPLC-ECD method was deemed linear over the concentration range of CLA investigated.

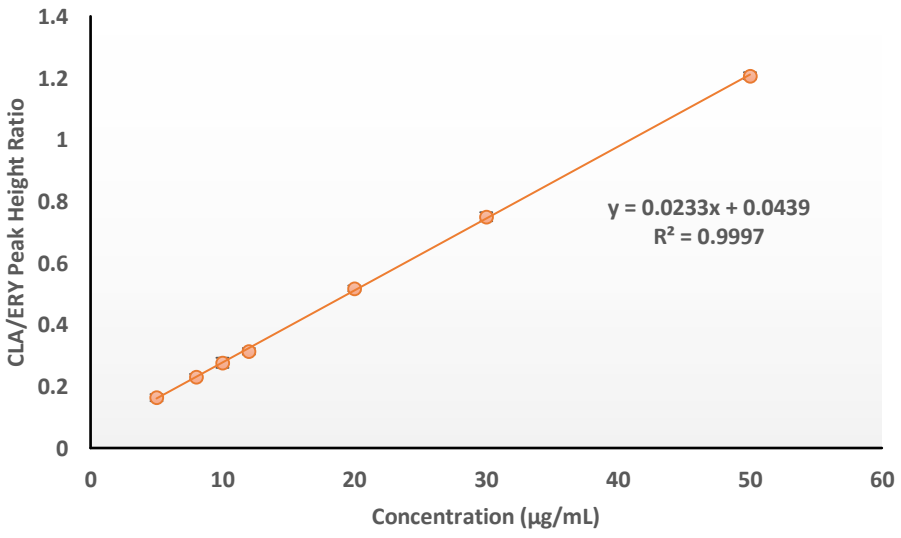

Figure 3.1 Typical calibration curve for CLA over the concentration range 0.5-50 µg/mL.

3.2.2 Precision

Analytical method precision is a measure of the ability of a method to generate reproducible results and may be assessed at three levels *viz.* repeatability or intra-day precision, intermediate or inter-day precision and reproducibility or between laboratory precision [132,194]. In these studies, the precision of the method was evaluated at two levels *viz*. repeatability and intermediate precision. All analyses were performed by the same analyst in one laboratory using the same equipment thus it was not necessary to establish the reproducibility of this method.

The repeatability for CLA was determined by analyzing a sample solution containing a target level of CLA. Ten replicates (n = 10) of the sample solution were analyzed as per the final method procedure [194]. Repeatability was determined using a 50 µg/mL sample solution. The inter-day precision for CLA was determined by analyzing sample solutions in replicate (n = 5) at three different concentrations *viz*. low (6.0 µg/mL), middle (25.0 µg/mL) and high (45.0 µg/mL) concentrations, within the range tested on three different days. The precision data for this method are summarized in Table 3.3. These data reveal that in all cases, the % RSD values were < 2%, indicating that the method is precise and can be used as intended.

Table 3.3 Intra-and inter-day precision data for CLA analysis

Intra-day precision % RSD (*n*=10)	1.2363
	Inter-day precision % RSD range (*n*=5)
Day 1	1.1409-1.9528
Day 2	0.2915-1.2201
Day 3	0.6229-1.1288

3.2.3 Accuracy and bias

The closeness in agreement of an accepted true value or a reference value to the actual results generated is referred to as the accuracy of an analytical method. Accuracy is determined by spiking a sample matrix with a known concentration of an analyte standard and analyzing the sample using the method under validation [132,192]. The accuracy of this method was determined by replicate analysis (n = 5) of samples containing known amounts of CLA at low (6.0 µg/mL), middle (25.0 µg/mL) and high (45.0 µg/mL) concentrations. A separate researcher from our laboratory, who was blinded to the concentration of the samples,

analyzed the accuracy data. The ICH guideline [189] recommends that accuracy be assessed using a minimum of nine analyses at three concentration levels within the specified calibration range. The accuracy data are reported as % recovery of the added amount of analyte in a sample or as the difference between the mean and accepted true value of a sample by use of confidence intervals [189]. The analytical method is considered accurate if the % recovery is close to 100% with a % bias < 2% for the samples [194]. The extent of deviation of the experimental data from the true value can be expressed as % Bias, which is calculated using Equation 3.2.

$$\% \text{ Bias} = \frac{True\ Value - Measured\ Value}{\text{True Value}} x100 \qquad \textbf{Equation 3.2}$$

The mean recovery was assessed for compliance according to the ICH guidelines [189]. The data generated for accuracy studies are summarized in Table 3.4 in which the % RSD values reported for all analyses were < 2%, indicating that the HPLC-ECD analytical method is accurate and suitable for the intended purpose.

Table 3.4 Accuracy results for blinded CLA samples (*n*=5)

Theoretical concentration µg/mL	Actual concentration µg/mL	% RSD	% Bias
6.00	6.11	1.63	+1.82
25.00	25.49	0.91	+1.94
45.00	45.20	1.22	+1.22

3.2.4 Limits of quantitation and detection

The limit of quantitation (LOQ) of a method is the lowest level of analyte that can be accurately and precisely determined whereas the limit of detection (LOD) of a method is the lowest analyte concentration that produces a response detectable above the noise level of the system and is typically, three times the noise level. The signal to noise ratio for the LOD should be 3:1 while that for the LOQ should be 10:1 [132,192,195]. The ICH guidelines [189] on method validation points out a number of ways to calculate the LOQ and the LOD. In these studies, the LOQ of the method was determined by evaluating the lowest concentration of CLA that resulted in a % RSD of < 5%, and the LOD was taken as the 0.3 × LOQ value. Alternatively, the LOD may be inferred from the concentration resulting in a % RSD of ≤ 20% when the LOQ results in a % RSD of ≤ 10% [193]. The LOQ for CLA was

0.05 µg/mL with an associated % RSD of 4.27% and by convention, the LOD was established as 0.02 µg/mL.

3.2.5 Robustness

As defined by the ICH [189], the robustness of an analytical procedure is reflected by the ability of the procedure to remain unaffected by small but deliberate changes in the method. Design of Experiments (DoE) was used to assess method robustness with two input factors being considered as described in § 2.2.1. The experimental domain for the selected responses is also described in § 2.3. Randomization of the experimental runs was used to minimize the effects of unknown factors likely to introduce bias when monitoring the ultimate method response. ANOVA data as reported in § 2.3.1 including analysis of the contour plots revealed that the retention time was not robust to slight changes in acetonitrile content and buffer molarity. Caution and attention to detail while preparing analytical mobile phase must therefore be taken when preparing for this analytical procedure as small changes in these factors may result in a change in retention time, which in turn may affect peak symmetry and the separation.

3.3 METHOD RE-VALIDATION AND SCALING

Following method development and validation using a Beckman® C_8, 150 × 4.0 mm i.d 4 µm analytical column, further analysis using the column could not be performed due to system suitability changes when evaluating the analytical response. Attempts to regenerate and/or purchase an identical column were unsuccessful as the specific column was phased out by the manufacturer. Consequently, re-validation and an investigation into the application of method scaling using a column of different L-designation was undertaken using a Phenomenex Luna® CN 150 × 4.6 mm i.d 5 µm (Phenomenex®, Torrace, CA, USA) which exhibited a −20% decrease in the L/dp value that fell within the range −25% to + 50% as defined in the USP method scaling guidelines [36]. Analysis was undertaken using a mobile phase flow rate of 1.058 mL/min that was calculated using Equation 3.1 (§ 3.1).

The USP system suitability requirements [36] for resolution, tailing factor and % RSD for PHR and retention time, were used to determine if the modified scaling of the HPLC-ECD

method resulted in outcomes that were comparable to those observed using a re-validation process thereby providing assurance of the applicability of scaling of this method for the analysis of CLA.

Method re-validation following the column change was successful. In addition, scaling of the method across analytical columns of different L-designation met all USP system suitability requirements for resolution, tailing factor and % RSD for this HPLC-ECD method, confirming the potential applicability of method scaling when changing to a stationary phase in a different class. This approach was deemed an efficient tool for this method with a result that a shorter run time, decreased solvent consumption and reduced cost were also achieved. The data generated from these studies are summarized in Tables 3.5 and 3.6.

Table 3.5 Summary of re-validation results for the HPLC method for CLA analysis

Parameter	CLA		
Linearity			
R^2	0.9999		
Equation	Y=0.0315x + 0.0176		
Intra-day precision % RSD (*n*=10)	1.7028		
Inter-day precision % RSD range (*n*=5)			
Day 1	1.0645-1.5675		
Day 2	1.1904-1.7166		
Day 3	0.9385-1.7849		
Accuracy (*n*=5)			
Theoretical concentration µg/mL	7.60	21.00	44.00
% Recovery ± % RSD	7.50±3.71	20.67±1.02	44.07±1.42
%Bias	-1.30	-1.58	+0.15
LOQ µg/mL (*n*=5)	1.5		
LOD µg/mL	0.5		

Table 3.6 USP scaling results for the CLA assay

	Resolution	**CLA tailing**	**CLA/ERY PHR**	**CLA retention time**
Average	1.509±0.015	4.083±0.039		
%RSD			1.145	0.187
Limits	**NMT 2.0**	**NLT 1.5**	**%RSD NMT 2%**	**%RSD NMT 2%**

The chromatographic responses before and after method re-validation and scaling are depicted in Figure 3.2. The scaled method revealed an improvement in peak asymmetry with sharp peaks and reduced tailing over a shorter analytical run time in comparison to the method developed using the Beckman® column. Columns in which CN functional groups are

used are more polar than C_8-based stationary phases and exhibit shorter retention times and different selectivity than C_8 columns [132]. Consequently, the repulsion of the ionized CLA moiety at pH 7.00 when using the CN column, led to reduced peak tailing and a shorter analytical run time.

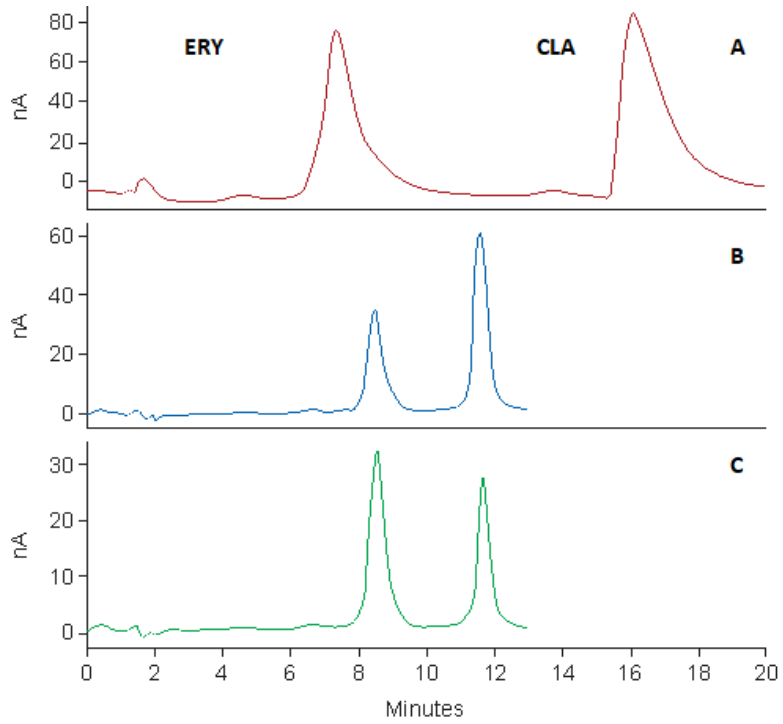

Figure 3.2 Typical chromatograms depicting the separation of CLA and ERY before method scaling (CLA 45 µg/mL, ERY 50 µg/mL) (A), after method scaling (CLA 50 µg/mL, ERY 50 µg/mL) (B) and for assay of Klarizon® 250 mg tablets (C)

3.3.1 Forced degradation studies

The ICH guidelines [196] on stress testing of new drug substances and products states that stress testing is intended to identify likely degradation products which further facilitates the determination of the intrinsic stability of a molecule, establishing degradation pathways and validation of the stability indicating procedures used. However, the regulatory guidance is very general when it comes to the conduct of forced degradation studies. In addition, the guidelines fail to provide details about the practical approaches needed for stress testing [191]. Degradation approaches and conditions often used during stress studies include acid and base hydrolysis, oxidation, photolytic and thermal degradation conditions at a tolerance level of between 5-20% API degradation [191,197]. Consequently, stress studies were conducted by exposing CLA to acidic, alkaline, thermal, hydrogen peroxide and light conditions. Stock solutions (100 µg/mL) were prepared as described in § 2.2.3.3 and exposed to different stress conditions *viz*. 0.1 M HCl, 0.1 M NaOH, 4% H_2O_2 at 80 °C and 500 W/m^2

(Suntest® CPS+, Atlas, Linsengericht, Germany) for 12 hours, prior to analysis using the validated analytical method. A tolerance of 10% was used to establish if CLA had degraded as a result of exposure to these stress conditions. These studies were also performed to identify interference, if any, by degradation products on the chromatographic separation that had been developed and validated.

The results of forced degradation studies can be used to establish the specificity and stability indicating characteristics of the HPLC-ECD method. Data from these studies are summarized in Table 3.7 and the resultant chromatograms following stress testing are depicted in Figure 3.3.

Table 3.7 Forced degradation data for CLA following exposure to stress conditions for 12 hours

Stress Condition	% Recovered	Remarks
Control in ACN	100±0.39	-
Thermal at 80°C	105.48±1.08	No degradation
UV exposure at 500 W/m^2	92.33±1.85	No degradation
Acid hydrolysis using 0.1M HCI	94.85±4.29	No Degradation
Alkaline hydrolysis using 0.1M NaOH	54.81±9.17	Degradation
Oxidation using 4% *v/v* H_2O_2	0.00	Degradation

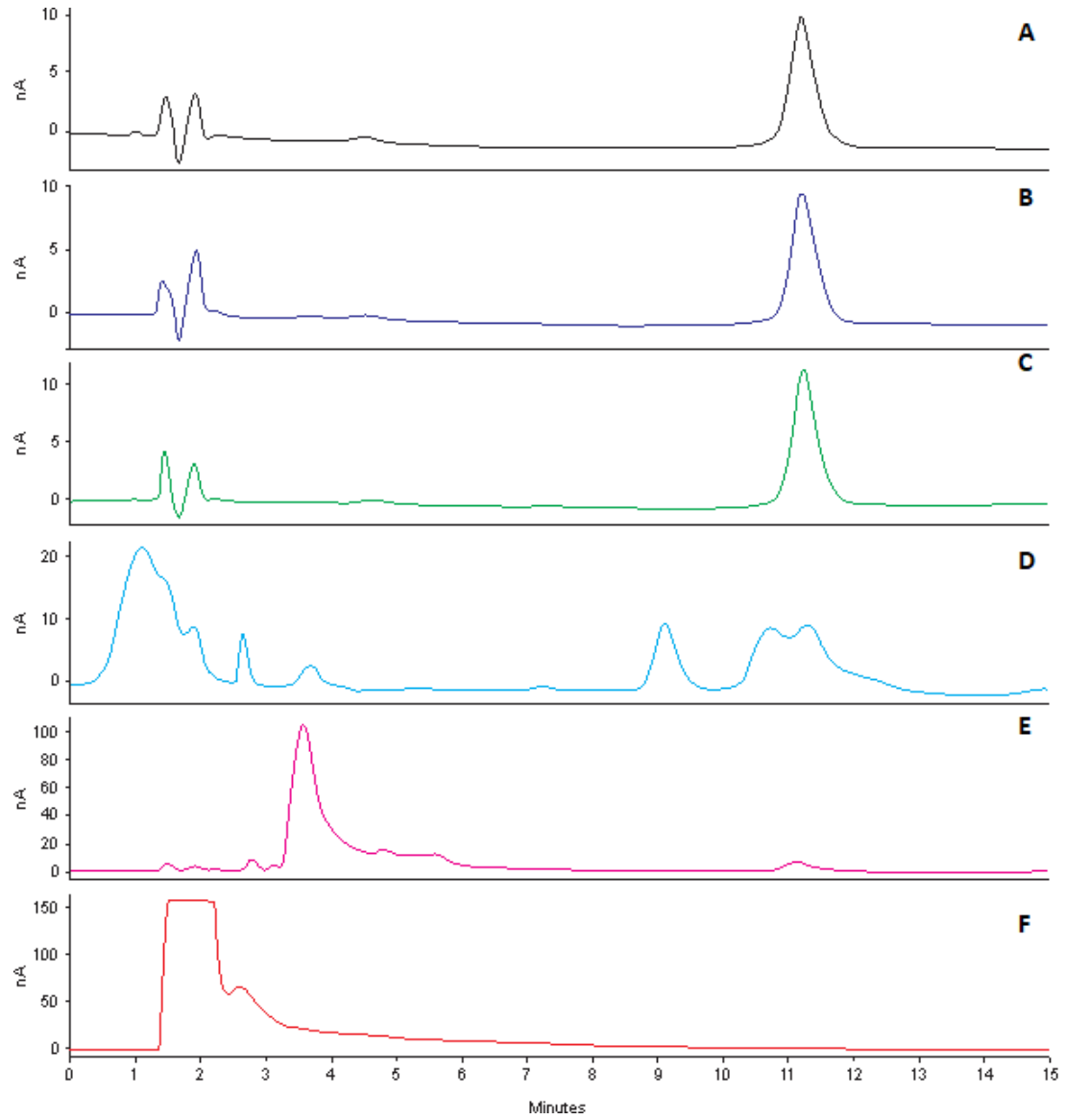

Figure 3.3 Typical chromatograms following degradation of CLA (10 µg/mL) following exposure to ACN (A), heat at 80 °C (B), 500 W/m^2 UV radiation (C), 0.1M HCI (D), 0.1M NaOH (E) and 4% *v/v* H_2O_2 (F)

The degradation data reveal that CLA undergoes extensive degradation when exposed to oxidative stress conditions. Oxidation of CLA has been reported to occur *via* reactivity of the tertiary amino group [51] and the reaction with hydrogen peroxide is thought to oxidise CLA, resulting in products that do not oxidise when using ECD for the analysis. Exposure of CLA to acidic conditions (pH 1.2) resulted in approximately 5% degradation, which is attributed to hydrolysis of the cladinose moieity [87], confirming previously published data which reported 90.2% and 41.1% loss of CLA from aqueous samples exposed in solutions of pH 1.00 and pH 2.00 for four hours [198]. However, one of the degradation products interferes with the chromatographic separation following acid hydrolysis (Figure 3.3D) thereby resulting on specificity failing for the method for these conditions. Nevertheless, the extreme

conditions used for these studies are unlikely to be used in any manufacturing or analytical procedures, therefore this outcome is of little concern for this research as the degradation study was conducted at a temperature and pH well in excess of the conditions used for this analyses or those intended to be used for the manufacture of carrier technologies of CLA. Exposure to alkaline conditions led to significant degradation of CLA that may be attributed to the presence of ester functional groups that are susceptible to hydrolysis in alkaline conditions. Acid and base hydrolysis does not result in the total loss of the oxidizing potential of CLA, implying the molecule may be detected and separated in the presence of degradation products but with some interference observed for acid hydrolysis samples. CLA was stable with < 10% degradation observed following exposure to heat and UV radiation for 12 hours.

3.3.2 Analyte Stability

The chemical stability of an analyte under specific conditions is determined by comparison of a response to that observed for freshly prepared samples. Analyte stability in mobile phase therefore ensures the integrity of the compound in question throughout the analytical process [199,200]. The stability of CLA in ACN was determined by analyzing a 10 µg/mL solution (n =5) maintained at 4 °C for a period of seven days and comparing it to a freshly prepared sample of the same concentration. A tolerance level of ±10% bias in PHR was considered acceptable in order to infer stability. The studies revealed that the concentration of CLA remained constant with a resultant bias of -5.73%. CLA was therefore considered stable in ACN, and the stock solution could be stored under the stated conditions and used within seven days of preparation. Furthermore, CLA in ACN stock solutions stored at 4 °C were found to be stable over a period of at least 21 days [155].

3.4 APPLICATION OF THE ANALYTICAL METHOD

In order to establish the applicability of the method for the analysis of CLA in dosage forms, six commercially available products were purchased form a local pharmacy and subjected to analysis. The analyzed products were, Clarihexal®, Klarithran®, Klarithran® MR 500 mg tablets, Klarizon® 250 mg tablets and Clarihexal®, Klarithran® 250 mg/mL granules for oral suspension.

3.4.1 Assay of Commercial Tablets

Briefly, 20 tablets were crushed using a mortar and pestle and an aliquot of powder equivalent to the mass of one tablet was quantitatively transferred to a 100 mL A-grade volumetric flask. Approximately 50 mL ACN was then added to the volumetric flask and the mixture sonicated using a bath sonicator (Ultrasonic Manufacturing Company (Pty), Ltd., Kenware, Krugersdorp, South Africa) with regular shaking at 20 minute intervals for 1 hour. The solution was allowed to cool to room temperature (22 °C) prior to making up to volume with ACN. A 5 mL aliquot of the resultant mixture was filtered through a 0.45 µm Millipore® Millex-HV Hydrophilic PVDF filter membrane (Millipore® Co., Bedford, MA, USA) and a 25 µg/mL sample solution in ACN was analyzed using the validated HPLC method (n =5).

3.4.2 Assay of Commercial Suspensions

The granules for suspension were reconstituted using HPLC-grade water as per the label instructions. A 5 mL aliquot of the reconstituted suspension was transferred to a 100 mL A-grade volumetric flask using a 10 mL A-grade measuring cylinder. Approximately 20 mL 50 mM phosphate buffer (pH 7.00) was then added to the volumetric flask and the mixture sonicated using a bath sonicator (Ultrasonic Manufacturing Company (Pty), Ltd., Kenware, Krugersdorp, South Africa) with regular shaking at 10 minute intervals for 30 minutes. Approximately 30 mL MeOH was added to the flask and the mixture was sonicated for a further 30 minutes. The solution was allowed to cool to room temperature (22 °C) prior to making up to volume with MeOH. The mixture was then stirred for one hour at 500 rpm using a digital hot plate stirrer (Lasec®, Port Elizabeth, South Africa). A 5 mL aliquot of the resultant mixture was filtered through a 0.45 µm Millipore® Millex-HV Hydrophilic PVDF filter membrane (Millipore® Co., Bedford, MA, USA) and analyzed using the validated HPLC method after dilution to obtain a 25 µg/mL solution in ACN (n=5).

The specificity of the method to resolve peak(s) of interest from any possible excipients or contaminants that may be present in a dosage form was established by quantitation of CLA in the commercially available tablets and suspensions. All tablet and suspension samples complied with USP assay specifications. The USP [36] assay limits for clarithromycin tablets of 90.0%–110.0% and suspensions 90.0%–115.0% were used as the acceptance criteria. The assay results are listed in Table 3.8. The analysis of CLA dosage forms resulted in clear, sharp, well-resolved peaks without interference from any excipients used for manufacture (Figure 3.2C).

Table 3.8 Analysis of commercially available CLA formulations (*n*=5)

Product and label claim	Dose mg	% Recovery	% RSD
Clarihexal®500 XL	500 mg	99.69	1.57
Klarithran®MR 500	500 mg	99.09	0.61
Klarithran® 500	500 mg	103.94	1.80
Klarizon® 250	250 mg	98.81	2.40
ClariHexal® 250 mg/5 mL	250 mg	110.04	2.23
Klarithran®250mg/5 mL	250 mg	106.94	1.75

3.5 CONCLUSIONS

The HPLC-ECD method developed and reported in Chapter 2 was validated using ICH guidelines with an analytical run time of 20 minutes. Method re-validation following a change in analytical column was successful in reducing the analytical run time to 13 minutes, decreasing solvent consumption thus facilitating environmental and financial sustainability. The applicability of using the USP method scaling approach in place of method re-validation using a column with a different L–designation to the original analytical column, was investigated. The scaled method met all USP system suitability requirements for resolution, tailing factor and % RSD. Method scaling allows for translation of an analytical method while achieving an equivalent separation without the need for re-validation. HPLC methods can thus be scaled on condition that they meet USP system suitability requirements, maintaining separation quality, thereby eliminating the need for method re-validation. The re-validated and scaled method was successfully used to resolve CLA from manufacturing excipients in commercially available dosage forms. Although USP method scaling is only permitted for columns within the same L-designation, its applicability should be investigated across analytical columns of different L-designation to further streamline regulatory requirements. This is, to the best of our knowledge, the first evaluation of an HPLC-ECD method using a modified scaling approach. The validated and scaled method was applied to the analysis of commercially available dosage forms and was found to be suitable for the analytical characterization studies of CLA in lipid nanocarriers developed in this research.

CHAPTER 4

SELECTION AND CHARACTERIZATION OF EXCIPIENTS FOR THE FORMULATION AND MANUFACTURE OF CLARITHROMYCIN LOADED NANOCARRIERS

4.1 INTRODUCTION

Solid lipid nanoparticles (SLN) and nanostructured lipid carriers (NLC) are two types of lipid-based nanocarriers that were developed to overcome the limitations of colloidal carriers, such as emulsions, liposomes and polymeric nanoparticles [201]. Some of the limitations of these conventional colloidal carriers include limited stability when stored over extended periods, poor batch-to-batch reproducibility, low drug loading capacity (LC), and failure to manipulate biological membrane barriers sufficiently to achieve the concentration of active pharmaceutical ingredient (API) in the systemic circulation for therapeutic activity [202,203]. The encapsulation of API molecules within nanoparticles shields them from the effect(s) of efflux transporters while the small particle size facilitates transport across biological membranes [204]. SLN and NLC are nanovectors manufactured using solid lipids or a combination of solid and liquid lipids [203,205]. SLN are usually used as aqueous dispersions and are produced using a solid lipid, an API and surfactant(s) which impart stability to the system [205]. NLC differ from SLN only from an excipient point of view, in that binary mixtures of solid and liquid lipids, as well as a surfactant(s), are used for their formulation [206]. In addition to excellent physical stability, SLN and NLC exhibit complex functions, such as an ability to achieve controlled delivery of API across different biological membranes and barriers which consequently impart an ability to target organs leading to adhesion and improved cellular uptake [201,203,204].

The manufacture of SLN or NLC involves melting a solid lipid or a binary mixture of solid and liquid lipid, followed by re-dispersion of the molten lipids as submicron-size droplets in an aqueous medium containing surfactant(s) *via* mechanical stirring [206]. Acute and/or chronic toxicity during *in vivo* use has been associated with traditional colloidal systems, including polymeric-based systems [207] therefore, a prerequisite for manufacture of SLN

and NLC is that only pharmaceutical grade excipients that are generally regarded as safe (GRAS) are used for production [207–209]. Mehnert and Mäder [205] and Souto and Müller [210], have reported broad lists of lipids and surfactants that can and have been used for the manufacture of SLN and NLC.

When formulating new products or re-formulating existing products, it is advantageous to use data of physical and chemical interactions between API and excipients which may give rise to changes in the chemical nature, stability, solubility, absorption and therapeutic response of drugs [211]. Pre-formulation testing is therefore the first step in a coherent dosage form drug development process. Pre-formulation can be defined as an investigation of physical and chemical properties of an API substance alone and in combination with potential excipients. In its entirety, pre-formulation testing generates information useful to a formulation scientist for the development of a stable dosage form that ensures the bioavailability of an API that can ultimately be mass produced [212]. Although excipients have traditionally been thought of as inert, they can and have shown possible interactions with API thereby limiting absorption with a reduction in bioavailability [213,214]. It is therefore necessary to study and understand the effects of excipients so as to ensure that the stability of a formulation is optimized. The type of information generated during pre-formulation studies is dependent on the dosage form to be produced including an understanding of the formulation and manufacturing steps required during dosage form development [211,212,214].

A formulation composition is considered appropriate when no drug-excipient or excipient-excipient interactions occur. In this sense, developing a rapid and accurate method to test and select the best excipients for the manufacture of stable dosage forms is the end-point of the pre-formulation stages of product development [213,215]. Although there is no standardized protocol for performing pre-formulation studies, some researchers have used the technique of annealing binary mixtures under stress conditions and then analyzing the mixtures using chromatographic techniques [216,217]. Despite requiring large amounts of API and excipients, the technique is time-consuming and ultimately very expensive. A number of researchers have thus used thermal analysis and spectroscopic techniques for the rapid evaluation and determination of compatibility of an API with pharmaceutical adjuncts or excipients [218–221]. Thermal analytical techniques such as differential scanning calorimetry

(DSC), differential thermal analysis (DTA) and thermogravimetric analysis (TGA) and spectroscopic techniques such as infrared spectroscopy (IR) and wide-angle x-ray diffraction scattering (WAXS) offer significant advantages in saving both time and raw materials when used to detect compatibility/incompatibility in physical mixtures directly thereby avoiding the time consuming step of annealing mixtures under stress conditions [61,222,223].

Different formulation approaches have been used for the manufacture of lipid nanocarriers including hot or cold high-pressure homogenization [171,224], ultrasonication or high speed homogenization [225,226], solvent emulsification-evaporation [227,228], supercritical fluid preparation [229,230], spray drying [231,232], double emulsion [233,234] amongst others or modifications of these techniques [235]. The pre-formulation experiments performed in these studies were undertaken with two manufacturing techniques in mind *viz.* hot emulsification ultrasonication (HEUS) and hot high-pressure homogenization (HHPH). These techniques involve exposing an API/ lipid(s) mixture to temperatures of 5-10 °C above the melting point of the solid lipid used, and then mixing with a surfactant solution maintained at the same temperature, resulting in the formation of a pre-emulsion [201,209]. The pre-emulsion is then passed through a high pressure homogenizer maintained at similar temperatures to ensure that the molten state of the lipid is preserved during production in the case of HHPH [236] or further sized reduced by cavitation using ultrasound techniques in the case of HEUS [237,238]. Furthermore, a practical consideration in the use of high pressure homogenizers is a constant supply of water to the spaces between the double piston seals of the instrument, which is essential in cooling the pistons, ultimately minimizing wear of the rear seals [239].

Production temperatures when using HEUS and/or HHPH may reach as high as 90 °C depending on the melting point of the solid lipid or solid lipid/liquid lipid mixtures used and/or the homogenization pressure or amplitude selected for the manufacturing process [240,241]. The use of high production temperatures may lead to the degradation of thermolabile API and/or lead to changes in the physicochemical properties of the API [240,242]. Therefore, it is vital that the thermal stability of an API be investigated and established prior to attempting to incorporate the molecule into nanoparticles using HEUS or HHPH. In addition, the potential effects of exposing an API to relatively high temperatures on the crystalline and polymorphic nature of the chemical entity must be elucidated during

pre-formulation studies. Consequently, TGA was used to investigate the thermal stability of CLA and to assess the feasibility of using HHPH and/or HEUS to manufacture CLA-loaded lipid nanocarriers. Similarly, DSC and WAXS have been used to assess the crystalline and polymorphic nature of API [243–245] and were used to evaluate the crystalline and polymorphic behaviour of CLA prior to and after exposing the molecule to the high temperatures in order to determine whether changes to the crystal structure of CLA occurred following exposure to heat.

Prior to the development and optimization of CLA-loaded lipid nanocarriers an investigation of the solubility of the molecule in the lipids to be used must be undertaken. To reduce the amount of lipid material required to make the nanocarriers, so as to maximize product quality, it is necessary to select lipid excipients that exhibit the highest loading capacity (LC) and encapsulation efficiency (EE) for an API [246]. An adequate LC and EE can only be achieved when the solubility of an API in the molten lipid is relatively high [209,247]. Screening for the solubility of an API in potential lipids to be used for the production of SLN and NLC has been performed using a traditional shake flask method in order to determine equilibrium solubility [245,248–250]. Modifications of the shake flask method have also been applied when evaluating poorly lipid soluble API [251,252]. The identification and selection of oily excipients for the production of nanoemulsions has been undertaken through investigation of API solubility in a variety of oils using the shake flask method followed by comparative stability studies of nanoemulsions using four oils in which the highest solubility for the API was observed [253]. Determination of the dissolution potential of different lipids for the API can be quantitated using HPLC analysis, UV spectrophotometry and/or by visual inspection [245,251–254]. The shake-flask technique is a simple procedure which is time consuming, costly and requires a number of laboratory experiments to be performed. Moreover, there is no accepted or standard approach for conducing these studies [255] and published solubility study data that have been reported reveal that a large variety of experimental conditions were used, in particular stirring/shake times, sample preparation and separation approaches prior to analysis, amongst others [256].

Recent advances in computational technologies have facilitated the development of powerful *in silico* simulation and modelling approaches to establishing solubility in which the

molecular structure, physiochemical properties and specific solute-solvent interactions may be taken into account [257–259]. The Hildebrand solubility parameter (δ) is a numerical value that indicates the relative solubilizing behavior of a specific solvent and is represented as Equation 4.1 [260]. The parameter expresses the square root of the cohesive energy density (CED) of the components that hold the substances together and is derived from the CED of the solvent, which in turn is derived from the heat of vaporization of the solvent [260,261].

$$\delta = (CED)^{1/2} = (\Delta Ev/Vm)^{1/2} \qquad \textbf{Equation 4.1}$$

Where,
ΔEv = the molar energy of vaporization
Vm = the molar volume of the solvent

The Hildebrand approach works well for low molecular weight non-polar solvents but fails to adequately describe the solubility behavior when polar and hydrogen bonding solvents are introduced into the system. Consequently, Hansen *et al* [262] developed an approach to solubility parameters that takes into account polar and hydrogen bonding forces. Hansen solubility parameters (HSP) have been applied to determine API-system affinities using a combination of the theoretical solubility parameters and experimentally determined partition coefficients of the API in the components of that system [263].

The HSP separates the total solubility parameter (δT) into individual components that include dispersion forces (δD), permanent dipole–permanent dipole forces (δP) and hydrogen bonding (δH) [262] that can be estimated using Equation 4.2.

$$\delta T^2 = \delta D^2 + \delta P^2 + \delta H^2 \qquad \textbf{Equation 4.2}$$

Where,
δD = dispersion forces
δP = permanent dipole–permanent dipole forces
δH = hydrogen bonding

The use of theoretical solubility parameter predictions based on the molecular structure of compounds provides an early, rapid screening approach for the selection of lipid candidates without the need for lengthy experimental procedures to generate the data [262,264,265].

According to the HSP, the best miscibility of an API and an excipient is predictable when intermolecular forces *viz*. dispersion, polar, and hydrogen bonding forces between the molecules of the solute and solvent are of similar strength [261,262,266]. The difference in the solubility parameters between an API and an excipient can be used to estimate the compatibility and thus miscibility of the components [267]. The HSP has been used to describe numerous physical properties of materials in addition to predicting the miscibility and compatibility of an API and potential excipients [267–270].

Makoni *et al.,* [256] investigated the use of quantitative analysis and HSP predictions for the selection of excipients for lipid nanocarriers to be loaded with water soluble and insoluble compounds. Minocycline hydrochloride, mometasone furoate, efavirenz, didanosine and CLA were the molecules investigated. Efavirenz, mometasone furoate and CLA have low aqueous solubility and high intestinal permeability and are classified as a Biopharmaceutical Classification System (BCS) Class II compounds [271–273] while minocycline hydrochloride and didanosine exhibit high aqueous solubility and low intestinal permeability and are classified as BCS Class III compounds [274,275]. During these studies with the five aforementioned API that exhibited different physicochemical characteristics, six solid lipids in addition to four liquid lipids, the authors concluded that there was no clear link between the physicochemical properties of each API, the BCS classification and the potential to be dissolved in the lipid excipients tested. The authors postulate that when the difference between API and lipid total solubility parameters is < 4.0 $MPa^{1/2}$, the best dissolution of an API is likely to result from that specific lipid when compared to other lipids and when the difference between API and lipid total solubility parameters is > 4.0 $MPa^{1/2}$, HSP predictions alone cannot be used to determine the lipid with the best dissolution potential for a specific API. In addition, the proposed model exhibited limitations when attempting to predict miscibility using HSP alone with molecules of more than 120 atoms other than H atoms, such as CLA for example. These molecules require splitting prior to using Hiroshi Yamamoto's molecular breaking method of HSP prediction in Practice software resulting in inaccurate predictions. Consequently, it is deemed important to evaluate the solubility of CLA quantitatively using laboratory experiments in the different solid and liquid lipids, with the primary aim of selecting a solid and/or liquid lipid combination with the best dissolution potential for this large molecular weight API.

The production of NLC involves mixing lipid molecules that are spatially different *viz*. solid and liquid lipids, and invariably results in the melting point of the solid lipid decreasing [207,252,276]. Nevertheless, the NLC must remain solid at room and body temperatures and therefore as a general rule the melting point of the solid lipid to be used should be > 40 °C [245,252] after combination with the liquid lipid used. In addition, the solid lipid should be miscible with the liquid lipid to permit the formation of imperfections in the crystal lattice structure of the solid lipid [121,277] therefore, the impact of the liquid lipid on the polymorphic nature of the solid lipid are an essential component of pre-formulation studies.

The overall aim of these studies was to investigate the possibility of using solubility parameters that are empirically derived from molecular structures to inform formulation efforts.

4.2 MATERIALS AND METHODS

4.2.1 Materials

CLA was purchased from Skyrun Industrial Co. Limited (Taizhou, China). Solid lipids *viz*. Gelucire® 48/16 (polyethylene glycol monostearate), Compritol® 888 (glyceryl behenate), Precirol® ATO 5 (glyceryl distearate), Geleol™ (glyceryl monostearate) and cetyl palmitate were donated by Gattefossé SAS (Gattefossé SAS, Saint-Priest Cedex, France). Stearic acid was purchased from Sigma Aldrich Chemical Co. (Milwaukee, WI, USA). Liquid lipids *viz*. Transcutol® HP (diethylene glycol monoethyl ether), Labrafac® PG (propylene glycol dicaprylate), Lauroglycol® FCC (propylene glycol monolaurate) and Capryol™ 90 (propylene glycol caprylate) were donated by Gattefossé SAS (Gattefossé SAS, Saint-Priest Cedex, France).

4.2.2 Methods

4.2.2.1 TGA Characterization of CLA

The thermal stability of CLA was investigated using a Perkin-Elmer® FT-IR thermogravimetric analyzer (Perkin-Elmer® Ltd, Connecticut, USA). A 5.827 mg aliquot of CLA was accurately weighed prior to analysis. The sample was heated from 30 to 345 °C at a heating rate of 10 °C/min. The TGA system was constantly purged with liquid nitrogen at a

flow rate of 20 ml/min, and the data generated were reduced using Pyris™ Manager Software version 4.01 (Perkin-Elmer® Ltd, Connecticut, USA).

4.2.2.2 FT-IR Characterization of CLA

The infrared spectrum of CLA was investigated using a Perkin-Elmer® Precisely FT-IR spectrophotometer Spectrum 100 (Perkin-Elmer® Pty Ltd, Beaconsfield, England) and the characteristic signal bands are depicted in Figure 1.3 of § 1.2.11.

4.2.2.3 DSC Characterization of CLA

The melting point of CLA was determined using a Model DSC-6000 PerkinElmer differential scanning calorimeter (Perkin-Elmer® Ltd, Connecticut, USA). A 3.419 g aliquot of CLA was weighed directly into a standard 40 µl aluminum open pan. The DSC scan was generated by heating the sample from 30 °C to 240 °C and then cooling for one cycle to 30 °C at heating and cooling rates of 10 °C/min. The system was purged with liquid nitrogen at a flow rate of 20 ml/min, and the resultant data were analyzed using version 4.01 Pyris™ Manger Software (Perkin-Elmer® Ltd, Connecticut, USA). The DSC data for CLA were generated prior to and following exposure to a temperature of 85 °C for one hour in order to establish whether thermal exposure had an impact on the physicochemical properties of the molecule *viz*. melting behaviour as well as crystalline and polymorphic nature.

4.2.2.4 WAXS Characterization of CLA

WAXS patterns of CLA were recorded using a Model D8 Discover X-ray diffractometer (Bruker, Billeria, MA, USA) that was equipped with a PSD LynxEye detector coupled to a copper anode set with Cu-Kα radiation at a $\lambda = 1.5405$ Å at 30 kV and fitted with a nickel filter. Samples were placed onto a zero background 511 silicon wafer embedded in a generic sample holder. The data were recorded at room temperature (22 °C) using a 2θ angle range between 10˚ and 100˚, a scanning rate of 1˚ min^{-1} with a filter time constant of 2.0 s per step and a slit width of 6.0 mm. The data were fitted using evaluation (Eva) curve-fitting software version V2.9.0.22 (Bruker, Billeria, MA, USA). All samples used for WAXS analysis were identical to those used for DSC studies in order to ensure ease of data comparison and enhance the characterization. The scattering angles observed from WAXS diffraction patterns

were transformed into short spacing using Bragg's equation (Equation 4.3) [171,278,279] so as to generate information about any potential lipid modifications.

$$d = \frac{\lambda}{sin\ 2\theta} \qquad \textbf{Equation 4.3}$$

Where,
d = inter-atomic distance
λ = wavelength of an X-ray beam
θ = the angle of incidence of the beam

4.2.2.5 Selection of Solid Lipids

The solubility of CLA in different solid lipids was determined by dissolving fixed amounts of API by addition of increasing amounts of solid lipid whilst heating and shaking the mixtures. Evaluation of the melt was performed visually [245,252]. The amount of API and/or solid lipid were accurately weighed using a Model PA 2102 Ohaus® top-loading analytical balance (Ohaus® Corp. Pine Brook, NJ USA) and transferred to individual test tubes (Pyrex® Laboratory Glassware, England). Aliquots (0.01 g) of CLA were accurately weighed and placed into a test tube and solid lipid added in 1.0 g aliquots after which the test tube was exposed to a temperature of 85 °C at 100 rpm with the aid of a LABOTEC® shaking water bath (Laboratory Thermal Equipment, Greenfield NR. Oldham). The amount of lipid required to dissolve the API whilst in the molten state was estimated as the point at which no further solid API could be visualized in the molten lipid after shaking at 100 rpm at 85 °C for 24 hours.

4.2.2.6 Selection of Liquid Lipids

The solubility of CLA in different liquid lipids was determined by dissolving increasing amounts of the API in a fixed amount of heated liquid lipid and evaluation of the melt visually as described in § 4.2.2.5. The amount of liquid lipid required to dissolve the API was estimated as the point at which no further solid API could be dissolved in the liquid lipid after shaking at 100 rpm at 85 °C for 24 hours.

4.2.2.7 Selection of a Binary Mixture of Solid and Liquid Lipid

The solid and liquid lipids with the best dissolution potential for CLA as identified from the studies described in § 4.2.2.5 and 4.2.2.6, were mixed in different ratios to identify a binary mixture of solid and liquid lipid that would be suitable for use for the manufacture of NLC. The miscibility of the two components was evaluated using a total lipid mass of 2.0 g in ratios of solid lipid : liquid lipid (*w/w*) of 95:5, 90:10, 85:15, 80:20, 75:25, 70:30, 60:40 and 50:50. Samples were weighed directly into a glass test tube and placed into a LABOTEC® shaking water bath (Laboratory Thermal Equipment, Greenfield NR. Oldham) for one hour with the temperature and speed set to 85 °C and 100 rpm, respectively. The samples were allowed to cool to room temperature (22 °C) for 24 hours prior to analysis. DSC was used to confirm the state of the cooled sample and therefore the miscibility of the solid lipid with the liquid lipid. DSC curves were generated by heating samples of between 2-5 mg, from 30 °C to 85 °C and subsequently cooling to 30 °C at heating and cooling rates of 10 °C/min. An empty aluminium pan was used as the reference. In addition, the miscibility of the two lipids was also evaluated by smearing a small sample of the dried binary mixture onto Whatman® 110 diameter hydrophilic filter papers (Whatman® International Ltd, Maidstone, England) prior to visual inspection for the presence of oil droplets. A miscible binary mixture of lipids for which CLA exhibited the highest solubility was identified and selected for formulation of NLC, and the melting point was determined using DSC to confirm that melting occurred at a temperature > 40 °C.

4.2.2.8 Polymorphism and Crystallinity of Bulk Lipids

The lipids used for the production of lipid nanocarriers include triglycerides and mixtures thereof, fatty acids, oils and waxes [279,280]. A requirement for the successful production of lipidic carriers is that the matrix remains in the solid state at room temperature. Therefore, the selection of lipids requires assessment of their polymorphism and crystallinity in addition to miscibility and physicochemical structure(s) [281]. Investigations of polymorphism is a necessity in the production of nanoparticles as these transitions have an influence on the EE, LC and expulsion of API on storage [282]. In addition, crystalline structures of triglycerides can occur in different polymorphic forms with the α-form exhibiting a lower melting point and latent heat of melting than the β-form which is the most stable and exhibits higher melting points and latent heat of melting. Transformation of α to β′ and β is irreversible and yields more hydrodynamic stable systems [279,283,284]. The production of SLN and/or NLC

using HHPH and/or HEUS requires the solid lipid to be molten prior to dissolving the API in the lipid. The API-containing lipid melt is then dispersed in a hot surfactant solution to yield a pre-emulsion. Homogenization or ultrasonication of the pre-emulsion produces a hot o/w nano-emulsion that on cooling results in recrystallization of the solid lipids with the subsequent formation of nanoparticles *in situ* [121,285]. Consequently, conducting an analysis of SLN and/or NLC using DSC for the determination of the impact of additional melting cycles on the properties of solid lipid(s) is essential. Therefore prior to homogenization or ultrasonication of a pre-emulsion, the lipid would have been melted to facilitate dissolution of the API, suggesting a second DSC scan of the bulk lipid(s) during characterization of the bulk material is necessary [285]. However the use of DSC to characterize bulk lipids following exposure to temperatures which mimic that for the dissolution stage of manufacture, would require only a single DSC scan corresponding to the analysis of SLN and/or NLC [277]. DSC and WAXS was therefore used to characterize polymorphic modifications, if any, of the bulk lipids. DSC and WAXS characterization of the lipids was performed using the procedures described in § 4.2.2.3 and 4.2.2.4. All samples were analyzed prior to and following exposure to a temperature of 85 °C for one hour. The samples that were subject to analysis were similar for both procedures in order to simplify assessment of data generated.

4.2.2.9 Interaction of Bulk Lipids with CLA

Potential physical interactions between lipid excipients and CLA were investigated using FT-IR, DSC and WAXS using the equipment and procedures described in § 4.2.2.2, 4.2.2.3 and 4.2.2.4, respectively. Binary mixtures of solid lipid and CLA in addition to a ternary mixture of the solid lipid, liquid lipid and CLA were analyzed prior to and following exposure to a temperature of 85 °C for one hour.

4.3 RESULTS AND DISCUSSION

4.3.1 TGA Characterization of CLA

TGA is used to determine the thermal stability of a material and the fraction of volatile components present by monitoring any weight change that occurs as the sample is heated at a constant rate [286]. The loss in weight of CLA and the first derivative of the TGA

thermogram for the molecule was recorded as a function of increasing temperature and was correlated to the thermal stability of the compound. These data are depicted in Figure 4.1.

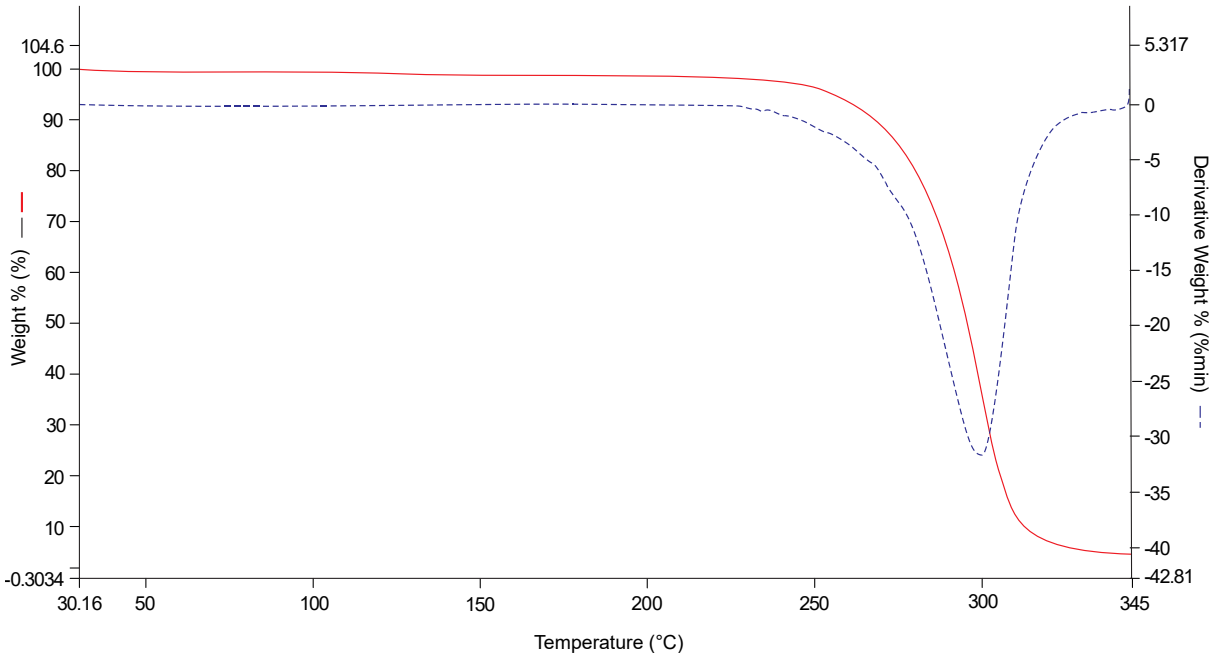

Figure 4.1 TGA curve for CLA (red) and the first derivative generated following heating at a rate of 10 °C/min

The TGA studies indicate the loss of more than 90% of the weight at temperatures > 300 °C and these results are in agreement with previously reported data [287]. It is evident that CLA is thermostable at temperatures ranging between 70 and 90 °C which are the temperatures of manufacture and exposure in these studies. Therefore, the molecule is unlikely to be unstable during solubility studies and the manufacture of SLN and/or NLC using HHPH and/or HEUS.

4.3.2 DSC Characterization of CLA

The melting behaviour, crystalline and polymorphic nature of anhydrous CLA prior to and following exposure to a temperature of 85 °C for one hour was evaluated using DSC. The molecule was exposed to heat for one hour to mimic the length of time over which the molecule was expected to be exposed to heat during the manufacture of the nanoparticles. The resultant DSC thermograms generated in these studies are depicted in Figure 4.2 and the relevant parameters are summarized in Table 4.1. Data in which the difference between the onset and melting temperature, or the width of the peak (WP) which can be used to determine lattice defects in crystalline materials [276,277] are also summarized in Table 4.1.

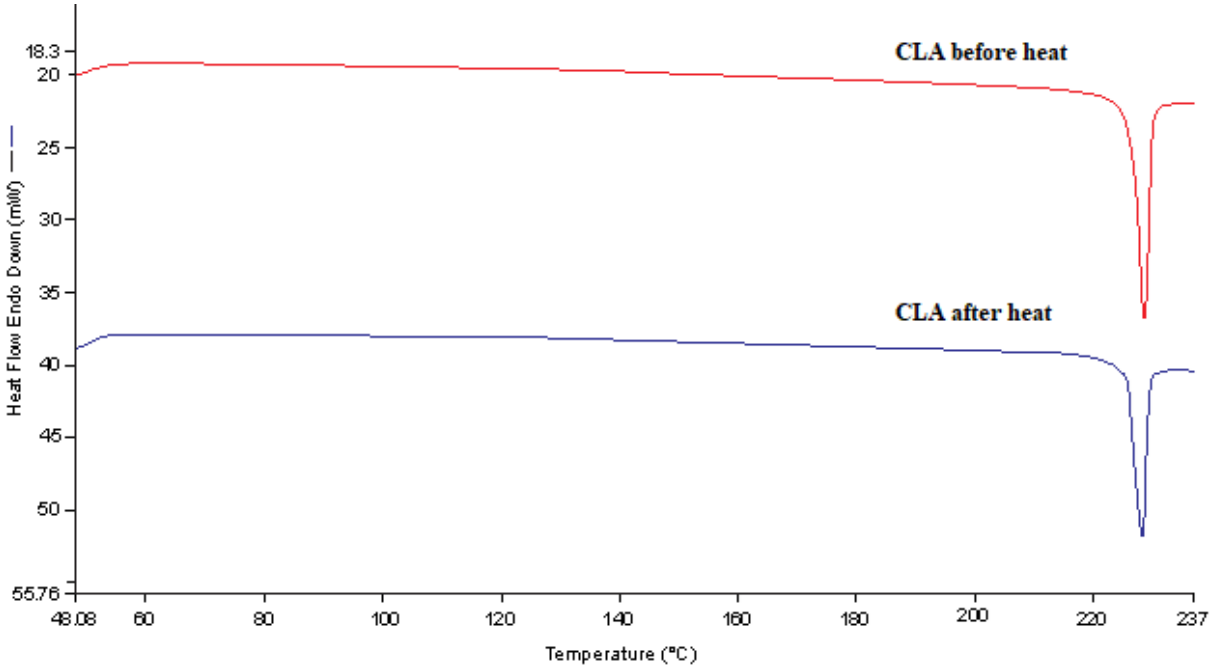

Figure 4.2 DSC thermograms for CLA prior to and following exposure to a temperature of 85 °C for one hour

Table 4.1 DSC parameters for CLA prior to and following exposure to a temperature of 85 °C for one hour

Clarithromycin	Thermal event	Onset (°C)	MP (°C)	Enthalpy (J/g)	WP (°C)
Before heating	Endothermic	228.12	229.25	57.42	1.13
After heating	Endothermic	227.07	228.86	42.57	1.79

The DSC data for CLA, prior to and following exposure to heating, revealed the presence of a sharp single melting endotherm at 229.25 °C with an enthalpy of 57.42 J/g and 228.86 °C with an enthalpy of 42.57 J/g, respectively. These data clearly indicate that CLA exists as a single polymorph and that the polymorphic nature of the molecule does not change following exposure to a temperature of 85 °C for one hour. The sharp nature of the peak and the narrow width (WP) of 1.13 observed prior to exposure to heat reveal that CLA is a highly crystalline material. Following exposure to heat the WP increases to 1.79, indicating that heating CLA may disrupt the crystal structure of the molecule to some extent. In addition, the decreased onset temperature and enthalpy and less intensive endothermic peak for CLA following heating can be attributed to a decrease in the degree of crystallinity and the polymorphic nature of the molecule. Nevertheless, the peak observed in the thermogram is still sharp, revealing a lack of significant change in the crystalline nature of the molecule following exposure to a temperature of 85 °C. The WAXS data were used to support and facilitate interpretation of the DSC data that had been generated.

4.3.3 WAXS Characterization of CLA

WAXS was used as a complementary analytical tool to DSC to facilitate analysis and support the DSC data generated and reported in § 4.3.2. The WAXS diffraction patterns of CLA prior to and following exposure of the API to 85 °C for one hour are depicted in Figure 4.3.

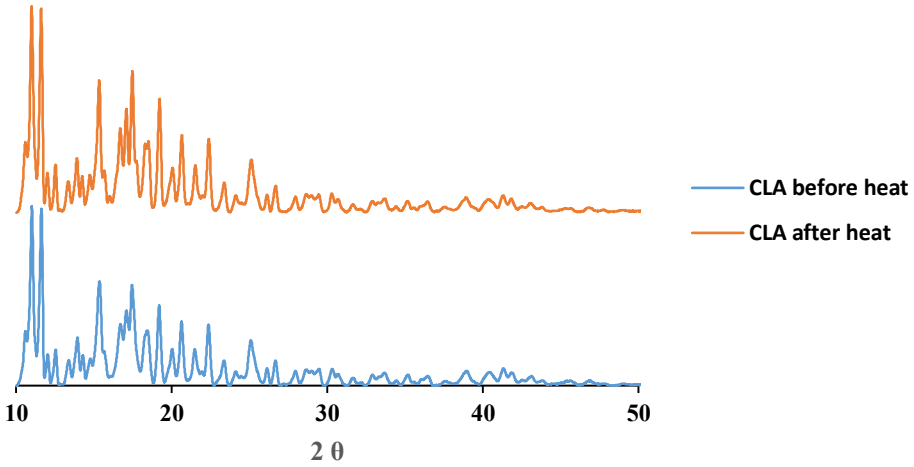

Figure 4.3 WAXS patterns for CLA prior to and following exposure to 85 °C for one hour

The WAXS diffraction patterns for CLA prior to and following exposure to heat show the presence of similar diffraction bands characteristic of the crystalline form of the molecule. The data confirm that CLA remains in a crystalline state following exposure to 85 °C for one hour. However, there appears to be a slight decrease in the sharpness of the diffraction pattern peaks for CLA following exposure to heat that may be attributed to a slight change or decrease in the degree of crystallinity of compound. These results are in agreement with those observed when evaluating the DSC data that revealed a slight disruption in the crystalline nature of CLA following exposure to 85 °C for one hour may have occurred.

4.3.4 Selection of Solid Lipids

The solubility of CLA in different solid lipids was determined with the primary aim of selecting a solid lipid with the best dissolution potential for CLA. The resultant data are listed in Table 4.2.

Table 4.2 The solubility of CLA in different solid lipid excipients

Solid lipid	Amount of lipid added (0.01 g CLA)	API solubility status
Compritol® 888 ATO	4.0 g	Insoluble
Precirol® ATO 5	4.0 g	Insoluble
Gelucire® 48/16	4.0 g	Insoluble
Cetyl palmitate	4.0 g	Insoluble
Stearic acid	3.0 g	Soluble
Geleol™	4.0 g	Insoluble

The chemical structures of the solid lipids investigated are depicted in Figure 4.4.

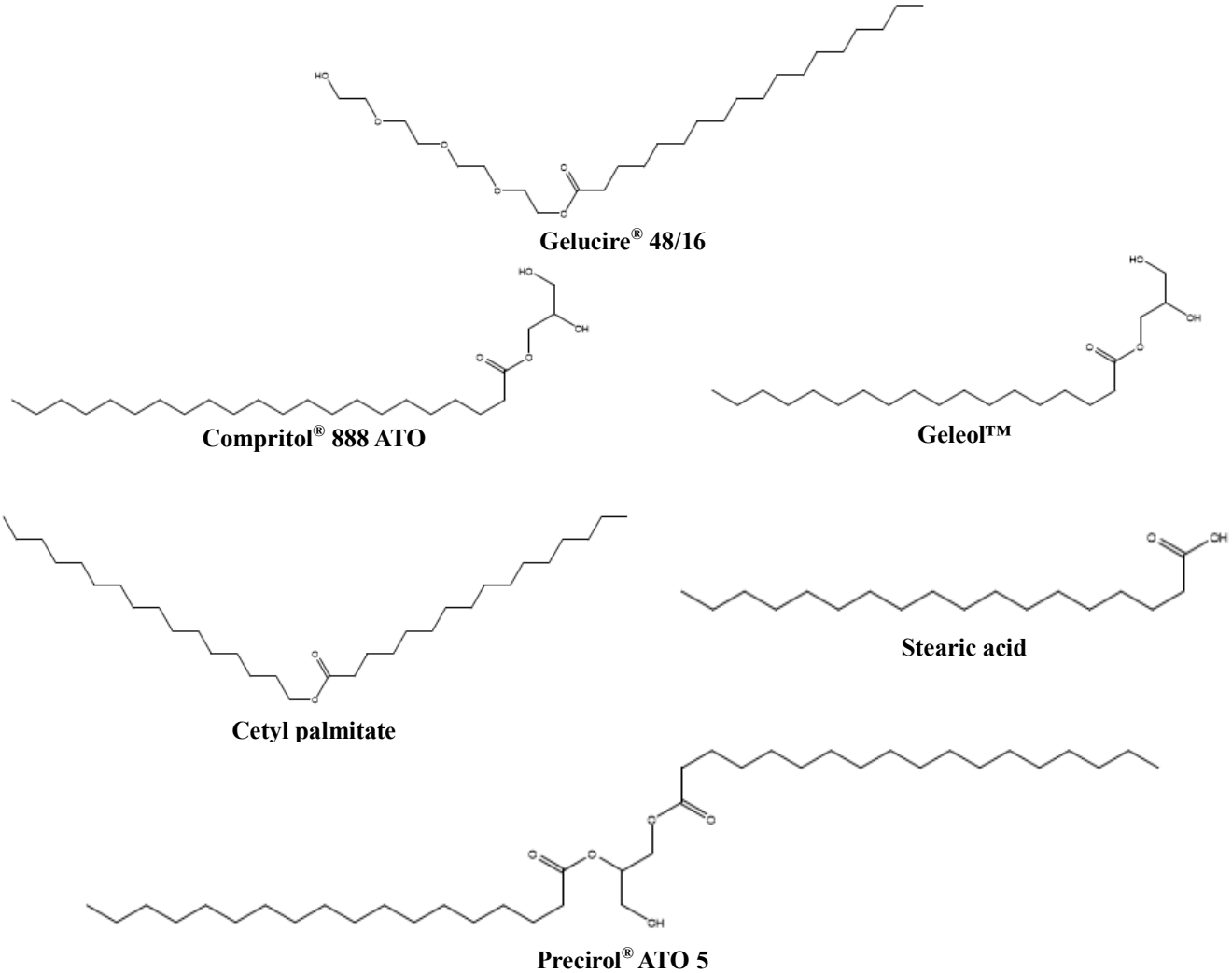

Figure 4.4 Chemical structures of solid lipids tested

The presence of oxygen and hydroxyl functional groups, such as those observed in Geleol™ and Compritol® 888 ATO, tend to increase the polarity and hydrogen bonding possibilities with compounds possibly contributing to the increase in API solubility in lipids [256]. In addition, the presence of mono- and diglycerides in the lipid matrices has promoted

dissolution of API [247]. Despite these reports, this was not the case with CLA as the data in Table 4.2 clearly suggests that CLA is most soluble in stearic acid (SA). Dissolution of an API in lipids is a complex process which is a function of different kinetic and thermodynamic factors that are affected by parameters such as interfacial tension, molecular volume, crystal structure, hydrophilicity, surface charge and/or charge density in addition to the physical and chemical environment of the reaction media used [261]. The solubility of ten compounds with different physicochemical profiles in ten lipid excipients was not successful in elucidating a clear link between the physicochemical properties of the API investigated and resultant solubility in the excipients tested [288].

4.3.5 Selection of Liquid Lipids

In contrast to SLN, the formulation of NLC requires the addition of a liquid lipid to the lipid mixture that results in the formation of a less ordered structural lipid matrix with imperfections that ultimately permit inclusion of larger amounts of API in the payload [171,276]. The identification and selection of a suitable liquid lipid for use in the formulation and manufacture of CLA-loaded NLC was therefore undertaken and the data are summarized in Table 4.3. The chemical structures of the liquid lipids are depicted in Figure 4.5.

Table 4.3 The solubility of CLA in different liquid lipid excipients

Liquid lipid l (2.0 g)	**Amount of CLA added**	**API solubility status**
Labrafac® PG	0.10 g	Insoluble
Transcutol® HP	0.20 g	Soluble
Capryol™ 90	0.10 g	Insoluble
Lauroglycol ® FCC	0.10 g	Insoluble

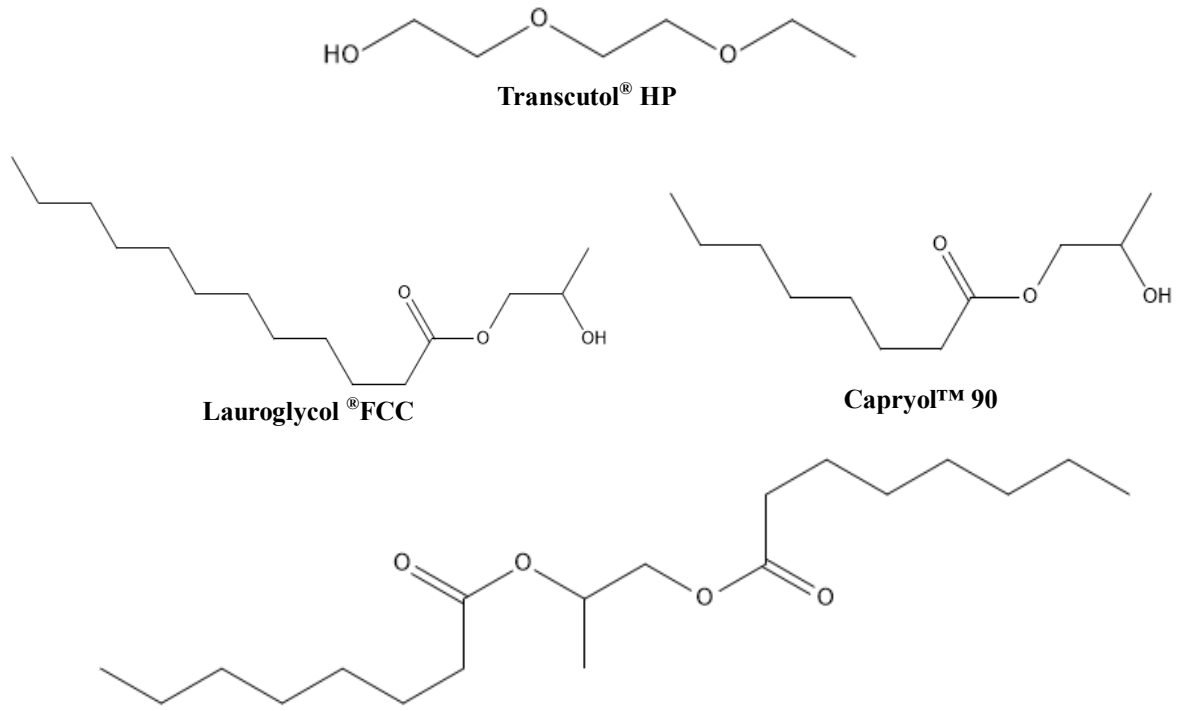

Figure 4.5 Chemical structures of liquid lipids tested

The data summarized in Table 2.3 reveal that CLA is highly soluble in Transcutol® HP (THP) which is a combination of diethylene glycol mono-ethyl ethers [289]. An investigation into the dispersion forces (δD), permanent dipole–permanent dipole forces (δP), and hydrogen bonding (δH) of the liquid lipids tested revealed that Transcutol® HP has the highest δP and δH values than the other lipids due to the presence of two ester and a single hydroxyl functional group in addition to possessing the shortest alkyl chain of all liquid lipids examined [256] resulting in the greatest dissolution potential for CLA. Consequently, THP was selected as the liquid lipid for use in formulation development and optimization studies for the preparation of CLA-loaded NLC.

4.3.6 Selection of a Binary Mixture of Solid and Liquid Lipids

Following the selection of SA and THP for evaluation in formulation development studies, the two lipids were mixed in different ratios in order to identify the best composition for a binary mixture for the formulation and manufacture of NLC containing CLA. Binary mixtures exhibiting melting points > 40 °C and were miscible were deemed suitable for consideration for use. The miscibility of the two lipids was established using DSC and also using visual assessment. The use of DSC to assess the miscibility of stearic acid and THP

was based on the fact that a depression in melting point of stearic acid would be observed following incorporation of THP into the lamellar structure of the solid lipid [245]. In terms of visual assessment, the presence of liquid lipid droplets on the filter paper used was considered a clear indication of poor miscibility of the lipids and any binary mixture in which droplets were observed was considered unsuitable for use. The influence of THP on the melting point and peak onset of SA in terms of liquid lipid content is depicted in Figure 4.6 and a summary of the melting events observed for the binary mixtures is summarized in Table 4.4.

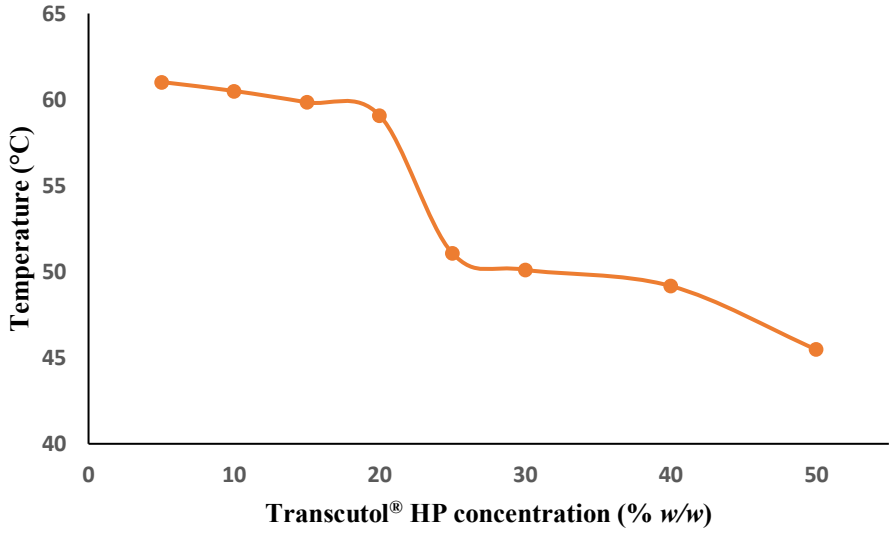

Figure 4.6 Impact of Transcutol® HP concentration on the melting point and peak onset for stearic acid

Table 4.4 DSC parameters for binary mixtures of stearic acid and Transcutol® HP following exposure to 85 °C for one hour

SA:THP (*w/w*)	Thermal event	Melting point (°C)	Onset (°C)	Enthalpy (J/g)
95:5	Endothermic	61.02	58.85	134.15
90:10	Endothermic	60.50	58.45	125.23
85:15	Endothermic	59.84	56.77	120.57
80:20	Endothermic	59.08	56.19	75.45
75:25	Endothermic	51.08	48.37	29.54
70:30	Endothermic	50.11	46.35	33.47
60:40	Endothermic	49.17	45.74	32.45
50:50	Endothermic	45.48	44.13	47.59

The data plotted in Figure 4.6 and listed in Table 4.4 reveal that all binary mixtures tested produced mixtures for which the melting point was > 40 °C. However, the onset melting point and enthalpy for the melting of stearic acid appears to decrease gradually with an increase in the amount of THP added to the mixture up to an amount of 20% *w/w* of the

liquid lipid. The gradual depression in the onset of melting of stearic acid when up to 20% *w/w* of THP is added to the solid lipid suggests that the two components are miscible when the liquid lipid is used in this concentration range. These results were confirmed by the presence of THP droplets on filter paper when amounts > 20% *w/w* of the liquid lipid were added to the mixture providing further evidence that THP and stearic acid are poorly miscible at these concentrations. The results suggest that a liquid lipid content of ≤ 20% *w/w* was optimal and concentrations higher than 20% *w/w* are likely to result in the production of immiscible mixtures. Consequently, a binary mixture in which 20% *w/w* Transcutol® HP and 80% *w/w* stearic acid was considered the most suitable combination for the formulation and manufacture of CLA-loaded NLC. In addition, the solubility of CLA in the selected binary mixture was investigated using the method described in § 4.2.2.6. The maximum solubility of CLA in a binary mixture of 80:20 (*w/w*) SA: THP was found to be 10% *w/w*.

4.3.7 Polymorphism and Crystallinity of Bulk Lipids

4.3.7.1 FT-IR Characterization of Stearic Acid

The FT-IR spectra generated for stearic acid prior to and following exposure to heat are depicted in Figure 4.7 and the relevant band assignments for the principal absorption peaks are summarized in Table 4.5.

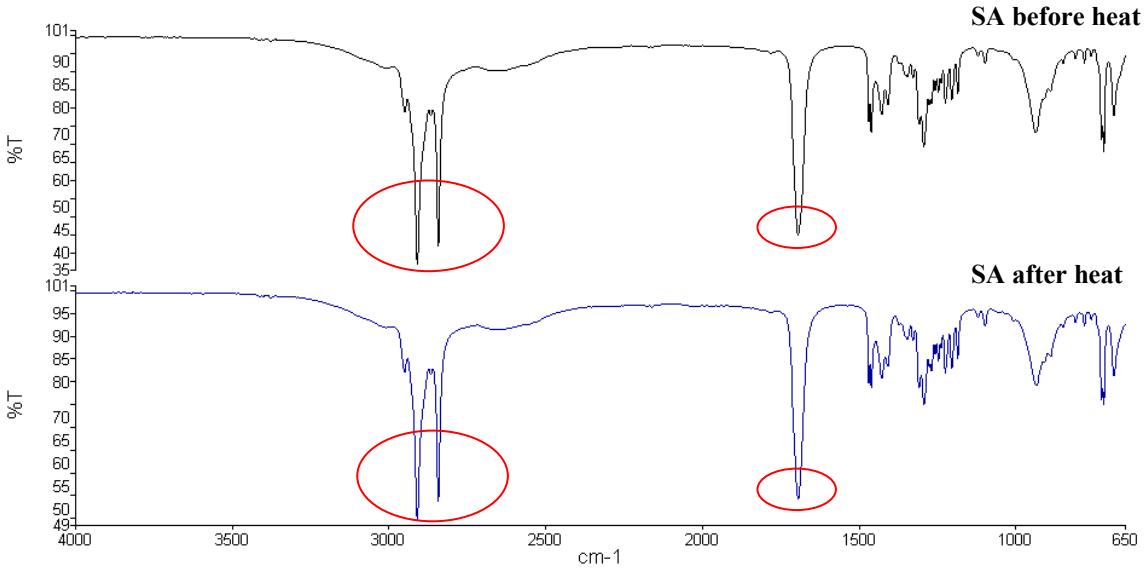

Figure 4.7 FT-IR spectra of SA prior to and following exposure to 85 °C for one hour

Table 4.5 FT-IR key frequency bands for stearic acid

Frequency (cm^{-1})	Vibrational Assignments
2918	C-H stretching of CH_2
2849	C-H stretching of CH_3
1698-1703	C=O stretching

The FT-IR spectrum of stearic acid reveals a characteristic peak at 1698 cm^{-1} due to a -C=O stretching vibration of that carboxyl group, 2918 cm^{-1} and 2849 cm^{-1} representing C-H stretching vibrations of $-CH_2$ and $-CH_3$, respectively that are characteristic of stearic acid [50,290]. Following exposure to heat, the major peaks (circled) of SA did not change, indicating that no vibrational energy changes of the chemical bonds were observed as depicted in Figure 4.7 implying the stability of the molecule during the manufacturing processes.

4.3.7.2 DSC Characterization of Stearic Acid

The DSC thermograms of SA prior to and following exposure to 85 °C for one hour are depicted in Figure 4.8 and the melting events observed are summarized in Table 4.6. Long-chain lipid compounds such as stearic acid, exhibit polymorphic transformations through crystallization in two or three different phases *viz.* α and/or β′, or α, β′ and/or β forms, respectively [279]. The melting and crystallization peaks of SA are broad, suggesting polymorphism that is consistent with the complex polymorphism usually observed for fatty acids. Particularly in SA, at least four polymorphic forms have been identified *viz.* A, B, C and E [291,292]. The thermogram generated prior to heating (run 1) reveals the presence of two peaks at an onset temperature and melting point of 60.25°C and 62.17°C, respectively. This is consistent with the presence of the B and C forms of SA. The B form is considered the most stable phase at room temperature [292] confirming that the solid lipid exists as a single polymorphic form prior to exposure to heat that transitions during and after heating. The DSC run following exposure of SA to heat reflects a melting point of 62.79°C with a melting enthalpy of 143.08 J/g, where the fraction corresponding to the B form of the lipid is practically absent. The higher input of energy post heat exposure is evident to lipid changes from a more unstable to a more stable polymorphic form, with the B form having been shown to irreversibly transform into form C at 46 °C [279,292].

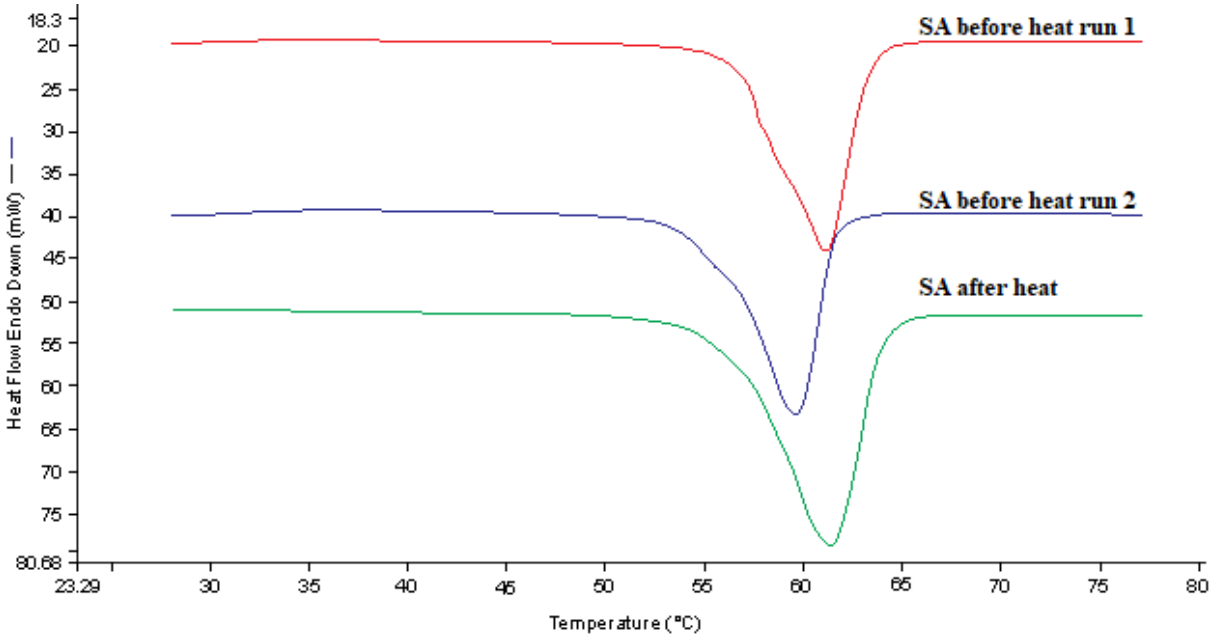

Figure 4.8 DSC thermograms of stearic acid generated prior to and following exposure to 85 °C for one hour

Table 4.6 DSC parameters for stearic acid prior to and following exposure to a temperature of 85 °C for one hour

Stearic acid	Thermal event	Onset (°C)	MP (°C)	Enthalpy (J/g)	WP (°C)
Prior to heating run 1	Endothermic	60.25	62.17	128.05	1.92
Prior to heating run 2	Endothermic	58.41	60.03	104.30	1.62
After heating	Endothermic	60.05	62.79	143.08	2.74

The thermogram generated following a second exposure of the sample to DSC analysis (SA run 2) reveals the presence of two peaks, with the onset temperature of the major peak decreasing from 60.25 to 58.41 °C indicating that SA undergoes an irreversible transition through recrystallization from the form B to form C polymorph following exposure to a temperature of 46 °C. It is also evident that the melting enthalpy of the thermogram following a second DSC run of 104.30 J/g is lower than the 128.05 J/g observed when the sample was subjected to a single DSC run which may be due to the fact that following an isothermal phase at 30 °C for approximately 10 minutes the molten lipid had not yet fully recrystallized.

Exposure of SA to 85 °C for one hour prior to DSC analysis revealed that a single endotherm peak was evident indicating that a single polymorphic form for SA existed which can be attributed to complete modification of the compound into to the form C polymorph. In

addition, the high enthalpy of 143.08 J/g suggests a more crystalline lattice structure of the form C polymorph when compared to the form B polymorph of SA.

4.3.7.3 WAXS Characterization of Stearic Acid

The WAXS diffraction patterns in which the lamellae arrangement of SA prior to and following exposure to 85 °C for one hour are depicted is reflected in Figure 4.9.

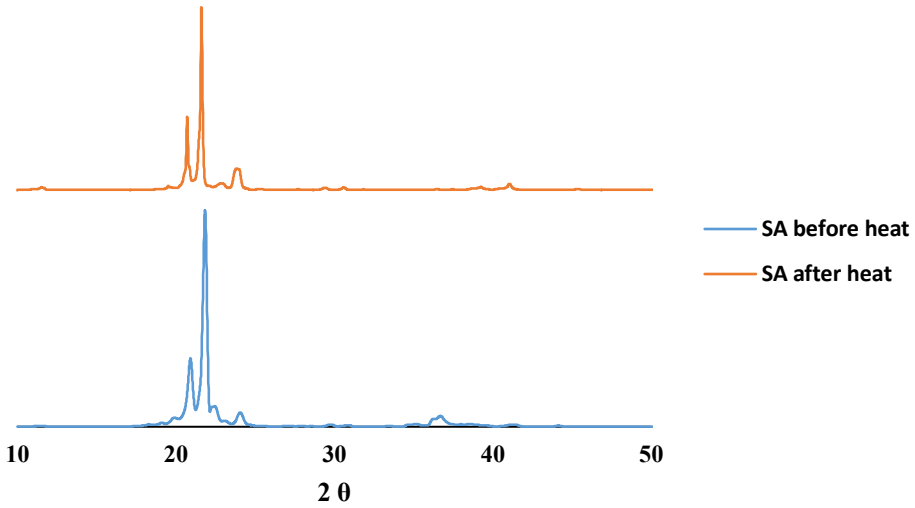

Figure 4.9 WAXS patterns for SA prior to and following exposure to 85 °C for one hour

The WAXS patterns at 21.5° (d = 0.421 nm) and 23.8° (d = 0.378 nm) prior to and following exposure to heat can be attributed to the crystalline structure of SA [279,290] and are indicative of the presence of the highly crystalline β'-modification form [171]. Although the diffraction patterns following exposure of SA to heat depict a reduced peak intensity, the peak width was generally similar albeit not as well defined, as that observed prior to exposure of the solid lipid to heat. However, it is evident that slight changes in the crystallinity of SA occur following heat exposure as observed in the DSC thermograms analysis and the absence of the diffraction band between 2θ (30°-40°) in the WAXS diffraction patterns. These results are in close agreement with those observed using DSC since the recorded melting point following exposure to heat was similar or slightly higher than that for the sample prior to exposure to heat. DSC and WAXS results for samples tested following exposure to heat are in agreement, as the decrease of the onset melting temperature corresponds to a decrease in the intensity of WAXS peaks.

4.3.7.4 FT-IR Characterization of Stearic Acid and Transcutol® HP

The FT-IR spectra of SA and that of a binary mixture of SA and THP in a 80:20 (*w/w*) ratio following exposure to 85 °C for one hour are depicted in Figure 4.10. It is clearly evident that both spectra reveal the presence of characteristic absorption bands for SA (circled) and that the incorporation of THP with SA did not result in the generation of additional peaks, confirming the lack of an interaction between these lipids. DSC analysis was also used to further investigate the impact of THP addition on the crystallinity and polymorphic nature of SA.

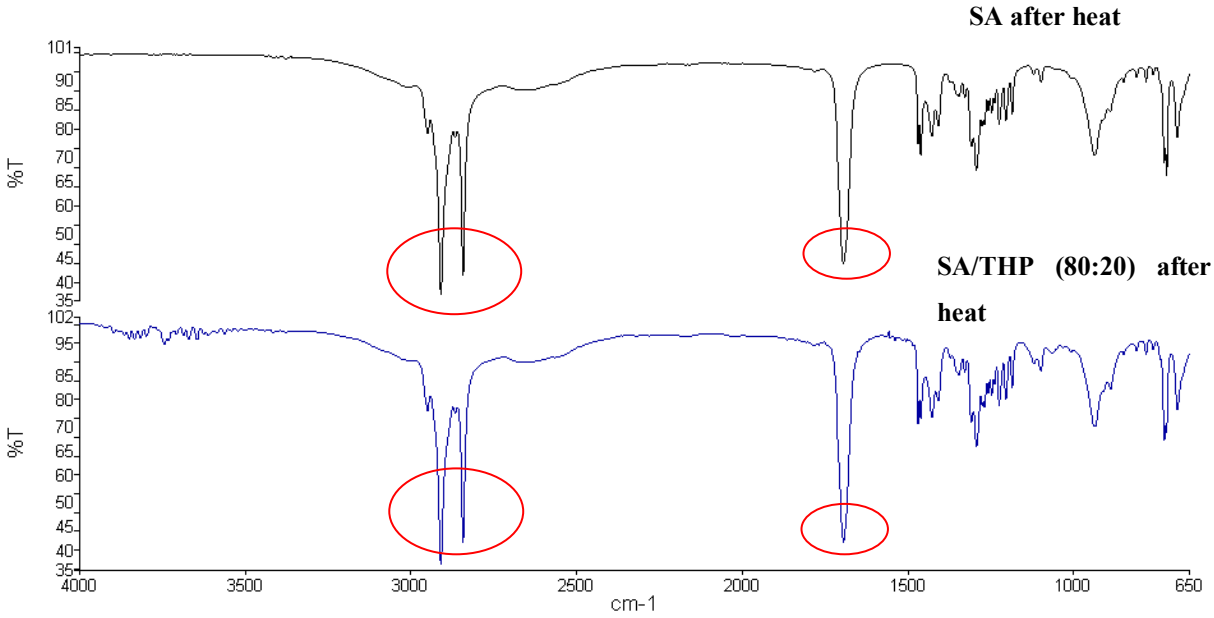

Figure 4.10 FT-IR spectra for SA and a 80:20 (*w/w*) binary mixture of SA and THP generated following exposure 85 °C for one hour

4.3.7.5 DSC Characterization of Stearic Acid and Transcutol® HP

The DSC thermogram generated for SA and for the 80:20 (*w/w*) binary mixture of SA and THP following exposure of both samples to 85 °C for one hour is depicted in Figure 4.11. The corresponding DSC parameters generated from the respective thermograms are summarized in Table 4.7.

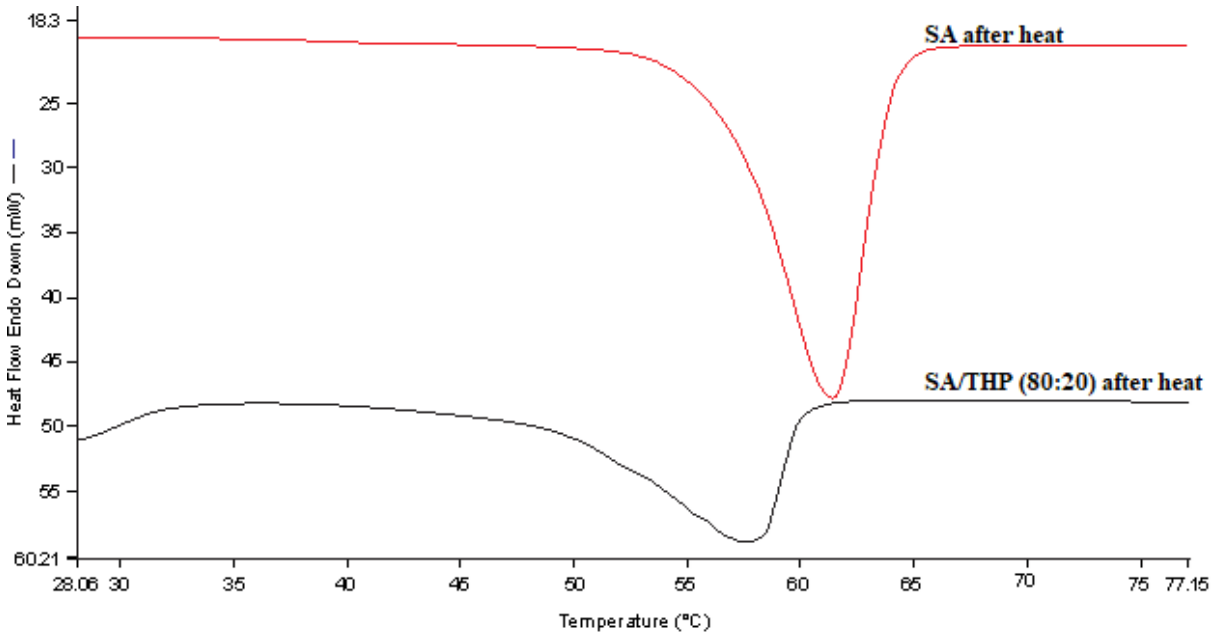

Figure 4.11 DSC thermograms of SA and a 80:20 (*w/w*) binary mixture of SA and THP (80:20) generated following exposure to 85 °C for one hour

Table 4.7 DSC parameters for SA and of an 80:20 (*w/w*) binary mixture of SA and THP generated following exposure to 85 °C for one hour

Material	Thermal event	Onset (°C)	MP (°C)	Enthalpy (J/g)	WP (°C)
SA after heating	Endothermic	60.05	62.79	143.08	2.74
SA/THP (80:20) after heating	Endothermic	56.23	59.10	86.20	2.87

The data reported in § 4.3.7.2 revealed that SA exists as the form B polymorph form prior to heating, and that following exposure to heat the polymorphic nature of SA changes to the more crystalline C modification. The DSC thermogram of the 80:20 (*w/w*) binary mixture of SA and THP following exposure to 85 °C for one hour reveals the presence of a broad single peak that is indicative of the existence of different polymorphic forms of SA, probably forms B and C, with form C the most likely dominant. The inclusion of THP into SA appears to create imperfections within the solid lipid matrix that consequently results in a depression of the melting point from 62.79 to 59.10 °C. The resultant binary mixture is also less crystalline in nature than SA alone, as confirmed by the decrease in enthalpy from 143.08 J/g to 86.20 J/g observed.

4.3.7.6 WAXS Characterization of Stearic Acid and Transcutol® HP

The WAXS diffraction patterns for the 80:20 (*w/w*) binary mixture of SA and THP generated following exposure of the lipid mixture to 85 °C for one hour is depicted in Figure 4.12. The WAXS profile for SA generated prior to heating was used as a reference diffractogram.

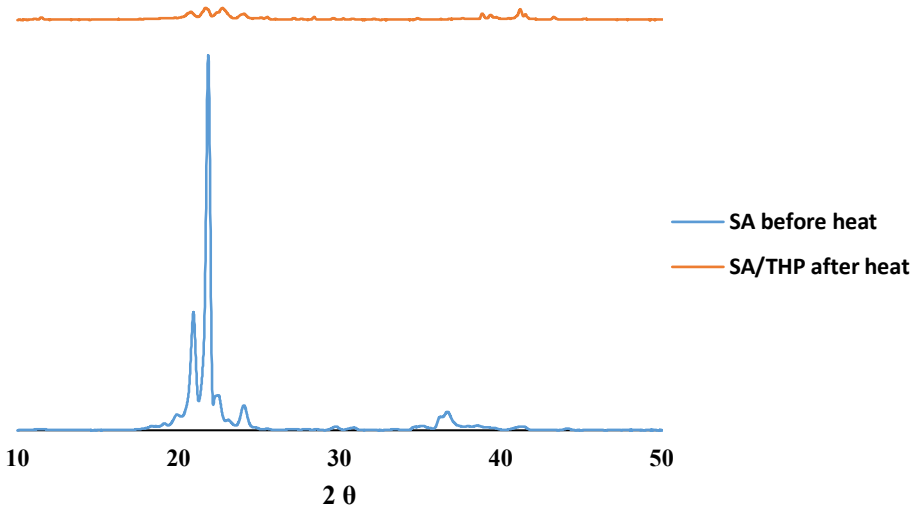

Figure 4.12 WAXS patterns for an 80:20 (*w/w*) binary mixture of SA and THP generated following exposure of the lipid mixture to 85 °C for one hour and that of SA prior to heat

Two scattering reflections for SA were observed prior to heating the material which corresponded to Bragg distances of 0.421 and 0.378 (§ 4.3.7.3). This is indicative of the presence of a highly crystalline form of SA. Evaluation of the diffractogram of the 80:20 (*w/w*) binary mixture of SA and THP following exposure to heat produced similar Bragg distances, with reduced intensity of the diffraction pattern and the absence of diffraction band between 2θ (30°- 40°) suggesting that heating the mixture produces different polymorphic forms. In addition, the aforementioned is evidence of the THP:SA mixture being completely amorphous. These data reflect the findings obtained when evaluating the DSC data in which the presence of a broad melting endotherm was observed for the binary mixture.

4.3.8 Interaction of Bulk Lipids with CLA

4.3.8.1 FT-IR Characterization of Stearic Acid and Clarithromycin

The FT-IR spectra of CLA and that of a 1:1 binary mixture of CLA and SA prior to heating is depicted in Figure 4.13.

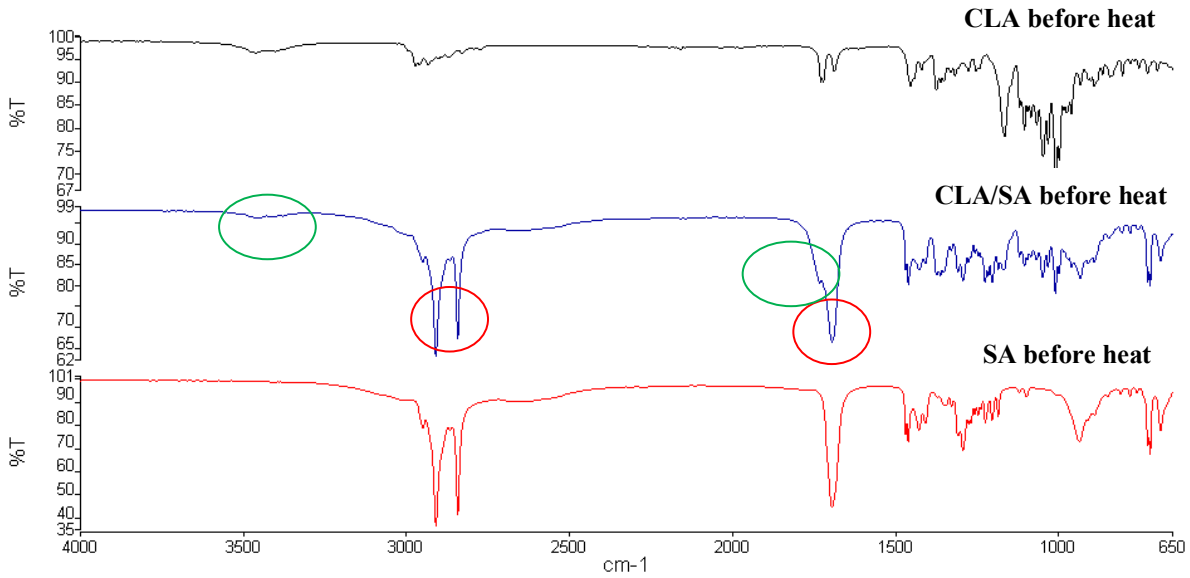

Figure 4.13 FT-IR spectra of CLA, SA and a 1:1binary mixture of CLA and SA generated prior to heating

The FTIR spectra depicted in Figure 4.13 reveal that additional peaks for SA in the 1:1 binary mixture with CLA occur in the frequency range between 2918 and 1698 cm^{-1}(circled in red). However, the spectrum of the 1:1 binary mixture also reveals the presence of frequency bands characteristic of CLA (circled in green), confirming the absence of an interaction between CLA and SA in this binary mixture. However, real time long term stability studies would be required to ensure this is indeed the case.

4.3.8.2 DSC Characterization of Stearic Acid and Clarithromycin

The DSC thermogram generated for the 1:1 binary mixture of CLA and SA prior to and following exposure to 85 °C for one hour is depicted in Figure 4.14 and the corresponding DSC parameters are summarized in Table 4.8.

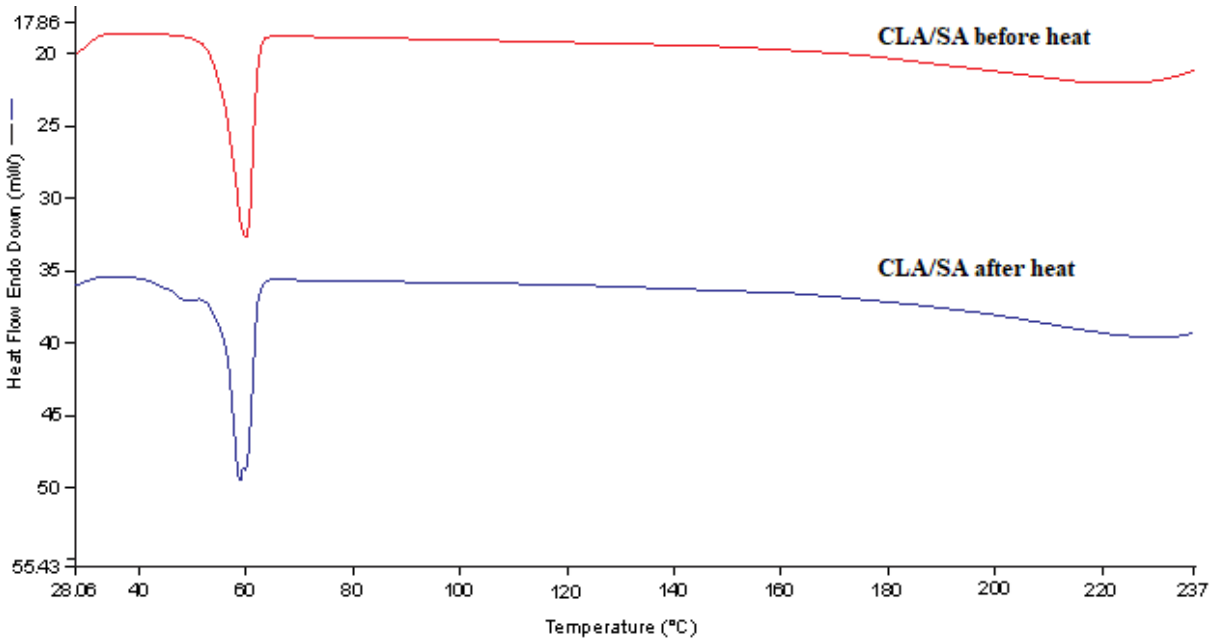

Figure 4.14 DSC thermogram for a 1:1 binary mixture of CLA and SA prior to and following exposure to 85 °C for one hour

Table 4.8 DSC parameters of a 1:1 binary mixture of CLA and SA prior to and following exposure to 85 °C for one hour

CLA and SA	Thermal event	Onset (°C)	MP (°C)	Enthalpy (J/g)	WP (°C)
Prior to heating	Endothermic	58.00	61.38	129.19	3.38
After heating	Endothermic	57.61	60.99	104.89	3.38

The DSC thermograms of the 1:1 binary mixture of CLA and SA prior to and following exposure to heat reveals the presence of endothermic peaks due to both CLA and SA that occur at the melting points reported in § 4.3.2 and 4.3.7.2, respectively suggesting clearly that no interaction between CLA and the SA occurs. However, the presence of SA in two polymorphic forms following exposure to heat suggests that disruption in the crystalline structure of SA after addition of CLA occurs that leads to a delay in the irreversible transformation of SA from the form B to form C polymorph as reported in § 4.3.7.2. Furthermore, the presence of the peak due to CLA prior to and following heating with the 1:1 binary mixture indicates that CLA is not completely dissolved in the SA and therefore remained in a crystalline state in the solid lipid when evaluated in these quantities as reported in § 4.3.3.

4.3.8.3 WAXS Characterization of Stearic Acid and Clarithromycin

The WAXS patterns of the 1:1 binary mixture of SA and CLA generated prior to and following exposure to 85 °C for one hour are depicted in Figure 4.15. The WAXS pattern for CLA following heating was used as a reference diffractogram to identify and distinguish the diffraction bands for CLA from those of the solid lipid matrix. The diffraction patterns of the 1:1 binary mixture prior to and following heating reveals the presence of a number of reflections consistent with those for CLA, which is an indication of the lack of complete dissolution of CLA in SA at the ratios used in these studies. CLA remains in a crystalline state following exposure to a temperature of 85 °C for one hour, which is consistent with the DSC data generated for the same samples.

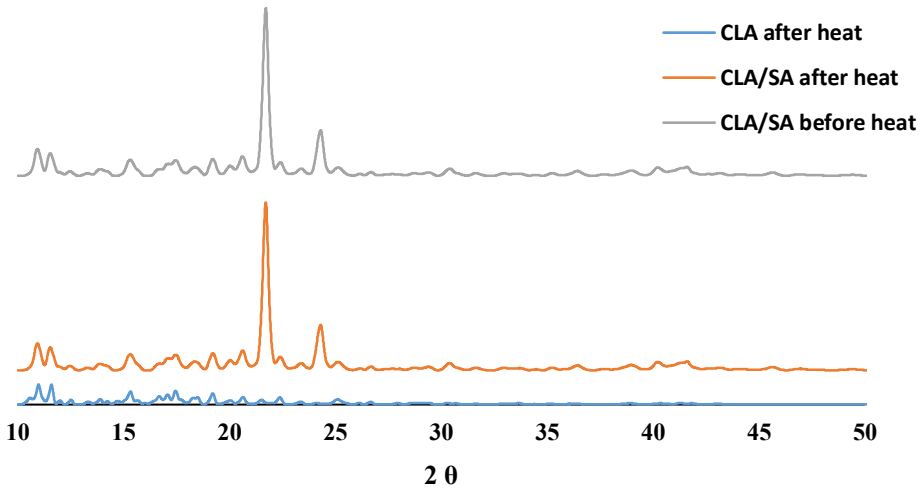

Figure 4.15 WAXS patterns of a 1:1 binary mixture of SA and CLA generated prior to and following exposure to 85 °C for one hour

4.3.8.4 FT-IR Characterization of CLA, SA and THP

The FT-IR spectra generated for CLA and SA prior to exposure to heat and that of a 1:1:1 ternary mixture of CLA, SA and THP following exposure to 85 °C for one hour are depicted in Figure 4.16. Evaluation of the FT-IR spectrum for the ternary mixture reveals the presence of peaks (circled in red) that are the same as those observed for SA, confirming that neither THP nor CLA appears to interact with the crystalline structure of the solid lipid. However, the presence of a peak representing the molecular vibrations for CLA (green) is most likely the result of CLA not forming a complete molecular dispersion in the ternary mixture.

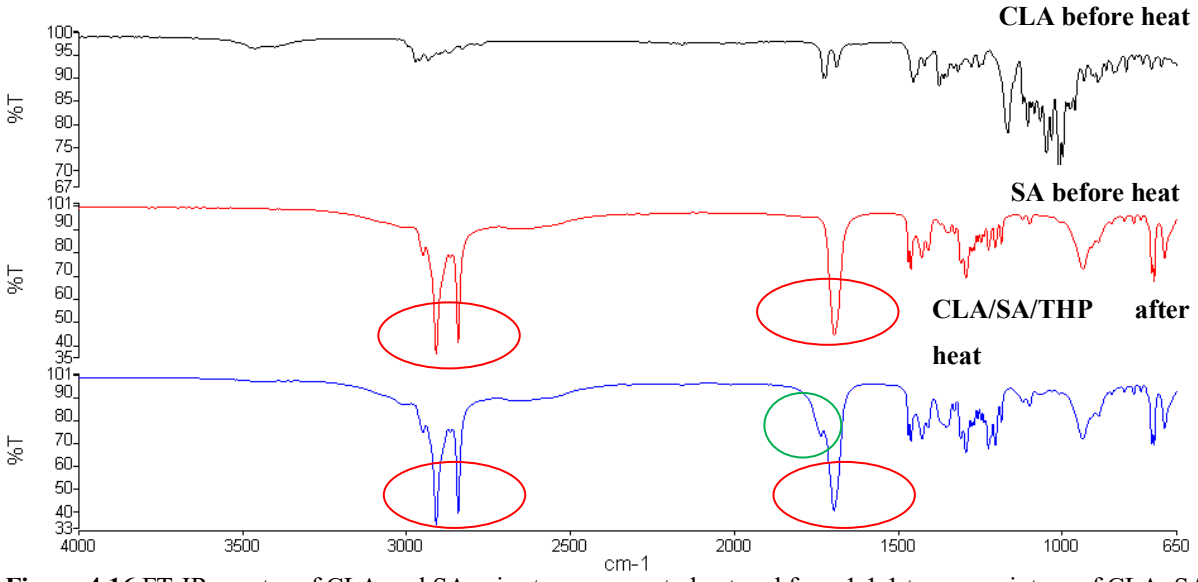

Figure 4.16 FT-IR spectra of CLA and SA prior to exposure to heat and for a 1:1:1 ternary mixture of CLA, SA and THP following exposure to 85 °C for one hour

4.3.8.5 DSC Characterization of CLA, SA and THP

The DSC thermogram generated for the 1:1:1 ternary mixture of CLA, SA and THP prior to and following exposure to 85 °C for one hour is depicted in Figure 4.17. The corresponding DSC parameters for these scans are summarized in Table 4.9.

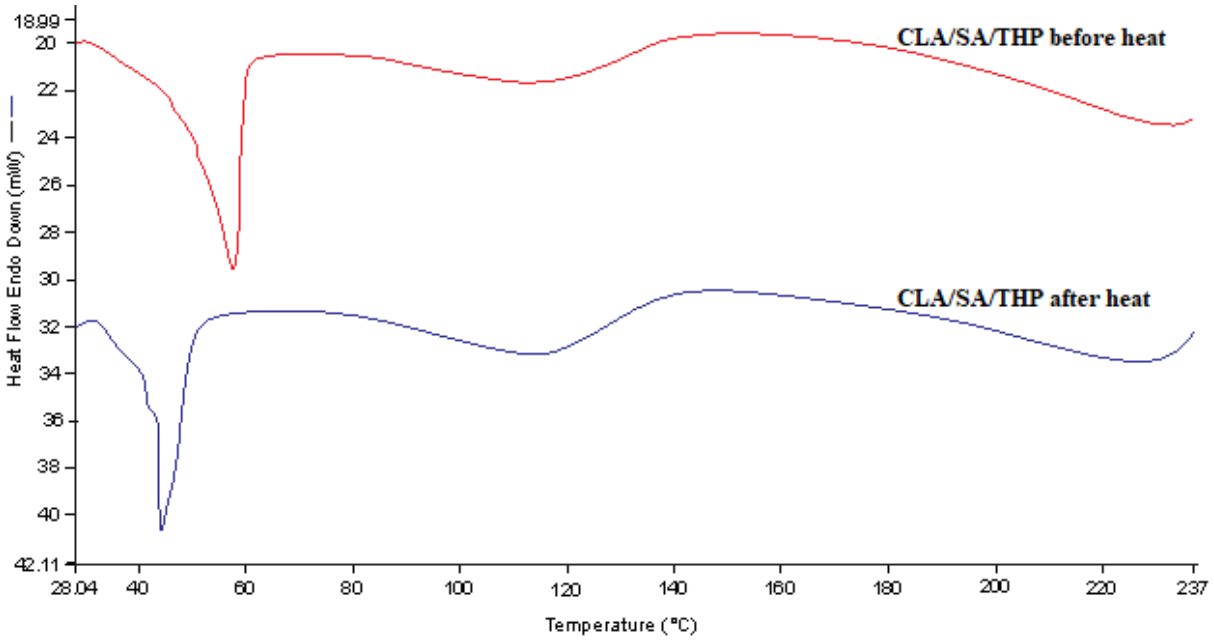

Figure 4.17 DSC thermogram for a 1:1:1 ternary mixture of CLA, SA and THP prior to and following exposure to 85 °C for one hour

Table 4.9 DSC parameters for a 1:1:1 ternary mixture of CLA, SA and THP prior to and following exposure to 85 °C for one hour

CLA/SA/THP	Thermal event	Onset (°C)	MP (°C)	Enthalpy (J/g)	WP (°C)
Prior to heating	Endothermic	56.65	58.68	68.70	2.03
After heating	Endothermic	43.84	47.78	39.68	3.94

The DSC thermograms of the 1:1:1 ternary sample prior to and following heating clearly reveals the presence of separate endothermic events consistent with those observed for the SA/THP lipid matrix and CLA. However, the markedly reduced enthalpy of 39.68 J/g for the 1:1:1 ternary mixture that was exposed to heat is indicative of the higher solubility of CLA in the molten lipid mixture while existing in a crystalline form in the solid lipid matrix or mixture of the solid and liquid lipids. This theoretically implies that a higher CLA payload will be achieved in NLC than SLN manufacture.

4.3.8.6 WAXS Characterization of CLA, SA and THP

The WAXS pattern generated for the 1:1:1 ternary mixture of CLA, SA and THP following exposure of the mixture to 85 °C for one hour, in addition to the WAXS pattern for CLA generated after exposure to heat, are depicted in Figure 4.18.

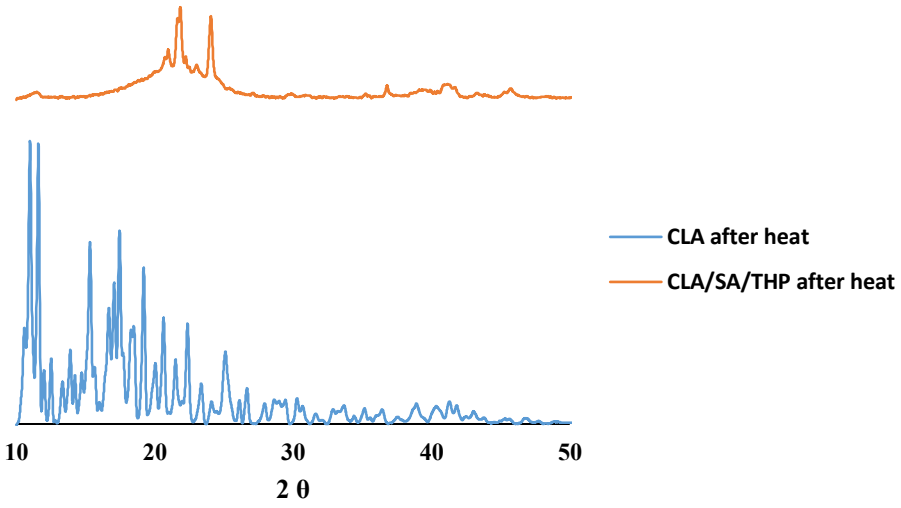

Figure 4.18 WAXS pattern of the 1:1:1 ternary mixture of CLA, SA and THP following exposure of the mixture 85 °C for one hour

The WAXS diffraction for the 1:1:1 ternary mixture revealed diffraction patterns matching those of CLA and SA. These data are consistent with those observed for DSC results analysis, and it can therefore be concluded that CLA is not completely dissolved in the

mixture of lipids and also exists in the crystalline form at the concentrations used in these studies. Formulation and manufacture of the nanocarriers will have to be optimized around API-solubility limits in the lipids as reported in § 4.3.4 and 4.3.5.

4.4 CONCLUSIONS

The pre-formulation studies undertaken reveal that CLA is thermostable when exposed to temperatures up to approximately 300 °C. Hot high-pressure homogenization (HHPH) and/or hot emulsion ultrasonication (HEUS) manufacturing procedures can therefore be used to manufacture CLA-loaded SLN and/or NLC. In addition, exposure of CLA to temperatures of approximately 85 °C for one hour revealed only slight disruptions in the crystallinity of CLA, without any changes to the polymorphic form of the molecule, confirming that the HHPH and/or HEUS would be suitable approaches for the manufacture of the nanoparticulate carrier technologies.

It is evident that CLA is poorly soluble in both solid and liquid lipids however a combination of stearic acid and Transcutol® HP exhibited the best solubilising potential for CLA of all the lipids tested. Stearic acid appears to exist in the B polymorphic form prior to exposure to heat however the form C polymorph was detected following heating at 85 °C for one hour. The best ratio for stearic acid and THP for the manufacture of CLA-NLC is an 80:20 (*w/w*) ratio of SA: THP. At this ratio the two lipids are miscible and assumed to have the greatest dissolution potential for CLA. DSC analysis revealed that the lipid samples had an onset of melting that is higher than the recommended minimum temperature for the formation and stability of lipid nanocarriers of 40 °C.

The addition of THP to SA resulted in a delay in the polymorphic transition of the solid lipid from the form B polymorph to the irreversible C polymorphic modification. In addition, the inclusion of THP into SA appears to create imperfections within the solid lipid matrix that consequently results in a melting point depression of the 1:1 binary mixture which could result in formulations with a higher API payload and low API leakage upon long term storage. Furthermore, these studies have revealed that CLA exists in a crystalline state when dispersed at high drug concentrations of 50% *w/w* in SA or at 33.3% *w/w* in a 1:1 binary

mixture of stearic acid and Transcutol® HP. It is also evident that potential interactions between CLA and the lipids did not occur however, real-time long-term stability studies would be required to ensure this is indeed the case.

Theoretically the relatively high solubility of CLA in THP in comparison to SA suggests that NLC are likely to have a higher LC and EE for CLA than SLN. Consequently, it was considered logical to investigate the feasibility of incorporating CLA into NLC and that investigation into the production of SLN not be considered as the production of these might not produce a delivery technology with the requisite EE and LC for CLA. Furthermore, in a study comparing HPH *versus* ultrasound in preparation, characterization and biocompatibility studies of risperidone-loaded SLN, the authors concluded that although HPH is a suitable method for SLN production in laboratory and scale-up activities, ultrasound could be used as an appropriate method for SLN production due to the ease of preparation and low cost of the required equipment [293]. Due to the erratic availability of municipal water required for cooling of the homogenizer block when using HHPH, HEUS was therefore used as the manufacturing approach for the production of CLA loaded nanocarriers.

CHAPTER 5

FORMULATION, DEVELOPMENT AND ASSESSMENT OF MUCO-ADHESIVE LIPID CLARITHROMYCIN CARRIERS FOR OPHTHALMIC USE

5.1 INTRODUCTION

The eye is an intricate organ with unique anatomy and physiology. Efficient protective mechanisms of the eye, such as the blinking reflex, lachrimal secretion and nasolacrimal drainage make it difficult to achieve the necessary target concentration at the site of treatment. Furthermore, the anatomy and barrier properties of the cornea, impede rapid absorption of active pharmaceutical ingredients (API) into the organ [294–296]. A number of ocular diseases are treated using topically applied or systemically delivered medicines [296,297]. The ease of administration and affordability make topical application of ocular medicine the preferred method for treatment of ocular disorders which affect the anterior segment of the eye. Anatomical and physiological barriers prevent drugs from reaching the posterior segment of the eye, particularly the choroid and retina [297,298]. The structure of the eye in which the anterior and posterior segments are shown is depicted in Figure 5.1 [297].

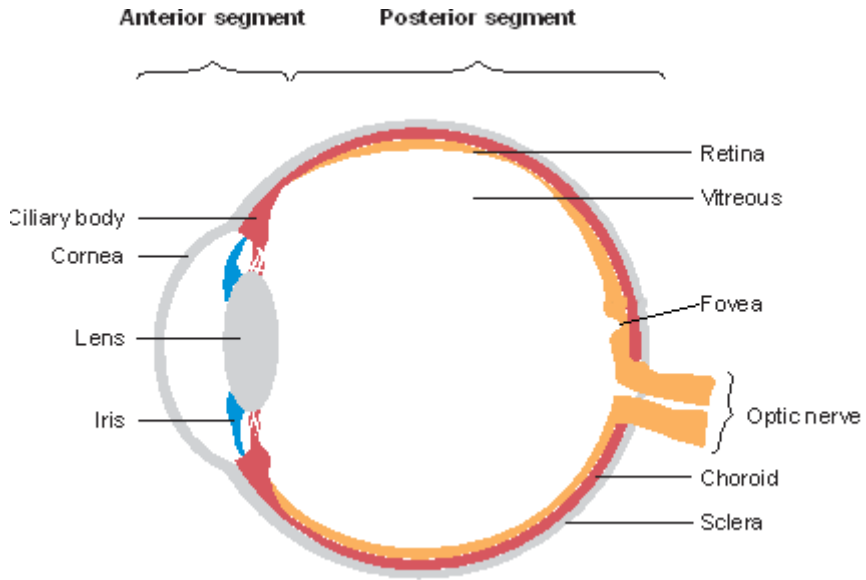

Figure 5.1 Structure of the eye (adapted from [296])

The tear film is comprised of three layers *viz*. a lipid, aqueous and mucous layer. The lipid layer is the outermost layer, which prevents evaporation of the aqueous layer, maintains surface tension of the tear film and lubricates the eyeball. The tear film is largely located in the aqueous layer, which maintains a smooth ocular surface and provides oxygen to the epithelial cells of the cornea. The mucous layer is important as it facilitates the corneal epithelium change from hydrophobic to hydrophilic by forming a hydrophilic gel layer that moves over the ocular surface, thereby allowing uniform distribution of the aqueous layer across the ocular surface. This aids in clearing cell debris, foreign bodies and pathogens while acting as a barrier to API delivery systems [299].

As much as topical instillation of eye-drops is non-invasive and the widely preferred mode for treating diseases affecting the anterior segment of the eye, elimination of the administered drops, irrespective of the volume instilled, occurs rapidly, usually within five to six minutes following administration. Therefore only a small amount of approximately 1–3% of the instilled drops may reach intraocular tissues. In order to maintain minimum inhibitory anti-bacterial concentrations there is a need to dose ocular formulations frequently which may result in poor patient adherence [295,297,300]. It is difficult to deliver and sustain the concentration of API in the precorneal region of the eye and ensure sufficient API reaches the target tissue(s). In order to exert an effective local effect, the residence time of the active compound in the tear film, should be increased. Furthermore, the use of once-a-day dosed ocular formulations may improve patient adherence. Consequently ophthalmic dosage forms such as viscous solutions, suspensions, emulsions, ointments, aqueous gels and polymeric inserts have been developed in an attempt to increase the bioavailability of API delivered *via* the ophthalmic route, through prolonging the contact time of formulation with the corneal/conjunctival epithelium [294,300].

Micro- and nanoparticle-based delivery systems have been used to increase the retention and contact time of API on ocular surfaces by interaction of functional groups and surface charges of micro- and nanoparticles with the mucin layer on ocular surfaces which prolong the interaction of the formulation at the corneal surface [301]. Furthermore encapsulation of API into nanoparticles to protect the compound from enzymatic degradation has been

successful, thereby permitting the use of lower doses to achieve a therapeutic effect whilst avoiding adverse events [302]. Nanoparticles are colloidal carriers of 10 to 1000 nm dimension and are gaining attention for ocular drug delivery applications as researchers attempt to develop nanoparticles for delivery of API to anterior and posterior ocular tissue(s) [303–308]. Lipid nanoparticles loaded with API have an ability to cross the corneal epithelium effectively, due to the lipophilic properties of the carrier technologies [309]. Lipid-based nanocarriers exhibit properties similar to films of tears and following instillation, the continuous phase is able to hydrate the aqueous layer of the film and moisten the corneal epithelium. As oil droplets are disrupted, encapsulated API is released permitting the oil phase to coalesce and increase the natural lipid layer in the ocular region, reducing fluid loss by evaporation. In addition the use of generally regarded as safe (GRAS) lipids for the production of the nanocarriers results in excellent ocular biocompatibility [299]. The use of biocompatible lipids for nanoencapsulation is an important approach for enhancing the bioavailability of encapsulated API and minimizes natural physiologic and manufacturing process effects which in turn improve dosing outcomes, due to the controlled delivery of API whilst permitting administration of low doses and exhibiting an improved shelf-life thereby reducing the potential emergence of side effects [310]. To date, state of the art lipid formulations of clarithromycin (CLA) have been manufactured as solid lipid nanoparticles (SLN) in an attempt to improve the antibacterial activity of encapsulated API against *Staphylococcus aureus* organisms [50,311].

Many polysaccharides exhibit muco-adhesive properties at low concentration and viscosity, making them suitable additives to prolong the contact time of ocular technologies with ophthalmic tissues thereby permitting reduced dosing frequencies and ultimately, enhancement of patient adherence. The ocular disposition, pharmacokinetics, efficacy and safety of nanoparticle-formulations for ophthalmic use has been documented [312] revealing that the products tested were well tolerated, with enhanced corneal and aqueous humor concentrations, improved ocular bioavailability and therapeutic efficacy observed when compared to the use of commercially available eye drops [312]. Polyethylene glycol (PEG), chitosan and hyaluronic acid have been investigated as precorneal residence time enhancers in nanoparticle products [312] of which the muco-adhesive properties of chitosan are well documented, with a variety of mechanisms of activity including the formation of hydrogen bonds and electrostatic interaction between positively charged amines and negatively charged

sialic acid residues of mucin, postulated. However, the limited solubility under physiological conditions of chitosan is a major drawback for successful translation into clinical practice requiring the chemical reactivity of the polymer to be harnessed to overcome this challenge [313]. PEG coating of nanoparticles enhances the transport of nanomaterials across the ocular epithelium by imparting muco-penetrative properties to the experimental technology [314]. Consequently, in an attempt to investigate possible muco-adhesive properties of NLC in these studies, PEG was used to coat the NLC.

The formulation for an NLC dispersion requires the inclusion of one or more emulsifying agents, solid and liquid lipids and water to impart and ensure stability to the carrier system as discussed in Chapter 4 of this thesis. The selection of surfactant is primarily based on the intended purpose of the formulation under development. As the objective of these studies was to develop muco-adhesive NLC for potential ophthalmic use it was necessary that a surfactant or combination of surfactants that exhibited a high degree of ocular tolerability, was identified. Tween®20 and Brij®35 are most effective in increasing corneal permeability [315] and exhibit low toxicity to epithelial cells of the rabbit cornea [316]. Consequently Tween®20 was selected for formulation development activities to produce CLA-loaded NLC as it is readily available, exhibits little or no cytotoxicity and is affordable. Stearic acid (SA) and Transcutol® HP (THP) were selected and used as the solid and liquid lipid for the NLC, as described in Chapter 4, *vide infra*.

5.2 MATERIALS AND METHODS

5.2.1 Materials

CLA was purchased from Skyrun Industrial Co. Limited (Taizhou, China). Stearic acid, PEG 6000, Tween® 20 (polysorbate 20) and porcine stomach type II mucin were purchased from Sigma Aldrich Chemical Co. (Milwaukee, WI, USA). Transcutol® HP (diethylene glycol monoethyl ether) was donated by Gattefossé SAS (Gattefossé SAS, Saint-Priest Cedex, France). Glycerine was purchased from Barrs Pharmaceutical Industries (Ndabeni, Cape Town, South Africa). HPLC grade water was prepared as described in § 2.2.3.1 in Chapter 2 of this thesis. All formulation excipients evaluated have GRAS status and are non-toxic and non-irritant [317]. All chemicals were used as received without further purification.

5.2.2 Methods

5.2.2.1 Experimental Design and Response Surface Methodology

Response Surface Methodology (RSM) includes a group of mathematical and statistical approaches used to develop, identify and elucidate appropriate functional relationships between a number of input variables and associated response(s). The responses can be plotted as 3- dimensional (3D) and/or contour plots to facilitate visualization of the shape of the resultant response surface(s) [318]. When using RSM as an optimization approach, different stages are followed during application of the design [319]. Initially independent variables likely to exhibit a major effect on the experimental system under investigation are selected with due consideration of the study objectives in addition to use of experience. The experimental design to be used is selected and the experiments conducted according to a pre-defined experimental matrix. The data are reduced by fitting data to polynomial functions, and the fitness of the model then established. Final analysis includes verification of the possibility of initiating steps necessary to perform displacement in the direction of an optimal region and subsequently generating an optimum value(s) for each of the variables investigated as discussed in Chapter 2 *vide infra*.

5.2.2.2 Manufacture of CLA-loaded NLC Formulations

CLA-loaded NLC were manufactured by hot emulsification ultrasonication (HEUS) [237,238]. A schematic representation of the manufacturing process is depicted in Figure 5.2. Briefly, the lipid phase containing CLA was heated to approximately 85 °C. An aqueous phase of Tween® 20 with or without PEG 6000 was heated to the same temperature, prior to dispersion using a Model T 18 Ultra-Turrax® BS2 homogenizer (Janke & Kunkel GmbH and Co KG, Staufen, Germany) in the molten lipid phase at 6000 rpm for one minute to produce a pre-emulsion. The pre-emulsion was subjected to ultrasound using a Sonopuls® HD 4200 probe sonicator (Bandelin, Berlin, Germany) fitted with a titanium flat tip (Bandelin, Berlin, Germany) at predetermined amplitude for a specific time. The nano-emulsion formed was filled into 100 mL siliconized glass vials (Lasec®, Port Elizabeth, South Africa), sealed and cooled to room temperature (22 °C) to permit recrystallization and *in situ* formation of CLA-loaded NLC. All batches produced were 100 mL in volume and were characterized 24 hours

after manufacture.

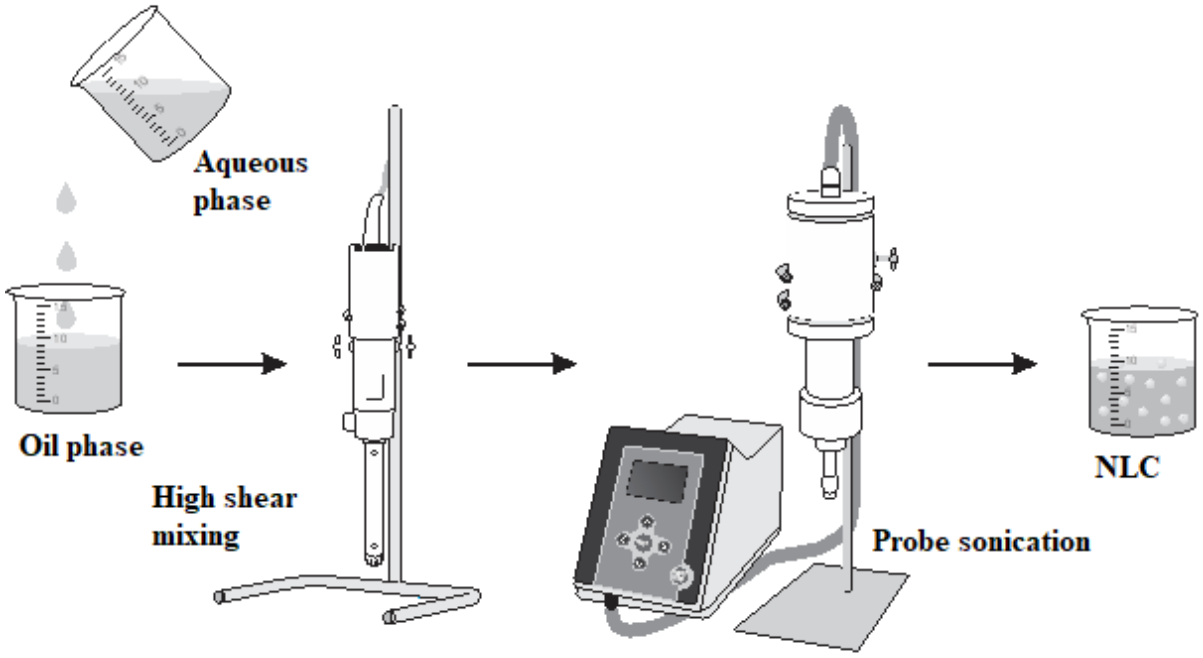

Figure 5.2 Schematic representation of the manufacture of CLA-NLC by HEUS

5.2.2.2.1 Screening of Formulation Parameters using Box Behnken Design (BBD)

Design of Experiments (DoE), specifically a BBD was used to investigate the impact of five input variables on the production of CLA-loaded NLC using HEUS. The variables tested included lipid content, Tween® 20, PEG 6000, amplitude and sonication time. The number of experimental runs for the BBD was established using Version 12 Design Expert® statistical software (Stat-Ease Inc., Minneapolis, MN, USA) and the concentration range, levels including composition for the input variables investigated are summarized in Table 5.1.

Table 5.1 Input variables and experimental design (BBD) values

Variable		Level		
Input		**-1**	**0**	**+1**
Lipids	**% *w/w***	1	3	5
Tween® 20	**% *w/w***	1	3	5
Sonication time	**min**	10	20	30
Amplitude	**%**	10	55	100
PEG 6000	**% *w/w***	0	1	2
Output monitored		**Constraint**		
EE	**%**	maximize		
LC	**%**	maximize		
ZP	**mV**	minimize		
PS	**nm**	minimize		
PDI		minimize		

HEUS was used to produce the NLC as described in §5.2.2.2. In total, forty-six (46) formulations with 10% *w/w* CLA loading relative to the lipid content, were manufactured in 100 mL batches. The Critical Quality Attributes (CQA) monitored were particle size (PS), Zeta Potential (ZP), polydispersity index (PDI), encapsulation efficiency (EE) and loading capacity (LC). Some test formulations formed a gel-like structure following 24 hours storage at 22 °C and were therefore not subject to further testing or analysis. The BBD is insensitive to outliers and missing data [320,321], consequently the experiments were continued in an attempt to monitor the target product attributes, as originally intended. Numerical optimization was used in an attempt to optimize the formulations however, the predicted formulation when manufactured, formed a cream gel-like structure following storage for 24 hours at room temperature (22 °C). Consequently, the experimental data generated using the BBD were rather used to identify a formulation composition which would produce a product that would meet the target CQA *viz.* PS in the nano-range, PDI < 0.5, ZP ≥ ± 30 mV, and EE > 80%. The formulation composition identified was then used for the subsequent optimization of the manufacturing parameters *viz.* sonication time and amplitude. ZP values of ± 30 mV are targeted to ensure NLC stabilized through electrostatic repulsion are produced, so as to prevent aggregation [322]. Stable nanocarriers for which the ZP was < 30 mV have been manufactured using Tween® 80 [244]. Polysorbate surfactants provide stability through both electrostatic and steric hindrance mechanisms mitigating the need for a target ZP of ± 30 mV to ensure stability of dispersions [244,323].

5.2.2.2.2 Optimization of Manufacturing Parameters using Central Composite Design (CCD)

Following identification of the most ideal formulation composition based on the CQA data,

process optimization in terms of the manufacturing parameters was undertaken in a specific attempt to increase EE, further reduce the PS and PDI and produce a stable formulation. Sonication time and amplitude of ultrasonic waves are important parameters when fabricating nanoparticles of small size using ultrasound [322]. An increase in time and amplitude of sonication results in a decrease in particle size [324]. However, high sonication amplitudes have also been shown to produce lipid nanoparticles of increased size, due to the formation of aggregates [322,324,325]. Consequently, the impact of sonication time and amplitude on the CQA of the NLC was investigated. The number of experimental runs required for the CCD was established using version 12 Design Expert® statistical software (Stat-Ease Inc., Minneapolis, MN, USA) and the input variables and ranges tested are summarized in Table 5.2.

Table 5.2 Variables and experimental design (CCD) values

Variable		**Level**			
Input		**-α**	**-1**	**1**	**+α**
Sonication time	**min**	5.86	10	30	34.14
Amplitude	**%**	12.57	25	85	97.43
Output monitored		**Constraints**			
EE	**%**	maximize			
LC	**%**	maximize			
ZP	**mV**	minimize			
PS	**nm**	minimize			
PDI		minimize			

5.2.2.2.3 pH and Osmolarity

The human eye can tolerate formulations of osmolality between 250–450 mOsm/kg and pH of 3.5–10.5 [326,327]. However, the extreme values of the pH range are unlikely considered for use, with formulators aiming for pH values that are aligned with lacrimal fluid isotonicity. The osmolarity of the optimized CLA-loaded NLC formulations was adjusted to physiological levels by adding glycerine and measuring the freezing point depression using a calibrated Gonotec Osmomat 3000 osmometer (Gonotec, Berlin, Germany). The pH of the nanocarrier suspensions was monitored at 22 °C using a calibrated Model GLP 20+ basic pH-meter (Crison Instruments, Barcelona, Spain).

5.2.2.3 Formulation Characterization

5.2.2.3.1 Particle size (PS), Polydispersity Index (PDI) and Zeta Potential (ZP)

The mean PS and PDI of NLC were measured using a Model Nano-ZS Zetasizer (Malvern Instruments Ltd, Worcestershire, UK) with the instrument set to photon correlation spectroscopy (PCS) mode. Approximately 30 µL of an aqueous dispersion of the NLC was diluted with 10 mL HPLC-grade water prior to analysis. The sample was placed into a 10 x 10 x 45 mm polystyrene cell and all measurements were performed in replicate (n = 10) at 25 °C using a standard 4 mW laser set at 633 nm at a scattering angle of 90°. Analysis of PCS data was achieved using Mie theory with the real and imaginary refractive indices set at 1.456 and 0.01, respectively.

The ZP was determined using a model Nano-ZS Zetasizer (Malvern Instruments Ltd, Worcestershire, UK) set in the laser doppler anemometry (LDA) mode at a wavelength of 633 nm. The sample was prepared as described for PS and PDI analysis and was placed into folded capillary cells for measurement. All measurements (n = 10) were performed at an applied field strength of 20 V/cm and the Helmholtz-Smoluchowsky equation [328] (Equation 5.1) was used, *in situ*, to calculate the ZP of each sample.

$$\gamma = \frac{\varepsilon_r \varepsilon_o}{\eta} \zeta \qquad \textbf{Equation 5.1}$$

Where,
γ = electrophoretic mobility
ε_r = relative permittivity
ε_o = permittivity of a vacuum
η = viscosity of surrounding fluid
ζ = Zeta Potential

5.2.2.3.2 Encapsulation Efficiency (EE) and Loading Capacity (LC)

The LC and EE for CLA in the NLC was investigated using a validated RP-HPLC-ECD method [63] (Chapter 3 *vide infra*) following filtration of an aqueous dispersion of the NLC using Centrisart® filter tubes (Sartorius AG, Goettingen, Germany). The filter tubes were fitted with a filter membrane of 200 KDa molecular cut-off of at the base of the sample recovery chamber. Approximately 2.5 mL of the aqueous dispersion of NLC was placed into the outer chamber of the tube after which the sample recovery chamber was fitted. The unit was centrifuged at 2500 rpm for 20 minutes using a Model HN-SII IEC centrifuge (Damon, Needham HTS, MA, USA) prior to analysis for CLA in the aqueous filtrate using a validated

RP-HPLC [63]. The LC and EE of CLA in the formulations was calculated using Equations 5.2 and 5.3 [63].

$$LC = \frac{W_a - W_s}{W_a - W_s + W_L} \, x \, 100 \qquad \textbf{Equation 5.2}$$

$$EE = \frac{W_a - W_s}{W_a} \, x \, 100 \qquad \textbf{Equation 5.3}$$

Where,
W_a = weight of CLA added to formulation
W_s = weight of CLA in supernatant after centrifugation
W_L = weight of lipid added to the formulation

5.2.2.3.3 Scanning Electron Microscopy (SEM) and Energy-Dispersive X-ray Spectroscopy (EDX)

SEM was used to evaluate the surface morphology of the NLC. Prior to SEM the aqueous dispersions of NLC were lyophilized without a cryoprotectant using a Vacutec freeze drier (Labconco®, Corp, Kansas City, Missouri, USA) at -51 °C and 0.315 Torr. Following lyophilization the powdered sample was mounted onto a carbon stub and sputter-coated with gold under vacuum (0.25 Torr) for 15 minutes using a sputter-coater (Balzers Union Ltd, Balzers, Lichtenstein). The sample was visualized using a Model TS 5136 LM Vega® Tescan SEM (Tescan, Vega LMU, Czechoslovakia Republic) at a voltage of 20 kV.

EDX was used for elemental analysis and determination of the presence of any metals on the surface of the lyophilized nanocarriers, since a metal probe with a titanium flat tip was used during the manufacturing process. The SEM sample was used for EDX analysis prior to sputter coating with gold. The sample was visualized using a Model TS 5136 LM Vega® Tescan SEM (Tescan, Vega LMU, Czechoslovakia Republic) fitted with an INCA PENTA FET probe at an accelerated voltage of 20 kV

5.2.2.3.4 Differential Scanning Calorimetry (DSC)

The degree of crystallinity and polymorphism of the lipids and nanocarriers was determined using a Model DSC-6000 Perkin-Elmer differential scanning calorimeter (Perkin-Elmer® Ltd, Connecticut, USA). Prior to analysis the liquid nanoemulsion was lyophilized without cryoprotectant (§ 5.2.2.3.3) after which NLC samples weighing between 3-5 mg were

weighed directly into standard 40 µl open aluminium pans. DSC curves were generated by heating the sample from 22 °C-240 °C and subsequent cooling to 22 °C at heating and cooling rates of 10 °C/min whilst purging with nitrogen at a flow rate of 20 mL/min. The resultant data was analyzed using Pyris™ Manger Software (Perkin-Elmer® Ltd, Connecticut, USA).

5.2.2.3.5 Wide-Angle X-ray Scattering (WAXS)

In order to facilitate complete interpretation of the DSC data, WAXS was used to monitor the degree of crystallinity and polymorphism of the raw materials and the NLC that were produced. WAXS patterns were generated using a Model D8 Discover X-ray diffractometer (Bruker, Billeria, MA, USA) that was equipped with a PSD LynxEye detector coupled to a copper anode using Cu-Kα radiation at $\lambda = 1.5405$ Å at 30 kV and fitted with a nickel filter. Samples were placed on a zero background (511) silicon wafer embedded in a generic sample holder and the data recorded at room temperature (22 °C) using 2θ range between 10˚ and 100˚ at a scanning rate of 1˚ min^{-1} using a filter time constant of 2.0 s per step at a slit width of 6.0 mm. All samples used for WAXS analysis were identical to those used for DSC studies in order to ensure data comparison and characterization was possible.

5.2.2.3.6 Fourier Transform Infrared Spectroscopy (FT-IR)

The crystalline and polymorphic nature of the NLC was also investigated using FT-IR as a complementary tool to DSC. Lyophilized NLC samples were mounted onto a diamond crystal using an applied force of approximately 100 N. The FT-IR spectrum was generated using a Precisely FT-IR Spectrum 100 spectrometer (Perkin-Elmer® Pty Ltd, Beaconsfield, England) over the scan range 4000-650 cm^{-1} at a resolution of 4 cm^{-1}.

5.2.2.3.7 Muco-adhesion

Nanoparticles with a negative ZP generally exhibit reduced ocular residence times since any interaction between the nanocarriers and mucin, a negatively charged glycoprotein, are unlikely to occur [322]. Consequently incorporation of PEG into the NLC formulation composition was considered and investigated to determine if muco-adhesive properties could be imparted to this experimental test technology.

The muco-adhesive properties of the NLC was evaluated by monitoring changes in ZP following incubation of the NLC with mucin [329], following preparation of a 0.1% *w/w* stock dispersion of mucin in HPLC-grade water. The dispersion was stirred for 30 minutes at 500 rpm using a hotplate stirrer (VWR®,Batavia, IL, USA) prior to filtration through a 0.45 µm Millipore® Millex-HV Hydrophilic PVDF filter membrane (Millipore® Co., Bedford, MA, USA). A 60 µL aliquot of the NLC dispersion was injected into 20 mL of the filtered mucin dispersion and the mixture stirred at 200 rpm for 6 hours at 32 °C in a glass beaker [330]. The temperature was used to simulate the temperature of the ocular surface and was maintained using a digital hotplate stirrer (VWR®,Batavia, IL, USA). The ZP of the mixtures was measured at 0, 30, 60, 120, 240 and 360 minutes and the data was analyzed as described in § 5.2.2.3.1. Aqueous dispersions of filtered mucin and NLC were also monitored and analyzed over a 6-hour period and the data used as a control. Confirmation of PEG coating on the nanocarriers was investigated using DSC with a Model DSC-6000 PerkinElmer differential scanning calorimeter (Perkin-Elmer® Ltd, Connecticut, USA).

5.2.2.3.8 *In vitro* Release and Data Modelling

The *in vitro* release of CLA from the optimized NLC dispersion after adjustment of the osmolarity with glycerine, was investigated using a dialysis method. One (1) milliliter of the nano-suspension was transferred into a closed dialysis bag of MWCO 14000 Da (Sigma Aldrich Chemical Co., Milwaukee, WI, USA) and placed into 70 mL borosilicate vials. The dissolution medium containing 20 mL HPLC-grade water (pH=7.20) was maintained at 32 °C, to simulate the temperature of the ocular surface, and stirred using a LABOTEC® shaking water bath (Laboratory Thermal Equipment, Greenfield NR. Oldham) set to 80 rpm. One (1) ml aliquots were withdrawn at 0.25, 0.50, 1, 3, 6, 12 and 24 hour intervals. Sink conditions were maintained by replacing 1.0 mL fresh dissolution medium at predetermined time intervals. The studies were performed in replicate (n = 3) over 24 hours. The amount of CLA in the receptor medium was determined using a validated RP-HPLC method [63] (Chapter 3 *vide infra*).

The *in vitro* release data for the optimized CLA-loaded NLC was fitted to first-order, Higuchi, Korsemeyer–Peppas, Hixson-Crowell and Baker-Lonsdale models using DDSolver, an add-in program for Microsoft Excel [331]. The model that best fitted the data was

identified based on the adjusted coefficient of determination (Rsqr_adj), Akaike Information Criterion (AIC) and Model Selection Criterion (MSC) which are popular evaluation criteria used for evaluating dissolution data [331]. The highest Rsqr_adj and MSC values and the lowest AIC values were used to identify the model that best fitted the release [311,331].

5.2.2.3.9 Cytotoxicity

Many authors have demonstrated that the organ and species of origin of cells used in cytotoxicity assays have a strong correlation to the results observed in such studies [332,333]. As a general rule, it is crucial to select an appropriate cell line for a study based on the expected target organ *in vivo* and application of the carrier system used [334,335]. Nevertheless in a study to assess the cytotoxicity of bio-active silica nanoparticles in 19 different cell lines representing all major organ types, the results revealed reduced toxicity in all cell types investigated, thereby implying the influence of the cell line characteristics on the final toxicity response observed was minimal [336]. Consequently, in an attempt to assess the biocompatibility of CLA-NLA for potential use in humans, a human cell line viz., human cervix adenocarcinoma cells, available in our institution was selected for evaluating potential cytotoxicity of the test technology.

Cytotoxicity was evaluated using HeLa (human cervix adenocarcinoma) cells (Cellonex, South africa) cultured in Dulbecco's Modified Eagle Medium (DMEM) – (Lonza, BioWhittaker®) supplemented with 10% fetal calf serum and a mixture of penicillin/streptomycin/amphotericin B (Lonza, BioWhittaker®) at 37 ºC in a 5% CO_2 incubator. The HeLa cells were inoculated into 96-well plates at a cell density of 1 x 10^4 cells per well in 150 µL culture medium and grown overnight. A single concentration of 50 µg/mL of the test compounds was incubated with the cells for an additional 48 hours, and cell viability in the wells assessed by adding 20 µL of 0.54 mM resazurin (Glentham Life Sciences, England) in phosphate buffered saline (PBS) for an additional 2-4 hours. The relative number of cells surviving treatment was determined by reading resorufin fluorescence at an excitation wavelength of 560 nm and emission wavelength of 590 nm with a SpectraMax® M3 plate reader (Molecular Devices, San Jose, CA, USA). Fluorescence readings for individual wells were converted to % cell viability, relative to the average

readings for untreated control wells (HeLa cells without test compounds) after subtracting background readings for wells without cells.

5.2.2.4 Statistical Analysis

Statistical analysis was performed using Version 12 Design Expert® statistical software (Stat-Ease Inc., Minneapolis, MN, USA) and the significance of relevant factors determined using Fisher's statistical test for Analysis of Variance (ANOVA) with models considered statistically significant when $p < 0.05$ at a 95 % level of confidence being observed. Three-dimensional (3-D) response surface plots were used to determine process parameters which resulted in the manufacture of CLA-loaded NLC that exhibited the pre-defined target CQA.

5.2.2.5 Stability

Short term stability testing of the optimized CLA-loaded NLC formulations were undertaken using a protocol based on existing global stability guidelines [337]. CLA-loaded NLC were packed into 50 g clear glass ointment jars and tightly sealed prior to being stored at room temperature (22 ˚C) and in a refrigerator (4 ˚C). Formulations were tested at each pull time and discarded after analysis. The PS, PDI, ZP, EE, pH and osmolarity were monitored for 28 days and samples were tested in triplicate ($n = 3$). Table 5.3 shows the stability protocol and the CQA tested at every pull point.

Table 5.3 Stability protocol for CLA-NLC

Storage Conditions	**Time points**				
	Number of bottles to be pulled per interval				
	Initial	7 days	14 days	21 days	28 days
4 °C	3	3	3	3	3
22 °C		3	3	3	3
Total bottles per time point	3	6	6	6	6
CQA tested	PS,PDI,ZP pH,EE Osmolarity	PS,PDI,ZP pH,EE Osmolarity	PS,PDI,ZP pH,Osmolarity	PS,PDI,ZP pH,EE Osmolarity	PS,PDI,ZP pH,EE Osmolarity

5.3 RESULTS AND DISCUSSION

5.3.1 Manufacture of CLA-loaded NLC Formulations

5.3.1.1 Formulation Screening using a Box Behnken Design (BBD)

The BBD design matrix for the responses monitored for formulations that did not form a gel-like mass and were analyzed 24 hours after manufacture are summarized in Table 5.4.

Table 5.4 Responses for stable BBD NLC formulations

	Input Variables					Responses (CQA)				
Run	**Lipid**	**Tween® 20**	**Amplitude**	**Time**	**PEG 6000**	**EE**	**LC**	**ZP**	**PS**	**PDI**
	% *w/w*	**% *w/w***	**%**	**min**	**% *w/w***	**%**	**%**	**mV**	**nm**	
1	5	3	55	20	2	76.67	7.12	-25.4	7095	0.716
6	3	1	55	20	2	76.06	7.07	-15.9	6196	0.963
7	3	1	100	20	1	78.7	7.3	-17	1568	0.846
9	3	3	55	30	2	67.83	6.35	-28	8306	0.762
10	3	1	55	20	0	82.13	7.59	-17.9	4053	0.721
11	1	3	100	20	1	58.99	5.57	-18.6	2483	0.866
12	5	3	55	10	1	79.47	7.36	-24.1	6864	0.614
13	3	3	10	20	0	79.85	7.4	-21.2	8184	0.877
16	1	3	10	20	1	65.9	6.18	-16.9	10770	0.785
17	3	1	55	30	1	65.61	6.16	-16.3	4084	0.893
20	1	5	55	20	1	36.97	3.57	-26.2	2607	0.887
22	1	3	55	30	1	38.25	3.68	-17	13390	0.743
23	1	1	55	20	1	26.86	2.62	-20.9	14180	0.577
26	5	3	10	20	1	55.78	5.28	-25.3	6869	0.807
29	1	3	55	10	1	32.68	3.16	-20.3	35380	0.793
33	3	1	55	10	1	70.57	6.59	-17.3	2494	0.901
37	1	3	55	20	2	30.56	2.97	-23.7	5800	0.803
41	1	3	55	20	0	38.51	3.71	-33.3	23910	0.878
43	3	3	55	10	0	66.49	6.23	-21.9	15710	0.738
*44	5	1	55	20	1	86.53	7.96	-20.3	499.8	0.456
45	3	1	10	20	1	75.02	6.98	-15.7	6130	0.738

The data listed in Table 5.4 reveal that formulation tested as run 44* (F 44) was the only formulation that met the specified CQA for EE, ZP, PS and PDI. Consequently, batch F 44 was further optimized in terms of process parameters in an attempt to assess the robustness of the formulation composition, to changes in process conditions.

5.3.1.2 Optimization of Process Parameters using a Central Composite Design (CCD)

The input variables used to optimize the manufacture of CLA-loaded NLC using the CCD in addition to the observed responses for these studies are summarized in Table 5.5

Table 5.5 Responses observed for CCD experiments during optimization of process conditions for the manufacture of NLC

	Input Variables		Responses (CQA)				
Run	**Sonication time**	**Amplitude**	**EE**	**LC**	**ZP**	**PS**	**PDI**
	min	**%**	**%**	**%**	**mV**	**nm**	
1	10	85	87.1	8	-18.5	661	0.668
2	30	25	88.1	8.1	-17.6	1008	0.948
3	10	25	88.1	8.1	-18.6	1130	0.886
4	20	55	88	8.1	-19.1	477.8	0.545
5	20	55	86.4	8	-21.8	511.3	0.487
*6	20	13	-	-	-	-	-
7	34.14	55	87.9	8	-26.1	477.2	0.531
8	20	55	87.8	8	-21.8	483.1	0.592
9	30	85	84.9	7.8	-25.6	495	0.555
10	6.15	55	87.1	8	-21.7	434.4	0.476
11	20	55	88.6	8.1	-23.8	424.6	0.454
12	20	97	84.3	7.8	-29.1	419.4	0.392
13	20	55	86.5	8	-21.4	441.0	0.479

* Formulation that was considered unstable following storage for 24 hours

The manufacturing parameters used for the production of CLA-loaded NLC were optimized using experimental design, specifically a CCD. The data was analyzed using Version 12 Design Expert® statistical software (Stat-Ease Inc., Minneapolis, MN, USA). Fisher's test for Analysis of Variance (ANOVA) was used to determine the significance of any difference(s) ($p = 0.05$) between the factors investigated. The overall design summary revealed that three linear and two quadratic models best described the relationship between the two independent input factors. Significant model variables were identified during optimization and the best combination of factors which yielded a product with the target CQA, identified.

The overall contribution of model factors used to produce the nanoparticles with the target EE, LC, ZP, PS and PDI were statistically significant and the models were used to navigate the design space. ANOVA analysis revealed that the significant model term for the linear models for EE, LC and ZP was amplitude of sonication ($p < 0.05$). The significant model term(s) for the quadratic models for PS and PDI established at $p < 0.05$ were amplitude of sonication and the quadratic effect(s) of amplitude. The best fit model, significant input factors and equations describing the relationship between the input variables and outputs monitored are summarized in Table 5.6.

The 3D response surface plots for these data are depicted in Figure 5.3 (A-E). The 3D response surface plots facilitate examination of the effect(s) of experimental variables and factors on the responses monitored. The graphical representation illustrates the responses to different experimental values and facilitates identification of major interactions between input variables. When using 3-D response surface plots, one variable must be set at an arbitrary and fixed value and the response surface plotted for the other two variables which are displayed on the X and Y-axes. The response surface generated is therefore a function of the value selected for the variable that is held constant and may differ as the actual value used, is changed [338].

Table 5.6 Best fit model, significant input factors and equations used to describe the relationship between input and output variables used for the CCD

Response	**Best fit model**	**Significant factors**	**Equation** (A=sonication time, B=amplitude)
EE	Linear	Amplitude ($p = 0.00686$)	EE = 90.05 - 0.01335A -0.04642B
LC	Linear	Amplitude ($p = 0.00146$)	LC = 8.278 - 0.00250A -0.0039102B
ZP	Linear	Amplitude ($p = 0.0209$)	ZP = -13.05 -0.1540A -0.1018B
PS	Quadratic	Amplitude ($p = 0.00123$)	PS = 2014 -13.32A - 40.51B - 0.03666A * B + $0.3085A^2$ + $0.2857B^2$
PDI	Quadratic	Amplitude ($p = 0.00679$)	PDI =1.354 - 0.003848A - 0.02269B -0.00014583A*B + $0.0003051A^2$ + $0.0001717B^2$

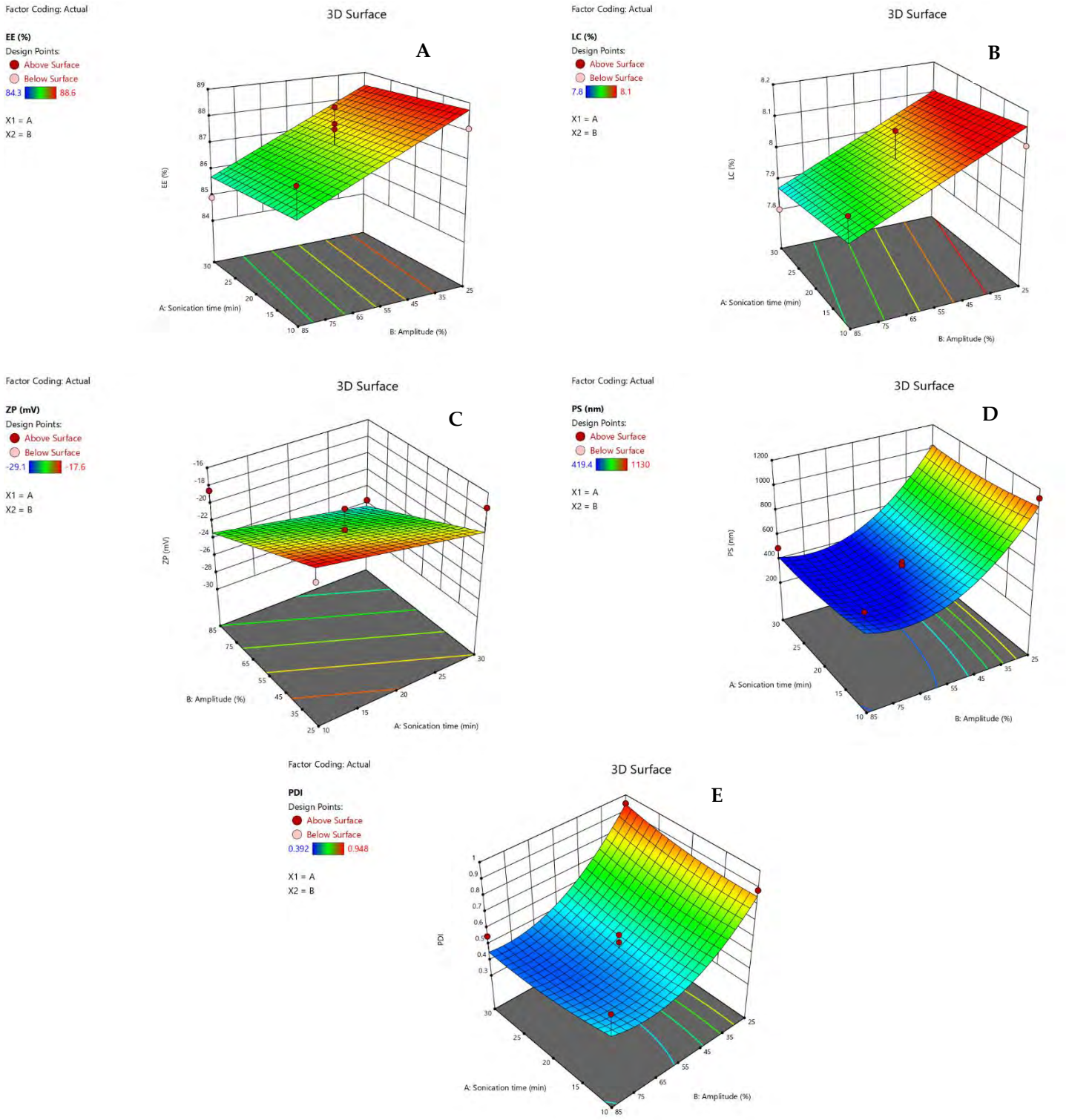

Figure 5.3 3-D response surface plots depicting the effect of sonication time and amplitude on encapsulation efficiency (A), loading capacity (B), Zeta Potential (C), particle size (D) and polydispersity index (E)

5.3.1.2.1 Encapsulation Efficiency (EE) and Loading Capacity (LC)

The LC of NLC is an essential parameter to monitor when establishing whether the novel

carrier has the potential for commercial use and has an impact on the long term stability of these systems if the API remains entrapped in the carriers [247]. The optimization process for NLC must include an investigation of the LC and EE [235]. The lipid core should shield the payload and minimize degradation whilst ensuring a sufficiently high EE and long term retention of the API in the lipid matrix [209]. The 3-D response surface plots (Figures 5.3A and 5.3B) reveal an inverse relationship between amplitude of sonication and the CQA monitored. The application of a higher amplitude during sonication on previously formed lipid carriers resulted in expulsion of entrapped CLA into the aqueous dispersion medium, resulting in a reduction in EE and LC [240,324]. Consequently, high amplitudes are likely to lead to CLA-NLC with a smaller payload, in addition to exposing CLA to possible hydrolytic degradation, which in turn requires the use of large amounts of the compound, to produce a dosage form that would exert a successful therapeutic effect, which if unstable or fails, may lead to the occurrence of adverse events.

5.3.1.2.2 Zeta Potential (ZP)

The ZP of the formulations tested, ranged between -17.6 and -29.8 mV. The 3-D response surface plot in which the effect of amplitude of sonication on ZP is depicted (Figure 5.3C) reveals that stable formulations with relatively high negative ZP values were produced with relatively high sonication amplitudes. The adsorption of non-ionic surfactant steric stabilizers decreases the ZP in colloidal systems, resulting in strong repulsive forces between particles thereby preventing aggregation [247,324]. An increase in amplitude is likely to generate increased temperatures during manufacture, which in turn may result in a reduction in adsorption and/or degradation of the surfactant used [237] and/or an increase in ZP. However, the ZP is primarily affected by the type and concentration of lipids and surfactants used in the technology and not the method of manufacture [339]. However this will have to be further monitored and investigated during long-term stability studies of CLA-loaded NLC intended for ophthalmic use.

5.3.1.2.3 Particle size (PS) and Polydispersity Index (PDI)

The mean PS of the CLA-loaded NLC ranged between 419.4 and 1130 nm. The particle size of the NLC produced are considered suitable for instillation into the eye, since the human eye can tolerate particles of up to 10 µm in diameter [340]. The PDI is a measure of the width of the size distribution of particles and completely monodisperse systems generally exhibit a

PDI close to 0 whereas a PDI of 0.500 is indicative of a relatively broad, particle size distribution [281,341]. The PDI for all formulations tested ranged between 0.392 and 0.948. The 3-D response surface plots in which the impact of amplitude of sonication on PS and PDI are depicted (Figures 5.3E and 5.3F) reveal an increase in PS and PDI when lower amplitudes are used in the manufacturing process. It has been suggested that low processing temperatures lead to the formation of nanoparticles of large particle size [206] and that high amplitudes of sonication lead to an increase in ultrasonic wave energy and temperatures, which in turn increase shear cavitation forces with an ultimate breakdown of the oil droplets into nanometric sized droplets [322]. Consequently, a compromise in terms of amplitude of sonication and the target PS and PDI must be reached to ensure the production of stable formulations.

5.3.1.3 Formulation Optimization

Numerical optimization was undertaken using Design Expert® software with the primary aim of identifying and selecting the optimum manufacturing parameters that would ensure the production of stable NLC formulations containing CLA. Numerical optimization is used to locate a point at which the desirability function for a system is maximized, while the characteristics of the target can be modified by adjusting the importance of that target [342]. The manufacturing parameters resulting in the highest desirability *viz.* a sonication time of 26.33 minutes and amplitude of 59.7 %, were used to manufacture the optimized NLC formulation, which was then characterized in terms of the pre-determined target CQA. The CQA responses for the optimized CLA-loaded NLC are summarized in Table 5.7 which also includes the experimental and predicted responses, with the corresponding % prediction error for each parameter. The size distribution curve depicted in Figure 5.4 reveals a Gausian distribution for PDI with the peak intensity ranging between 400-500 nm which correlates well with the observed PDI of < 0.5.

Table 5.7 Comparison of predicted and observed responses for the optimized formulation

Response		Experimental value	Predicted value	% prediction error
EE	**%**	89.75 ± 0.19	86.93	3.14
LC	**%**	8.24 ± 0.68	7.98	3.16
ZP	**mV**	-20.4 ± 5.21	-23.19	-13.68
PS	**nm**	489.1 ± 41.62	419.4	14.25
PDI		0.486 ± 0.097	0.493	-1.44

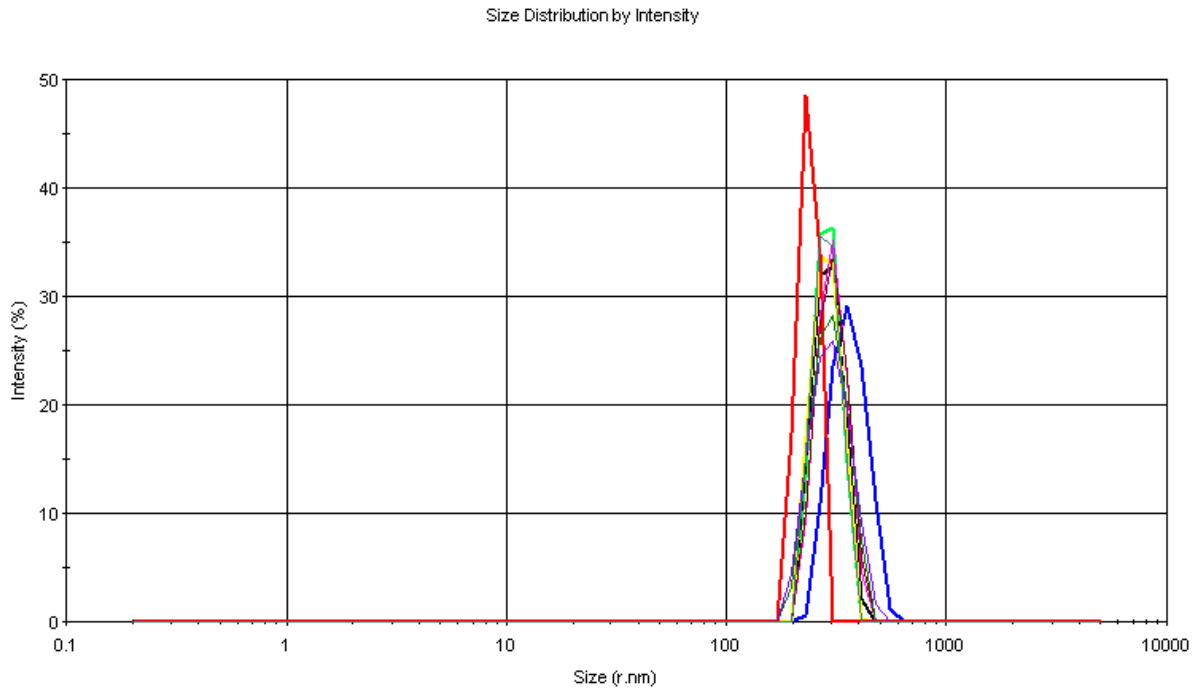

Figure 5.4 Particle size distribution by intensity for the optimized CLA-NLC formulation (n = 10)

The low magnitude of the percent prediction error indicates the robustness of the mathematical model used. The prediction errors for the ZP and PS are > 10% implying that the model may have a poor predictive ability for these parameters. However, the NLC produced were considered stable and the PS was in the nanometer size range. The high predictive ability of DoE has been demonstrated suggesting the efficiency of DoE as a tool, for process optimization, particularly when developing and optimizing pharmaceutical dosage forms [182].

5.3.2 pH and Osmolarity

The pH of the optimized CLA-loaded NLC dispersion was 7.73 ± 0.01 which suggests it would be well tolerated, when administered to the human eye [326]. The osmolarity was adjusted to 250–450 mOsm/kg by adding glycerine so as to ensure the formulation fell within

the physiological range for osmolarity to ensure it is suitable for ophthalmic administration [327]. The final pH and osmolarity of the optimized CLA-loaded NLC formulation was 7.76 ± 0.01 and 316 ± 2 mOsm/Kg. It was established that the CQA of the NLC did not change following addition of glycerine to the dispersion and the values for EE, ZP, PS and PDI were 88.62 ± 0.23 %, -20.5 ± 4.82 mV, 461.9 ± 40.16 nm and 0.523 ± 0.104, respectively. These are comparable to the EE, ZP, PS and PDI of 89.75 ± 0.19 %, -20.4 ± 5.21 mV, 489.1 ± 41.62 nm and 0.486 ± 0.097 observed prior to osmolarity adjustment. The ultimate impact of inclusion of glycerine in the formulation would need to be monitored during future, long-term stability studies.

5.3.3 Scanning Electron Microscopy (SEM) and Energy-Dispersive X-ray Spectroscopy (EDX)

The surface morphology and elemental analysis of optimized CLA-loaded NLC following lyophilization was evaluated using SEM and EDX and the data are depicted graphically in Figures 5.5 and 5.6, respectively. Elemental analysis indicates the presence of elemental carbon and oxygen in the CLA-NLC product and the absence of titanium confirms the absence of any metal that might have been shed by the probe fitted to the sonicator used during formulation, development and processing studies. In addition, elemental analysis of the pure CLA raw material reveals an increase is C atoms on the surface of the NLC, which can be attributed to PEG which coats the nanocarriers thereby confirming encapsulation of the molecule in this technology. SEM reveals anisometric shaped microparticles which is likely due to agglomeration of particles during the lyophilization process undertaken prior to SEM experiments. It should be noted that pre-treatment of the aqueous NLC sample, prior to SEM analysis and/or visualization of the particles under high vacuum conditions and at accelerated voltages, may result in shrinking of the nanoparticles and/or potentially modified shape and surface morphology of the particles [276].

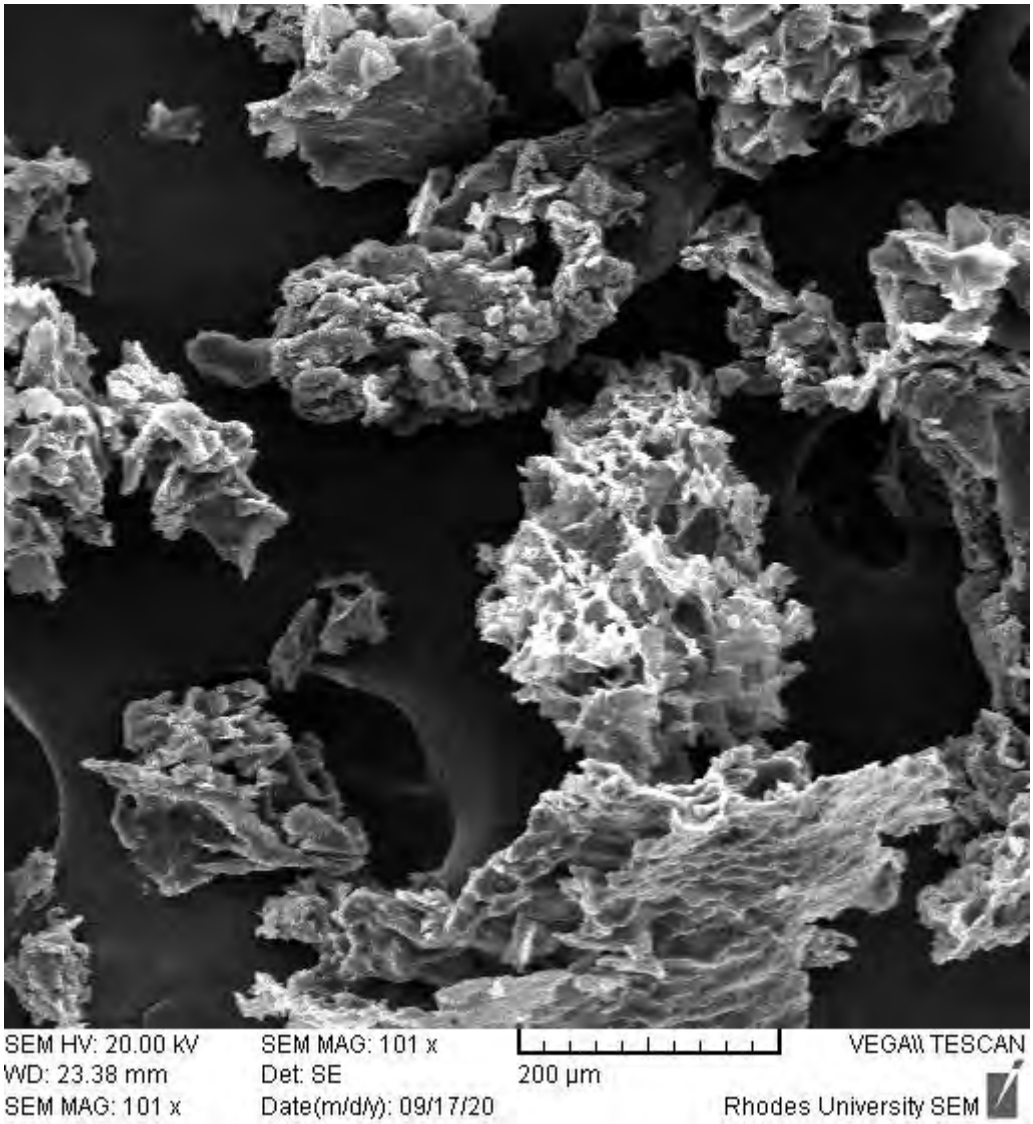

Figure 5.5 SEM micrograph of CLA-loaded NLC

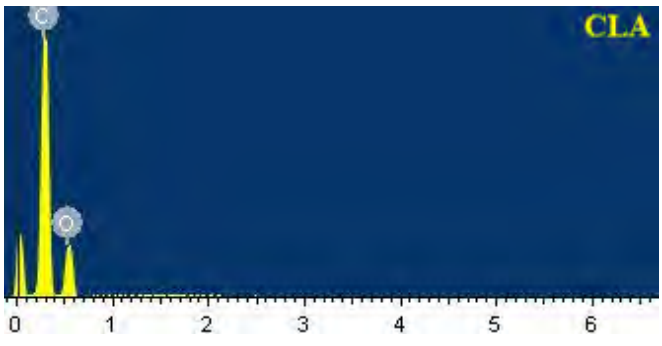

C_K = 70.96%
O_K = 29.04%

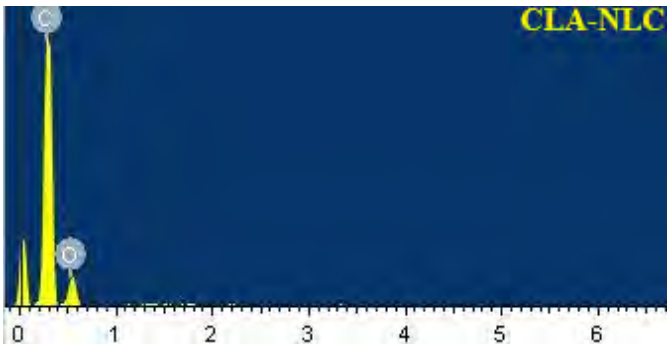

C_K = 78.73%
O_K = 21.27%

Figure 5.6 EDX spectra illustrating elemental surface composition of CLA and CLA-NLC

5.3.4 Differential Scanning Calorimetry (DSC)

DSC was used to establish if polymorphism of the optimized CLA-loaded NLC was evident and these data are depicted in Figure 5.7.

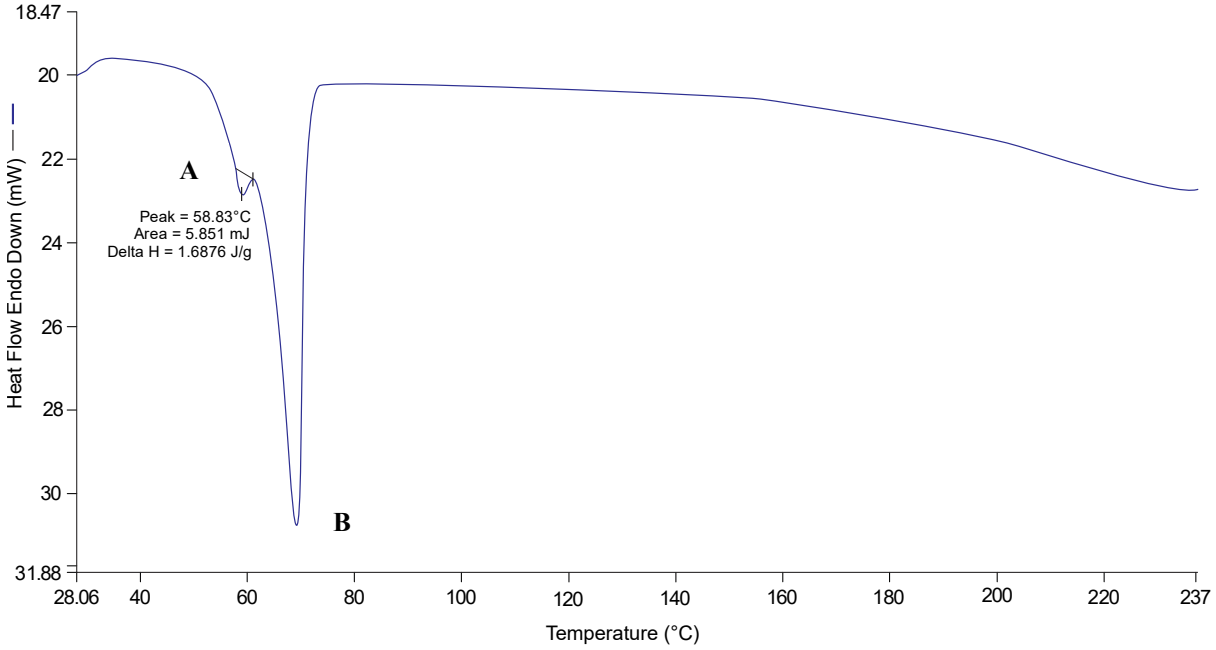

Figure 5.7 DSC thermogram for the optimized CLA-loaded NLC

The thermogram for CLA-loaded NLC reveals the presence of two endothermic events which are characteristic of the solid and liquid lipid mixture (A) in addition to PEG 6000 (B), suggesting the existence of single polymorphic forms of these excipients. The thermogram also confirms the absence of a peak which would be characteristic for CLA melting thereby indicating that CLA is molecularly dispersed in the NLC. The melting point observed at 58.83 °C is consistent with the presence of polymorphic form C of SA, also reported in § 4.3.6.5. However, the melting point of 58.83 °C for CLA-NLC is slightly lower than that of the lipid mixture (59.10 °C) which may be attributed to the smaller particle size of the particles using this production method leading to an increased surface area. The lyophilized NLC is also less crystalline than the binary mixture of the lipids, as confirmed by the decrease in enthalpy from 86.20 J/g to 1.6876 J/g. During the production of nanoparticulate formulations, the surfactant used, may lead to defects in the crystalline lattice of the lipid particles [247,311] leading to reduced crystallinity of the formed nanocarriers.

5.3.5 Wide Angle X-ray Scattering (WAXS)

The WAXS diffraction patterns for the optimized CLA-NLC, generated following lyophilization and for CLA following application of heat are depicted in Figure 5.8. The diffractogram reveals the absence of the principle bands for CLA in the optimized NLC sample tested. These results are in close agreement with those observed for DSC data that revealed that CLA was molecularly dispersed in the NLC when evaluated. The characteristic bands for PEG 6000 matched well with literature reports at 2θ = 18.75, 23.15 and 26.60 values [343] further confirming that CLA was dissolved in the PEG-coated NLC.

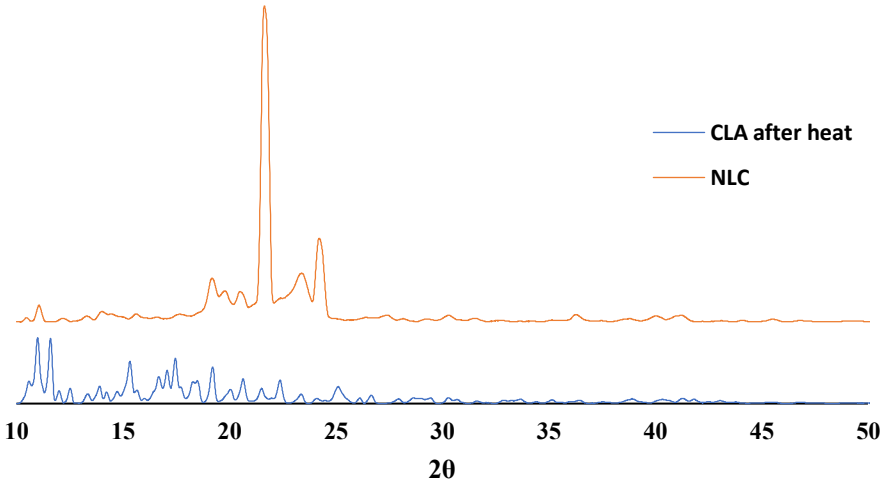

Figure 5.8 WAXS patterns for optimized CLA-NLC and CLA generated following exposure to 85 °C heat for one hour

5.3.6 Fourier Transform Infrared Spectroscopy (FT-IR)

FT-IR spectroscopy was used to assess the crystalline state of the CLA-NLC, and the spectra are depicted in Figure 5.9. These data also reveal the FT-IR spectra for PEG 6000, SA: THP in a ratio of 80:20 (*w/w*) and CLA following exposure to a temperature of 85 °C so as to facilitate comparisons and data interpretation.

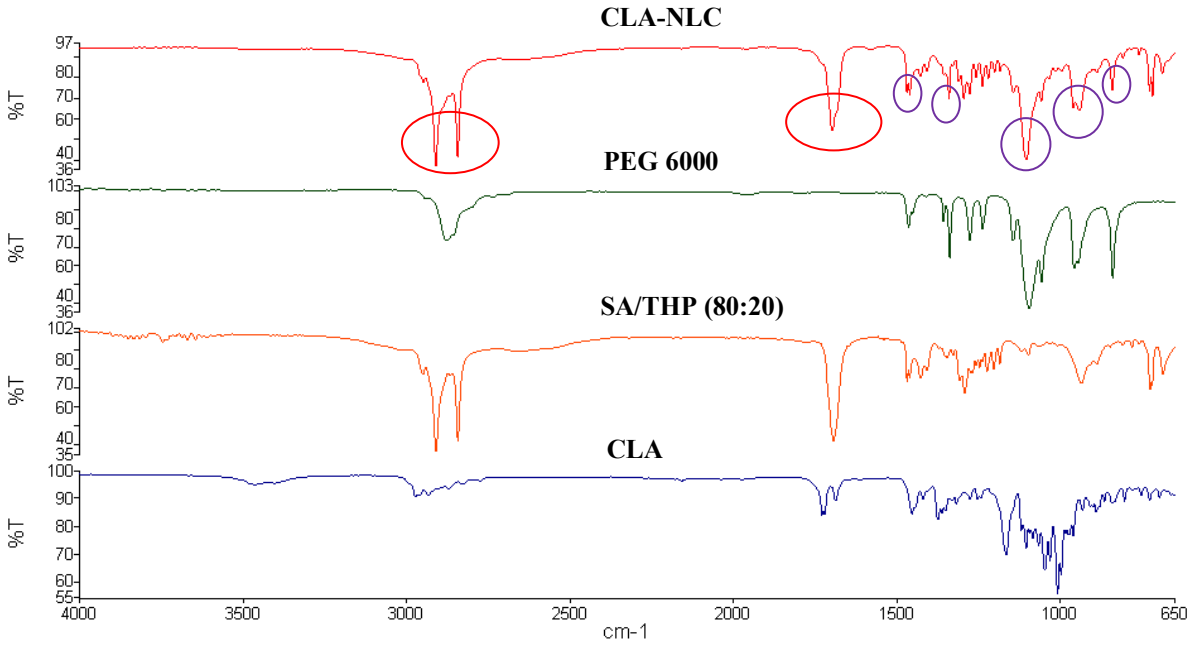

Figure 5.9 FT-IR spectra for CLA-NLC, PEG 6000, an 80:20 (*w/w*) binary mixture of SA and THP and CLA generated following exposure to 85 °C for one hour

The FT-IR spectrum for CLA-NLC reveals the presence of the characteristic bands of SA (circled in red). However, the characteristic bands for molecular vibrations of CLA were not observed for this colloidal system, thereby confirming the DSC and WAXS results which suggest that CLA was molecularly dispersed in the lipid matrix. The spectrum for the NLC also reveal the presence of characteristic bands consistent with molecular vibrations of PEG 6000 (circled in purple) suggesting that PEG was exterior to the nanoparticle structure suggesting it is performing as a coating and is not dispersed in the interior of the nanoparticles. The intensity of the bands in the CLA-NLC spectrum are lower in intensity to those observed for the excipients used during the manufacturing process, which may indicate the amorphous nature of the nanocarriers that were manufactured.

5.3.7 Muco-adhesion

The interaction of the CLA-NLC with mucin was investigated as was the use of PEG in the formulation. The adsorption of PEG onto the surfaces of the NLC due to the hydrophilic nature of the polymer was intended to promote a muco-adhesive interaction with mucin, which in turn suggests interaction with the surfaces of the eye and results in enhanced precorneal retention and a possible increase in ocular availability, thereby permitting dose reduction and use of a longer dosing frequencies.

Muco-adhesion occurs *via* different mechanisms *viz.* electrostatic, adsorption, wetting, and diffusion that allow the inter-penetration of polymer chains and mucin, entanglement and subsequent formation of interactive bonds [344,345]**.** Sequentially, the polymer swells on wetting, forms non-covalent bonds at the mucus-polymer interface *via* electrostatic interaction and adsorption after which the polymer and mucin interpenetrate and entangle to form bonds [344]. A decrease in the magnitude of ZP for NLC following incubation with mucin was observed (Figure 5.10) suggesting that the NLC with surface adsorbed/coated PEG would likely exhibit enhanced muco-adhesive properties. The DSC thermograms depicted in Figure 5.11 reveal the presence of melting endotherms consistent with those for PEG in the thermogram of the lyophilized NLC providing additional evidence to suggest that the hydrophilic polymer is adsorbed onto the surface of the nanocarriers and is not molecularly dispersed on the interior of the NLC.

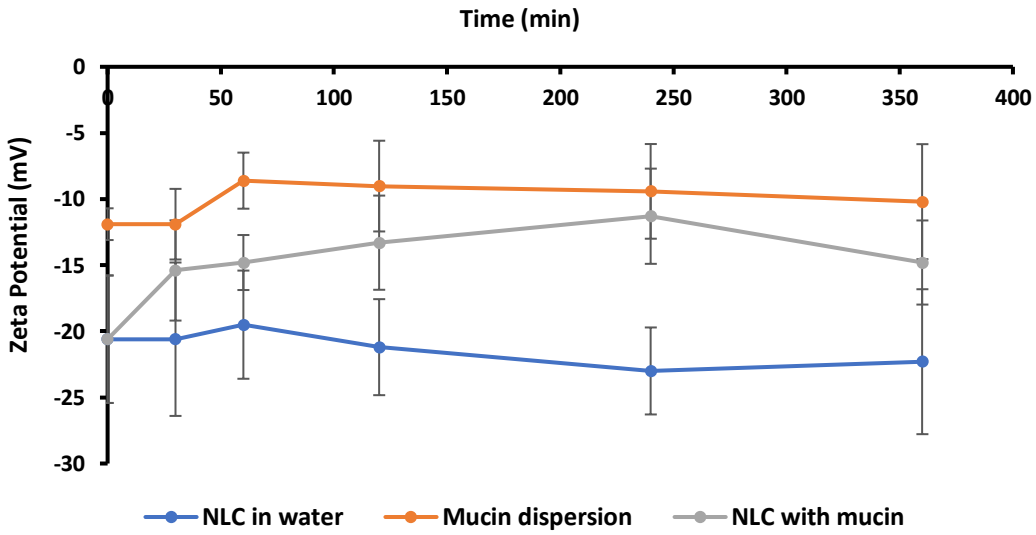

Figure 5.10 Zeta Potential of CLA- NLC incubated in a 0.1 % *m/v* aqueous dispersion of mucin

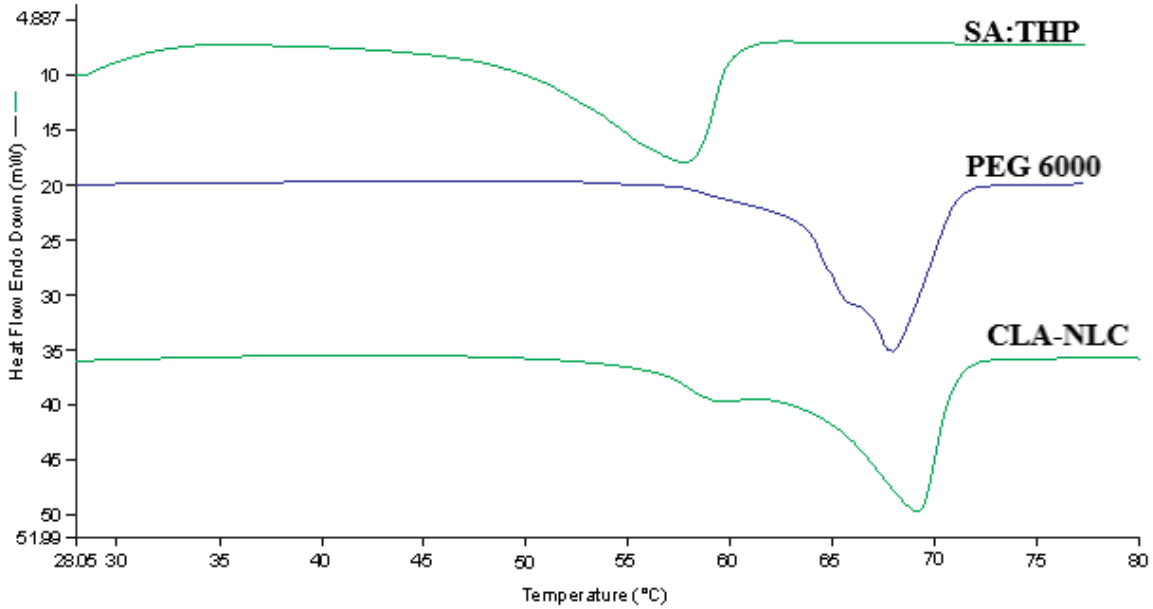

Figure 5.11 DSC thermograms of an 80:20 (*w/w*) binary mixture of SA and THP, PEG 6000 and lyophilized CLA-NLC

Adsorption is the most likely mechanism by which muco-adhesion of the NLC produced in these studies occurs as these are negatively charged particles that would be unlikely to exhibit an electrostatic interaction with the negatively charged mucin. However, it should be noted that demonstration of muco-adhesive properties of nanoparticles should be evaluated using multiple approaches in which particle diffusion, attachment and aggregation are also monitored in order to accurately classify a system as being muco-penetrative or muco-adhesive [346]. Nevertheless, this is positive data but would need confirmation through nanoparticle tracking analysis and quartz crystal microbalance with dissipation technology.

5.3.8 *In vitro* Release and Data Modelling

The *in vitro* release profile of CLA release from the optimized NLC formulation is depicted in Figure 5.12.

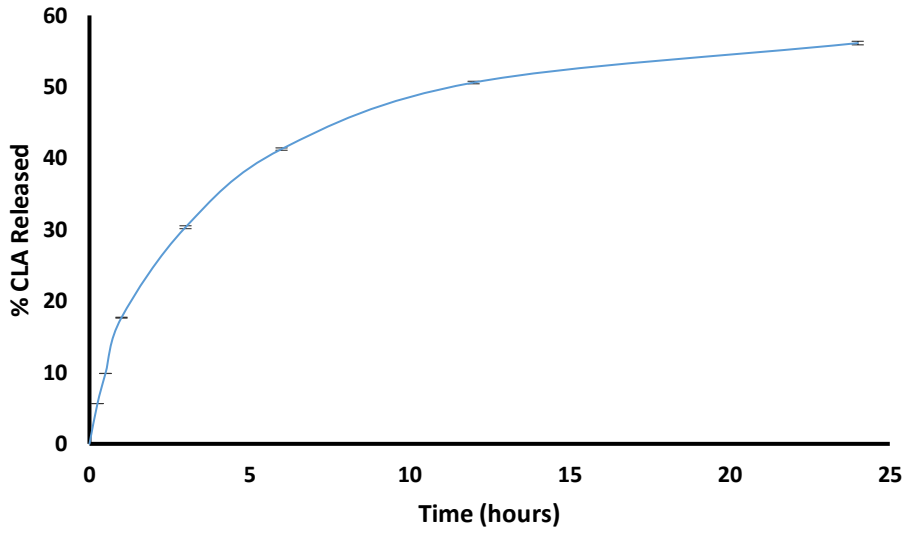

Figure 5.12 *In vitro* release of CLA from the optimized NLC formulation (n = 3)

The *in vitro* release data reveal that the cumulative amount CLA released from the NLC over a 24-hour period was 56.13 ± 0.23%. Mass balance analysis of the lipid formulations remaining in the dialysis tubing yielded an amount of CLA of 41.38 ± 0.02% indicating that these NLC release CLA in a controlled and sustained manner. Drug release from nanoparticles has been shown to be affected by factors such as intrinsic solubility of the API in the lipid matrix, movement of API across depleted layers of the formulation, composition of the lipid matrix used and diffusion across and from interfacial barriers such as that used as the dialysis membrane [50]. Consequently, kinetic modelling of the release profile was undertaken using DDSolver in order to identify the factors that influenced CLA release from these lipid carriers.

The release kinetic data generated following fitting of CLA release to a variety of models using DDSolver are depicted graphically in Figure 5.13 and are summarized in Table 5.8 and include the corresponding criteria used to evaluate the release data. The highest R^2 adjusted, MSC and lowest AIC values were used to evaluate *in vitro* CLA release data fitted to First-order, Higuchi, Korsmeyer-Peppas, Hixson- Crowell and the Baker-Lonsdale models [331].

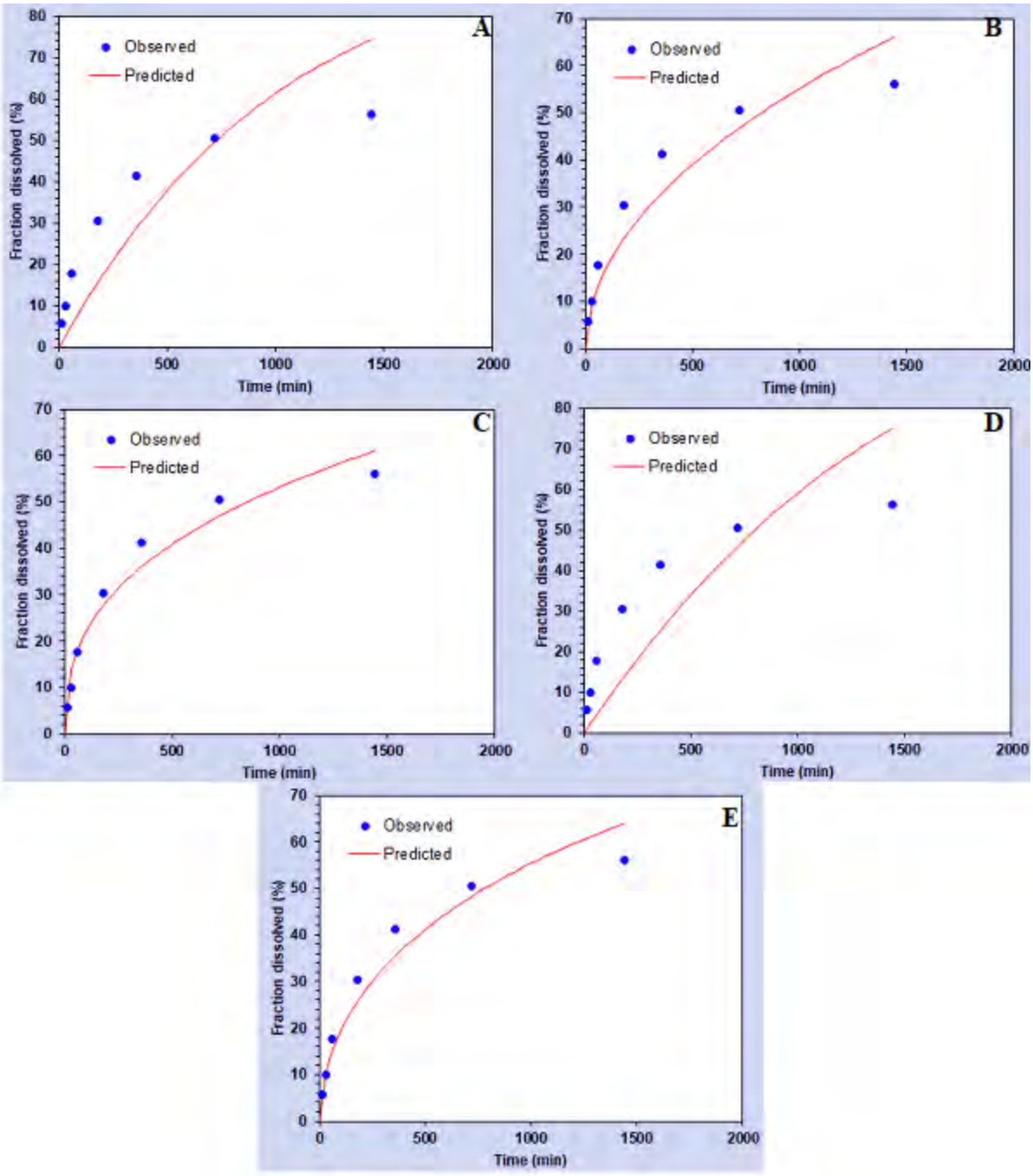

Figure 5.13 Results of model fitting for CLA-NLC to First order (A), Higuchi (B), Korsmeyer-Peppas (C), Hixson- Crowell (D) and Baker-Lonsdale (E) models automatically generated from DDSolver

Table 5.8 Kinetic models and best fit criteria for CLA release from NLC

Model and Equation	Code Evaluation Criteria		
	Rsqr_adj	**AIC**	**MSC**
First order (A) F=100*[1-Exp(-k1*t)]	0.6142	49.7717	0.6667
Higuchi (B) F=kH*t^0.5	0.8954	40.6333	1.9722
Korsmeyer-Peppas (C) F=kKP*t^n	0.9416	37.2827	2.4509
Hixson-Crowell (D) F=100*[1-(1-kHC*t)^3]	0.5067	51.4924	0.4209
Baker-Lonsdale (E) 3/2*[1-(1-F/100)^(2/3)]-F/100=kBL*t	0.9442*	36.2357*	2.6004*

* Best fit model

The highest R^2 adjusted and MSC values and the lowest AIC for the models investigated are summarized in Table 5.8. The data revealed that the Baker-Lonsdale model was best to fit these data. The Baker-Lonsdale model is derived from the Higuchi model and describes controlled release mechanisms for CLA, in this case, from spherical shaped lipid matrices, involving diffusion and degradation as the primary factors affecting release and model [347]. However, The Korsmeyer Peppas model analyzes both Fickian and non-Fickian release of API from swelling and non-swelling polymeric delivery systems while the Baker-Lonsdale model explains drug release from spherical matrices. The aforementioned could possibly explain the observed similarity in generated profiles [348].

5.3.9 Cytotoxicity

The effect of encapsulating CLA into NLC and the biocompatibility of the lipids used for production of the carrier was investigated. None of the samples tested produced a significant cytotoxic effect assessed as a reduction of viability of HeLa cells to < 50% using a test concentration of 50 µg/mL. CLA-NLC exhibited improved cell viability, when compared to that observed when testing CLA alone, which may be due to a shielding effect imparted by encapsulating lipids revealing the protective nature of these nanocarriers. In addition, PEG is assumed to form a hydrophilic and protective layer on the surfaces of the nanoparticle opposing interaction and ultimate uptake by HeLa cells [349,350]. Furthermore, the high % viability of HeLa cells following exposure to control/blank NLC confirms that the lipids and excipients used in these studies are safe and comply with GRAS status. A graphic summary of the *in vitro* cytotoxicity data is depicted in Figure 5.14.

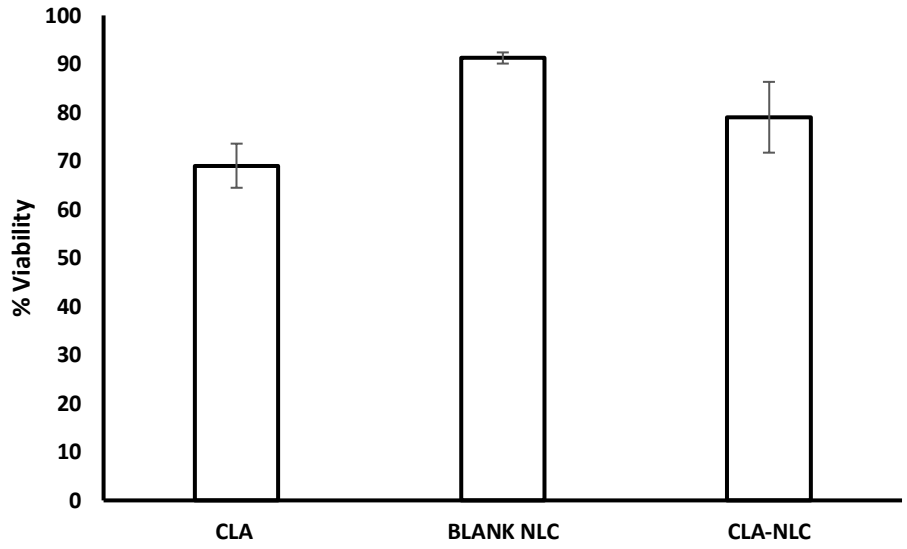

Figure 5.14 Cytotoxicity results for CLA (50 µg/mL), control/blank-NLC and CLA-NLC (50 µg/mL) tested in HeLa cells

5.3.10 Stability Studies

The PS, PDI, EE, ZP, pH and osmolarity of CLA-NLC generated following storage at 4 °C and 22 °C for 28 days are summarized in Table 5.9 and corresponding graphical representations of PS, PDI, EE and ZP are depicted in Figure 5.15.

Table 5.9 Critical Quality Attributes monitored for CLA-NLC stored at 4 °C and 22 °C for 28 days

Time days	Storage Conditions	PS nm	PDI	EE %	ZP mV	pH	Osmolarity mOsm/kg
0	4°C	461.9±40.16	0.523±0.104	88.62±0.23	-20.5±4.82	7.75±0.01	314±2
	22°C	461.9±40.16	0.523±0.104	88.62±0.23	-20.5±4.82	7.76±0.01	314±2
7	4°C	581.6±84.47	0.504±0.129	83.18±0.55	-27.4±5.46	7.58±0.02	316±1
	22°C	624.5±81.5	0.613±0.218	86.5±0.01	-14.7±2.10	7.65±0.01	312±2
14	4°C	466±32.8	0.331±0.126	NP	-31.5±2.01	7.30±0.01	313±2
	22°C	1148±60.4	0.919±0.118	NP	-23.1±5.38	7.53±0.01	310±2
21	4°C	478.9±10.8	0.462±0.119	78.11±0.13	-19.3±4.17	7.35±0.01	318±1
	22°C	973.9±34.8	0.910±0.137	84.6±0.11	-23.4±6.20	7.47±0.01	314±2
28	4°C	578.1±21	0.452±0.179	74.2±0.14	-32.2±3.90	7.42±0.01	317±1
	22°C	1754±100	0.890±0.103	83.48±0.08	-33.7±4.14	7.24±0.02	316±2

NP=Not performed

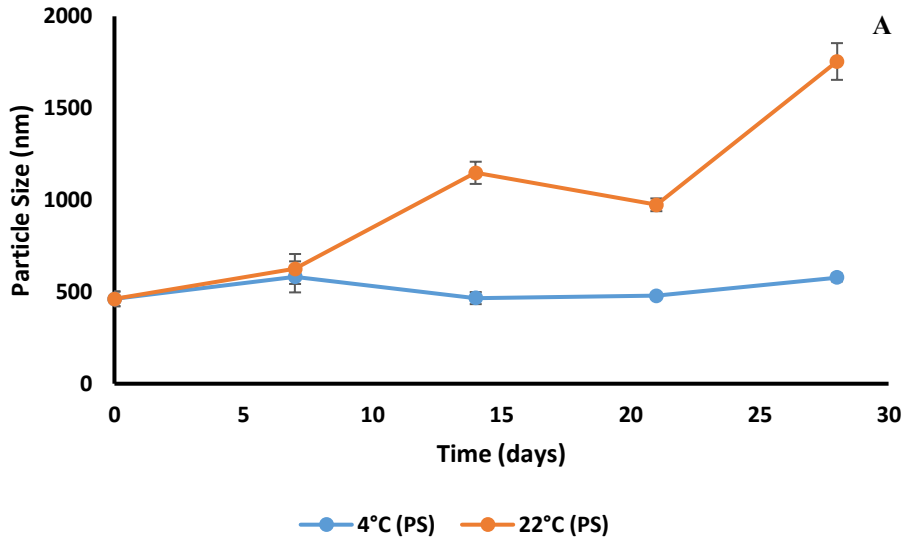
A
2000
1500
1000
500
0
Particle Size (nm)
0
5
10
15
20
25
30
Time (days)
4°C (PS)
22°C (PS)

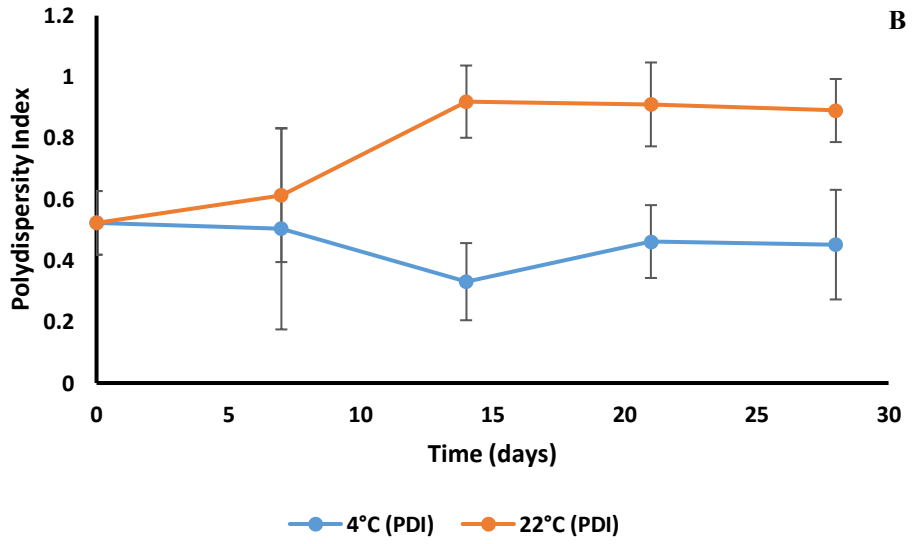
B
1.2
1
0.8
0.6
0.4
0.2
0
Polydispersity Index
0
5
10
15
20
25
30
Time (days)
4°C (PDI)
22°C (PDI)

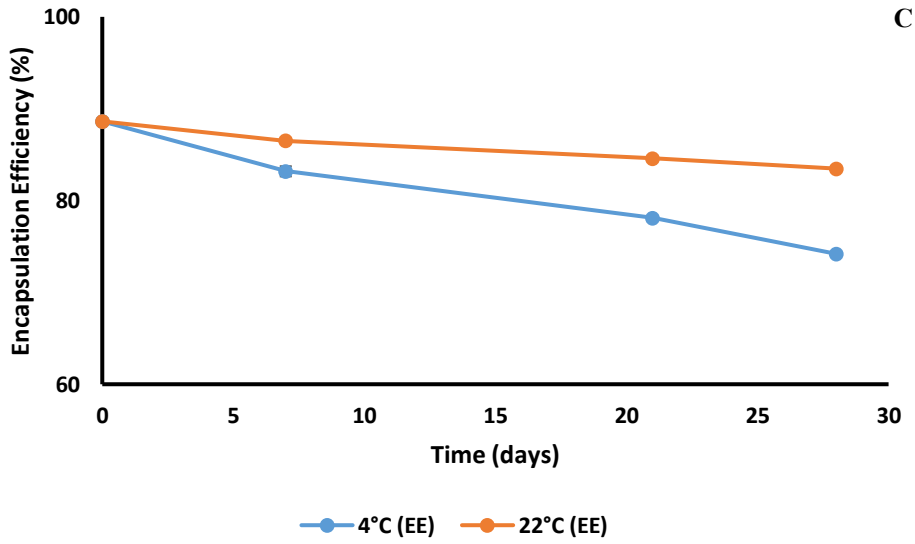
C
100
80
60
Encapsulation Efficiency (%)
0
5
10
15
20
25
30
Time (days)
4°C (EE)
22°C (EE)

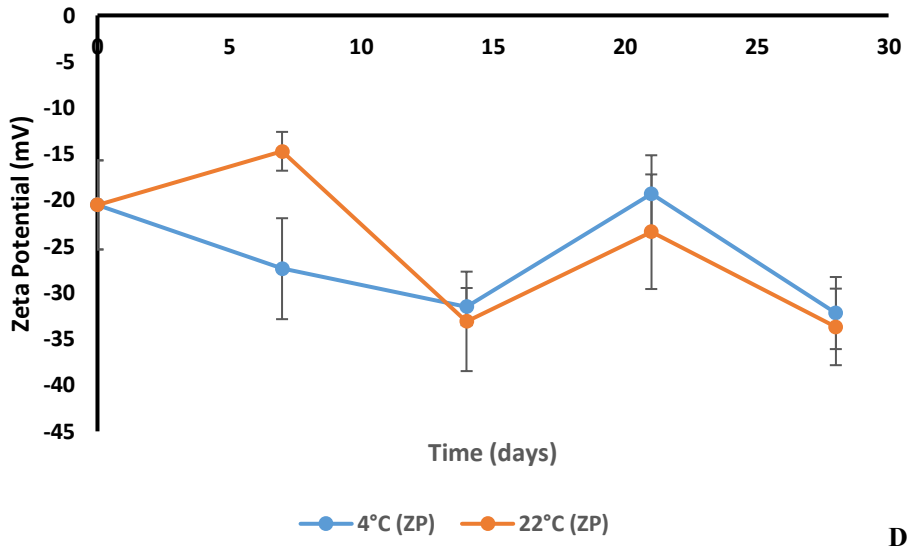

Figure 5.15 Particle size (A), polydispersity index (B), encapsulation efficiency (C) and Zeta Potential (D) of CLA-NLC analyzed over 28 days (n = 3) stability study

The results following stability studies reveal a relatively constant PS and PDI for CLA-NLC stored at 4 °C in comparison to those products stored at 22 °C which show an increase in both PS and PDI. Higher temperatures increase the kinetic energy of particles, which in turn leads to a greater number of collisions between particles and the possibility of agglomeration and an increase in particle size [244]. The PS for CLA-NLC stored at 4 °C remained within the nanometer range during the incubation period whereas those stored at 22 °C increased to approximately 1.8 µm in diameter. However, despite this increase in size these formulations are suitable for ocular use as the human eye can tolerate particles of up to 10 µm in diameter [340]. Nonetheless, it should be noted that changes in particle size changes may influence formulation performance, likely both muco-adhesion behavior and drug release rates. Storage at 22 °C is therefore not advised given the potential impact on performance of the formulations.

An unexpected loss of CLA of approximately 14.42% occurred at 4 °C in comparison to 5.14% for the CLA-NLC stored at 22 °C after storage for 28 days. The leakage of API from SLN stored at 4 °C were postulated be a consequence of temporary non-homogeneity in the phospholipid bilayers around the nanoparticles when stored at these conditions [351]. Consequently DSC analysis was performed on lyophilized CLA-NLC following storage at 4 °C and 22 °C so as to elucidate the reasons for this anomaly and the resultant thermograms are depicted in Figure 5.16.

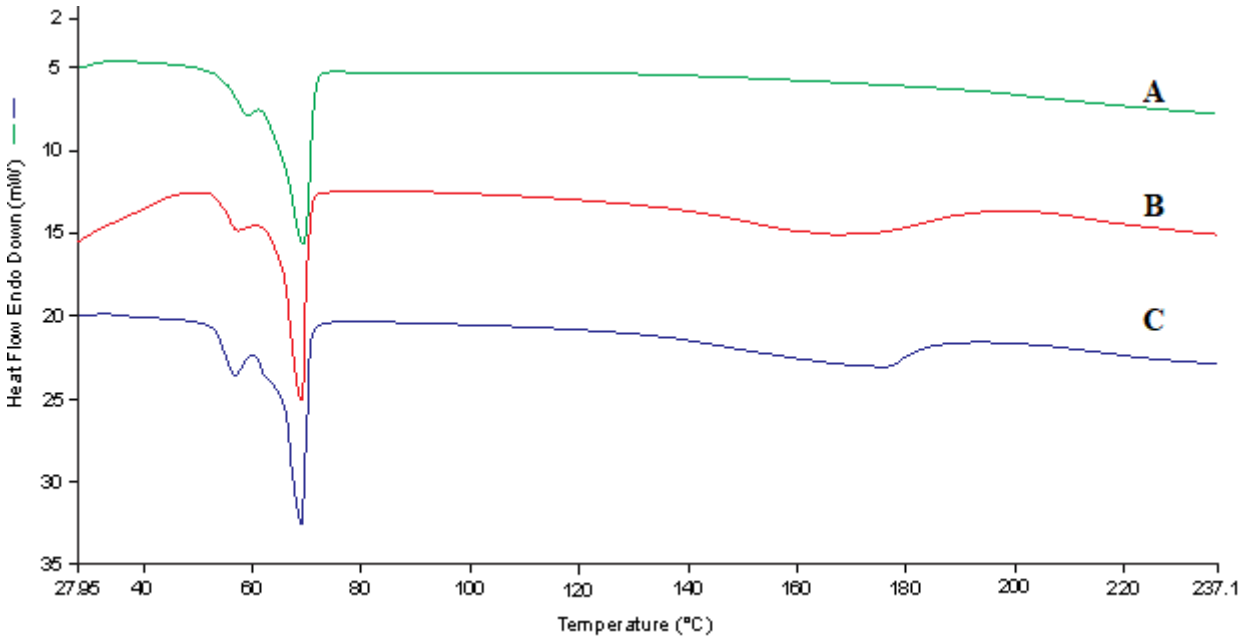

Figure 5.16 DSC thermograms of lyophilized CLA-NLC 24 hours after production (A) and storage for 28 days at 22 °C (B) and 4 °C (C)

The thermogram for the CLA-NLC formulations stored at 4 °C (Figure 5.16 C) reveal a change in the polymorphic form of the PEG 6000 used to coat and impart muco-adhesive properties to the nanoparticles. In addition, PEG has a depolarizing effect which alters the partition of hydrophobic molecules between the interior and the exterior of lipid bilayers [352].

The ZP of ≥ -30 mV for CLA-NLC generally indicates good physical stability of the nanoparticles at days 14 and 28 following storage at 4 °C and 22 °C. However, although the ZP for the formulations was lower than -30 mV between day 0 and day 7 and at day 21, the stability of the nanoparticles may be inferred, since polysorbate surfactants provide stability through both electrostatic and steric hindrance mechanisms. The ZP for the formulations were relatively higher following storage for 28 days in comparison to when assessed 24 hours following manufacture. Furthermore an increase in the negative charges on the surface of the particles, did not appear to enhance the stability of the formulations, since particle growth was observed for formulations stored at 22 °C. It is possible that the increase and decrease in the negative potential observed was unrelated to the presence of the surfactant but is rather due to an increase in the amount of CLA, either in the ionized or unionized form, on the surfaces of the particles which also corresponds to a reduction in EE over time. No agglomeration of formulations was observed following storage for 28 days and is supported

by the ZP not reaching the agglomeration threshold range of -20 to -11 mV [244].
The pH and osmolarity of the NLC formulations stored at 4 °C and 22 °C for 28 days were within 3.5-10.5 and 250-450 mOsm/kg, respectively which is also tolerable to the human eye [326,327].

5.4 CONCLUSIONS

CLA-loaded NLC formulations were manufactured using hot emulsification ultrasonication and were successfully optimized using a Design of Experiments approach with the inclusion of Tween® 20 to stabilize the nanocarriers. A Central Composite Design was used to identify optimum process parameters and a sonication time of 26.33 minutes and amplitude of 59.7% was identified as appropriate. The optimized formulation included SA and Transcutol® HP in a 4:1% *w/w* ratio with Tween® 20 and polyethylene glycol included at 1% *w/w* content. The particle size of the optimized NLC particles was in the nano range and > 80% of the theoretical CLA load was encapsulated in the NLC.

The optimized CLA-loaded NLC for which the osmolality was adjusted to between 250–450 mOsm/kg exhibited muco-adhesive properties when tested under stationary conditions using laser doppler anemometry. The optimized formulation exhibited sustained release of CLA over 24 hours *in vitro* and was best described using the Baker-Lonsdale model. *In vitro* cytotoxicity data reveal that the CLA-NLC were less cytotoxic to HeLa cells when compared to CLA alone and further confirmed that the lipids and excipients used in these studies are of GRAS status.

Stability studies revealed a reduction in encapsulation efficiency over 28 days when stored at 4 °C and 22 °C and the particle size increased into the µm range at 22 °C. The findings are a good starting point but require further optimization to ensure prolongation of stability. In addition, the technology requires additional development possibly as a powder for reconstitution for use as a single-dose. The concept of single dose packaging may be a solution to the compromised formulation stability observed. The CLA-NLC produced in these studies exhibit sound product attributes which serve as a useful starting point for the novel delivery of antibiotics to the eye. However, further evaluation and elucidation of the minimum inhibitory concentration for development of clinically relevant single-dose therapy against *Mycobacterium fortuitum* and *Mycobacterium chelonae* when using these CLA-

loaded NLC is required. A structured and well-designed ocular absorption study, conducted using an appropriate *ex vivo* set up (porcine or bovine excised cornea and sclera) would be of use in elucidating the ocular absorption pathway/mechanism of CLA. In addition, the effect of the developed formulations on ocular absorption of CLA would be better understood. Furthermore, keratitis induces drastic changes in the barrier properties of the cornea where the epithelium and the stroma lose much of their barrier properties. Consequently, the use of an appropriate animal model of bacterial keratitis would provide an ideal opportunity to investigate the hypothesis that CLA-NLC would improve ocular efficacy of CLA.

The aforementioned results suggest that the optimized NLC have the potential to enhance precorneal retention and increase ocular availability of CLA, which in turn may be useful to reduce the required dose and dosing frequency when administering CLA to treat susceptible organisms. Given the sensitivity of the ocular system, future research would include production of the nanocarriers under sterile conditions and addition of antimicrobial preservatives prior to determining the ocular disposition, pharmacokinetics, efficacy and safety of CLA-NLC *in vivo*.

CHAPTER 6

CONCLUSIONS

Non-tuberculous precipitating *mycobacteria* are ecological pathogens which are a significant cause of a number of different human diseases. *Mycobacterium fortuitum* and *Mycobacterium chelonae* are examples of such *mycobacteria* and are a leading cause of infectious keratitis. The development of ocular non-tuberculous mycobacterial (NTM) keratitis has been attributed to trauma following penetration of the corneal epithelium. The use of topical corticosteroids suppresses granulomatous inflammation facilitating the growth of NMT in the eye. Outbreaks of NTM keratitis following laser-assisted *in situ* keratomileusis (LASIK) has been reported in Brazil, USA and Japan and are due to improper sterilization of surgical fluids and instruments subsequently leading to the introduction of pathogens to the corneal stroma during surgery. NTM is a common pathogen causing post-LASIK keratitis (47%) however causative agents of infectious keratitis vary by region with the highest rates being observed in developing countries.

The macrolide, clarithromycin (CLA) is a structural analogue of erythromycin A which is used in combination for the treatment of *Mycobacterium avium* complex and *Helicobacter pylori* infections. CLA exhibits inhibitory activity against > 275 NTM clinical isolates. The treatment of NTM keratitis with topical CLA has been successful however, toxic reactions, intolerance and patient discomfort due to frequent instillation of topical solutions of CLA is of concern. Commercially available CLA dosage forms for ocular use are not readily available and the *in vivo* efficacy of CLA for the treatment of NTM keratitis has, to date, been determined by reconstitution and use of lyophilized parenteral formulations administered *via* the ocular route. It is therefore imperative that research and development be focused on improving the delivery of CLA to the eye thereby addressing some or all of these unmet clinical needs.

An area of concern when considering ocular drug delivery is that only moderately-charged small molecules are likely to penetrate, albeit poorly, through the corneal epithelium. The passage of hydrophilic molecules is limited due to the tight junctions of the corneal epithelial cells while charged collagen fibres of the corneal stroma limit the successful passage of

hydrophobic molecules. Furthermore the collagen fibres of the stroma are organized into an ordered structure and can act as a sieve to large molecules, such as CLA. In addition, the constant flow of tears and tear films across the outer surfaces of the cornea, naso-lachrimal drainage and blinking contribute to a reduction in the availability of active pharmaceutical ingredients (API) to the anterior segment of the eye. Nano-particulate formulations have been investigated as potential ocular delivery systems intended to enhance corneal permeation thereby improving API availability to the eye whilst ensuring access to safe, non-invasive treatment approaches that also facilitate patient adherence. The muco-adhesive nature of some lipid-based nanocarriers can improve interaction with ocular membrane, resulting in prolonged residence times, enhanced availability and fewer local and/or systemic side effects.

Nanostructured lipid carriers (NLC) are innovative carrier technologies that are an alternative delivery approach to colloidal systems such as emulsions, liposomes and polymeric nanoparticles. NLC offer a number of advantages in comparison to the other colloidal carriers, including protecting the API and reducing potential degradation, facilitating targeting, reducing potential side effects and control of API release, *in vivo*. Consequently one objective of these studies, was to investigate the feasibility of developing CLA-loaded NLC that would have the potential to enhance precorneal retention of the API and increase ocular availability, which in turn may be useful to reduce the dose and dosing frequency when administering this antibiotic to treat NTM. The manufacture of NLC involves melting a binary mixture of a solid and liquid lipid, followed by re-dispersion of the molten lipids as submicron-sized droplets in an aqueous medium containing surfactant(s) with the aid of mechanical stirring. Although there are different methods of producing NLC the feasibility of encapsulation of CLA into colloidal carriers was investigated using a hot emulsification ultrasonication (HEUS) approach.

A vast number of analytical techniques can be used for the characterization of colloidal systems. Photon correlation spectroscopy (PCS) was used to determine the particle size (PS) and polydispersity index (PDI) of the systems manufactured in these studies. Although PCS is used to determine the PS and PDI of NLC, this technique does not provide information pertaining to the elemental and surface properties of the nanoparticles. Scanning electron microscopy (SEM) and energy-dispersive x-ray spectroscopy (EDX) were used to determine the topological characteristics of the colloidal systems produced in these studies. Laser

doppler anemometry (LDA) was used to determine the Zeta Potential of the systems which was used as a means of assessing the stability of the colloidal system. Crystallization and polymorphic transitions of the NLC were investigated using differential scanning calorimetry (DSC), wide-angle x-ray scattering (WAXS) and fourier transform infrared spectroscopy (FT-IR). FT-IR was used to investigate interactions between CLA and lipid raw materials. The osmolarity of NLC dispersions was determined by using freezing point depression. The loading capacity (LC), encapsulation efficiency (EE) and *in vitro* release of CLA from the NLC was evaluated using a reversed-phase high performance liquid chromatography (RP-HPLC) method developed and validated in these studies.

RP-HPLC is commonly used for the analysis of pharmaceutical products and is used for evaluation of a variety of sample matrices in the pharmaceutical industry. RP-HPLC can be used for the *in vitro* analysis of formulations such as NLC that possess lipid based complex matrices. Prior to initiating pre-formulation and formulation development studies Response Surface Methodology (RSM) using a Central Composite Design (CCD) was used for the development and validation of a RP-HPLC method coupled to an electrochemical detector (ECD) for the quantitative analysis of CLA in formulations and during *in vitro* dissolution testing conducted in these studies. Following a change to the stationary phase, the analytical run time was reduced and solvent consumption decreased facilitating environmental and financial sustainability of the method. Such a change in the method parameters requires re-validation of the method. The applicability of using the United States Pharmacopeia (USP) scaling approach in place of method re-validation using a column with a different L– designation to the original analytical column was also investigated. The scaled method met all USP system suitability requirements for resolution, tailing factor and % relative standard deviation (% RSD). The re-validated and scaled method was successfully used to resolve CLA from excipients used for the manufacture of pharmaceutical formulations and during *in vitro* dissolution testing. The scaled HPLC-ECD method was simple, precise, accurate, sensitive and stability indicating for the analysis of CLA, specifically for the determination of LC, EE and CLA release from the NLC. The separation between CLA and erythromycin (ERY) which was the internal standard was achieved using an isocratic separation with a Phenomenex Luna® CN, 5 µm 150 mm × 4.6 mm i.d cartridge column and a mobile phase of 36.5 % *v/v* acetonitrile, 5 % *v/v* methanol, a 50 mM phosphate buffer of pH = 7.00 set at a flow rate of 1.0 mL/min. The temperature of the analytical column was 30 °C and the

injection volume was 10 µL. The analytical electrode of the ECD was set at an oxidation potential of 1200 mV to monitor the eluent and the total run time for the analysis was 13 minutes. The method was validated according to ICH guidelines and was found to be suitable for the routine analysis of CLA-loaded NLC. Stock solutions of CLA in acetonitrile were found to be stable over seven days at 4 °C.

Prior to commencing formulation and development studies of CLA-NLC, pre-formulation studies aimed at investigating the thermal stability of CLA and characterization of the excipients were undertaken to facilitate the selection of suitable lipids for use in the manufacture of CLA-NLC. HEUS was selected as the method of production of CLA-NLC which would necessitate exposure of CLA to temperatures of approximately 85 °C and therefore an investigation of the thermal stability of CLA in addition to its crystalline and polymorphic state prior to and following exposure to heat was required. Thermogravimetric analysis (TGA) was used to evaluate the thermal stability of CLA and DSC and WAXS used to establish the crystalline and polymorphic nature of CLA prior to and following exposure to a temperature of 85 °C for one hour. TGA data revealed that CLA is thermostable up to a temperature of approximately 300 °C thereby confirming that the use of HEUS for the manufacture of CLA-NLC was unlikely to have any impact on the stability of the molecule. DSC and WAXS data revealed that exposure to a temperature of 85 °C would not result in a change in the crystallinity of CLA and no change in the polymorphic form of CLA, further confirming the suitability of HEUS for the production of the lipid nanocarriers.

The selection of lipid materials for the NLC formulation was undertaken following investigating the solubility of CLA in different solid and liquid lipids at 85 °C in order to select a binary mixture of a solid and liquid lipid with the best dissolution potential for CLA. The results of solubility studies revealed that CLA is poorly soluble in solid and liquid lipids however a combination of stearic acid (SA) and Transcutol® HP (THP) exhibited the best dissolution potential for CLA of all lipids tested. Consequently SA and THP were selected for use in the formulation and manufacture of CLA-loaded NLC.

The production process for NLC using HEUS may result in polymorphic modification(s) of the lipid matrices from which the lipid nanocarriers are produced. The degree of crystallization and polymorphic transition of lipids following exposure to heat during HEUS may also influence API incorporation, release and product quality. DSC and WAXS were

used to investigate the polymorphic and crystalline state of the lipid materials in addition to their potential to interact with CLA prior to and following exposure to 85 °C for one hour. The data generated revealed that SA appears to exist as the form B polymorph prior to exposure to heat and the form C polymorph following heating to 85 °C for one hour. The addition of THP to SA resulted in a delay in this transition of the solid lipid from the form B polymorph to the irreversible form C modification. It is therefore likely that NLC produced using SA and THP would exist as the form C polymorph of the lipid resulting in a hydrodynamic and stable system. However, the stability of these carriers, in terms of EE would have to be investigated.

The production and use of NLC requires that the mixture of solid and liquid lipids be solid at room and body temperatures implying that binary mixtures should possess a melting temperature onset > 40 °C. Consequently, the miscibility of SA and THP was investigated using different proportions of the solid and liquid lipids using DSC and an in-house filter paper test to determine the miscibility of the different lipid blends in order to identify the most suitable binary mixture of lipids that would be used for the formulation and manufacture of CLA-NLC. The optimum ratio of SA and THP used for the manufacture of NLC was 80:20 (*w/w*) and the binary mixture was miscible and had an onset melting point > 40 °C. The DSC, WAXS and FT-IR profiles for a ternary mixture of SA, THP and CLA generated prior to and following exposure to 85 °C for one hour revealed that any interaction between CLA and the lipid mixture selected for the production of the NLC was unlikely although, long term stability studies would be required to ensure this is indeed the case.

A Design of Experiments (DoE) approach, specifically a Box-Behnken Design (BBD) was used as a screening method to investigate the impact of five input variables on the production of CLA-loaded NLC. The input variables investigated included lipid content, Tween® 20 and PEG 6000 content, amplitude and sonication time. Further optimization with respect to the process parameters was undertaken in an attempt to establish the robustness of the formulation composition and performance to changes in process conditions using a CCD. Consequently, the effect of sonication time and amplitude of sonication on the target Critical Quality Attributes (CQA) *viz*. EE, LC, ZP, PS and PDI of the NLC, was investigated. In addition, the pH, osmolarity, muco-adhesive nature, cytotoxicity, *in vitro* CLA release, degree of crystallinity and lipid modification of the optimized NLC were investigated to

ensure that a product of desirable quality had been produced. The ZP of the optimized nanocarriers was determined in HPLC grade water and ranged between -19.3 to -32.2 mV and -14.7 to -33.7 mV following storage for 28 days at 4 °C and 22 °C, respectively. The agglomeration threshold for dispersions is defined at a ZP range of -20 to -11 mV and was not achieved following assessment after 28 days storage at 4 °C and 22 °C which is consistent with the data generated as none of the products tested were observed to agglomerate over the stability test period.

The optimized NLC exhibited muco-adhesive properties under stationary conditions assessed using LDA and sustained release of CLA was observed over the 24-hour test period. *In vitro* cytotoxicity studies revealed that the CLA-NLC exhibited improved cell viability when compared to pure CLA which was attributed to the shielding effect of the encapsulating lipids used further emphasizing the protective nature of NLC technology. In addition, the use of PEG may form a hydrophilic and protective layer on the surface of the nanoparticles resulting in a reduction in the interaction and subsequent uptake of the CLA-NLC by human cervix adenocarcinoma (HeLa) cells. Furthermore, the high % viability of HeLa cells was observed following exposure of the cells to control/blank NLC confirming that the excipients used in these studies are generally regarded as safe (GRAS).

The DSC thermogram for the optimized CLA-NLC revealed the presence of two endothermic events, characteristic of the solid and liquid lipids in the mixture and PEG 6000. The thermogram confirmed the absence of characteristic events for CLA indicating the existence of single polymorphic forms of the excipients used and that CLA was molecularly dispersed internally in the NLC. The melting point of the lipid mixture observed was consistent of the presence of the form C polymorph of SA.

The WAXS diffractogram for the optimized CLA-NLC revealed the absence of the principle bands for CLA and these findings are in agreement with those observed when evaluating the DSC data that revealed that CLA was molecularly dispersed within the NLC. The characteristic bands for PEG 6000 matched well with literature reports [343], further confirming that CLA was dissolved in the PEG-coated NLC.

The FT-IR spectra for optimized CLA-NLC product revealed the presence of all characteristic bands for SA. The frequency bands consistent with molecular vibrations of CLA were not observed in the colloidal system, confirming the DSC and WAXS data that suggested CLA was molecularly dispersed within the lipid matrix. The NLC also revealed the presence of characteristic bands consistent with molecular vibrations for PEG 6000 suggesting that PEG was on the exterior surface and coated the nanoparticles. The band intensity for the optimized CLA-NLC was lower than that of the intensity observed for the excipients used during the manufacturing process, which may indicate the amorphous nature of the manufactured nanocarrier formulation.

The results of stability studies revealed fairly constant PS and PDI data for NLC stored at 4 °C in comparison to the formulations stored at 22 °C which exhibited an increase in the PS and PDI. Storage at elevated temperatures are known to increase the kinetic energy of particles, which in turn lead to increased numbers of collisions between particles with a corresponding increase in particle size due to agglomeration. The PS for NLC stored at 4 °C remained within the nanometer size range during the incubation period with those stored at 22 °C increasing to approximately 1.8 μm in diameter.

The unexpected loss of CLA of up to 14.42% at 4 °C in comparison to that of 5.14% from the NLC stored at 22 °C following storage for 28 days may be a consequence of the depolarizing effect of PEG, which alters the partitioning of hydrophobic molecules between the interior and the exterior of lipid bilayers under these conditions. The pH and osmalirity of the NLC formulations stored at 4 °C and 22 °C for 28 days were between 3.5-10.5 and 250-450 mOsm/kg, respectively which is readily tolerated by the human eye.

This research has demonstrated the feasibility of using HEUS to manufacture CLA-loaded NLC stabilized with Tween®20. The CLA-NLC have the potential to enhance ocular permeability and reduce toxicity and the optimized formulation exhibited sustained and controlled release of CLA when fitted to a number of kinetic models. The results of kinetic modelling revealed that CLA release from the optimized NLC was best fitted by the Baker-

Lonsdale model which describes controlled release mechanisms for CLA from spherical shaped lipid matrices, involving diffusion and degradation as the primary factors affecting release. The *in vitro* release and muco-adhesive properties of the optimized CLA-NLC indicate that these systems have the potential to enhance precorneal retention, increase ocular availability and permit dose reduction or permit use of a longer dosing frequency. However, additional and alternate *in vitro* and appropriately designed *in vivo* studies are necessary to establish if this is indeed the case.

The findings are a good starting point but require further optimization to ensure prolongation of stability. In addition, the technology should be further investigated and the use of a powder for reconstitution as a single-dose so as to optimize formulation stability can be considered. In addition, a structured and well-designed ocular absorption study, conducted using an appropriate *ex vivo* set up (porcine or bovine excised cornea and sclera) would be of use in elucidating the ocular absorption pathway/mechanism of CLA as well as understanding the effect of the developed formulations on ocular absorption of CLA. Furthermore, keratitis induces drastic changes in the barrier properties of the cornea where the epithelium and the stroma lose much of their barrier properties. Consequently, the use of an appropriate animal model of bacterial keratitis would provide an ideal opportunity to investigate the hypothesis that CLA-NLC would improve ocular efficacy of CLA. The CLA-NLC produced in these studies have provided a useful foundation for investigating the delivery of antibiotics to the eye, however further evaluation as mentioned above, and determination of the minimum inhibitory concentration for development of a clinically relevant single-dose therapy against *Mycobacterium fortuitum and Mycobacterium chelonae* should be undertaken.

HEUS is a relatively easy laboratory-scale method commonly used for NLC manufacture. However, the quality and narrow size distribution of the nanocarriers produced is generally compromised by the presence of microparticles. Furthermore, metallic contamination from the ultrasonic probe used during sonication may also occur [121,240,353]. High pressure homogenization (HPH) is the most reliable and scalable technique for the production of NLC [205]. In contrast to HEUS, HPH manufacturing can be applied to laboratory and industrial scale production of NLC while avoiding the introduction of microparticles and metallic contamination in the dispersions. The feasibility of producing CLA loaded NLC for

ophthalmic used using HEUS has been demonstrated however, formulations of CLA-NLC manufactured using HPH should be investigated to establish the feasibility of manufacturing these on a large scale. In addition, enhanced formulation stability and more homogenous particles may be a potential outcome using this approach.

The research outcomes reported *vide infra* have been published in peer-reviewed journals as follows and the full manuscripts are included in Appendix II.

1. **Makoni, P.A.**; Chikukwa, M.T.R.; Khamanga, S.M.; Walker, R.B. Stability Indicating HPLC-ECD Method for the Analysis of Clarithromycin in Pharmaceutical Dosage Forms: Method Scaling versus Re-Validation. *Sci. Pharm.* **2019**, *87*, 31

2. **Makoni, P.A.**; Ranchhod, J.; WaKasongo, K.; Khamanga, S.M.; Walker, R.B. The use of quantitative analysis and Hansen solubility parameter predictions for the selection of excipients for lipid nanocarriers to be loaded with water soluble and insoluble compounds. *Saudi Pharm.* J. **2020**, *28*, 305–315.

3. **Makoni, P.A.**; Khamanga, S.M.; Walker, R.B. Muco-adhesive Clarithromycin-Loaded Nanostructured Lipid Carriers for Ocular Delivery: Formulation, Characterization, Cytotoxicity and Stability. *J Drug Deliv Sci Technol*. **(In Press)** https://doi.org/10.1016/j.jddst.2020.102171

REFERENCES

1. L.K. Bekele and G.G. Gebeyehu, Application of Different Analytical Techniques and Microbiological Assays for the Analysis of Macrolide Antibiotics from Pharmaceutical Dosage Forms and Biological Matrices, ***ISRN Analytical Chemistry*** 2012 (2012) 1–17.
2. I. Kanfer, M.F. Skinner, and R.B. Walker, Analysis of macrolide antibiotics, ***Journal of Chromatography A*** 812 (1998) 255–286.
3. G.-F. Pang, Macrolides, *in Anal. Methods Food Saf. by Mass Spectrom. Elsevier*, (2018): pp. 195–264.
4. T. Kaneko, T.J. Dougherty, and T.V. Magee, Macrolide Antibiotics, *in Compr. Med. Chem. II. Elsevier*, (2007): pp. 519–566.
5. Z. Ma, A.M. Ginsberg, and M. Spigelman, Antimycobacterium agents, *in Compr. Med. Chem. II. Elsevier Ltd.*, (2006): pp. 699–730.
6. R. Vardanyan and V. Hruby, Chapter 30 – Antibiotics, *in Synth. Best-Seller Drugs*. (2016): pp. 573–643.
7. A. Dasgupta, Advances in antibiotic measurement, *in Adv. Clin. Chem. Academic Press Inc.*, (2012): pp. 75–104.
8. J.M. Zuckerman, F. Qamar, and B.R. Bono, Macrolides, Ketolides, and Glycylcyclines: Azithromycin, Clarithromycin, Telithromycin, Tigecycline, ***Infectious Disease Clinics of North America*** 23 (4) (2009) 997–1026.
9. D. Jelić and R. Antolović, From erythromycin to azithromycin and new potential ribosome-binding antimicrobials, ***Antibiotics*** 5 (3) (2016).
10. K.A. Rodvold, Clinical pharmacokinetics of clarithromycin, ***Clinical Pharmacokinetics*** 37 (5) (1999) 385–398.
11. D. Rossiter and University of Cape Town. Division of Clinical Pharmacology., *South African medicines formulary*, 12th ed., *Health and Medical Pub. Group*, Claremont South Africa, (2016).
12. W. Nie, H. Duan, H. Huang, Y. Lu, and N. Chu, Species Identification and Clarithromycin Susceptibility Testing of 278 Clinical Nontuberculosis Mycobacteria Isolates, ***BioMed Research International*** 2015 (2015).
13. B.A. Brown, R.J. Wallace, G.O. Onyi, V. De Rosas, and R.J. Wallace, Activities of Four Macrolides, Including Clarithromycin, against Mycobacterium fortuitum,

Mycobacterium chelonae, and M chelonae-Like Organisms, ***Antimicrobial Agents and Chemotherapy*** 36 (1) (1992) 180–184.

14. S.C.M. Huang, H.K. Soong, J.S. Chang, and Y.S. Liang, Non-tuberculous mycobacterial keratitis: A study of 22 cases, ***British Journal of Ophthalmology*** 80 (11) (1996) 962–968.
15. H.S. Chu and F.R. Hu, Non-tuberculous mycobacterial keratitis, ***Clinical Microbiology and Infection*** 19 (3) (2013) 221–226.
16. F.R. Hu, W.J. Huang, and S.F. Huang, Clinicopathologic study of satellite lesions in nontuberculous mycobacterial keratitis, ***Japanese Journal of Ophthalmology*** 42 (2) (1998) 115–118.
17. N.S. Chandra, M.F. Torres, K.L. Winthrop, D.A. Bruckner, D.G. Heidemann, H.M. Calvet, M. Yakrus, B.J. Mondino, and G.N. Holland, Cluster of Mycobacterium chelonae keratitis cases following laser in-situ keratomileusis, ***American Journal of Ophthalmology*** 132 (6) (2001) 819–830.
18. T. Yamaguchi, H. Bissen-Miyajima, Y. Hori-Komai, Y. Matsumoto, N. Ebihara, H. Takahashi, K. Tsubota, and J. Shimazaki, Infectious keratitis outbreak after laser in situ keratomileusis at a single laser center in Japan, ***Journal of Cataract and Refractive Surgery*** 37 (5) (2011) 894–900.
19. D. Freitas, L. Alvarenga, J. Sampaio, M. Mannis, E. Sato, L. Sousa, L. Vieira, M.C. Yu, M.C. Martins, A. Hoffling-Lima, and R. Belfort, An outbreak of Mycobacterium chelonae infection after LASIK, ***Ophthalmology*** 110 (2) (2003) 276–285.
20. M.A. Chang, S. Jain, and D.T. Azar, Infections following laser in situ keratomileusis: An Integration of the published literature, ***Survey of Ophthalmology*** 49 (3) (2004) 269–280.
21. P.A. Thomas and P. Geraldine, Infectious keratitis, ***Current Opinion in Infectious Diseases*** 20 (2) (2007) 129–141.
22. M.J. Doughty and M.L. Zaman, Human corneal thickness and its impact on intraocular pressure measures: A review and meta-analysis approach, ***Survey of Ophthalmology*** 44 (5) (2000) 367–408.
23. A. Edwards and M.R. Prausnitz, Predicted permeability of the cornea to topical drugs, ***Pharmaceutical Research*** 18 (11) (2001) 1497–1508.
24. M.R. Prausnitz and J.S. Noonan, Permeability of cornea, sclera, and conjunctiva: A literature analysis for drug delivery to the eye, ***Journal of Pharmaceutical Sciences*** 87 (12) (1998) 1479–1488.

25. Y.C. Kim, B. Chiang, X. Wu, and M.R. Prausnitz, Ocular delivery of macromolecules, ***Journal of Controlled Release*** 190 (2014) 172–181.
26. L.L. Mitic, C.M. Van Itallie, and J.M. Anderson, Molecular physiology and pathophysiology of tight junctions I Tight junction structure and function: Lessons from mutant animals and proteins, ***American Journal of Physiology - Gastrointestinal and Liver Physiology*** 279 (2 42-2) (2000).
27. T. John and E. Velotta, Nontuberculous (Atypical) Mycobacterial Keratitis After LASIK, ***Cornea*** 24 (3) (2005) 245–255.
28. R.S. Moorthy, S. Valluri, and N.A. Rao, Nontuberculous Mycobacterial Ocular and Adnexal Infections, ***Survey of Ophthalmology*** 57 (3) (2012) 202–235.
29. F.R. Hu, Extensive lamellar keratectomy for treatment of nontuberculous mycobacterial keratitis, ***American Journal of Ophthalmology*** 120 (1) (1995) 47–54.
30. M. Lazar, P. Nemet, R. Bracha, and A. Campus, Mycobacterium fortuitum keratitis, ***American Journal of Ophthalmology*** 78 (3) (1974) 530–532.
31. R.H. Gross, G.N. Holland, S.J. Elias, and R. Tuz, Corneal pharmacokinetics of topical clarithromycin, ***Investigative Ophthalmology and Visual Science*** 36 (5) (1995) 965–968.
32. J.G. Ford, A.J.W. Huang, S.C. Pflugfelder, E.C. Alfonso, R.K. Forster, and D. Miller, Nontuberculous mycobacterial keratitis in South Florida, ***Ophthalmology*** 105 (9) (1998) 1652–1658.
33. C.J. Helm, G.N. Holland, R. Lin, O.G.W. Berlin, and D.A. Bruckner, Comparison of Topical Antibiotics for Treating Mycobacterium fortuitum Keratitis in an Animal Model, ***American Journal of Ophthalmology*** 116 (6) (1993) 700–707.
34. *Moorfields Eye Hospital Ophthalmic Formulary Medicines Information Publication Ophthalmic Formulary NICE*, (2017).
35. E.C. Ogoko, S.A. Odoemelam, B.I. Ita, and N.O. Eddy, Adsorption and Inhibitive Properties of Clarithromycin for the Corrosion of Zn in 001 to 005 M H 2 SO 4, ***Portugaliae Electrochimica Acta*** 27 (6) (2009) 713–724.
36. United States Pharmacopoeia, ***United States Pharmacopoeia 43-National Formulary 38*** (2019).
37. Chemmart Clarithromycin, ***Symbion Pharmacy Services Pty Ltd*** (2009) 1–18.
38. Y. Nakagawa, S. Itai, T. Yoshida, and T. Nagai, Physicochemical Properties and Stability in the Acidic Solution of a New Macrolide Antibiotic, Clarithromycin, in Comparison with Erythromycin, ***Chemical & Pharmaceutical Bulletin*** 40 (3) (1992)

725–728.

39. A. Tanigake, Y. Miyanaga, T. Nakamura, E. Tsuji, K. Matsuyama, M. Kunitomo, and T. Uchida, The Bitterness Intensity of Clarithromycin Evaluated by a Taste Sensor, ***Chemical & Pharmaceutical Bulletin*** 51 (11) (2003) 1241–1245.
40. S. Shinoda and P. Becher, *Principles of Solution and Solubility*, *Marcel Dekker, Inc*, New York, USA, (1978).
41. Clarithromycin, ***Tuberculosis*** 88 (2) (2008) 92–95.
42. E. Esfandi, V. Ramezani, A. Vatanara, A.R. Najafabadi, S. Pouya, and H. Moghaddam, Clarithromycin Dissolution Enhancement by Preparation of Aqueous Nanosuspensions Using Sonoprecipitation Technique, ***Iranian Journal of Pharmaceutical Research*** 13 (3) (2014) 809–818.
43. S. Babić, A.J.M. Horvat, D. Mutavdžić Pavlović, and M. Kaštelan-Macan, Determination of pKa values of active pharmaceutical ingredients, ***TrAC - Trends in Analytical Chemistry*** 26 (11) (2007) 1043–1061.
44. J.G. Speight, Molecular Interactions, Partitioning, and Thermodynamics, *in React. Mech. Environ. Eng. Elsevier*, (2018): pp. 307–336.
45. C.C. Bannan, G. Calabró, D.Y. Kyu, and D.L. Mobley, Calculating Partition Coefficients of Small Molecules in Octanol/Water and Cyclohexane/Water, ***Journal of Chemical Theory and Computation*** 12 (8) (2016) 4015–4024.
46. P.B. Fernandes, D.J. Hardy, D. McDaniel, C.W. Hanson, and R.N. Swanson, In vitro and in vivo activities of clarithromycin against Mycobacterium avium, ***Antimicrobial Agents and Chemotherapy*** 33 (9) (1989) 1531–1534.
47. F. Doucet-Populaire, Molecular basis of clarithromycin activity against Mycobacterium avium and Mycobacterium smegmatis, ***Journal of Antimicrobial Chemotherapy*** 41 (2) (1998) 179–187.
48. S. Naveed and F. Qamar, Simple UV spectrophotometric assay of Clarithromycin, ***International Journal of Pharma Sciences and Research*** 5 (9) (2014) 582–585.
49. I.I. Salem, *Analytical Profiles of Drug Substances and Excipients*, *Academic Press Inc.*, (1996).
50. M. Sharma, N. Gupta, and S. Gupta, Implications of designing clarithromycin loaded solid lipid nanoparticles on their pharmacokinetics, antibacterial activity and safety, ***RSC Advances*** 6 (80) (2016) 76621–76631.
51. M.M. Huber, S. Korhonen, T.A. Ternes, and U. von Gunten, Oxidation of pharmaceuticals during water treatment with chlorine dioxide, ***Water Research*** 39 (15)

(2005) 3607–3617.

52. Y. Tozuka, A. Ito, H. Seki, T. Oguchi, and K. Yamamoto, Characterization and Quantitation of Clarithromycin Polymorphs by Powder X-Ray Diffractometry and Solid-State NMR Spectroscopy, ***Chemical & Pharmaceutical Bulletin*** 50 (8) (2002) 1128–1130.
53. G.A. Stephenson, J.G. Stowell, P.H. Toma, R.R. Pfeiffer, and S.R. Byrn, Solid-state investigations of erythromycin A dihydrate: Structure, NMR spectroscopy, and hygroscopicity, ***Journal of Pharmaceutical Sciences*** 86 (11) (1997) 1239–1244.
54. Y.T. Sohn, J.K. Rhee, and W.B. Im, Polymorphism of clarithromycin, ***Archives of Pharmacal Research*** 23 (4) (2000) 381–4.
55. J.-H. Liu, R.F. Henry, S.G. Spanton, and D.A. Riley, US6627743B1 - 6-O-methylerythromycin A crystal form III - Google Patents, 1999.
56. K.-H. Suh, S.-M. Yun, M.-R. Seong, G.-J. Kim, G.-S. Lee, and N.-D. Kim, US Patent for Method of preparing form II crystals of clarithromycin Patent - Justia Patents, 2003.
57. I. Avrutov, I. Lifshitz, R. Borochovitz, B. Masarwa, and E. Schwartz, US20040058879A1 - Processes for preparing clarithromycin polymorphs and novel polymorph IV - Google Patents, 2000.
58. F. Faghihzadeh, N.M. Anaya, L.A. Schifman, and V. Oyanedel-Craver, Fourier transform infrared spectroscopy to assess molecular-level changes in microorganisms exposed to nanoparticles, ***Nanotechnology for Environmental Engineering*** 1 (1) (2016).
59. J.P. Coates, The interpretation of infrared spectra: Published reference sources, ***Applied Spectroscopy Reviews*** 31 (1–2) (1996) 179–192.
60. S. Hardikar and A. Bhosale, Formulation and evaluation of gastro retentive tablets of clarithromycin prepared by using novel polymer blend, ***Bulletin of Faculty of Pharmacy, Cairo University*** 56 (2) (2018) 147–157.
61. S.M. Khamanga, Formulation and evaluation of captopril loaded polymethacrylate and hydropropyl methylcellulose microcapsules, Rhodes University, 2010.
62. A. Awan, J. Barber, R.J. Brennan, and J.A. Parkinson, Structural studies on clarithromycin (6-O-methylerythromycin A): Assignments of the1H and13C NMR spectra in organic and aqueous solutions, ***Magnetic Resonance in Chemistry*** 30 (12) (1992) 1241–1246.
63. P.A. Makoni, M.T.R. Chikukwa, S.M. Khamanga, and R.B. Walker, Stability

Indicating HPLC-ECD Method for the Analysis of Clarithromycin in Pharmaceutical Dosage Forms: Method Scaling versus Re-Validation, ***Scientia Pharmaceutica*** 87 (4) (2019) 31.

64. V.K. Kansal, D.N. Mistry, M. Gandhi, and R.R. Patel, United States Patent Application: 0090054634-Process for the preparation of clarithromycin, 2008.
65. S. Mabe, J. Eller, and W.S. Champney, Structure-Activity Relationships for Three Macrolide Antibiotics in Haemophilus influenzae, ***Current Microbiology*** 49 (2004) 248–254.
66. I. Odenholt-Tornqvist, E. Löwdin, and O. Cars, Postantibiotic effects and postantibiotic sub-MIC effects of roxithromycin, clarithromycin, and azithromycin on respiratory tract pathogens, ***Antimicrobial Agents and Chemotherapy*** 39 (1) (1995) 221–6.
67. F. Schlünzen, J.M. Harms, F. Franceschi, H.A.S. Hansen, H. Bartels, R. Zarivach, and A. Yonath, Structural basis for the antibiotic activity of ketolides and azalides, ***Structure (London, England : 1993)*** 11 (3) (2003) 329–38.
68. J.L. Hansen, J.A. Ippolito, N. Ban, P. Nissen, P.B. Moore, and T.A. Steitz, The structures of four macrolide antibiotics bound to the large ribosomal subunit, ***Molecular Cell*** 10 (1) (2002) 117–28.
69. Z.J. Zhu, O. Krasnykh, D. Pan, V. Petukhova, G. Yu, Y. Liu, H. Liu, S. Hong, Y. Wang, B. Wan, W. Liang, and S.G. Franzblau, Structure-activity relationships of macrolides against Mycobacterium tuberculosis, ***Tuberculosis*** 88 (SUPPL. 1) (2008).
70. R. Piccolomini, G. Catamo, and G. Di Bonaventura, Bacteriostatic and bactericidal in vitro activities of clarithromycin and erythromycin against periodontopathic Actinobacillus actinomycetemcomitans, ***Antimicrobial Agents and Chemotherapy*** 42 (11) (1998) 3000–1.
71. S. McKenna and G.A. Evans, Macrolides: A Canadian infectious disease society position paper, ***Canadian Journal of Infectious Diseases*** 12 (4) (2001) 218–231.
72. Y. Cohen, C. Perronne, C. Truffot-Pernot, J. Grosset, J.L. Vilde, and J.J. Pocidalo -, Activities of WIN-57273, minocycline, clarithromycin, and 14-hydroxy-clarithromycin against Mycobacterium avium complex in human macrophages, ***Antimicrobial Agents and Chemotherapy*** 36 (10) (1992) 2104–2107.
73. K. Takeshita, I. Yamagishi, M. Harada, S. Otomo, T. Nakagawa, and Y. Mizushima, Immunological and anti-inflammatory effects of clarithromycin: inhibition of interleukin 1 production of murine peritoneal macrophages, ***Drugs under***

Experimental and Clinical Research 15 (11–12) (1989) 527–33.

74. M.S. Whitman and A.R. Tunkel, Azithromycin and Clarithromycin: Overview and Comparison with Erythromycin, ***Infection Control and Hospital Epidemiology*** 13 (6) (1992) 357–368.
75. J.P. Gisbert, L. González, X. Calvet, N. García, T. López, M. Roqué, R. Gabriel, and J.M. Pajares, Proton pump inhibitor, clarithromycin and either amoxycillin or nitroimidazole: A meta-analysis of eradication of Helicobacter pylori, ***Alimentary Pharmacology and Therapeutics*** 14 (10) (2000) 1319–1328.
76. J.Q. Huang and R.H. Hunt, The importance of clarithromycin dose in the management of Helicobacter pylori infection: a meta-analysis of triple therapies with a proton pump inhibitor, clarithromycin and amoxycillin or metronidazole, ***Alimentary Pharmacology and Therapeutics*** 13 (6) (1999) 719–729.
77. D.R.P. Guay, D.R. Patterson, N. Seipman, and J.C. Craft, Overview of the Tolerability Profile of Clarithromycin in Preclinical and Clinical Trials, ***Drug Safety*** 8 (5) (1993) 350–364.
78. M. LeBel, Pharmacokinetic Properties of Clarithromycin: A Comparison with Erythromycin and Azithromycin, ***Canadian Journal of Infectious Diseases*** 4 (3) (1993) 148–152.
79. F. Bril, C. Gonzalez, and G. Di Girolamo, Antimicrobial Agents-Associated with QT Interval Prolongation, ***Current Drug Safety*** 5 (1) (2009) 85–92.
80. S.C. Ausband and P.E. Goodman, An unusual case of clarithromycin associated ergotism, ***The Journal of Emergency Medicine*** 21 (4) (2001) 411–3.
81. R.S. Horowitz, R.C. Dart, and H.F. Gomez, Clinical ergotism with lingual ischemia induced by clarithromycin-ergotamine interaction, ***Archives of Internal Medicine*** 156 (4) (1996) 456–8.
82. M. Kawada, K. Okuzumi, S. Hitomi, and C. Sugishita, Transmission of Staphylococcus aureus between healthy, lactating mothers and their infants by breastfeeding, ***Journal of Human Lactation : Official Journal of International Lactation Consultant Association*** 19 (4) (2003) 411–7.
83. P.B. Bookstaver, C.M. Bland, B. Griffin, K.R. Stover, L.S. Eiland, and M. McLaughlin, A Review of Antibiotic Use in Pregnancy, ***Pharmacotherapy: The Journal of Human Pharmacology and Drug Therapy*** 35 (11) (2015) 1052–1062.
84. J.T. Andersen, M. Petersen, E. Jimenez-Solem, K. Broedbaek, N.L. Andersen, C. Torp-Pedersen, N. Keiding, and H.E. Poulsen, Clarithromycin in Early Pregnancy and

the Risk of Miscarriage and Malformation: A Register Based Nationwide Cohort Study, ***PLoS ONE*** 8 (1) (2013) e53327.

85. C.R. Drinkard, D. Shatin, and J. Clouse, Postmarketing surveillance of medications and pregnancy outcomes: Clarithromycin and birth malformations, ***Pharmacoepidemiology and Drug Safety*** 9 (7) (2000) 549–556.
86. A. Einarson, E. Phillips, F. Mawji, D. D'Alimonte, B. Schick, A. Addis, P. Mastroiacova, T. Mazzone, D. Matsui, and G. Koren, A prospective controlled multicentre study of clarithromycin in pregnancy, ***American Journal of Perinatology*** 15 (9) (1998) 523–525.
87. P.G. Davey, The pharmacokinetics of clarithromycin and its 14-OH metabolite, ***Journal of Hospital Infection*** 19 (1991) 29–37.
88. S. -y Chu, G.R. Granneman, P.J. Pichotta, J.P. Decourt, J. Girault, and J.B. Fourtillan, Effect of Moderate or Severe Hepatic Impairment on Clarithromycin Pharmacokinetics, ***The Journal of Clinical Pharmacology*** 33 (5) (1993) 480–485.
89. D. Pessayre, M. Tinel, D. Larrey, B. Cobert, C. Funck-Brentano, and G. Babany, Inactivation of cytochrome P-450 by a troleandomycin metabolite Protective role of glutathione, ***The Journal of Pharmacology and Experimental Therapeutics*** 224 (3) (1983) 685–91.
90. G. Danan, V. Descatoire, and D. Pessayre, Self-induction by erythromycin of its own transformation into a metabolite forming an inactive complex with reduced cytochrome P-450, ***The Journal of Pharmacology and Experimental Therapeutics*** 218 (2) (1981) 509–14.
91. M.P. Pai, D.M. Graci, and G.W. Amsden, Macrolide drug interactions: an update, ***The Annals of Pharmacotherapy*** 34 (4) (2000) 495–513.
92. B. Cronnolly and H. Pegrum, Fentanyl - clarithromycin interaction, ***Case Reports*** 2012 (jul06 1) (2012) bcr0220125936–bcr0220125936.
93. N. Yasui, K. Otani, S. Kaneko, R. Shimoyama, T. Ohkubo, and K. Sugawara, Carbamazepine toxicity induced by clarithromycin coadministration in psychiatric patients, ***International Clinical Psychopharmacology*** 12 (4) (1997) 225–229.
94. G.W. Amsden, K.L. Cheng, C.A. Peloquin, and A.N. Nafziger, Oral cimetidine prolongs clarithromycin absorption, ***Antimicrobial Agents and Chemotherapy*** 42 (7) (1998) 1578–1580.
95. R.K. Piquette, Torsade de pointes induced by cisapride/clarithromycin interaction, ***The Annals of Pharmacotherapy*** 33 (1) (1999) 22–6.

96. M.A. Sekkarie, Torsades de pointes in two chronic renal failure patients treated with cisapride and clarithromycin, ***American Journal of Kidney Diseases*** 30 (3) (1997) 437–439.

97. P.B. Watkins, The role of cytochromes P-450 in cyclosporine metabolism, ***Journal of the American Academy of Dermatology*** 23 (6) (1990) 1301–1311.

98. B. Sadaba, A. Lopez de Ocariz, J.R. Azanza, J. Quiroga, and J.A. Cienfuegos, Concurrent clarithromycin and cyclosporin A treatment, ***Journal of Antimicrobial Chemotherapy*** 42 (3) (1998) 393–395.

99. I.S. Sketris, M.R. Wright, and M.L. West, Possible role of the intestinal P-450 enzyme system in a cyclosporine-clarithromycin interaction, ***Pharmacotherapy*** 16 (2 I) (1996) 301–305.

100. A. Sutton and M.A. Pilot, Digoxin toxicity and erythromycin, ***British Medical Journal*** 298 (6680) (1989) 1101.

101. S.E. Guerriero, E. Ehrenpreis, and K.L. Gallagher, Two cases of clarithromycin-induced digoxin toxicity, ***Pharmacotherapy*** 17 (5 I) (1997) 1035–1037.

102. J. Yan, J. Shen, Y. Li, F. Tang, and N. Chen, Survey about the use of clarithromycin in an ENT outpatient department of a tertiary hospital, ***European Archives of Oto-Rhino-Laryngology*** 274 (8) (2017) 3103–3107.

103. R.A. Yeates, H. Laufen, and T. Zimmermann, Interaction between midazolam and clarithromycin: Comparison with azithromycin, ***International Journal of Clinical Pharmacology and Therapeutics*** 34 (9) (1996) 400–405.

104. D.A. Flockhart, M.D. Drici, T. Kerbusch, N. Soukhova, E. Richard, P.L. Pearle, S.K. Mahal, and V.J. Babb, Studies on the mechanism of a fatal clarithromycin-pimozide interaction in a patient with Tourette syndrome, ***Journal of Clinical Psychopharmacology*** 20 (3) (2000) 317–24.

105. E. Rubinstein, Comparative safety of the different macrolides, ***International Journal of Antimicrobial Agents*** 18 (SUPPL.1) (2001) 71–76.

106. G. Apseloff, G. Foulds, L. LaBoy-Goral, S. Willavize, and J. Vincent, Comparison of azithromycin and clarithromycin in their interactions with rifabutin in healthy volunteers, ***Journal of Clinical Pharmacology*** 38 (9) (1998) 830–5.

107. N. Corti, A. Taegtmeyer, and A. Imhof, Miscellaneous antibacterial drugs, *in Side Eff. Drugs Annu.* (2011): pp. 509–540.

108. M.W. Recker and K.L. Kier, Potential interaction between clarithromycin and warfarin, ***The Annals of Pharmacotherapy*** 31 (9) (1997) 996–8.

109. K.C. Oberg, Delayed elevation of international normalized ratio with concurrent clarithromycin and warfarin therapy, ***Pharmacotherapy*** 18 (2 I) (1998) 386–391.
110. M.A. Polis, S.C. Piscitelli, S. Vogel, F.G. Witebsky, P.S. Conville, B. Petty, J.A. Kovacs, R.T. Davey, R.E. Walker, J. Falloon, J.A. Metcalf, C. Craft, H.C. Lane, and H. Masur, Clarithromycin lowers plasma zidovudine levels in persons with human immunodeficiency virus infection, ***Antimicrobial Agents and Chemotherapy*** 41 (8) (1997) 1709–1714.
111. M.N. Alekshun and S.B. Levy, Molecular Mechanisms of Antibacterial Multidrug Resistance, ***Cell*** 128 (6) (2007) 1037–1050.
112. C.A. Widdowson and K.P. Klugman, Molecular mechanisms of resistance to commonly used non-betalactam drugs in Streptococcus pneumoniae, ***Seminars in Respiratory Infections*** 14 (3) (1999) 255–68.
113. J. Zhang, L. Wang, J. Zhou, L. Zhang, H. Xia, T. Zhou, and H. Zhang, Ocular penetration and pharmacokinetics of topical clarithromycin eye drops to rabbits, ***Journal of Ocular Pharmacology and Therapeutics*** 30 (1) (2014) 42–48.
114. M.B. Al-Sibai, A.S. Al-Kaff, D. Raines, and A. El-Yazigi, Ocular Penetration of Oral Clarithromycin in Humans, ***Journal of Ocular Pharmacology and Therapeutics*** 14 (6) (1998) 575–583.
115. M. Bin-Jumah, S.J. Gilani, M.A. Jahangir, A. Zafar, S. Alshehri, M. Yasir, C. Kala, M. Taleuzzaman, and S.S. Imam, Clarithromycin-Loaded Ocular Chitosan Nanoparticle: Formulation, Optimization, Characterization, Ocular Irritation, and Antimicrobial Activity , ***International Journal of Nanomedicine*** Volume 15 (2020) 7861–7875.
116. D.H. Peters and S.P. Clissold, Clarithromycin A review of its antimicrobial activity, pharmacokinetic properties and therapeutic potential, ***Drugs*** 44 (1) (1992) 117–164.
117. J.L. Ferrero, B.A. Bopp, K.C. Marsh, S.C. Quigley, M.J. Johnson, D.J. Anderson, J.E. Lamm, K.G. Tolman, S.W. Sanders, and J.H. Cavanaugh, Metabolism and disposition of clarithromycin in man, ***Drug Metabolism and Disposition: The Biological Fate of Chemicals*** 18 (4) (n.d.) 441–6.
118. P.A. Lartey, H.N. Nellans, and S.K. Tanaka, New Developments in Macrolides: Structures and Antibacterial and Prokinetic Activities, *in Adv. Pharmacol.* (1994): pp. 307–343.
119. V. Agrahari, A. Mandal, V. Agrahari, H.M. Trinh, M. Joseph, A. Ray, H. Hadji, R. Mitra, D. Pal, and A.K. Mitra, A comprehensive insight on ocular pharmacokinetics,

Drug Delivery and Translational Research 6 (6) (2016) 735–754.

120. D. Ghate and H.F. Edelhauser, Barriers to Glaucoma Drug Delivery, ***Journal of Glaucoma*** 17 (2) (2008) 147–156.
121. A. Khosa, S. Reddi, and R.N. Saha, Nanostructured lipid carriers for site-specific drug delivery, ***Biomedicine and Pharmacotherapy*** 103 (2018) 598–613.
122. M.R. Siddiqui, Z.A. AlOthman, and N. Rahman, Analytical techniques in pharmaceutical analysis: A review, ***Arabian Journal of Chemistry*** 10 (2017) S1409–S1421.
123. L.R. Snyder and J.J. Kirkland, *Introduction to Modern Liquid Chromatography*, 2nd ed., *John Wiley*, New York, United States of America, (1979).
124. R.J. Flanagan, D. Perrett, and R. Whelpton, *Electrochemical detection in HPLC : analysis of drugs and poisons*, *Royal Society of Chemistry*, (2005).
125. C. Wang, J. Xu, G. Zhou, Q. Qu, G. Yang, and X. Hu, Electrochemical Detection Coupled with High-Performance Liquid Chromatography in Pharmaceutical and Biomedical Analysis: A Mini Review, ***Combinatorial Chemistry & High Throughput Screening*** 10 (7) (2007) 547–554.
126. G.W. Fong and S.K. Lam, *HPLC in the pharmaceutical industry*, *Marcel Dekker, Inc*, (1991).
127. M. Swartz, HPLC detectors: A brief review, ***Journal of Liquid Chromatography & Related Technologies*** 33 (9–12) (2010) 1130–1150.
128. K. Robards, P.R. Haddad, and P.E. Jackson, High-performance Liquid Chromatography—Instrumentation and Techniques, *in Princ. Pract. Mod. Chromatogr. Methods*. *Elsevier*, (2004): pp. 227–303.
129. K. Honeychurch, Review: The application of liquid chromatography electrochemical detection for the determination of drugs of abuse, ***Separations*** 3 (4) (2016).
130. G. Horvai, E. Pungor, and W.A. MacCrehan, Electrochemical Detectors in HPLC and Ion Chromatography, ***Critical Reviews in Analytical Chemistry*** 21 (1) (1989) 1–28.
131. H.B. Hanekamp, W.H. Voogt, P. Bos, and R.W. Frei, An electrochemical scrubber for the elimination of eluent background effects in polarographic flow-through detection, ***Analytica Chimica Acta*** (1980).
132. M.W. Dong, *Modern HPLC for practicing scientists*, 1st ed., *Wiley Interscience*, Hoboken, New Jersey, (2006).
133. S.A. Özkan, LC with electrochemical detection Recent application to pharmaceuticals and biological fluids, ***Chromatographia*** 66 (SUPPL. 1) (2007).

134. P.T. Kissinegr, K. Bratin, W.P. King, and J.R. Rice, Electrochemical Detection of Picomole Amounts of Oxidizable and Reducible Residues Separated by Liquid Chromatography, *in* (1980): pp. 57–88.

135. R.A. Moore, D. Baldwin, H.J. Mcquay, and R.E.S. Bullingham, HPLC of Morphine with Electrochemical Detection: Analysis in Human Plasma, ***Annals of Clinical Biochemistry*** 21 (2) (1984) 125–130.

136. A. Chmielewska, L. Konieczna, A. Plenis, M. Bieniecki, and H. Lamparczyk, Determination of diclofenac in plasma by high-performance liquid chromatography with electrochemical detection, ***Biomedical Chromatography*** 20 (1) (2006) 119–124.

137. F. Kees, S. Spangler, and M. Wellenhofer, Determination of macrolides in biological matrices by high-performance liquid chromatography with electrochemical detection, ***Journal of Chromatography A*** 812 (1–2) (1998) 287–293.

138. C.M. Selavka, I.S. Krull, and K. Bratin, Analysis for penicillins and cefoperazone by HPLC-photolysis-electrochemical detection (HPLC-hv-EC), ***Journal of Pharmaceutical and Biomedical Analysis*** 4 (1) (1986) 83–93.

139. W.R. LaCourse and C.O. Dasenbrock, Pulsed electrochemical detection of sulfur-containing antibiotics following high performance liquid chromatography, ***Journal of Pharmaceutical and Biomedical Analysis*** 19 (1–2) (1999) 239–252.

140. L. Liu and Z. Chen, Analysis of four alkaloids of Coptis chinensis in rat plasma by high performance liquid chromatography with electrochemical detection, ***Analytica Chimica Acta*** 737 (2012) 99–104.

141. V.P. Ranta, J.C. Callaway, and T. Naaranlahti, Electrochemical Detection of Alkaloids in HPLC, *in Mod. Methods Plant Anal.* Linskens/Jackson (Ed.), *Springer-Verlag*, (1994): pp. 91–114.

142. T.A. Ivandini, B. V. Sarada, C. Terashima, T.N. Rao, D.A. Tryk, H. Ishiguro, Y. Kubota, and A. Fujishima, Electrochemical detection of tricyclic antidepressant drugs by HPLC using highly boron-doped diamond electrodes, ***Journal of Electroanalytical Chemistry*** 521 (1–2) (2002) 117–126.

143. F.S. Messiha, Determination of carbamazepine by HPLC electrochemical detection and application for estimation of imipramine desipramine, doxepin and nordoxepin, ***Alcohol*** 3 (2) (1986) 135–138.

144. P.A. Makoni, S.M. Khamanga, K. Wa Kasongo, and R.B. Walker, The use of experimental design for the development and validation of an HPLC-ECD method for the quantitation of efavirenz, ***Die Pharmazie*** 73 (10) (2018) 570–578.

145. K. Suzuki, M. Katayama, K. Takamatsu, S. Kaneko, K. Miyaji, H. Ishikawa, and Y. Matsuda, Improvement of sensitivity and selectivity of high-performance liquid chromatography for anti-retroviral drugs (non-reverse transcriptase inhibitors) by diamond-electrode electrochemical and fluorescence detection, ***Journal of Chromatography A*** 1216 (15) (2009) 3117–3121.

146. S.M. Khamanga and R.B. Walker, The use of experimental design in the development of an HPLC–ECD method for the analysis of captopril, ***Talanta*** 83 (3) (2011) 1037–1049.

147. C. Stubbs, J.M. Haigh, and I. Kanfer, A stability-indicating liquid chromatographic method for the analysis of erythromycin in stored biological fluids using amperometric detection, ***Journal of Liquid Chromatography*** 10 (11) (1987) 2547–2557.

148. R.B. Walker and I. Kanfer, Sensitive high-performance liquid chromatographic determination of cyclizine and its demethylated metabolite, norcyclizine, in biological fluids using coulometric detection, ***Journal of Chromatography B: Biomedical Sciences and Applications*** 672 (1) (1995) 172–177.

149. C. Taninaka, H. Ohtani, E. Hanada, H. Kotaki, H. Sato, and T. Iga, Determination of erythromycin, clarithromycin, roxithromycin, and azithromycin in plasma by high-performance liquid chromatography with amperometric detection, ***Journal of Chromatography B: Biomedical Sciences and Applications*** 738 (2) (2000) 405–411.

150. M.F. Zaater, Y.R. Tahboub, and E. Ghanem, Determination and Stability Assessment of Clarithromycin in Human Plasma using RP-LC with Electrochemical Detection, ***Journal of Chromatographic Science*** 50 (9) (2012) 763–768.

151. M. Lohitnavy, O. Lohitnavy, K. Sareekan, and W. Chaiyaput, Average bioequivalence study of clarithromycin tablets in healthy male volunteers, ***Journal of Clinical Pharmacy and Therapeutics*** 28 (3) (2003) 187–190.

152. P.O. Erah, D.A. Barrett, and P.N. Shaw, Ion-pair high-performance liquid chromatographic assay method for the assessment of clarithromycin stability in aqueous solution and in gastric juice, ***Journal of Chromatography B: Biomedical Sciences and Applications*** 682 (1) (1996) 73–78.

153. W. Li, H. Jia, and K. Zhao, Determination of clarithromycin in rat plasma by HPLC–UV method with pre-column derivatization, ***Talanta*** 71 (1) (2007) 385–390.

154. F. Lange, S. Cornelissen, D. Kubac, M.M. Sein, J. von Sonntag, C.B. Hannich, A. Golloch, H.J. Heipieper, M. Möder, and C. von Sonntag, Degradation of macrolide antibiotics by ozone: A mechanistic case study with clarithromycin, ***Chemosphere*** 65

(1) (2006) 17–23.

155. J. Sastre Toraño and H.-J. Guchelaar, Quantitative determination of the macrolide antibiotics erythromycin, roxithromycin, azithromycin and clarithromycin in human serum by high-performance liquid chromatography using pre-column derivatization with 9-fluorenylmethyloxycarbonyl chloride and fluorescence detection, ***Journal of Chromatography B: Biomedical Sciences and Applications*** 720 (1–2) (1998) 89–97.

156. S.-Y. Chu, L.T. Sennello, and R.C. Sonders, Simultaneous determination of clarithromycin and 14(R)-hydroxyclarithromycin in plasma and urine using high-performance liquid chromatography with electrochemical detection, ***Journal of Chromatography B: Biomedical Sciences and Applications*** 571 (1–2) (1991) 199–208.

157. M. Hedenmo and B.-M. Eriksson, Liquid chromatographic determination of the macrolide antibiotics roxithromycin and clarithromycin in plasma by automated solid-phase extraction and electrochemical detection, ***Journal of Chromatography A*** 692 (1–2) (1995) 161–166.

158. S.J. Choi, S.B. Kim, H.-Y. Lee, D.H. Na, Y.S. Yoon, S.S. Lee, J.H. Kim, K.C. Lee, and H.S. Lee, Column-switching high-performance liquid chromatographic determination of clarithromycin in human plasma with electrochemical detection, ***Talanta*** 54 (2) (2001).

159. J. Wibawa, P. Shaw, and D. Barrett, Quantification of clarithromycin, its 14-hydroxy and decladinose metabolites in rat plasma, gastric juice and gastric tissue using high-performance liquid chromatography with electrochemical detection, ***Journal of Chromatography B*** 783 (2) (2003) 359–366.

160. S.M. Foroutan, A. Zarghi, A. Shafaati, B. Madadian, and F. Abolfathi, Rapid high performance liquid chromatographic method for determination of clarithromycin in human plasma using amperometric detection: application in pharmacokinetic and bioequivalence studies, ***Iranian Journal of Pharmaceutical Research*** 12 (Suppl) (2013) 65–9.

161. Y. Vander Heyden, A. Nijhuis, J. Smeyers-Verbeke, B. Vandeginste, and D. Massart, Guidance for robustness/ruggedness tests in method validation, ***Journal of Pharmaceutical and Biomedical Analysis*** 24 (5–6) (2001) 723–753.

162. B. Jančić-Stojanović and T. Rakić, Chemometrics in Data Analysis and Liquid Chromatographic Method Development, *in Anal. Sep. Sci. Wiley-VCH Verlag GmbH & Co. KGaA*, Weinheim, Germany, (2015): pp. 279–298.

163. V.F. Samanidou, Basic LC Method Development and Optimization, *in Anal. Sep. Sci. Wiley-VCH Verlag GmbH & Co. KGaA*, Weinheim, Germany, (2015): pp. 25–42.

164. V. Gupta, A. Deep, K. Jain, N.S. Gill, and K. Gupta, Development and validation of HPLC method-a review, ***Int. Res J Pharm. App Sci*** 2 (4) (2012) 17–25.

165. P.K. Sahu, N.R. Ramisetti, T. Cecchi, S. Swain, C.S. Patro, and J. Panda, An overview of experimental designs in HPLC method development and validation, ***Journal of Pharmaceutical and Biomedical Analysis*** 147 (2018) 590–611.

166. R.E. Bruns, I.S. Scarminio, and B. de Barros Neto, Statistical design-chemometrics, *in Data Handl. Sci. Technol.* R.E. Bruns, I.S. Scarminio, B. de Barros Neto (Eds.), 1st ed., *Elsevier*, (2006): p. 412.

167. B. Dejaegher and Y. Vander Heyden, Experimental designs and their recent advances in set-up, data interpretation, and analytical applications, ***Journal of Pharmaceutical and Biomedical Analysis*** 56 (2) (2011) 141–158.

168. G.A. Lewis, D. Mathieu, and R. Phan-Tan-Luu, eds., *Pharmaceutical Experimental Design*, 1st ed., *CRC Press*, Boca Raton, USA, (1998).

169. B. Dejaegher and Y. Vander Heyden, The use of experimental design in separation science, ***Acta Chromatographica*** 21 (2) (2009) 161–201.

170. D.L. Massart, B.G. Vandeginste, L.M.C. Buydens, P.J. Lewi, J. Smeyers-Verbeke, and S. De Jong, *Handbook of chemometrics and qualimetrics*, *Elsevier*, New York, USA, (1997).

171. P.A. Makoni, Formulation, development and assment of efavirenz-loaded lipid nanocarriers, Rhodes University, South Africa, 2014.

172. A. Pappa-Louisi, A. Papageorgiou, A. Zitrou, S. Sotiropoulos, E. Georgarakis, and F. Zougrou, Study on the electrochemical detection of the macrolide antibiotics clarithromycin and roxithromycin in reversed-phase high-performance liquid chromatography, ***Journal of Chromatography B: Biomedical Sciences and Applications*** 755 (1–2) (2001) 57–64.

173. T.D. Rotsch, M. Spanton, P. Cugier, and A.C. Plasz, Determination of Clarithromycin as a Contaminant on Surfaces by High-Performance Liquid Chromatography Using Electrochemical Detection, ***Pharmaceutical Research: An Official Journal of the American Association of Pharmaceutical Scientists*** 8 (8) (1991) 989–991.

174. I. Niopas and A.C. Daftsios, Determination of clarithromycin in human plasma by HPLC with electrochemical detection: validation and application in pharmacokinetic study, ***Biomedical Chromatography*** 15 (8) (2001) 507–508.

175. *Center for Drug Evaluation and Research (CDER) Reviewer Guidance' Validation of Chromatographic Methods*, (1994).
176. F. Zhang and H. Li, Resolution of overlapping capillary electrophoresis peaks by using chemometric analysis: Improved quantification by using internal standard, ***Chemometrics and Intelligent Laboratory Systems*** 82 (1-2 SPEC. ISS) (2006) 184–192.
177. K. Tsuji and J.F. Goetz, High-performance liquid chromatographic determination of erythromycin, ***Journal of Chromatography*** 147 (1978) 359–67.
178. M. Brisaert, M. Heylen, and J. Plaizier-Vercammen, Investigation on the chemical stability of erythromycin in solutions using an optimization system, ***Pharmacy World and Science*** 18 (5) (1996) 182–186.
179. J.J. Kirkland, J.W. Henderson, J.J. DeStefano, M.A. van Straten, and H.A. Claessens, Stability of silica-based, endcapped columns with pH 7 and 11 mobile phases for reversed-phase high-performance liquid chromatography, ***Journal of Chromatography A*** 762 (1–2) (1997) 97–112.
180. L.R. Snyder, J.J. Kirkland, and J.L. Glajch, *Practical HPLC method development*, *Wiley*, (1997).
181. S. Zhang, X. Huang, N. Yao, and C. Horváth, Preparation of monodisperse porous polymethacrylate microspheres and their application in the capillary electrochromatography of macrolide antibiotics, ***Journal of Chromatography A*** 948 (1–2) (2002) 193–201.
182. A.F.B. Fauzee, S.M. Khamanga, and R.B. Walker, The impact of manufacturing variables on in vitro release of clobetasol 17-propionate from pilot scale cream formulations, ***Drug Development and Industrial Pharmacy*** 40 (12) (2014) 1683–1692.
183. G. Bahrami and B. Mohammadi, Determination of clarithromycin in human serum by high-performance liquid chromatography after pre-column derivatization with 9-fluorenylmethyl chloroformate: Application to a bioequivalence study, ***Journal of Chromatography B*** 850 (1–2) (2007) 417–422.
184. J. You, Y. Ming, Y. Shi, X. Zhao, Y. Suo, H. Wang, Y. Li, and J. Sun, Development of a sensitive fluorescent derivatization reagent 1,2-benzo-3,4-dihydrocarbazole-9-ethyl chloroformate (BCEOC) and its application for determination of amino acids from seeds and bryophyte plants using high-performance liquid chromatography wi, ***Talanta*** 68 (2) (2005) 448–458.

185. A.M. Di Pietra, R. Gatti, V. Andrisano, and V. Cavrini, Application of high-performance liquid chromatography with diode-array detection and on-line post-column photochemical derivatization to the determination of analgesics, ***Journal of Chromatography A*** 729 (1–2) (1996) 355–361.
186. K.M. Darwish, I. Salama, S. Mostafa, and M. El-Sadek, RP-HPLC/Pre-Column Derivatization for Analysis of Omeprazole, Tinidazole, Doxycycline and Clarithromycin, ***Journal of Chromatographic Science*** 51 (6) (2013) 566–576.
187. S. Bansal and A. DeStefano, Key elements of bioanalytical method validation for small molecules, ***AAPS Journal*** 9 (1) (2007).
188. I.S. Krull and M. Swartz, Analytical method development and validation for the academic researcher, ***Analytical Letters*** 32 (6) (1999) 1067–1080.
189. ICH, Q2 (R1) Harmonised tripatite guidline validation of analytical procedures, texts and methodology, (2005).
190. J. Dolan, Method Adjustment the USP Way, (2017).
191. M. Blessy, R.D. Patel, P.N. Prajapati, and Y.K. Agrawal, Development of forced degradation and stability indicating studies of drugs-A review, ***Journal of Pharmaceutical Analysis*** 4 (3) (2014) 159–165.
192. T.N. Rao, Validation of Analytical Methods, *in Calibration Valid. Anal. Methods - A Sampl. Curr. Approaches*. *InTech*, (2018).
193. R. LoBrutto and T. Patel, Method Validation HPLC for Pharmaceutical Scientists, *in Method Validation. HPLC Pharm. Sci. John Wiley & Sons, Inc.*, Hoboken, NJ, USA, (2006): pp. 455–502.
194. G.A. Shabir, W. John Lough, S.A. Arain, and T.K. Bradshaw, Evaluation and Application of Best Practice in Analytical Method Validation, ***Journal of Liquid Chromatography & Related Technologies*** 30 (3) (2007) 311–333.
195. A. Marín, E. García, A. García, and C. Barbas, Validation of a HPLC quantification of acetaminophen, phenylephrine and chlorpheniramine in pharmaceutical formulations: Capsules and sachets, ***Journal of Pharmaceutical and Biomedical Analysis*** 29 (4) (2002) 701–714.
196. ICH Topic Q1 A (R2) Stability testing on new drug sunstances and products, ***European Medicines Agency*** (2003) 1–20.
197. G. Ngwa, Forced Degradation as an Integral Part of HPLC Stability-Indicating Method Development, ***Drug Delivery Technology*** 10 (5) (2010).
198. P. Erah, A.F. Goddard, D.A. Barrett, P.N. Shaw, and R.C. Spiller, The stability of

amoxycillin, clarithromycin and metronidazole in gastric juice: relevance to the treatment of Helicobacter pylori infection, ***Journal of Antimicrobial Chemotherapy*** 39 (1) (1997) 5–12.

199. H. Rosing, W.Y. Man, E. Doyle, A. Bult, and J.H. Beijnen, Bioanalytical Liquid Chromatographic Method Validation A Review of Current Practices and Procedures, ***Journal of Liquid Chromatography & Related Technologies*** 23 (3) (2000) 329–354.
200. D. Dadgar and P.E. Burnett, Issues in evaluation of bioanalytical method selectivity and drug stability, ***Journal of Pharmaceutical and Biomedical Analysis*** 14 (1–2) (1995) 23–31.
201. N. Naseri, H. Valizadeh, and P. Zakeri-Milani, Solid Lipid Nanoparticles and Nanostructured Lipid Carriers: Structure, Preparation and Application, ***Advanced Pharmaceutical Bulletin*** 5 (3) (2015) 305–13.
202. M. Beija, R. Salvayre, N. Lauth-de Viguerie, and J.-D. Marty, Colloidal systems for drug delivery: from design to therapy, ***Trends in Biotechnology*** 30 (9) (2012) 485–496.
203. K. Riehemann, S.W. Schneider, T.A. Luger, B. Godin, M. Ferrari, and H. Fuchs, Nanomedicine-Challenge and Perspectives, ***Angewandte Chemie International Edition*** 48 (5) (2009) 872–897.
204. N. Ahmad, M.A. Alam, R. Ahmad, S. Umar, and F. Jalees Ahmad, Improvement of oral efficacy of Irinotecan through biodegradable polymeric nanoparticles through in vitro and in vivo investigations, ***Journal of Microencapsulation*** 35 (4) (2018) 327–343.
205. W. Mehnert and K. Mader, Solid lipid nanoparticles Production, characterization and applications, ***Advanced Drug Delivery Reviews*** 47 (2–3) (2002) 165–196.
206. M. Uner, Preparation, characterization and physico-chemical properties of solid lipid nanoparticles (SLN) and nanostructured lipid carriers (NLC): their benefits as colloidal drug carrier systems, ***Die Pharmazie*** 61 (5) (2006) 375–86.
207. R.H. Müller, M. Radtke, and S.A. Wissing, Nanostructured lipid matrices for improved microencapsulation of drugs, ***International Journal of Pharmaceutics*** 242 (1–2) (2002) 121–128.
208. M. Muchow, P. Maincent, and R.H. Müller, Lipid Nanoparticles with a Solid Matrix (SLN®, NLC®, LDC®) for Oral Drug Delivery, ***Drug Development and Industrial Pharmacy*** 34 (12) (2008) 1394–1405.
209. S.A. Wissing, O. Kayser, and R.H. Müller, Solid lipid nanoparticles for parenteral drug

delivery, ***Advanced Drug Delivery Reviews*** 56 (9) (2004) 1257–1272.

210. E.B. Souto and R.. Müller, Lipid nanoparticles (SLN and NLC) for drug delivery, *in Nanoparticles Pharm. Appl.* A. Domb, M. Tabata, R. Kumar, S. Farber (Eds.), *American Scientific Publishers*, (2007): pp. 103–122.
211. P. Mura, M.T. Faucci, A. Manderioli, S. Furlanetto, and S. Pinzauti, Thermal analysis as a screening technique in preformulation studies of picotamide solid dosage forms, ***Drug Development and Industrial Pharmacy*** 24 (8) (1998) 747–756.
212. H.A. Lieberman, L. Lachman, and J.B. Schwartz, *PHARMACEUTICAL DOSAGE FORMS*, 2nd ed., *Marcel Dekker Inc.*, New York, (1989).
213. L.M. Rus, I. Tomuta, C. Iuga, C. Maier, I. Kacso, G. Borodi, I. Bratu, and M. Bojita, Compatibility Studies of Indapamide/Pharmaceutical Excipients used in Tablet Preformulation, ***FARMACIA*** 60 (2012) 1.
214. D.C. Monkhouse, Stability aspects of preformulation and formulation of solid pharmaceuticals, ***Drug Development and Industrial Pharmacy*** 10 (8–9) (1984) 1373–1412.
215. G. Bruni, L. Amici, V. Berbenni, A. Marini, and A. Orlandi, Drug-excipient compatibility studies: Search of interaction indicators, *in J. Therm. Anal. Calorim.* (2002): pp. 561–573.
216. A.T.M. Serajuddin, A.B. Thakur, R.N. Ghoshal, M.G. Fakes, S.A. Ranadive, K.R. Morris, and S.A. Varia, Selection of solid dosage form composition through drug-excipient compatibility testing, ***Journal of Pharmaceutical Sciences*** 88 (7) (1999) 696–704.
217. C.E.P. Malan, M.M. De Villiers, and A.P. Lötter, Evaluation of compatibility of tablet excipients with albendazole and closantel using DSC and HPLC, ***Drug Development and Industrial Pharmacy*** 23 (6) (1997) 533–537.
218. I. Alves-Silva, L.C.L. Sá-Barreto, E.M. Lima, and M.S.S. Cunha-Filho, Preformulation studies of itraconazole associated with benznidazole and pharmaceutical excipients, ***Thermochimica Acta*** 575 (2014) 29–33.
219. A.M. Lira, A.A.S. Araújo, I.D.J. Basílio, B.L.L. Santos, D.P. Santana, and R.O. Macedo, Compatibility studies of lapachol with pharmaceutical excipients for the development of topical formulations, ***Thermochimica Acta*** 457 (1–2) (2007) 1–6.
220. N.R. Pani, L.K. Nath, S. Acharya, and B. Bhuniya, Application of DSC, IST, and FTIR study in the compatibility testing of nateglinide with different pharmaceutical excipients, ***Journal of Thermal Analysis and Calorimetry*** 108 (1) (2012) 219–226.

221. A. V. Singh and L.K. Nath, Evaluation of compatibility of tablet excipients and novel synthesized polymer with lamivudine, ***Journal of Thermal Analysis and Calorimetry*** 108 (1) (2012) 263–267.

222. H. Jacobson and G. Reier, Application of differential thermal analysis to compatibility and stability problems in penicillin-stearic acid mixtures, ***Journal of Pharmaceutical Sciences*** 58 (5) (1969) 631–633.

223. A. Marini, V. Berbenni, S. Moioli, G. Bruni, P. Cofrancesco, C. Margheritis, and M. Villa, Drug-excipient compatibility studies by physico-chemical techniques: The case of indomethacin, ***Journal of Thermal Analysis and Calorimetry*** 73 (2) (2003) 529–545.

224. K. Wa Kasongo, R.H. Müller, and R.B. Walker, The use of hot and cold high pressure homogenization to enhance the loading capacity and encapsulation efficiency of nanostructured lipid carriers for the hydrophilic antiretroviral drug, didanosine for potential administration to paediatric patients, ***Pharmaceutical Development and Technology*** 17 (3) (2012) 353–362.

225. M. Niu, K. Shi, Y. Sun, J. Wang, and F. Cui, Preparation of CyA-loaded solid lipid nanoparticles and application on ocular preparations, ***Journal of Drug Delivery Science and Technology*** 18 (4) (2008) 293–297.

226. M.D. Triplett and J.F. Rathman, Optimization of β-carotene loaded solid lipid nanoparticles preparation using a high shear homogenization technique, ***Journal of Nanoparticle Research*** 11 (3) (2009) 601–614.

227. D. Liu, S. Jiang, H. Shen, S. Qin, J. Liu, Q. Zhang, R. Li, and Q. Xu, Diclofenac sodium-loaded solid lipid nanoparticles prepared by emulsion/solvent evaporation method, ***Journal of Nanoparticle Research*** 13 (6) (2011) 2375–2386.

228. D. Pooja, L. Tunki, H. Kulhari, B.B. Reddy, and R. Sistla, Optimization of solid lipid nanoparticles prepared by a single emulsification-solvent evaporation method, ***Data in Brief*** 6 (2016) 15–19.

229. P. Chattopadhyay, B.Y. Shekunov, D. Yim, D. Cipolla, B. Boyd, and S. Farr, Production of solid lipid nanoparticle suspensions using supercritical fluid extraction of emulsions (SFEE) for pulmonary delivery using the AERx system, ***Advanced Drug Delivery Reviews*** 59 (6) (2007) 444–453.

230. Y. Chen, R. Jin, Y. Zhou, J. Zeng, H. Zhang, and Q. Feng, Preparation of solid lipid nanoparticles loaded with Xionggui powder-supercritical carbon dioxide fluid extraction and their evaluation in vitro release, ***Zhongguo Zhong Yao Za Zhi*** =

Zhongguo Zhongyao Zazhi = China Journal of Chinese Materia Medica 31 (5) (2006) 376–9.

231. T. Wang, Q. Hu, M. Zhou, Y. Xia, M.P. Nieh, and Y. Luo, Development of "all natural" layer-by-layer redispersible solid lipid nanoparticles by nano spray drying technology, ***European Journal of Pharmaceutics and Biopharmaceutics*** 107 (2016) 273–285.
232. T. Wang, Q. Hu, M. Zhou, J. Xue, and Y. Luo, Preparation of ultra-fine powders from polysaccharide-coated solid lipid nanoparticles and nanostructured lipid carriers by innovative nano spray drying technology, ***International Journal of Pharmaceutics*** 511 (1) (2016) 219–222.
233. C. Chen, T. Fan, Y. Jin, Z. Zhou, Y. Yang, X. Zhu, Z.R. Zhang, Q. Zhang, and Y. Huang, Orally delivered salmon calcitonin-loaded solid lipid nanoparticles prepared by micelle-double emulsion method via the combined use of different solid lipids, ***Nanomedicine*** 8 (7) (2013) 1085–1100.
234. L. Becker Peres, L. Becker Peres, P.H.H. de Araújo, and C. Sayer, Solid lipid nanoparticles for encapsulation of hydrophilic drugs by an organic solvent free double emulsion technique, ***Colloids and Surfaces B: Biointerfaces*** 140 (2016) 317–323.
235. E.B. Souto and R.H. Muller, Solid Lipid Nanoparticles and Nanostructured Lipid Carriers-Lipid Nanoparticles for Medicals and Pharmaceuticals, ***Encyclopedia of Nanoscience and Nanotechnology*** 23 (2011) 313–328.
236. S. Shidhaye, R. Vaidya, S. Sutar, A. Patwardhan, and V. Kadam, Solid Lipid Nanoparticles and Nanostructured Lipid Carriers – Innovative Generations of Solid Lipid Carriers, ***Current Drug Delivery*** 5 (4) (2008) 324–331.
237. B. Abismaïl, J.P. Canselier, A.M. Wilhelm, H. Delmas, and C. Gourdon, Emulsification by ultrasound: Drop size distribution and stability, ***Ultrasonics Sonochemistry*** 6 (1–2) (1999) 75–83.
238. A.C. Taylor, Advances in nanoparticle reinforcement in structural adhesives, *in Adv. Struct. Adhes. Bond. Elsevier Inc.*, (2010): pp. 151–182.
239. R.A. Wilbey, Homogenization, *in Encycl. Food Sci. Nutr.* B. Caballero (Ed.), 2nd ed., *Academic Press*, (2003): pp. 3119–3125.
240. W. Mehnert and K. Mäder, Solid lipid nanoparticles: Production, characterization and applications, ***Advanced Drug Delivery Reviews*** 64 (SUPPL.) (2012) 83–101.
241. A.M. Hashtjin and S. Abbasi, Optimization of ultrasonic emulsification conditions for the production of orange peel essential oil nanoemulsions, ***Journal of Food Science***

and Technology 52 (5) (2015) 2679–2689.

242. E.B. Souto and R.H. Müller, SLN and NLC for topical delivery of ketoconazole, ***Journal of Microencapsulation*** 22 (5) (2005) 501–510.
243. D. Hou, C. Xie, K. Huang, and C. Zhu, The production and characteristics of solid lipid nanoparticles (SLNs), ***Biomaterials*** 24 (10) (2003) 1781–5.
244. P.A. Makoni, K.W. Kasongo, and R.B. Walker, Short Term Stability Testing of Efavirenz-Loaded Solid Lipid Nanoparticle (SLN) and Nanostructured Lipid Carrier (NLC) Dispersions, ***Pharmaceutics*** 11 (8) (2019) 397.
245. K.W. Kasongo, J. Pardeike, R.H. Muller, and R.B. Walker, Selection and Characterization of Suitable Lipid Excipients for use in the Manufacture of Didanosine-Loaded Solid Lipid Nanoparticles and Nanostructured Lipid Carriers, ***J Pharm Sci*** 100 (12) (2011) 5185–5196.
246. N.P. Aditya and S. Ko, Solid lipid nanoparticles (SLNs): Delivery vehicles for food bioactives, ***RSC Advances*** 5 (39) (2015) 30902–30911.
247. R.H. Müller, K. Mäder, and S. Gohla, Solid lipid nanoparticles (SLN) for controlled drug delivery- a review of the state of the art, ***European Journal of Pharmaceutics and Biopharmaceutics*** 50 (1) (2000) 161–177.
248. E. Baka, J.E.A. Comer, and K. Takács-Novák, Study of equilibrium solubility measurement by saturation shake-flask method using hydrochlorothiazide as model compound, ***Journal of Pharmaceutical and Biomedical Analysis*** 46 (2) (2008) 335–341.
249. M. Cirri, L. Maestrini, F. Maestrelli, N. Mennini, P. Mura, C. Ghelardini, and L. Di Cesare Mannelli, Design, characterization and in vivo evaluation of nanostructured lipid carriers (NLC) as a new drug delivery system for hydrochlorothiazide oral administration in pediatric therapy, ***Drug Delivery*** 25 (1) (2018) 1910–1921.
250. G.-H. Son, Y.-G. Na, H.W. Huh, M. Wang, M.-K. Kim, M.-G. Han, J.-J. Byeon, H.-K. Lee, and C.-W. Cho, Systemic Design and Evaluation of Ticagrelor-Loaded Nanostructured Lipid Carriers for Enhancing Bioavailability and Antiplatelet Activity, ***Pharmaceutics*** 11 (5) (2019) 222.
251. M. Joshi and V. Patravale, Nanostructured lipid carrier (NLC) based gel of celecoxib, ***International Journal of Pharmaceutics*** 346 (1–2) (2008) 124–132.
252. M. Joshi and V. Patravale, Formulation and Evaluation of Nanostructured Lipid Carrier (NLC)–based Gel of Valdecoxib, ***Drug Development and Industrial Pharmacy*** 32 (8) (2006) 911–918.

253. N. Ahmad, R. Ahmad, M.A. Alam, F.J. Ahmad, and M. Amir, Impact of ultrasonication techniques on the preparation of novel Amiloride-nanoemulsion used for intranasal delivery in the treatment of epilepsy, ***Artificial Cells, Nanomedicine, and Biotechnology*** 46 (sup3) (2018) S192–S207.

254. R. Parveen, S. Baboota, J. Ali, A. Ahuja, S.S. Vasudev, and S. Ahmad, Oil based nanocarrier for improved oral delivery of silymarin: In vitro and in vivo studies, ***International Journal of Pharmaceutics*** 413 (1–2) (2011) 245–253.

255. K.J. Box, G. Völgyi, E. Baka, M. Stuart, K. Takács-Novák, and J.E.A. Comer, Equilibrium versus kinetic measurements of aqueous solubility, and the ability of compounds to supersaturate in solution—a validation study, ***Journal of Pharmaceutical Sciences*** 95 (6) (2006) 1298–1307.

256. P.A. Makoni, J. Ranchhod, K. WaKasongo, S.M. Khamanga, and R.B. Walker, The use of quantitative analysis and Hansen solubility parameter predictions for the selection of excipients for lipid nanocarriers to be loaded with water soluble and insoluble compounds, ***Saudi Pharmaceutical Journal*** 28 (3) (2020) 305–315.

257. A.O. Kasimova, G.M. Pavan, A. Danani, K. Mondon, A. Cristiani, L. Scapozza, R. Gurny, and M. Möller, Validation of a Novel Molecular Dynamics Simulation Approach for Lipophilic Drug Incorporation into Polymer Micelles, ***The Journal of Physical Chemistry B*** 116 (14) (2012) 4338–4345.

258. L.C. Persson, C.J.H. Porter, W.N. Charman, and C.A.S. Bergström, Computational prediction of drug solubility in lipid based formulation excipients, ***Pharmaceutical Research*** 30 (12) (2013) 3225–37.

259. S.S. Rane, Y. Cao, and B.D. Anderson, Quantitative Solubility Relationships and the Effect of Water Uptake in Triglyceride/Monoglyceride Microemulsions, ***Pharmaceutical Research*** 25 (5) (2008) 1158–1174.

260. A. Martin, J. Newburger, and A. Adjei, Extended hildebrand solubility approach: Solubility of theophylline in polar binary solvents, ***Journal of Pharmaceutical Sciences*** 69 (5) (1980) 487–491.

261. M. Shah and Y. Agrawal, High throughput screening: an *in silico* solubility parameter approach for lipids and solvents in SLN preparations, ***Pharmaceutical Development and Technology*** 18 (3) (2013) 582–590.

262. C.M.H. and H.Y. Steven Abbott, *Hansen Solubility Parameters in Practice*, 5th ed., *Hansen-Solubility.com*, (2015).

263. B. Hossin, K. Rizi, and S. Murdan, Application of Hansen Solubility Parameters to

predict drug–nail interactions, which can assist the design of nail medicines, ***European Journal of Pharmaceutics and Biopharmaceutics*** 102 (2016) 32–40.

264. C.M. Hansen and A.L. Smith, Using Hansen solubility parameters to correlate solubility of C60 fullerene in organic solvents and in polymers, ***Carbon*** 42 (8–9) (2004) 1591–1597.
265. E. Stefanis and C. Panayiotou, Prediction of Hansen Solubility Parameters with a New Group-Contribution Method, ***International Journal of Thermophysics*** 29 (2) (2008) 568–585.
266. D. Medarević, J. Djuriš, P. Barmpalexis, K. Kachrimanis, and S. Ibrić, Analytical and Computational Methods for the Estimation of Drug-Polymer Solubility and Miscibility in Solid Dispersions Development, ***Pharmaceutics*** 11 (8) (2019) 372.
267. C. Long, L. Zhang, and Y. Qian, Preparation and Crystal Modification of Ibuprofen-Loaded Solid Lipid Microparticles, ***Chinese Journal of Chemical Engineering*** 14 (4) (2006) 518–525.
268. A. Forster, J. Hempenstall, I. Tucker, and T. Rades, Selection of excipients for melt extrusion with two poorly water-soluble drugs by solubility parameter calculation and thermal analysis, ***International Journal of Pharmaceutics*** 226 (1–2) (2001) 147–161.
269. R.C. Rowe, Adhesion of film coatings to tablet surfaces —a theoretical approach based on solubility parameters, ***International Journal of Pharmaceutics*** 41 (3) (1988) 219–222.
270. A.B. Kovačević, R.H. Müller, and C.M. Keck, Formulation development of lipid nanoparticles: Improved lipid screening and development of tacrolimus loaded nanostructured lipid carriers (NLC), ***International Journal of Pharmaceutics*** 576 (2020) 118918.
271. F. Kristin, H. René, M. Boontida, J.V. Buraphacheep, A. Maximilian, M. Johanna, and L. Peter, Dissolution and dissolution/permeation experiments for predicting systemic exposure following oral administration of the BCS class II drug clarithromycin, ***European Journal of Pharmaceutical Sciences*** 101 (2017) 211–219.
272. A.R. Madgulkar, R.R. Padalkar, and S.K. Amale, Preformulation Studies of Intranasal Solid Lipid Nanoparticles of Mometasone Furoate, ***Journal of Drug Delivery and Therapeutics*** 9 (4) (2019) 526–528.
273. S. Taneja, S. Shilpi, and K. Khatri, Formulation and optimization of efavirenz nanosuspensions using the precipitation-ultrasonication technique for solubility enhancement, ***Artificial Cells, Nanomedicine and Biotechnology*** 44 (3) (2016) 978–

984.

274. M.G. Papich and M.N. Martinez, Applying Biopharmaceutical Classification System (BCS) Criteria to Predict Oral Absorption of Drugs in Dogs: Challenges and Pitfalls, ***AAPS Journal*** 17 (4) (2015) 948–964.

275. E. Pretorius and P.J.D. Bouic, Permeation of four oral drugs through human intestinal mucosa, ***AAPS PharmSciTech*** 10 (1) (2009) 270–275.

276. K. WaKasongo, An investigation into the feasability of incorporating didanosine into innovative solid lipid nanocarriers, Rhodes University, South Africa, 2010.

277. E.B. Souto, W. Mehnert, and R.H. Müller, Polymorphic behaviour of Compritol®888 ATO as bulk lipid and as SLN and NLC, ***Journal of Microencapsulation*** 23 (4) (2006) 417–433.

278. V.I. Mikla and V. V. Mikla, Advances in Imaging from the First X-Ray Images, ***Medical Imaging Technology*** (2014) 1–22.

279. P. Severino, S.C. Pinho, E.B. Souto, and M.H.A. Santana, Polymorphism, crystallinity and hydrophilic-lipophilic balance of stearic acid and stearic acid-capric/caprylic triglyceride matrices for production of stable nanoparticles, ***Colloids and Surfaces B: Biointerfaces*** 86 (1) (2011) 125–130.

280. E.B. Souto, S. Doktorovova, and P. Boonme, Lipid-based colloidal systems (nanoparticles, microemulsions) for drug delivery to the skin: Materials and end-product formulations, ***Journal of Drug Delivery Science and Technology*** (2011).

281. B. Heurtault, P. Saulnier, B. Pech, J.-E. Proust, and J.-P. Benoit, Physico-chemical stability of colloidal lipid particles, ***Biomaterials*** 24 (23) (2003) 4283–4300.

282. H. Bunjes, K. Westesen, and M.H.J. Koch, Crystallization tendency and polymorphic transitions in triglyceride nanoparticles, ***International Journal of Pharmaceutics*** 129 (1–2) (1996) 159–173.

283. A. Kovacevic, S. Savic, G. Vuleta, R.H. Müller, and C.M. Keck, Polyhydroxy surfactants for the formulation of lipid nanoparticles (SLN and NLC): Effects on size, physical stability and particle matrix structure, ***International Journal of Pharmaceutics*** 406 (1–2) (2011) 163–172.

284. R.E. Timms, Physical properties of oils and mixtures of oils, ***Journal of the American Oil Chemists' Society*** 62 (2) (1985) 241–249.

285. R.H. Müller, S.A. Runge, V. Ravelli, A.F. Thünemann, W. Mehnert, and E.B. Souto, Cyclosporine-loaded solid lipid nanoparticles (SLN): drug-lipid physicochemical interactions and characterization of drug incorporation, ***European Journal of***

Pharmaceutics and Biopharmaceutics 68 (3) (2008) 535–544.

286. K.R. Rajisha, B. Deepa, L.A. Pothan, and S. Thomas, Thermomechanical and spectroscopic characterization of natural fibre composites, *in Interface Eng. Nat. Fibre Compos. Maximum Perform. Elsevier*, (2011): pp. 241–274.
287. I.I. Salem, Clarithromycin, *in Anal. Profiles Drug Subst. Excipients*. K. Florey (Ed.), *Academic Press Inc.*, New York, (1996): pp. 45–85.
288. T. Thi, M. Speybroeck, V. Barillaro, J. Martens, P. Annaert, P. Augustijns, J. Humbeck, J. Vermant, and Gv. Mooter, Formulate-ability of ten compounds with different physicochemical profiles in SMEDDS, ***European Journal of Pharmaceutical Sciences*** 38 (5) (2009) 479–488.
289. Gattefosse, Gattefosse-Personal care ingredients and pharmaceutical excipients, (2020).
290. K. Peng, L. Fu, X. Li, J. Ouyang, and H. Yang, Stearic acid modified montmorillonite as emerging microcapsules for thermal energy storage, ***Applied Clay Science*** 138 (2017) 100–106.
291. F. Kaneko, M. Kobayashi, Y. Kitagawa, and Y. Matsuura, Structure of stearic acid E form, ***Acta Crystallographica Section C Crystal Structure Communications*** 46 (8) (1990) 1490–1492.
292. A.C.T. Teixeira, A.R. Garcia, L.M. Ilharco, A.M.P.S. Gonçalves Da Silva, and A.C. Fernandes, Phase behaviour of oleanolic acid, pure and mixed with stearic acid: Interactions and crystallinity, ***Chemistry and Physics of Lipids*** 163 (7) (2010) 655–666.
293. A.C. Silva, E. González-Mira, M.L. García, M.A. Egea, J. Fonseca, R. Silva, D. Santos, E.B. Souto, and D. Ferreira, Preparation, characterization and biocompatibility studies on risperidone-loaded solid lipid nanoparticles (SLN): High pressure homogenization versus ultrasound, ***Colloids and Surfaces B: Biointerfaces*** 86 (1) (2011) 158–165.
294. A. Ludwig, The use of mucoadhesive polymers in ocular drug delivery, ***Advanced Drug Delivery Reviews*** 57 (11) (2005) 1595–1639.
295. J. Hao, X. Wang, Y. Bi, Y. Teng, J. Wang, F. Li, Q. Li, J. Zhang, F. Guo, and J. Liu, Fabrication of a composite system combining solid lipid nanoparticles and thermosensitive hydrogel for challenging ophthalmic drug delivery, ***Colloids and Surfaces B: Biointerfaces*** 114 (2014) 111–120.
296. A. Patel, Ocular drug delivery systems: An overview, ***World Journal of***

Pharmacology 2 (2) (2013) 47.

297. R. Gaudana, J. Jwala, S.H.S. Boddu, and A.K. Mitra, Recent perspectives in ocular drug delivery, ***Pharmaceutical Research*** 26 (5) (2009) 1197–1216.
298. V.H.L. Lee and J.R. Robinson, Topical Ocular Drug Delivery: Recent Developments and Future Challenges, ***Journal of Ocular Pharmacology*** 2 (1) (1986) 67–108.
299. L. Gan, J. Wang, M. Jiang, H. Bartlett, D. Ouyang, F. Eperjesi, J. Liu, and Y. Gan, Recent advances in topical ophthalmic drug delivery with lipid-based nanocarriers, ***Drug Discovery Today*** 18 (5–6) (2013) 290–297.
300. N. Kuno and S. Fujii, Recent Advances in Ocular Drug Delivery Systems, ***Polymers*** 3 (1) (2011) 193–221.
301. D.R. Janagam, L. Wu, and T.L. Lowe, Nanoparticles for drug delivery to the anterior segment of the eye, ***Advanced Drug Delivery Reviews*** 122 (2017) 31–64.
302. C. Jumelle, S. Gholizadeh, N. Annabi, and R. Dana, Advances and limitations of drug delivery systems formulated as eye drops, ***Journal of Controlled Release*** 321 (2020) 1–22.
303. K.L. Nair, S. Vidyanand, J. James, and G.S.V. Kumar, Pilocarpine-loaded poly(DL-lactic-co-glycolic acid) nanoparticles as potential candidates for controlled drug delivery with enhanced ocular pharmacological response, ***Journal of Applied Polymer Science*** 124 (3) (2012) 2030–2036.
304. R.C. Nagarwal, R. Kumar, and J.K. Pandit, Chitosan coated sodium alginate-chitosan nanoparticles loaded with 5-FU for ocular delivery: In vitro characterization and in vivo study in rabbit eye, ***European Journal of Pharmaceutical Sciences*** 47 (4) (2012) 678–685.
305. H. Gupta, M. Aqil, R.K. Khar, A. Ali, A. Bhatnagar, and G. Mittal, Sparfloxacin-loaded PLGA nanoparticles for sustained ocular drug delivery, ***Nanomedicine: Nanotechnology, Biology, and Medicine*** 6 (2) (2010) 324–333.
306. S.M. Agnihotri and P.R. Vavia, Diclofenac-loaded biopolymeric nanosuspensions for ophthalmic application, ***Nanomedicine: Nanotechnology, Biology, and Medicine*** 5 (1) (2009) 90–95.
307. H.K. Ibrahim, I.S. El-Leithy, and A.A. Makky, Mucoadhesive nanoparticles as carrier systems for prolonged ocular delivery of gatifloxacin/prednisolone bitherapy, ***Molecular Pharmaceutics*** 7 (2) (2010) 576–585.
308. P. Bhagav, H. Upadhyay, and S. Chandran, Brimonidine tartrate-eudragit long-acting nanoparticles: Formulation, optimization, in vitro and in vivo evaluation, ***AAPS***

PharmSciTech 12 (4) (2011) 1087–1101.

309. A. Seyfoddin, J. Shaw, and R. Al-Kassas, Solid lipid nanoparticles for ocular drug delivery, ***Drug Delivery*** 17 (7) (2010) 467–489.
310. B.A. Witika, P.A. Makoni, S.K. Matafwali, B. Chabalenge, C. Mwila, A.C. Kalungia, C.I. Nkanga, A.M. Bapolisi, and R.B. Walker, Biocompatibility of Biomaterials for Nanoencapsulation: Current Approaches, ***Nanomaterials*** 10 (9) (2020) 1649.
311. A.A. Öztürk, A. Aygül, and B. Şenel, Influence of glyceryl behenate, tripalmitin and stearic acid on the properties of clarithromycin incorporated solid lipid nanoparticles (SLNs): Formulation, characterization, antibacterial activity and cytotoxicity, ***Journal of Drug Delivery Science and Technology*** 54 (2019) 101240.
312. H.-Z. Bu, H. Gukasyan, L. Goulet, X.-J. Lou, C. Xiang, and T. Koudriakova, Ocular Disposition, Pharmacokinetics, Efficacy and Safety of Nanoparticle-Formulated Ophthalmic Drugs, ***Current Drug Metabolism*** 8 (2) (2007) 91–107.
313. A. Kumar, P.K. Naik, D. Pradhan, G. Ghosh, and G. Rath, Mucoadhesive Formulations: Innovations, Merits, Drawbacks and Future Outlook, ***Pharmaceutical Development and Technology*** (2020) 1–43.
314. A.M. De Campos, A. Sánchez, R. Gref, P. Calvo, and M.J. Alonso, The effect of a PEG versus a chitosan coating on the interaction of drug colloidal carriers with the ocular mucosa, ***European Journal of Pharmaceutical Sciences*** 20 (1) (2003) 73–81.
315. T. Hua, X. Zhang, B. Tang, C. Chang, G. Liu, L. Feng, Y. Yu, D. Zhang, and J. Hou, Tween-20 transiently changes the surface morphology of PK-15 cells and improves PCV2 infection, ***BMC Veterinary Research*** 14 (1) (2018).
316. R.K. Sahoo, N. Biswas, A. Guha, N. Sahoo, and K. Kuotsu, Nonionic Surfactant Vesicles in Ocular Delivery: Innovative Approaches and Perspectives, (2014).
317. R. Rowe, P. Sheskey, and M. Quinn, *Handbook of pharmaceutical excipients*, 6th ed., *The Pharmaceutical Press*, London, (2009).
318. A.I. Khuri and S. Mukhopadhyay, Response surface methodology, ***WIREs Computational Statistics*** 2 (2010) 128–149.
319. A.B. Marcos, E.S. Ricardo, P.O. Eliane, S.V. Leonardo, and A.E. Luciane, Response surface methodology (RSM) as a tool for optimization in analytical chemistry, ***Talanta*** 76 (5) (2008) 965–977.
320. *Handbook for Experimenters A conscise collection of handy tips to help you set up and analyze your designed experiments*, *Stat-Ease Inc.*, Minneapolis, (2014).
321. D.C. Whittinghill, A note on the robustness of Box-Behnken designs to the

unavailability of data, ***Metrika*** 48 (1) (1998) 49–52.

322. S. Cunha, C.P. Costa, J.A. Loureiro, J. Alves, A.F. Peixoto, B. Forbes, J.M.S. Sousa Lobo, and A.C. Silva, Double Optimization of Rivastigmine-Loaded Nanostructured Lipid Carriers (NLC) for Nose-to-Brain Delivery Using the Quality by Design (QbD) Approach: Formulation Variables and Instrumental Parameters, ***Pharmaceutics*** 12 (7) (2020) 599.
323. J.Y. Fang, C.L. Fang, C.H. Liu, and Y.H. Su, Lipid nanoparticles as vehicles for topical psoralen delivery: Solid lipid nanoparticles (SLN) versus nanostructured lipid carriers (NLC), ***European Journal of Pharmaceutics and Biopharmaceutics*** 70 (2) (2008) 633–640.
324. B. Shah, D. Khunt, H. Bhatt, M. Misra, and H. Padh, Application of quality by design approach for intranasal delivery of rivastigmine loaded solid lipid nanoparticles: Effect on formulation and characterization parameters, ***European Journal of Pharmaceutical Sciences*** 78 (2015) 54–66.
325. T. Alam, S. Khan, B. Gaba, M.F. Haider, S. Baboota, and J. Ali, Adaptation of Quality by Design-Based Development of Isradipine Nanostructured–Lipid Carrier and Its Evaluation for In Vitro Gut Permeation and In Vivo Solubilization Fate, ***Journal of Pharmaceutical Sciences*** 107 (11) (2018) 2914–2926.
326. J.F. Charlton, K.P. Dalla, and A. Kniska, Storage of extemporaneously prepared ophthalmic antimicrobial solutions, ***Am J Health-Syst Pharm*** 55 (1998).
327. R. Mazet, L. Choisnard, D. Levilly, D. Wouessidjewe, and A. Gèze, Investigation of Combined Cyclodextrin and Hydrogel Formulation for Ocular Delivery of Dexamethasone Acetate by Means of Experimental Designs, ***Pharmaceutics*** 10 (4) (2018) 249.
328. A. Sze, D. Erickson, L. Ren, and D. Li, Zeta-potential measurement using the Smoluchowski equation and the slope of the current-time relationship in electroosmotic flow, ***Journal of Colloid and Interface Science*** 261 (2003) 402–410.
329. R.S. Bhatta, H. Chandasana, Y.S. Chhonker, C. Rathi, D. Kumar, K. Mitra, and P.K. Shukla, Mucoadhesive nanoparticles for prolonged ocular delivery of natamycin: In vitro and pharmacokinetics studies, ***International Journal of Pharmaceutics*** 432 (1–2) (2012) 105–112.
330. E. Terreni, P. Chetoni, S. Tampucci, S. Burgalassi, A. Al-kinani, R. Alany, and D. Monti, Assembling Surfactants-Mucoadhesive Polymer Nanomicelles (ASMP-Nano) for Ocular Delivery of Cyclosporine-A, ***Pharmaceutics*** 12 (3) (2020) 253.

331. Y. Zhang, M. Huo, J. Zhou, A. Zou, W. Li, C. Yao, and S. Xie, DDSolver: An add-in program for modeling and comparison of drug dissolution profiles, ***AAPS Journal*** 12 (3) (2010) 263–271.

332. R. Foldbjerg, J. Wang, C. Beer, K. Thorsen, D.S. Sutherland, and H. Autrup, Biological effects induced by BSA-stabilized silica nanoparticles in mammalian cell lines, ***Chemico-Biological Interactions*** 204 (1) (2013) 28–38.

333. D.R. Nogueira, M. Carmen Morán, M. Mitjans, V. Martínez, L. Pérez, and M. Pilar Vinardell, New cationic nanovesicular systems containing lysine-based surfactants for topical administration: Toxicity assessment using representative skin cell lines, ***European Journal of Pharmaceutics and Biopharmaceutics*** 83 (1) (2013) 33–43.

334. I. Bácskay, D. Nemes, F. Fenyvesi, J. Váradi, G. Vasvári, P. Fehér, M. Vecsernyés, and Z. Ujhelyi, Role of Cytotoxicity Experiments in Pharmaceutical Development, *in Cytotoxicity*. *InTech*, (2018).

335. D. Nogueira, M. Mitjans, C. Rolim, and M. Vinardell, Mechanisms Underlying Cytotoxicity Induced by Engineered Nanomaterials: A Review of In Vitro Studies, ***Nanomaterials*** 4 (2) (2014) 454–484.

336. S.W. Ha, J.A. Sikorski, M.N. Weitzmann, and G.R. Beck, Bio-active engineered 50nm silica nanoparticles with bone anabolic activity: Therapeutic index, effective concentration, and cytotoxicity profile in vitro, ***Toxicology in Vitro*** 28 (3) (2014) 354–364.

337. B.R. Matthews and G.M. Wall, Stability Storage and Testing of Ophthalmic Products for Global Registration, ***Drug Development and Industrial Pharmacy*** 26 (12) (2000) 1227–1237.

338. A.A. Ahmad, B.H. Hameed, and A.L. Ahmad, Removal of disperse dye from aqueous solution using waste-derived activated carbon: Optimization study, ***Journal of Hazardous Materials*** 170 (2–3) (2009) 612–619.

339. A. Siddiqui, A. Alayoubi, Y. El-Malah, and S. Nazzal, Modeling the effect of sonication parameters on size and dispersion temperature of solid lipid nanoparticles (SLNs) by response surface methodology (RSM), ***Pharmaceutical Development and Technology*** 19 (3) (2014) 342–346.

340. E. Gonzalez-Mira, M.A. Egea, M.L. Garcia, and E.B. Souto, Design and ocular tolerance of flurbiprofen loaded ultrasound-engineered NLC, ***Colloids and Surfaces B: Biointerfaces*** 81 (2) (2010) 412–421.

341. A. Radomskasoukharev, Stability of lipid excipients in solid lipid nanoparticles☆, ***Advanced Drug Delivery Reviews*** 59 (6) (2007) 411–418.
342. A. Nath and P.K. Chattopadhyay, Optimization of oven toasting for improving crispness and other quality attributes of ready to eat potato-soy snack using response surface methodology, ***Journal of Food Engineering*** 80 (4) (2007) 1282–1292.
343. R.P. Patel, D.J. Patel, D.B. Bhimani, and J.K. Patel, Physicochemical Characterization and Dissolution Study of Solid Dispersions of Furosemide with Polyethylene Glycol 6000 and Polyvinylpyrrolidone K30, ***Dissoltion Technologies*** 15 (3) (2018) 17–25.
344. N. Dubashynskaya, D. Poshina, S. Raik, A. Urtti, and Y.A. Skorik, Polysaccharides in ocular drug delivery, ***Pharmaceutics*** 12 (1) (2020) 22.
345. S. Rossi, B. Vigani, M.C. Bonferoni, G. Sandri, C. Caramella, and F. Ferrari, Rheological analysis and mucoadhesion: A 30 year-old and still active combination, ***Journal of Pharmaceutical and Biomedical Analysis*** 156 (2018) 232–238.
346. R. Machado Cruz, M.J. Santos-Martinez, and L. Tajber, Impact of polyethylene glycol polymers on the physicochemical properties and mucoadhesivity of itraconazole nanoparticles, ***European Journal of Pharmaceutics and Biopharmaceutics*** 144 (2019) 57–67.
347. S. Scioli Montoto, M.L. Sbaraglini, A. Talevi, M. Couyoupetrou, M. Di Ianni, G.O. Pesce, V.A. Alvarez, L.E. Bruno-Blanch, G.R. Castro, M.E. Ruiz, and G.A. Islan, Carbamazepine-loaded solid lipid nanoparticles and nanostructured lipid carriers: Physicochemical characterization and in vitro/in vivo evaluation, ***Colloids and Surfaces B: Biointerfaces*** 167 (2018) 73–81.
348. M. Padmaa Paarakh, P. Ani Jose, C.M. Setty, and G.V.P. Christoper, RELEASE KINETICS-CONCEPTS AND APPLICATIONS, ***International Journal of Pharmacy Research & Technology*** 8 (2018) 12–20.
349. B.A. Witika, V.J. Smith, and R.B. Walker, Quality by Design Optimization of Cold Sonochemical Synthesis of Zidovudine-Lamivudine Nanosuspensions, ***Pharmaceutics*** 12 (4) (2020) 367.
350. B. Romberg, W.E. Hennink, and G. Storm, Sheddable coatings for long-circulating nanoparticles, ***Pharmaceutical Research*** 25 (1) (2008) 55–71.
351. H. Heiati, R. Tawashi, and N.C. Phillips, Drug retention and stability of solid lipid nanoparticles containing azidothymidine palmitate after autoclaving, storage and lyophilization, ***Journal of Microencapsulation*** 15 (2) (1998) 173–184.

352. L.T. Boni, T.P. Stewart, and S.W. Hui, Alterations in phospholipid polymorphism by polyethylene glycol, ***The Journal of Membrane Biology*** 80 (1) (1984) 91–104.
353. S. Das and A. Chaudhury, Recent Advances in Lipid Nanoparticle Formulations with Solid Matrix for Oral Drug Delivery, ***AAPS PharmSciTech*** 12 (1) (2010) 62–76.

APPENDIX I

BATCH PRODUCTION RECORDS

Note that only the production records for F44 and the optimized CLA-NLC (CLA-NLC-OPT) are included here. The batch production records for all other formulations manufactured and assessed during formulation development and optimization studies are available on request. All formulations manufactured and assessed during formulation development and optimization studies were manufactured using Good Manufacturing Practice (GMP).

RHODES UNIVERSITY, FACULTY OF PHARMACY

MAKHANDA, 6140, SOUTH AFRICA

BATCH PRODUCTION RECORD

Product name: CLA-loaded NLC **Page 1 of 5**

Batch ID: F44 **Batch size: 100 g**

MANUFACTURING APPROVALS

Batch record issued by_____ **Date**_____

Master record issued by_____ **Date**_____

RHODES UNIVERSITY, FACULTY OF PHARMACY

MAKHANDA, 6140, SOUTH AFRICA

BATCH PRODUCTION RECORD

Product name: CLA-loaded NLC

Batch ID: F44 **Batch size: 100 g**

Item	Material	Quantity (% *w/w*)	Amount/batch (g)	Dispensed by	Checked by
1	CLA	0.50	0.50		
2	Stearic acid	4.00	4.00		
3	Transcutol® HP	1.00	1.00		
4	Tween® 80	1.00	1.00		
5	PEG 6000	1.00	1.00		
6	Aqua (ad)	93.00	93.00		

RHODES UNIVERSITY, FACULTY OF PHARMACY

MAKHANDA, 6140, SOUTH AFRICA

BATCH PRODUCTION RECORD

Product name: CLA-loaded NLC **Page 3 of 5**

Batch ID: F44 **Batch size: 100 g**

EQUIPMENT VERIFICATION			
Description	**Type**	**Verified by**	**Confirmed by**
High speed homogenizer	Model T 18 Ultra-Turrax®		
Probe sonicator	Sonoplus® HD 4200		

RHODES UNIVERSITY, FACULTY OF PHARMACY

MAKHANDA, 6140, SOUTH AFRICA

BATCH PRODUCTION RECORD

Product name: CLA-loaded NLC

Batch ID: F44 **Batch size: 100 g**

MANUFACTURING PROCEDURE				
Step	**Procedure**	**Time**	**Done by**	**Checked by**
1	Weigh all the materials.			
2	Heat water (item 6) to 85 °C in a beaker and disperse Tween® 20 and PEG 6000 (items 4 and 5) into the hot water until a clear solution is obtained. Maintain the temperature of the resultant aqueous phase at 85 °C.			
3	Heat stearic acid and Transcutol® HP (items 2 and 3) at 85 °C until a clear melt is obtained. Disperse CLA (item 1) in the lipid melt and maintain at 85 °C.			
4	Disperse the heated aqueous phase in the molten lipid phase using high speed stirring at 6000 rpm for 1 minute to form a pre-emulsion.			
5	Sonicate the pre-emulsion at 85 °C using the probe sonicator set an amplitude of 55% for 20 minutes.			
6	Fill and seal the hot o/w nanoemulsion immediately in a siliconized glass vial and allow the product to cool to room temperature (22 ºC).			
7	Store all samples at room temperature for at least 24 hours prior to characterization.			

RHODES UNIVERSITY, FACULTY OF PHARMACY

MAKHANDA, 6140, SOUTH AFRICA

BATCH PRODUCTION RECORD

Product name: CLA-loaded NLC

Batch ID: F44 **Batch size: 100 g**

SIGNATURE AND INITIAL REFERENCE			
Full name (Print)	**Signature**	**Initials**	**Date**

RHODES UNIVERSITY, FACULTY OF PHARMACY

MAKHANDA, 6140, SOUTH AFRICA

BATCH PRODUCTION RECORD

Product name: CLA-loaded NLC **Page 1 of 5**

Batch ID: CLA-NLC-OPT **Batch size: 100 g**

MANUFACTURING APPROVALS

Batch record issued by_____ Date_____

Master record issued by_____ Date_____

RHODES UNIVERSITY, FACULTY OF PHARMACY

MAKHANDA, 6140, SOUTH AFRICA

BATCH PRODUCTION RECORD

Product name: CLA-loaded NLC

Batch ID: CLA-NLC-OPT **Batch size: 100 g**

Item	Material	Quantity (% w/w)	Amount/batch (g)	Dispensed by	Checked by
1	CLA	0.50	0.50		
2	Stearic acid	4.00	4.00		
3	Transcutol® HP	1.00	1.00		
4	Tween® 80	1.00	1.00		
5	PEG 6000	1.00	1.00		
6	Aqua (ad)	93.00	93.00		

RHODES UNIVERSITY, FACULTY OF PHARMACY

MAKHANDA, 6140, SOUTH AFRICA

BATCH PRODUCTION RECORD

Product name: CLA-loaded NLC

Batch ID: CLA-NLC-OPT **Batch size: 100 g**

EQUIPMENT VERIFICATION			
Description	**Type**	**Verified by**	**Confirmed by**
High speed homogenizer	Model T 18 Ultra-Turrax®		
Probe sonicator	Sonoplus® HD 4200		

RHODES UNIVERSITY, FACULTY OF PHARMACY

MAKHANDA, 6140, SOUTH AFRICA

BATCH PRODUCTION RECORD

Product name: CLA-loaded NLC **Page 4 of 5**

Batch ID: CLA-NLC-OPT **Batch size: 100 g**

MANUFACTURING PROCEDURE				
Step	**Procedure**	**Time**	**Done by**	**Checked by**
1	Weigh all the materials.			
2	Heat water (item 6) to 85 °C in a beaker and disperse Tween® 20 and PEG 6000 (items 4 and 5) into the hot water until a clear solution is obtained. Maintain the temperature of the resultant aqueous phase at 85 °C.			
3	Heat stearic acid and Transcutol® HP (items 2 and 3) at 85 °C until a clear melt is obtained. Disperse CLA (item 1) in the lipid melt and maintain at 85 °C.			
4	Disperse the heated aqueous phase in the molten lipid phase using high speed stirring at 6000 rpm for 1 minute to form a pre-emulsion.			
5	Sonicate the pre-emulsion at 85 °C using the probe sonicator set an amplitude of 60% for 26.33 minutes.			
6	Fill and seal the hot o/w nanoemulsion immediately in a siliconized glass vial and allow the product to cool to room temperature (22 ºC).			
7	Store all samples at room temperature for at least 24 hours prior to characterization.			

RHODES UNIVERSITY, FACULTY OF PHARMACY

MAKHANDA, 6140, SOUTH AFRICA

BATCH PRODUCTION RECORD

Product name: CLA-loaded NLC **Page 5 of 5**

Batch ID: CLA-NLC-OPT **Batch size: 100 g**

SIGNATURE AND INITIAL REFERENCE			
Full name (Print)	**Signature**	**Initials**	**Date**

APPENDIX II

PUBLICATIONS

Scientia Pharmaceutica

ÖSTERREICHISCHE PHARMAZEUTISCHE GESELLSCHAFT

MDPI

Article

Stability Indicating HPLC-ECD Method for the Analysis of Clarithromycin in Pharmaceutical Dosage Forms: Method Scaling versus Re-Validation

Pedzisai A. Makoni, Mellisa T. R. Chikukwa, Sandile M. M. Khamanga and Roderick B. Walker *

Division of Pharmaceutics, Faculty of Pharmacy, Rhodes University, 6140 Grahamstown, South Africa; P.Makoni@ru.ac.za (P.A.M.); MTRChikukwa@gmail.com (M.T.R.C.); S.Khamanga@ru.ac.za (S.M.M.K.)

* Correspondence: R.B.Walker@ru.ac.za

Received: 16 October 2019; Accepted: 6 November 2019; Published: 16 November 2019

Abstract: An isocratic high-performance liquid chromatographic method using electrochemical detection (HPLC-ECD) for the quantitation of clarithromycin (CLA) was developed using Response Surface Methodology (RSM) based on a Central Composite Design (CCD). The method was validated using International Conference on Harmonization (ICH) guidelines with an analytical run time of 20 min. Method re-validation following a change in analytical column was successful in reducing the analytical run time to 13 min, decreasing solvent consumption thus facilitating environmental and financial sustainability. The applicability of using the United States Pharmacopeia (USP) method scaling approach in place of method re-validation using a column with a different L–designation to the original analytical column, was investigated. The scaled method met all USP system suitability requirements for resolution, tailing factor and % relative standard deviation (RSD). The re-validated and scaled method was successfully used to resolve CLA from manufacturing excipients in commercially available dosage forms. Although USP method scaling is only permitted for columns within the same L-designation, these data suggest that it may also be applicable to columns of different designation.

Keywords: clarithromycin; electrochemical detection; central composite design; method validation; USP method scaling; stability-indicating

1. Introduction

Clarithromycin (CLA) is a semi-synthetic macrolide derivative of erythromycin A comprised of 14-cladisone and desosamine residues attached at positions 3 and 5 (Figure 1) [1,2]. CLA is a biopharmaceutical classification system (BCS) class II molecule that is poorly soluble and highly permeable. CLA exhibits an aqueous solubility of approximately 0.342 µg/mL at 25 °C, and has a pKa of 8.8 [3]. CLA is acid-stable and has a broad spectrum of antimicrobial activity, inhibiting a range of Gram-positive and Gram-negative organisms, atypical pathogens and some anaerobic organisms [4,5]. CLA lacks a chromophore as it has no conjugated double bond in the lactone ring therefore, significant UV absorbance is only observed at wavelengths < 210 nm [6]. Detection at these wavelengths is suitable for most in vitro samples but lack the necessary sensitivity for the quantitation of low concentrations of CLA, such as those observed in biological matrices [2,7] and nanoparticles [8]. CLA has a tertiary amino group which is reactive for electrochemical oxidation [9], making electrochemical detection (ECD) a potentially useful tool for ensuring the accurate determination of CLA in dosage forms. Quantitative analysis of CLA has been achieved in biological samples using high-performance liquid chromatography (HPLC) with ECD [10–12], UV [2,13], LCMS [14] and fluorescence detection [15].

Published HPLC-ECD methods have reported detection limits of 10.03 μg/mL [16], 0.5 μg/mL [17], 0.03 μg/mL [18], 0.01 μg/mL [19], 0.15 μg/mL [20] and 0.02 μg/mL [21]. In addition, characterization of degradation products of CLA have been reported using HPLC-MS [22,23] and HPLC-UV [5,13].

Sci. Pharm. 2019, 87, 31 2 of 20

and 0.02 μg/mL [21]. In addition, characterization of degradation products of CLA have been reported using HPLC-MS [22,23] and HPLC-UV [8,13].

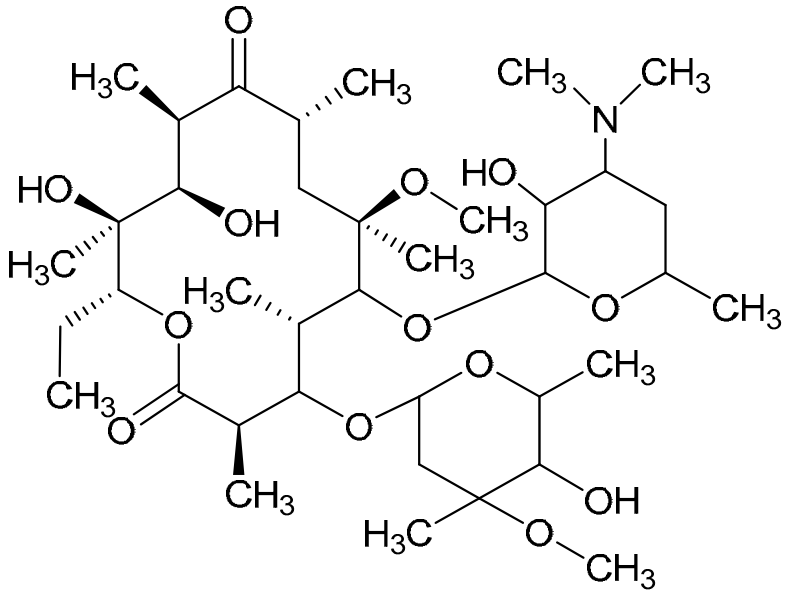

Figure 1. Chemical structure of clarithromycin (CLA) ($C_{38}H_{69}NO_{13}$, MW = 747.96 g/mol) [24].

Figure 1. Chemical structure of clarithromycin (CLA) ($C_{38}H_{69}NO_{13}$, MW = 747.96 g/mol) [24].

It has been established that step-by-step optimization procedures for any reliable HPLC method requires good peak resolution with acceptable retention time(s), the absence of 'ghost' peaks, stable sensitivity with minimal peak tailing [25]. The initial aim of these studies was to screen factors that would hinder achievement of the appropriate chromatographic conditions and performance, with the ultimate goal of developing a rapid, simple and sensitive analytical method using a minimum number of experimental runs.

It has been established that step-by-step optimization procedures for any reliable HPLC method requires good peak resolution with acceptable retention time(s), the absence of 'ghost' peaks, stable sensitivity with minimal peak tailing [25]. The initial aim of these studies was to screen factors that would hinder achievement of the appropriate chromatographic conditions and performance, with the ultimate goal of developing a rapid, simple and sensitive analytical method using a minimum number of experimental runs.

Prior to using Design of Experiments (DoE), a conventional approach was used to establish the optimum operating conditions so as to eliminate factors that resulted in a long retention time, baseline drift and background noise. DoE was ultimately used to identify the optimum analytical conditions for this separation.

Prior to using Design of Experiments (DoE), a conventional approach was used to establish the optimum operating conditions so as to eliminate factors that resulted in a long retention time, baseline drift and background noise. DoE was ultimately used to identify the optimum analytical conditions for this separation.

DoE is a chemometric approach that allows for a reduction in the number of experiments conducted associated with lower reagent consumption and less laboratory work [26]. The use of statistical experimental design modelling methods and response optimization based on derived models reduces the time and effort required for the development of complex multi-variable analyses. Furthermore, optimization of HPLC methods are complex processes since, several variables including mobile phase pH and composition, buffer concentration, flow rate, injection volume, column temperature and detector settings must be controlled to achieve an appropriate separation [27]. The approach facilitates the development of suitable polynomial regression models and the addition of valuable scientific information in support of an ability to assess the statistical significance of the influence of input variables on target chromatographic responses [26]. In these studies, a Central Composite Design (CCD) was used to identify the optimum conditions for the HPLC-ECD method.

DoE is a chemometric approach that allows for a reduction in the number of experiments conducted associated with lower reagent consumption and less laboratory work [26]. The use of statistical experimental design modelling methods and response optimization based on derived models reduces the time and effort required for the development of complex multi-variable analyses. Furthermore, optimization of HPLC methods are complex processes since, several variables including mobile phase pH and composition, buffer concentration, flow rate, injection volume, column temperature and detector settings must be controlled to achieve an appropriate separation [27]. The approach facilitates the development of suitable polynomial regression models and the addition of valuable scientific information in support of an ability to assess the statistical significance of the influence of input variables on target chromatographic responses [26]. In these studies, a Central Composite Design (CCD) was used to identify the optimum conditions for the HPLC-ECD method.

The development of an HPLC-UV analytical method for the quantification of CLA in pharmaceutical dosage forms using DoE has been reported [28]. The CCD is a three-level full factorial design covering a symmetrical domain with a center point used to estimate experimental error [29]. A CCD may include a two-level full factorial design (2^f experiments), a star design ($2f$ experiments) and a center point, requiring $N = 2^f + 2f + 1$ experiments to examine f factors [30,31]. The points of the full factorial design are located at factor levels −1 and +1 and for the star design at factor levels 0, $-\alpha$ and $+\alpha$, whereas for the center point at a factor level 0 [32].

The development of an HPLC-UV analytical method for the quantification of CLA in pharmaceutical dosage forms using DoE has been reported [28]. The CCD is a three-level full factorial design covering a symmetrical domain with a center point used to estimate experimental error [29]. A CCD may include a two-level full factorial design (2^f experiments), a star design ($2f$ experiments) and a center point, requiring $N = 2^f + 2f + 1$ experiments to examine f factors [30,31].

Method validation is a process that demonstrates that a method will successfully meet or exceed the minimum standards recommended by regulatory authorities for accuracy, precision, selectivity,

The points of the full factorial design are located at factor levels −1 and +1 and for the star design at factor levels 0, $-\alpha$ and $+\alpha$, whereas for the center point at a factor level 0 [32].

Method validation is a process that demonstrates that a method will successfully meet or exceed the minimum standards recommended by regulatory authorities for accuracy, precision, selectivity, sensitivity, reproducibility and stability [33]. According to the USP [34], certain parameters of a method may be adjusted or scaled on the condition that allowable limits and equivalency are maintained.

The objective of these studies was to develop a stability indicating the HPLC-ECD method for the quantitative determination of CLA in pharmaceutical formulations and monitoring CLA incorporation into lipid nano-carrier technologies. The method was developed and validated according to International Conference of Harmonization (ICH) guidelines [35]. Method re-validation in addition to modified method scaling as per United States Pharmacopeia (USP) [34] guidelines was also investigated in order to assess and assure the performance of the method when moving across analytical columns of different packing material (L-designation). To our knowledge, this is the first time an experimental design has been applied to the development of a simple, rapid, sensitive and reliable HPLC method using amperometric detection for the quantification of CLA in dosage forms. Furthermore, this is the first study to develop a stability indicating the HPLC-ECD method for CLA whilst investigating a modified USP scaling approach through use of a column of different L-designation.

2. Materials and Methods

2.1. Chemicals and Reagents

All reagents were at least of analytical reagent grade and used without further purification. CLA was purchased from Skyrun Industrial Co. Limited (Taizhou, China) and the internal standard, erythromycin (ERY) was purchased from Sigma Aldrich Chemical Co. (Milwaukee, WI, USA). Clarihexal®, Klarithran®, Klarithran® MR 500 mg tablets, Klarizon 250 mg tablets and Clarihexal®, Klarithran® 250 mg/mL granules for oral suspension were purchased from a local pharmacy. HPLC-grade water was prepared by reverse osmosis using a RephiLe® Direct-Pure UP ultrapure and RO water system (Microsep®, Johanessburg, South Africa), consisting of a deionization RephiDuO® H PAK cartridge and a polishing RephiDuO® PAK cartridge. The water was filtered through a 0.22 µm PES high-flux capsule filter (Microsep®, Johannesburg, South Africa) and used to prepare all buffer solutions. HPLC far UV-grade acetonitrile (ACN) and methanol (MeOH) was purchased from Anatech® Instruments Pty, Ltd. (Randburg, Johannesburg, South Africa). Potassium dihydrogen orthophosphate, sodium chloride and sodium hydroxide pellets were purchased from Merck® Laboratories (Merck®, Wadeville, South Africa).

2.2. Instrumentation and Analytical Conditions

The HPLC system was a Waters® Alliance Model 2695 separation module equipped with a solvent delivery module, an autosampler, an online degasser and a Model 2465 Electrochemical Detector (Waters®, Milford, MA, USA). Data acquisition, processing and reporting were achieved using Waters® Empower 3 software (Waters®, Milford, MA, USA). The separation was achieved under isocratic conditions using a Beckman® C_8, 4 µm (150 mm × 4.0 i.d) (Beckman Instruments, Inc., San Ramon, CA, USA) cartridge column with a mobile phase consisting of 50 mM phosphate buffer (pH 7.0), ACN and MeOH in a 58.5:36.5:5.0 *v/v/v* ratio. The flow rate of the mobile phase and the injection volume were 1.0 mL/min and 10 µL, respectively. The analytical column was maintained at 30 °C using an integral column heater (Waters®, Milford, MA, USA).

2.3. Preparation of Solutions

2.3.1. Stock solution and calibration standards

Standard stock solutions of CLA (100 µg/mL) and ERY (50 µg/mL) were prepared by accurately weighing approximately 10 mg and 5 mg of each API using a Model AE 163 Mettler® analytical balance (Mettler® Inc., Zurich, Switzerland) into 100 mL A-grade volumetric flasks and dissolving in a small volume of ACN. The stock solutions were sonicated using an ultrasonic bath (Ultrasonic Manufacturing Company (Pty), Ltd., Kenware, Krugersdorp, South Africa) until a clear solution formed, after which the solutions were made up to volume with ACN. Calibration standards of CLA over the concentration range 5–50 µg/mL were prepared by serial dilution of the standard stock solution on the day of analysis, using ACN as a diluent. A 0.75 mL aliquot of the 50 µg/mL ERY stock solution was added to all calibration standards and test samples prior to analysis.

2.3.2. Buffer and Mobile Phase

Phosphate buffer solutions (50 mM) were prepared by accurately weighing 6.0845 g potassium dihydrogen orthophosphate into a 1 L A-grade volumetric flask and making up to volume with HPLC grade water. A 0.11 g aliquot of sodium chloride was added to the buffer solution to produce 2 mM equivalent chloride ions. The pH of the buffers was monitored at 22 °C using a Model Basic 20+ Grison pH-meter (Crison Instruments, Barcelona, Spain) and was adjusted to 7.0 using sodium hydroxide pellets. The buffer was degassed under vacuum with the aid of a Model A-2S Eyela Aspirator degasser (Rikakikai Co., Ltd., Tokyo, Japan) and filtered through a 0.2 µm cellulose membrane filter (Sartorius Stedim Biotech GmbH, Goettingen, Germany) prior to being transferred into a 1 L Schott® Duran bottle (Schott Duran GmbH, Wertheim, Germany).

2.4. Statistical Analysis

Data generated were analyzed using Design Expert® version 8.0.2 statistical software (Stat-Ease Inc., Minneapolis, MN, USA). The significance of relevant factors was determined using Fisher's statistical test for Analysis of Variance (ANOVA). Models were estimated and run to compare first-order interaction terms. ANOVA for linear regression, partitions the total variation of a sample into components that are then used to compute an F-ratio which is used to evaluate the effectiveness of the model. If the probability associated with the F-ratio is low, the model is considered to better fit the data statistically. In these calculations, the higher-order interaction terms are assumed not to contribute, to any great extent, to the behavior of the statistical model.

2.5. Method Validation

2.5.1. Linearity and Range

The linearity was determined using a minimum of five standards injected five times as per the ICH [35] guidelines. The linearity of the method was evaluated over the concentration range of 5–50 µg/mL and least squares linear regression analysis of the peak height ratio (PHR) versus concentration data was used to evaluate the linearity of the method.

2.5.2. Precision

The precision of the method was evaluated at two different levels *viz*., repeatability (intra-day precision) and intermediate precision (inter-day precision). The repeatability for CLA was determined by analysing a sample solution containing the target level of CLA. Ten replicates (n = 10) of the sample solution were analysed as per the final method procedure [36]. Repeatability was determined using a 50 µg/mL sample solution. The inter-day precision for CLA was determined by analysing sample solutions in replicate (n = 5) at three different concentrations *viz*., low, middle and high, within the range tested on three different days.

2.5.3. Accuracy

The accuracy of the method was determined by replicate analysis (n = 5) of samples containing known amounts of CLA at low (6.0 µg/mL), middle (25.0 µg/mL) and high (45.0 µg/mL) concentrations. The mean recovery was assessed for compliance according to the ICH guidelines.

2.5.4. LOQ and LOD

The limit of quantitation (LOQ) of the method was determined by evaluating the lowest concentration of CLA that resulted in a precision of < 5% RSD, and the limit of detection (LOD) was taken as the 0.3 × LOQ value. Alternatively, the LOD may be inferred from the concentration resulting in a % RSD of ≤ 20% when the LOQ results in a % RSD of ≤ 10% [37].

2.6. Method Scaling and Re-Validation

Method scaling is used when an adjustment of the method is required and where parameters are changed within permitted limits, to preserve the chromatographic separation. When a change is made to the column, flow rates may need to be adjusted to maintain the separation and chromatographic performance of a method [34,38]. Scaling methods can be used to ensure the same quality of separation while reducing run times, with a reduction in solvent consumption thus ensuring environmental and financial sustainability. In addition, reduced run times result in increased throughput, efficiency of operation and overall profitability.

Chapter 621 of the USP [34] defines permitted adjustments, for a method, for the purposes of scaling without the need for re-validation. These adjustments are permissible provided system suitability requirements, as described in the monograph, are met when the changes are implemented [34,38].

Any column changes must stay within the original method L-designation. For isocratic separations, the particle size and/or the length of the column may be modified provided that the ratio of column length (L) to particle size (dp) (the L/dp) remains constant or falls within the limits of −25%–+50%. When the particle size is changed, the flow rate may require adjustment and can be calculated using Equation (1) [34].

$$F_2 = F_1 \times [(dc_2{}^2 x dp_1)/(dc_1{}^2 x dp_2)] \quad (1)$$

where, F_1 and F_2 are the flow rates for the original and modified conditions, dc_1 and dc_2 are the respective column diameters and dp_1 and dp_2 are the particle sizes of the stationary phase used. Following method development and validation using a Beckman® C_8, 4 µm (150 mm × 4.0 i.d) analytical column, further analysis using the column could not be performed. Attempts to regenerate and/or purchase an identical column were unsuccessful as the specific column has been phased out by the manufacturer. Consequently, re-validation and an investigation into the application of method scaling using a different L-designation column were undertaken using a Phenomenex Luna® CN, 5 µm 150 mm × 4.6 mm i.d (Phenomenex®, Torrace, CA, USA) which exhibited a −20% decrease in the L/dp value that fell within the range of −25% to + 50% as per the USP [34] method scaling guidelines. Analysis was undertaken using a mobile phase flow rate of 1.058 mL/min that was calculated using Equation (1).

USP [34] system suitability requirements for resolution, tailing factor and % RSD for peak height ratio (PHR) and retention time, were used to determine if the modified scaling for the HPLC-ECD method resulted in outcomes that were comparable to those observed using re-validation and thus assess, the applicability of the scaled method for the determination of CLA.

2.7. Assay of Clarithromycin Dosage Forms

2.7.1. Assay of Commercial Tablets

Briefly, 20 tablets were crushed using a mortar and pestle and an aliquot of powder equivalent to the mass of one tablet transferred quantitatively to a 100 mL A-grade volumetric flask. Approximately

50 mL ACN was then added to the volumetric flask and the mixture sonicated using a bath sonicator (Ultrasonic Manufacturing Company (Pty), Ltd., Kenware, Krugersdorp, South Africa) with regular shaking at 20 min intervals for 1 h. The solution was allowed to cool to room temperature (22 °C) prior to making up to volume with ACN. A 5 mL aliquot of the resultant mixture was filtered through a 0.45 µm Millipore® Millex-HV Hydrophilic PVDF filter membrane (Millipore® Co., Bedford, MA, USA) and a 25 µg/mL sample solution in ACN was analyzed using the validated HPLC method.

2.7.2. Assay of Commercial Suspensions

The granules for suspension were reconstituted using HPLC-grade water as per the label instructions. A 5 mL aliquot of the reconstituted suspension was transferred to a 100 mL A-grade volumetric flask. Approximately 20 mL 50 mM phosphate buffer (pH 7.00) was then added to the volumetric flask and the mixture sonicated using a bath sonicator (Ultrasonic Manufacturing Company (Pty), Ltd., Kenware, Krugersdorp, South Africa) with regular shaking at 10 min intervals for 30 min. Approximately 30 mL MeOH was added to the flask and the mixture was sonicated for a further 30 min. The solution was allowed to cool to room temperature (22 °C) prior to making up to volume with MeOH. The mixture was then stirred for one hour using a digital hot plate stirrer (Lasec®, Port Elizabeth, South Africa). A 5 mL aliquot of the resultant mixture was filtered through a 0.45 µm Millipore® Millex-HV Hydrophilic PVDF filter membrane (Millipore® Co., Bedford, MA, USA) and analyzed using the validated HPLC method after dilution to obtain a 25 µg/mL solution in ACN.

2.8. Forced Degradation Studies

Stress studies were conducted by exposing CLA to acidic, alkaline, hydrogen peroxide and light conditions [39]. Stock solutions (100 µg/mL) were prepared as described in Section 2.3. These solutions were then exposed to different stress conditions viz., 0.1 M HCL, 0.1 M NaOH, 4% H_2O_2 at 80 °C and 500 W/m^2 for 12 h, prior to analysis using the validated analytical method. A tolerance level of 10% degradation is considered optimal for the purposes of validating the analytical method intended for assay [39]. Consequently, a tolerance of 10% was used to determine if CLA had degraded as a result of exposure to stress conditions. These studies were also performed to determine interference, if any, of degradation products with the chromatography.

3. Results and Discussion

3.1. Method Development and Optimization

3.1.1. Method Development

During the development of the analytical method, a Phenomenex® C_{18} 5 µm Luna column, (150 mm × 2 mm, i.d) and a Beckman®Ultrashere C_8 4 µm (150 mm × 4.0 i.d.) column were tested. The Beckman® column produced a better peak shape than the Phenomenex® column. Decreasing the particle size while keeping the column length constant, increases column efficiency and peak resolution [40]. Although C_{18} and C_8 columns have similar selectivity, C_8 columns are much less likely to retain compounds due to shorter alkyl chains, resulting in improved peak shape [40], as observed with the Beckman® column. The Beckman® column was selected as the column of choice for use in the analysis of CLA.

Hydrodynamic voltammetric (HDV) studies were undertaken to identify the optimum working electrode potential for the analysis of CLA. The HDV of CLA and ERY generated in direct current (DC) mode at potential settings ranging between +900 mV and +1300 mV at a scan background current of 100 nA is depicted in Figure 2.

These data reveal that a limiting current plateau occurred at a potential of +1200 mV for both CLA and ERY. The response of both macrolides was sigmoidal and can be explained mathematically as a logistic function voltammogram [41]. The background current that exhibited the best signal to noise

compromise was 100 nA and was selected for use. In addition, preliminary screening chromatographic experiments were performed to identify factors for optimization. Inclusion of methanol (MeOH) in the mobile phase improved chromatographic behavior and influenced the detector signal positively. However, MeOH increased the retention time significantly due to a low solvent strength based on the Hildebrand's elution strength scale for reversed-phase liquid chromatography [40]. Consequently, MeOH content was maintained at 2% *v/v* of the organic phase composition during optimization studies. An increase in column temperature resulted in a prolonged retention time and an increase in baseline noise, possibly due to an increase in the oxidation of mobile phase impurities at the higher temperatures. However, the drift in baseline was reduced at temperatures above ambient (22 °C) conditions. Consequently, a temperature of 30 °C was selected as a compromise and used during optimization studies. Buffer pH was maintained at 7.00 since ERY is stable between pH 7.00 and 8.00 [19,42,43] and the life of silica-based stationary phases is significantly reduced under alkaline conditions [44].

Sci. Pharm. **2019**, *87*, x FOR PEER REVIEW 7 of 20

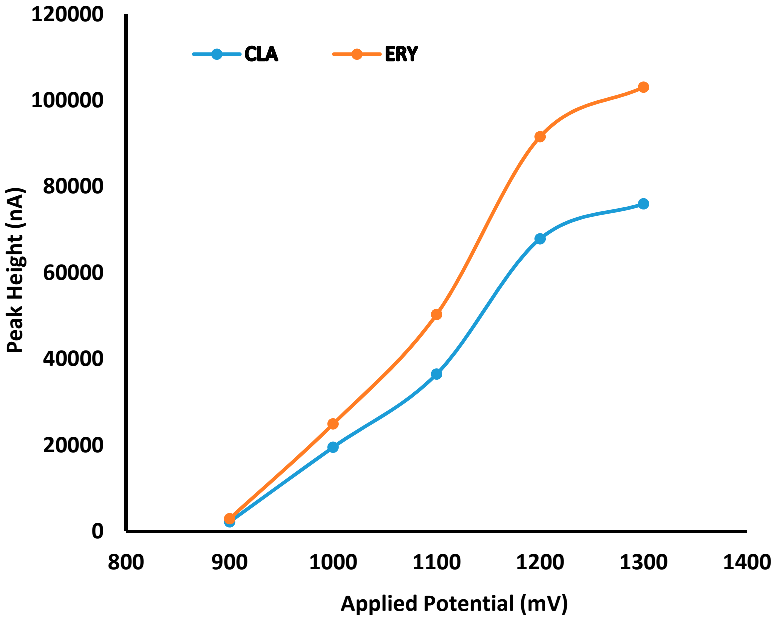

Figure 2. Hydrodynamic voltammogram (HDV) for CLA and erythromycin (ERY) generated in direct current (DC) mode at a sensitivity of 100 nA.

Figure 2. Hydrodynamic voltammogram (HDV) for CLA and erythromycin (ERY) generated in direct current (DC) mode at a sensitivity of 100 nA.

3.1.2. Method Optimization

All experiments undertaken during optimization studies were performed in randomized order to minimize bias of uncontrolled factors. A computer-generated rotatable CCD design consisting of 13 experiments with 5 center points and 8 axial points was generated using Design Expert® version 8.0.2 statistical software (Stat-Ease Inc., Minneapolis, MN, USA). The experimental levels investigated and responses monitored are listed in Table 1. The minimum and maximum values for buffer molarity ($X1$) were 10 mM and 50 mM, with the lower and upper axial levels of 1.72 mM and 58.28 mM. Similarly, ACN concentration ($X2$) was kept at minimum and maximum levels of 40% *v/v* and 50% *v/v* with respect to mobile phase composition, with the lower and upper axial levels of 37.9% *v/v* and 52.1% *v/v*, respectively. The independent input variables and ranges were selected on the basis of preliminary studies, and the retention time ($Y1$) of the last peak eluted, peak asymmetry ($Y2$) and peak resolution ($Y3$) were the responses monitored. The data generated from the responses were analysed using Design Expert® version 8.0.2 statistical software (Stat-Ease Inc., Minneapolis, MN, USA). Fisher's test for Analysis of Variance (ANOVA) was used to establish the significance of any difference(s) between the factors investigated. The overall design summary consisted of three quadratic mathematical variables was undertaken to identify the best combination of factors that would yield the desired responses.

Table 1. Variables and experimental design values.

Variable	Level

models for two independent factors. Optimization of significant model variables was undertaken to identify the best combination of factors that would yield the desired responses.

Table 1. Variables and experimental design values.

Variable	Level				
Input	$-\alpha$	−1	1	$+\alpha$	
Mobile phase mM (X_1)	1.72	10	50	58.28	
ACN content % *v/v* (X_2)	37.9	40	50	52.1	
Output	**Constraints**				
Retention time	$Y_1 \leq 10$ min				
Peak asymmetry	Y_2 = minimize				
Peak resolution	Y_3 = maximize				

Sci. Pharm. 2019, *87*, x FOR PEER REVIEW 8 of 20

Input	$-\alpha$	−1	1	$+\alpha$
Mobile phase mM (X_1)	1.72	10	50	58.28
ACN content % *v/v* (X_2)	37.9	40	50	52.1
Output	**Constraints**			
Retention time	$Y_1 \leq 10$ min			
Peak asymmetry	Y_2 = minimize			
Peak resolution	Y_3 = maximize			

Retention Time

3.1.2.1. Retention Time

The retention time (Y_1) is the most critical response as it has an effect on the length of the analytical run and cost of using a method. ACN concentration and buffer molarity were found to be the statistically significant factors that affected retention time. The influence of ACN concentration and buffer molarity on retention time is depicted in Figure 3.

The retention time (Y_1) is the most critical response as it has an effect on the length of the analytical run and cost of using a method. ACN concentration and buffer molarity were found to be the statistically significant factors that affected retention time. The influence of ACN concentration and buffer molarity on retention time is depicted in Figure 3.

These data reveal that a decrease in retention time of CLA occurs when the ACN content is increased from 40–50% *v/v* and the buffer molarity is increased form 10–50 mM. ACN is a strong solvent according to Hilderbrand's elution strength scale, thereby reducing mobile phase polarity when ACN concentrations are increased [40], leading to preferential partitioning of CLA into the mobile phase resulting in rapid elution and shorter retention times. The decrease in retention time observed with increased buffer molarity can be attributed to increased competition of buffer cations for active silanol sites on the stationary phase, leading to preferential partitioning of CLA into the mobile phase [41].

These data reveal that a decrease in retention time of CLA occurs when the ACN content is increased from 40–50% *v/v* and the buffer molarity is increased form 10–50 mM. ACN is a strong solvent according to Hilderbrand's elution strength scale, thereby reducing mobile phase polarity when ACN concentrations are increased [40], leading to preferential partitioning of CLA into the mobile phase resulting in rapid elution and shorter retention times. The decrease in retention time observed with increased buffer molarity can be attributed to increased competition of buffer cations for active silanol sites on the stationary phase, leading to preferential partitioning of CLA into the mobile phase [41].

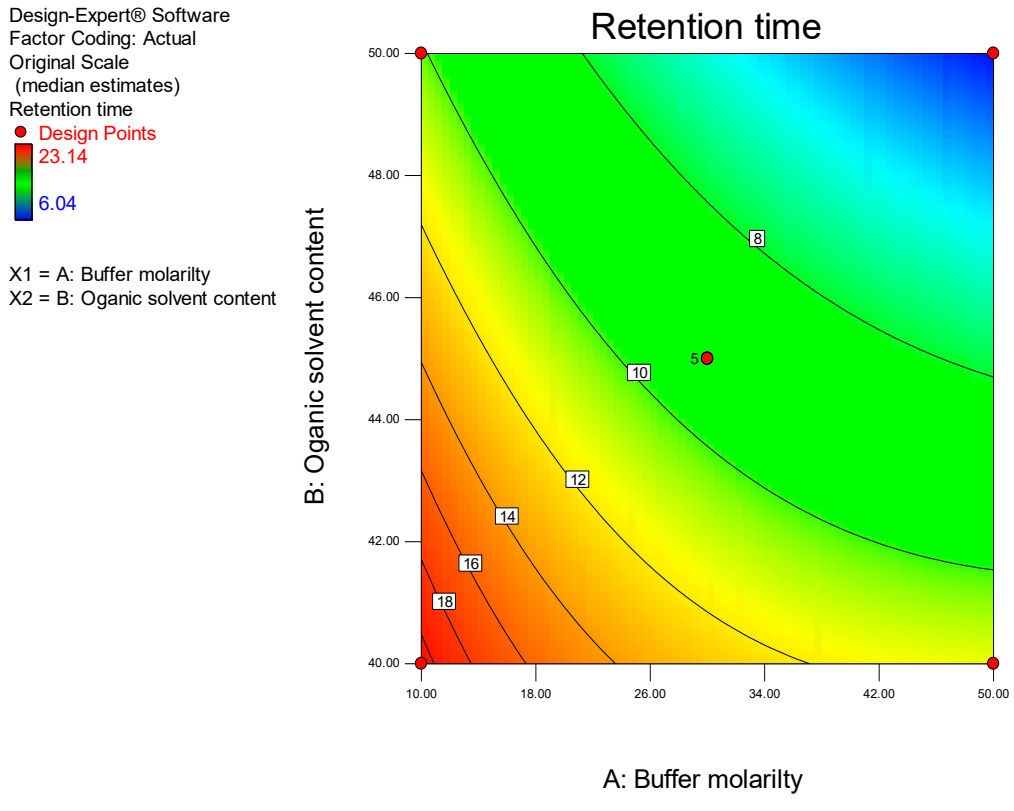

Figure 3. Contour plot depicting the impact of ACN content and buffer molarity on retention time.

Figure 3. Contour plot depicting the impact of ACN content and buffer molarity on retention time.

Examination of the model Box-Cox plot (Figure 4) inferred the need to transform the model. The plot reveals that the blue line fell outside the 95% confidence interval, indicating that the model was

Sci. Pharm. **2019**, *87*, x FOR PEER REVIEW 9 of 20

Examination of the model Box-Cox plot (Figure 4) inferred the need to transform the model. The plot reveals that the blue line fell outside the 95% confidence interval, indicating that the model was not located in the optimum region of the parabola. Consequently, a power transformation of the model was undertaken using model reduction by backward elimination in order to improve the fit of the data to the model, thereby permitting navigation of the design space [45].

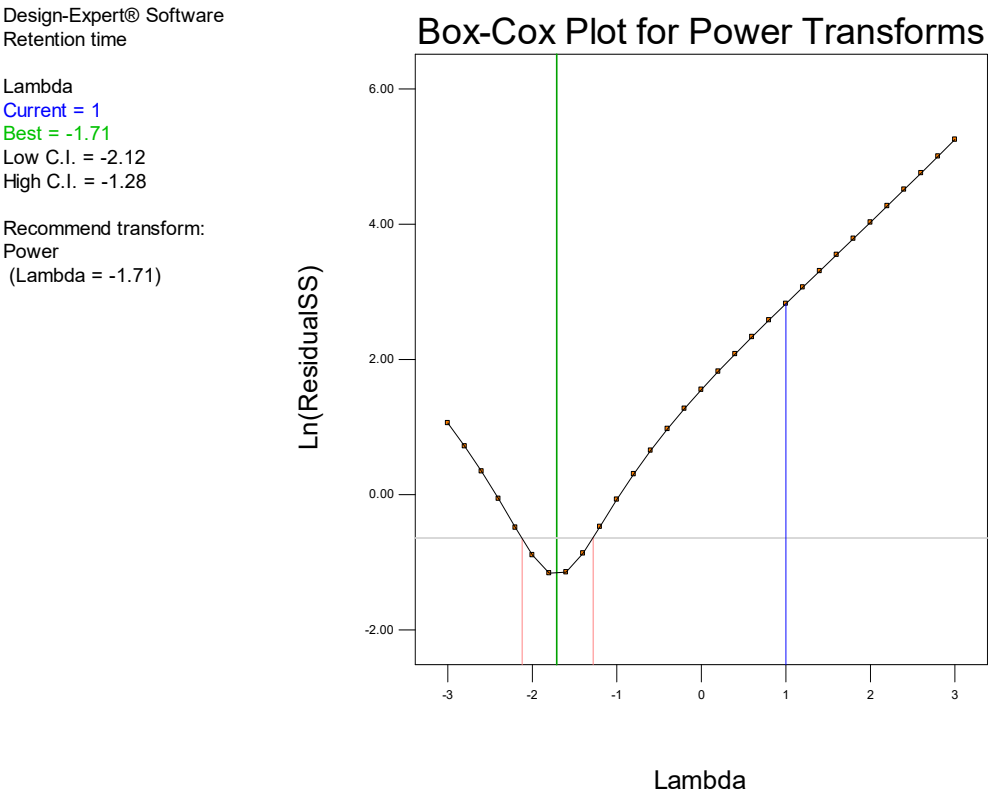

Figure 4. Box-Cox plot for power transformation for retention time prior to transformation.

Figure 4. Box-Cox plot for power transformation for retention time prior to transformation.

The Box-Cox plot (Figure 5) generated following power transformation of the data using backward elimination reveals the blue line falls within the confidence interval, confirming that the data fell in the optimum region of the parabola and indicates model adequacy.

ANOVA was used to evaluate the quadratic model for retention time and Fisher's F-ratio was calculated to identify significant terms in the model, with the error term set at $p = 0.05$. Values of Prob > F < 0.0500 indicate model terms that are significant; however, values > 0.1000 indicate that the model terms are not significant. The overall contribution of model factors to retention time were statistically significant, as summarized in Table 2.

The Model F-value of 902.59 implies the model is significant and there is only a 0.01% chance that a Model F-Value this large could occur due to noise. The Pred R-Squared of 0.9892 is in reasonable agreement with the Adj R-Squared of 0.9973. Adeq Precision measures the signal to noise ratio. A ratio > 4 is desirable and the ratio of 96.322 indicates an adequate signal. This model can thus be used to navigate the design space and, therefore, the method developed was able to be applied to predict the retention time of CLA within the limits of the identified design space. The equation for Y_1 (retention time) is reported in Equation (2).

$$Y_1^{-1.71} = +0.023 + 9.208E-003A + 0.011B + 4.248E-003AB - 2.301E-003A^2 + 1.276E-003B^2 \quad (2)$$

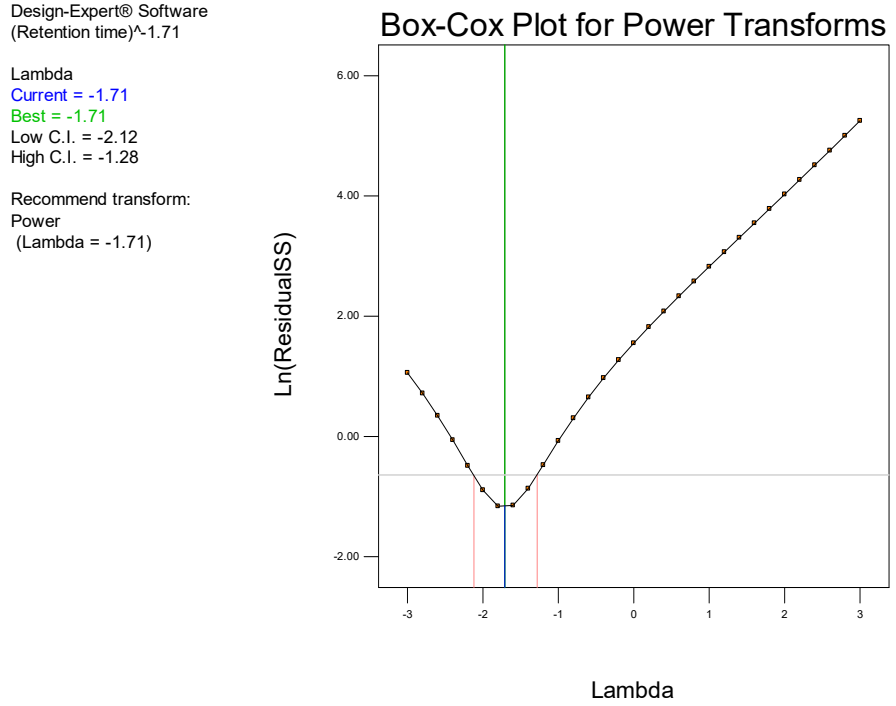

Figure 5. Box–Cox plot for power transformation for retention time following transformation.

Table 2. ANOVA table for response surface quadratic model for retention time.

Source	Sum of Squares	df	Mean Square	F Value	p-Value Prob>F	
Model	1.78×10^{-3}	5	3.56×10^{-4}	902.59	< 0.0001	significant
A-Buffer molarilty	6.78×10^{-4}	1	6.78×10^{-4}	1719.85	< 0.0001	
B-Oganic solvent content	9.75×10^{-4}	1	9.75×10^{-4}	2472.06	< 0.0001	
AB	7.22×10^{-5}	1	7.22×10^{-5}	183.05	< 0.0001	
A^2	3.68×10^{-5}	1	3.68×10^{-5}	93.42	< 0.0001	
B^2	1.13×10^{-5}	1	1.13×10^{-5}	28.74	0.0011	
Residual	2.76×10^{-6}	7	3.94×10^{-7}			
Lack of Fit	2.70×10^{-6}	3	9.00×10^{-7}	57.93	0.0009	significant
Pure Error	6.21×10^{-8}	4	1.55×10^{-8}			
Cor Total	1.78×10^{-3}	12				
Std. Dev.	6.28×10^{-4}					
Mean	0.022					
C.V. %	2.86					
PRESS	1.93×10^{-5}					
R-Squared	0.9985					
Adj R-Squared	0.9973					
Pred R-Squared	0.9892					
Adeq Precision	96.322					

The Model F-value of 902.59 implies the model is significant and there is only a 0.01% chance that a Model F-Value this large could occur due to noise. The Pred R-Squared of 0.9892 is in reasonable agreement with the Adj R-Squared of 0.9973. Adeq Precision measures the signal to noise ratio. A ratio > 4 is desirable and the ratio of 96.322 indicates an adequate signal. This model can thus be used to navigate the design space and, therefore, the method developed was able to be applied to predict the retention time of CLA within the limits of the identified design space. The equation for Y_1 (retention time) is reported in Equation 2.

Peak Symmetry

The asymmetry factor was used to evaluate the response, peak symmetry (Y_2). Excellent chromatographic columns have been reported to produce asymmetry factor values between 0.95 and 1.1 [46]. Due to the molecular mass and the basic nature of CLA, interaction with silica-based

$$Y_1^{-1.71} = +0.023 + 9.208E-003A + 0.011B + 4.248E-003AB - 2.301E-003A^2 + 1.276E-003B^2 \quad (2)$$

3.1.2. Peak Symmetry

The asymmetry factor was used to evaluate the response, peak symmetry (Y_2). Excellent chromatographic columns have been reported to produce asymmetry factor values between 0.95 and 1.1 [46]. Due to the molecular mass and the basic nature of CLA, interaction with silica-based reversed-phase columns results in marked tailing of the peaks, due to interaction with residual silanols of the stationary phase [47], resulting in poor peak symmetry.

ANOVA analysis reveals that the model for peak symmetry was significant (p = 0.0149). The significant model term established was ACN content (p = 0.0011). The influence of ACN concentration on CLA peak symmetry is depicted in Figure 6.

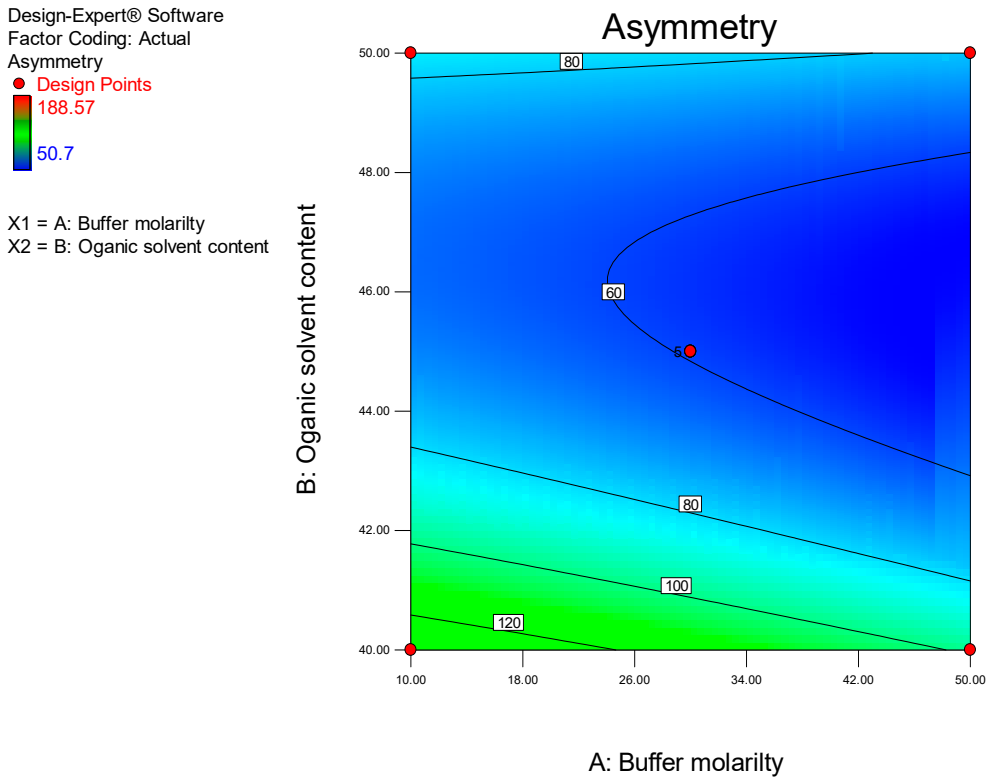

Figure 6. Contour plot depicting the impact of ACN content and buffer molarity on peak asymmetry.

The best peak shape with minimal tailing can be obtained at an ACN concentration of approximately 46% *v/v*. Due to peak tailing, the experimental run time was increased to 20 min to permit the chromatograms to return to baseline. The equation for peak symmetry (Y_2) is reported in Equation 3.

$$1/Sqrt(Asymmetry) = +0.13 - 5.545E-003A - 8.462E-003B + 3.692E-003AB - 0.073A^2 - 0.073B^2 \quad (3)$$

Peak Resolution

The goal of the HPLC analysis was to separate CLA from all other components present. Resolution is a measure of the degree of separation of two adjacent analytes [40]. Ideally, most HPLC methods should achieve a baseline separation between 1.5 and 2.0 for all analytes of interest [48].

ANOVA analysis reveals that the model for peak resolution was significant (p < 0.0001). The significant model terms were buffer molarity and ACN content with p values of 0.0028 and <0.0001, respectively. The two-dimensional contour plot of the influence of the two factors on peak resolution is depicted in Figure 7.

ACN content and buffer molarity can be manipulated to improve peak resolution. The contour plot suggests that increased peak resolution will be obtained when a buffer molarity of 50 mM and ACN content of approximately 40% *v/v* is used. The equation for peak resolution (Y_3) is reported in Equation (4).

3.1.2.3. Peak Resolution

The goal of the HPLC analysis was to separate CLA from all other components present. Resolution is a measure of the degree of separation of two adjacent analytes [40]. Ideally, most HPLC methods should achieve a baseline separation between 1.5 and 2.0 for all analytes of interest [48].

ANOVA analysis reveals that the model for peak resolution was significant ($p < 0.0001$). The significant model terms were buffer molarity and ACN content with p values of 0.0028 and <0.0001, respectively. The two-dimensional contour plot of the influence of the two factors on peak resolution is depicted in Figure 7.

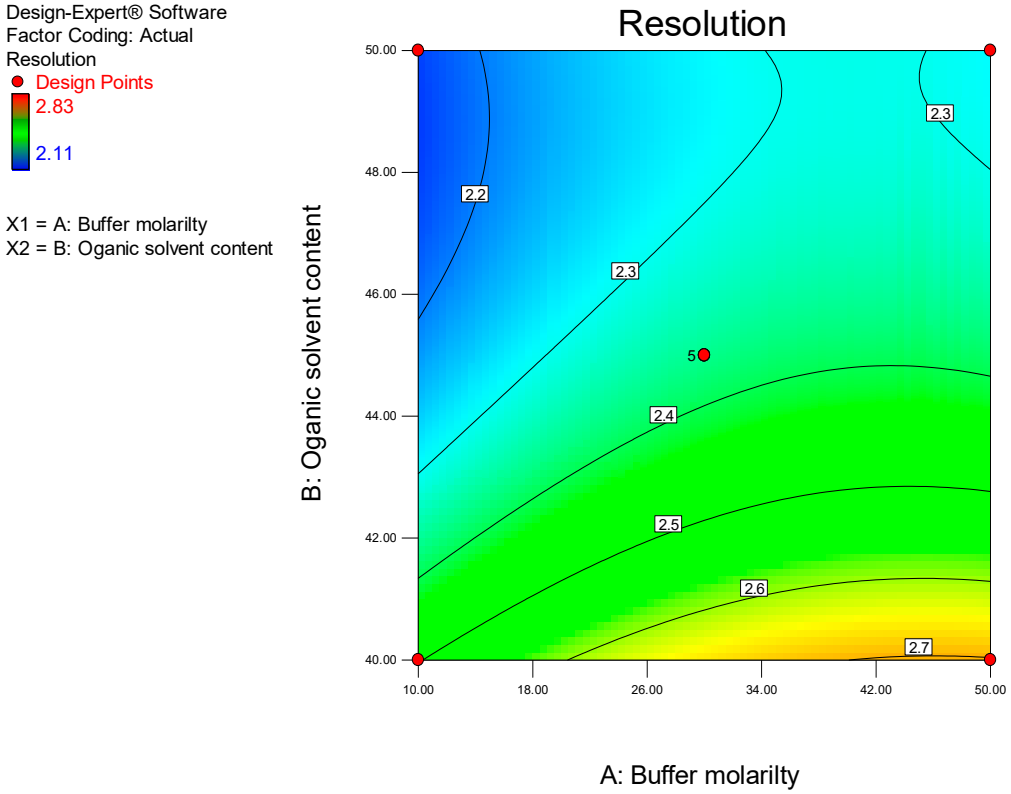

Figure 7. Contour plot depicting the impact of ACN content and buffer molarity on peak resolution.

ACN content and buffer molarity can be manipulated to improve peak resolution. The contour plot suggests that increased peak resolution will be obtained when a buffer molarity of 50 mM and ACN content of approximately 40% *v/v* is used. The equation for peak resolution (Y_3) is reported in Equation 4.

$$\text{Resolution} = +2.37 + 0.083A - 0.19B - 0.020AB - 0.064A^2 + 0.11B^2 \quad (4)$$

3.1.3. Optimized Chromatographic Conditions

The overall solutions for chromatographic analysis of CLA and ERY were identified by optimization of the quadratic models using Design Expert statistical software Version 8.0.2 Design Expert® statistical software (Stat-Ease Inc., Minneapolis, MN, USA). A series of compromises is required when evaluating outputs from Design Expert®. For example, for a retention time of ≤ 10 min, minimum peak asymmetry and maximum resolution between CLA and ERYthe impact of MeOH was largely avoided, by maintaining the content at 2.0% *v/v* and therefore ensured the benefits of using this solvent were achieved. Elegant multi-criteria statistical solutions are possible; however, they may be considered if required when this pragmatic approach to optimization is not adequate. Solutions to quadratic models have been generated by matrix calculation using Cramer's rule, Eigenvalues and Eigenfunctions, for the optimized conditions of chromatography for captopril [41] but were not considered necessary for this separation. The optimized conditions for the overall separation are summarized in Table 3.

Table 3. Optimized chromatographic conditions for the overall separation of CLA and ERY.

Parameter	Results
Buffer molarity	50 mM
Organic phase content	41.5% *v/v*
Flow rate	1.00 mL/min
Column temperature	30 °C
Mode	Isocratic
Detection voltage	+1200 mV
Injection volume	10 µL

The optimized chromatographic separation was applied to the quantitative analysis of CLA and the final separation produced well resolved peaks for CLA and ERY (Figure 8). The % prediction error for retention time of CLA using the optimized conditions in relation to the predicted retention time was −6.19%. The % prediction errors for resolution and asymmetry were −2.38% and −10.13%, respectively. The low values for the calculated percentage prediction errors indicate the robustness of the mathematical models used. In addition, the high predictive ability of DoE is also demonstrated, suggesting the efficiency of DoE, for process optimization [49].

Prior to validation of the analytical method, an attempt was made to improve peak shape and detector sensitivity by investigating the effect of the amount of MeOH as a component of the mobile phase.

Effect of Methanol

The inclusion of MeOH in the mobile phase was found to have a positive effect on peak and chromatographic responses during method development. MeOH inclusion in the mobile phase was investigated over a 2 to 10% *v/v* range. Well resolved chromatographic responses were achieved for all concentrations of MeOH investigated. The average peak height ratios of CLA and ERY over the concentration range investigated are summarized in Table 4.

Table 4. Chromatographic response of CLA and ERY with changes in mobile phase content (n = 3).

MeOH % *v/v*	PHR (CLA/ERY)	%RSD	Run Time (min)
2	0.1272 ± 0.0034	2.698	15
5	0.1424 ± 0.0023	1.627	20
10	0.1605 ± 0.0025	1.533	30

The increase in MeOH content in the mobile phase resulted in an increase in the retention time of CLA and ERY. The % RSD of the peak response decreases with an increase in MeOH content. Consequently, 5% *v/v* MeOH was used in the mobile phase for all validation studies as the run time of 20 min was deemed suitable for this analysis.

3.2. Method Validation

3.2.1. Linearity and Range

The calibration curve was found to be linear with a R^2 of 0.9997, a slope of 0.0233 and a y-intercept of 0.0439, yielding a regression equation of y = 0.0233 + 0.0439. Correlation coefficients of >0.990 are generally considered as evidence of acceptable linearity fora regression line [37]. Consequently, the HPLC-ECD method was linear over the concentration range of CLA investigated.

3.2.2. Precision

The precision data are summarized in Table 5. These data reveal that in all cases, the % RSD values were < 2%, indicating that the method is precise and can be used as intended.

Table 5. Intra-and inter-day precision data for CLA analysis.

Intra-day Precision % RSD (n = 10)	1.2363
	Inter-day precision % RSD range (n = 5)
Day 1	1.1409–1.9528
Day 2	0.2915–1.2201
Day 3	0.6229–1.1288

3.2.3. Accuracy

The data for accuracy are listed in Table 6 and % RSD values for all analyses were < 2%, indicating that the HPLC-ECD analytical method is accurate and suitable for its intended purpose.

Table 6. Accuracy results for blinded CLA samples (n = 5).

Theoretical Concentration µg/mL	Actual Concentration µg/mL	% RSD	% Bias
6.00	6.11	1.63	+1.82
25.00	25.49	0.91	+1.94
45.00	45.20	1.22	+1.22

3.2.4. LOQ and LOD

The LOQ was 0.05 µg/mL with an associated % RSD of 4.27% and by convention, the LOD was 0.02 µg/mL.

3.3. Re-Validation and Method Scaling

Method re-validation following the column change was deemed successful. In addition, scaling of the method across analytical columns of different L-designation met all USP system suitability requirements for resolution, tailing factor and % RSD for this HPLC-ECD method, confirming the potential applicability of method scaling using a different stationary phase in a different class as an efficient tool for this method resulting in a shorter run time, decreased solvent consumption and reduced cost. The data generated from these studies are listed in Tables 7 and 8.

Table 7. Summary of re-validation results for HPLC method for CLA analysis.

Parameter	CLA		
Linearity			
R^2	0.9999		
Equation	Y = 0.0315x + 0.0176		
Intra-day precision % RSD (n = 10)	1.7028		
Inter-day precision % RSD range (n = 5)			
Day 1	1.0645–1.5675		
Day 2	1.1904–1.7166		
Day 3	0.9385–1.7849		
Accuracy (n = 5)			
Theoretical concentration µg/mL	7.60	21.00	44.00
% Recovery ± % RSD	7.50 ± 3.71	20.67 ± 1.02	44.07 ± 1.42
%Bias	−1.30	−1.58	+0.15
LOQ µg/mL (n = 5)	1.5		
LOD µg/mL	0.5		

Table 8. USP scaling assay results for CLA.

	Resolution	CLA Tailing	CLA/ERY PHR	CLA Retention Time
Average	1.509 ± 0.015	4.083 ± 0.039		
%RSD			1.145	0.187
Limits	NMT 2.0	NLT 1.5	%RSD NMT 2%	%RSD NMT 2%

Sci. Pharm. **2019**, *87*, 31 15 of 20

%RSD			1.145	0.187
Limits	NMT 2.0	NLT 1.5	%RSD NMT 2%	%RSD NMT 2%

Chromatographic responses before and after method re-validation and scaling are depicted in Figure 8. The scaled method revealed an improvement in peak asymmetry, producing sharp peaks with reduced tailing in a shorter analytical run time in comparison to the method developed using the Beckman® column. Columns in which CN functional groups are used are more polar than C_8 based phases and exhibit shorter retention times and exhibit different selectivity than C_8 columns [40]. Consequently, the repulsion of the ionized CLA moiety at pH 7.00 when using the CN column, led to reduced peak tailing and shorter analytical run times.

Chromatographic responses before and after method re-validation and scaling are depicted in Figure 8. The scaled method revealed an improvement in peak asymmetry, producing sharp peaks with reduced tailing in a shorter analytical run time in comparison to the method developed using the Beckman® column. Columns in which CN functional groups are used are more polar than C_8 based phases and exhibit shorter retention times and exhibit different selectivity than C_8 columns [40]. Consequently, the repulsion of the ionized CLA moiety at pH 7.00 when using the CN column, led to reduced peak tailing and shorter analytical run times.

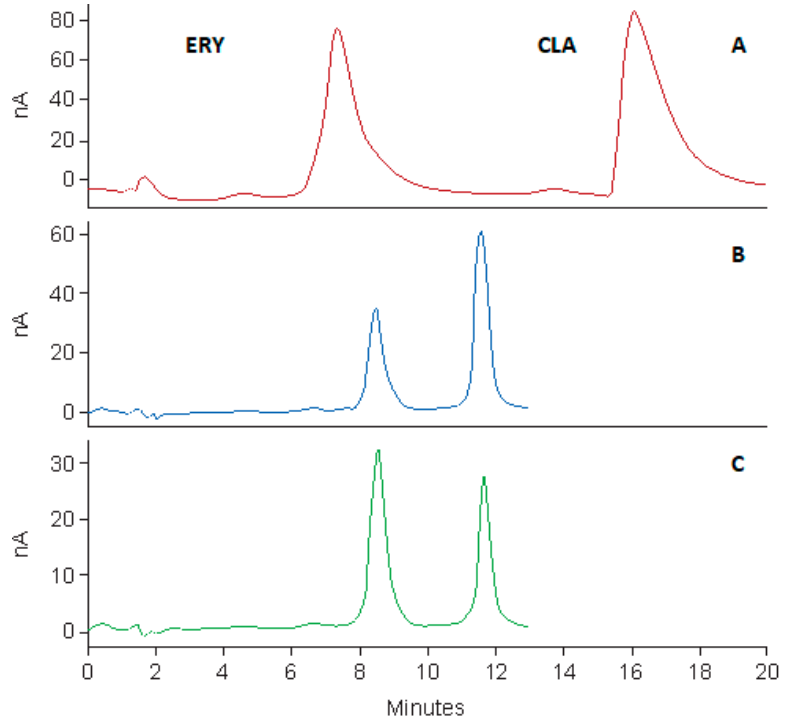

Figure 8. Typical chromatograms depicting the separation of CLA and ERY before method scaling (CLA 45 µg/mL, ERY 50 µg/mL) (**A**), after method scaling (CLA 50 µg/mL, ERY 50 µg/mL) (**B**) and for assay of Klarizon 250 mg tablets (**C**).

Figure 8. Typical chromatograms depicting the separation of CLA and ERY before method scaling (CLA 45 µg/mL, ERY 50 µg/mL) (**A**), after method scaling (CLA 50 µg/mL, ERY 50 µg/mL) (**B**) and for assay of Klarizon 250 mg tablets (**C**).

3.4. Forced Degradation Studies

3.4. Forced Degradation Studies

The results of forced degradation studies can be used to establish specificity and stability indicating characteristics of the HPLC-ECD method. Data from these studies are summarized in Table 9 and the resultant chromatograms are depicted in Figure 9.

The results of forced degradation studies can be used to establish specificity and stability indicating characteristics of the HPLC-ECD method. Data from these studies are summarized in Table 9 and the resultant chromatograms are depicted in Figure 9.

Table 9. Forced degradation data for CLA following exposure to stress conditions for 12 h.

Table 9. Forced degradation data for CLA following exposure to stress conditions for 12 h.

Stress Condition	% Recovered	Remarks
Control in ACN	100	-
Thermal at 80 °C	105.48	No degradation
UV exposure at 500 W/m^2	92.33	No degradation
Acid hydrolysis using 0.1 M HCL	94.85	No Degradation
Alkaline hydrolysis using 0.1 M NaOH	54.81	Degradation
Oxidation using 4% *v/v* H_2O_2	0.00	Degradation

Stress Condition	% Recovered	Remarks
Control in ACN	100	-
Thermal at 80 °C	105.48	No degradation
UV exposure at 500 W/m^2	92.33	No degradation
Acid hydrolysis using 0.1 M HCL	94.85	No Degradation
Alkaline hydrolysis using 0.1 M NaOH	54.81	Degradation
Oxidation using 4% *v/v* H_2O_2	0.00	Degradation

Sci. Pharm. **2019**, *87*, x FOR PEER REVIEW 16 of 20

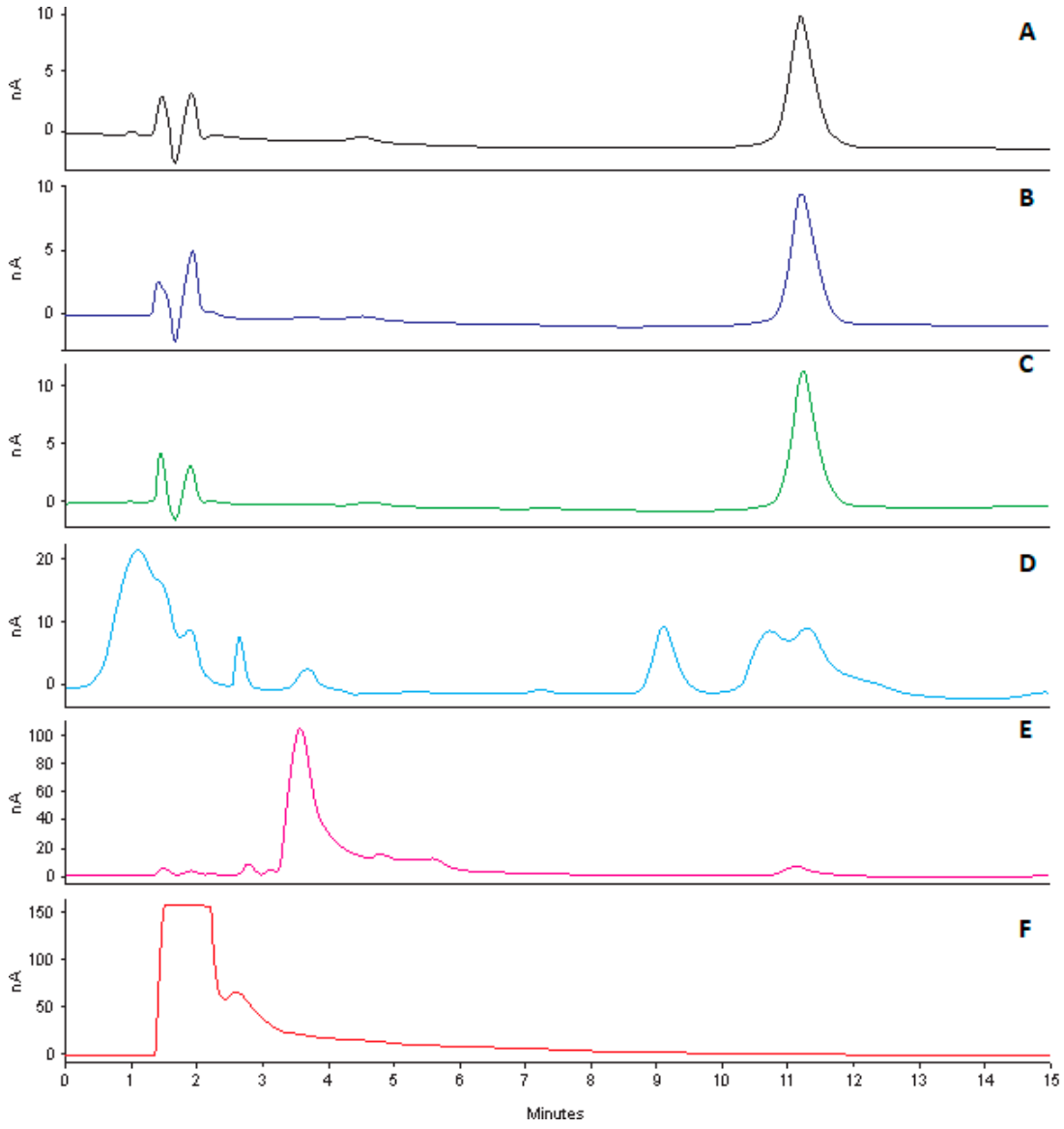

Figure 9. Typical chromatograms following degradation of CLA (10 µg/mL) following exposure to ACN (**A**), heat at 80 °C (**B**), 500 W/m² UV radiation (**C**), 0.1 M HCl (**D**), 0.1 M NaOH (**E**) and 4% *v/v* H_2O_2 (**F**).

The data reveal that CLA undergoes extensive degradation when exposed to oxidative stress conditions. Oxidation of CLA has been reported to occur via reactivity of the tertiary amino group [9]. Consequently, the reaction with hydrogen peroxide is thought to oxidise CLA, resulting in products that cannot oxidise during analysis. Exposure of CLA to acidic conditions (pH 1.2) resulted in approximately 5% degradation, which could be attributed to hydrolysis of cladinose [50], confirming previously published data which reported 90.2% and 41.1% loss of CLA from aqueous samples exposed in solution to pH 1.0 and pH 2.0 for four hours [51]. However, one of the degradants interferes with the chromatogram following acid hydrolysis and can be seen in Figure 9D, thus failing to infer specificity of the method for these conditions. Nevertheless, the extreme conditions used for these studies are unlikely to be used in any of the manufacturing or analytical procedures, therefore this outcome is of little concern as the study was conducted at a temperature well in excess of the normal conditions used for analyses. Exposure to alkaline conditions led to significant degradation of CLA that may be attributed to the presence of ester functional groups that are susceptible to hydrolysis in alkaline conditions. Acid and base hydrolysis does not result in the total loss of the oxidizing potential of CLA, implying the molecule may be detected and separated in the presence of

implying the molecule may be detected and separated in the presence of degradation products but with some interference observed in acid hydrolysis. CLA was stable with < 10% degradation observed following exposure to heat and UV radiation for 12 h.

3.5. Assay

The specificity of the method to resolve peak(s) of interest from any possible excipients or contaminants that may be present in a dosage form was established by quantitation of CLA in commercially available tablets and suspensions. All tablet and suspension samples complied with USP assay specifications. The USP assay limits for clarithromycin tablets of 90.0%–110.0% [52] and suspensions 90.0%–115.0% [53] were used as the acceptance criteria. The assay results are listed in Table 10. The analysis of CLA dosage forms resulted in clear, sharp, well-resolved peaks without interference from any excipients used for manufacture (Figure 8).

Table 10. Analysis of commercially available CLA formulations (n = 5).

Product and Label Claim	Dose mg	% Recovery	% RSD
Clarihexal®500 XL	500 mg	99.69	1.57
Klarithran®MR 500	500 mg	99.09	0.61
Klarithran® 500	500 mg	103.94	1.80
Klarizon 250	250 mg	98.81	2.40
ClariHexal 250 mg/5 mL	250 mg	110.04	2.23
Klarithran®250mg/5 mL	250 mg	106.94	1.75

4. Conclusions

A simple, selective and sensitive high-performance liquid chromatographic method with electrochemical detection for the quantitation of clarithromycin in bulk samples and oral dosage forms has been developed. The method complies with ICH validation parameters. In addition, an attempted investigation into the applicability of USP method scaling across different L-designation proved feasible. Method scaling allows for translation of an analytical method while achieving an equivalent separation without the need for re-validation. In this study, a revalidation was undertaken and confirmed the applicability of method scaling across analytical columns of different L-designation, to the HPLC-ECD analytical determination of CLA. This, in turn, saves costs and is environmentally sustainable as less solvent is used and reduced analytical run times can be achieved. The scaled method resulted in an increase in throughput with shorter run times that resulted in less solvent consumption in the laboratory. HPLC methods can thus be scaled on condition that they meet USP system suitability requirements, maintaining separation quality, thereby eliminating the need for method re-validation. Although USP method scaling is only permitted for columns within the same L-designation, its applicability should be investigated across analytical columns of different L-designation to further streamline regulatory requirements. This is, to the best of our knowledge, the first evaluation of an HPLC-ECD method using a modified scaling approach.

Author Contributions: P.A.M. and M.T.R.C. performed the experiments, analyzed the data and wrote the article. R.B.W. and S.M.M.K. contributed to the conceptualization, supervision, bibliographical research and proof reading of the manuscript.

Funding: The authors acknowledge funding support from the Rhodes University Research Committee.

Acknowledgments: The authors wish to acknowledge the Research Committee of Rhodes University (R.B.W.) for financial assistance.

Conflicts of Interest: The authors report no conflict of interest and the authors are responsible for the content and writing of this manuscript.

References

1. Kanfer, I.; Skinner, M.; Walker, R. Analysis of macrolide antibiotics. *J. Chromatogr. A* **1998**, *812*, 255–286. [CrossRef]
2. Li, W.; Jia, H.; Zhao, K. Determination of clarithromycin in rat plasma by HPLC–UV method with pre-column derivatization. *Talanta* **2007**, *71*, 385–390. [CrossRef] [PubMed]
3. Esfandi, E.; Ramezani, V.; Vatanara, A.; Najafabadi, A.R.; Pouya, S.; Moghaddam, H. Clarithromycin Dissolution Enhancement by Preparation of Aqueous Nanosuspensions Using Sonoprecipitation Technique. *Iran. J. Pharm. Res.* **2014**, *13*, 809–818. [PubMed]
4. Peters, D.H.; Clissold, S.P. Clarithromycin. A review of its antimicrobial activity, pharmacokinetic properties and therapeutic potential. *Drugs* **1992**, *44*, 117–164. [CrossRef]
5. Abuga, K.O.; Chepkwony, H.K.; Roets, E.; Hoogmartens, J. A stability-indicating HPLC method for the separation of clarithromycin and related substances in bulk samples. *J. Sep. Sci.* **2001**, *24*, 849–855. [CrossRef]
6. Bekele, L.K.; Gebeyehu, G.G. Application of Different Analytical Techniques and Microbiological Assays for the Analysis of Macrolide Antibiotics from Pharmaceutical Dosage Forms and Biological Matrices. *Anal. Chem.* **2012**, *2012*, 1–17. [CrossRef]
7. Bahrami, G.; Mohammadi, B. Determination of clarithromycin in human serum by high-performance liquid chromatography after pre-column derivatization with 9-fluorenylmethyl chloroformate: Application to a bioequivalence study. *J. Chromatogr. B* **2007**, *850*, 417–422. [CrossRef]
8. Sharma, M.; Gupta, N.; Gupta, S. Implications of designing clarithromycin loaded solid lipid nanoparticles on their pharmacokinetics, antibacterial activity and safety. *RSC Adv.* **2016**, *6*, 76621–76631. [CrossRef]
9. Huber, M.M.; Korhonen, S.; Ternes, T.A.; von Gunten, U. Oxidation of pharmaceuticals during water treatment with chlorine dioxide. *Water Res.* **2005**, *39*, 3607–3617. [CrossRef]
10. Taninaka, C.; Ohtani, H.; Hanada, E.; Kotaki, H.; Sato, H.; Iga, T. Determination of erythromycin, clarithromycin, roxithromycin, and azithromycin in plasma by high-performance liquid chromatography with amperometric detection. *J. Chromatogr. B Biomed. Sci. Appl.* **2000**, *738*, 405–411. [CrossRef]
11. Zaater, M.F.; Tahboub, Y.R.; Ghanem, E. Determination and stability assessment of clarithromycin in human plasma using RP-LC with electrochemical detection. *J. Chromatogr. Sci.* **2012**, *50*, 763–768. [CrossRef] [PubMed]
12. Lohitnavy, M.; Lohitnavy, O.; Sareekan, K.; Chaiyaput, W. Average bioequivalence study of clarithromycin tablets in healthy male volunteers. *J. Clin. Pharm. Ther.* **2003**, *28*, 187–190. [CrossRef] [PubMed]
13. Erah, P.O.; Barrett, D.A.; Shaw, P.N. Ion-pair high-performance liquid chromatographic assay method for the assessment of clarithromycin stability in aqueous solution and in gastric juice. *J. Chromatogr. B Biomed. Sci. Appl.* **1996**, *682*, 73–78. [CrossRef]
14. Lange, F.; Cornelissen, S.; Kubac, D.; Sein, M.M.; von Sonntag, J.; Hannich, C.B.; Golloch, A.; Heipieper, H.J.; Möder, M.; von Sonntag, C. Degradation of macrolide antibiotics by ozone: A mechanistic case study with clarithromycin. *Chemosphere* **2006**, *65*, 17–23. [CrossRef] [PubMed]
15. Sastre Toraño, J.; Guchelaar, H.-J. Quantitative determination of the macrolide antibiotics erythromycin, roxithromycin, azithromycin and clarithromycin in human serum by high-performance liquid chromatography using pre-column derivatization with 9-fluorenylmethyloxycarbonyl chloride and fluorescence detection. *J. Chromatogr. B Biomed. Sci. Appl.* **1998**, *720*, 89–97.
16. Chu, S.-Y.; Sennello, L.T.; Sonders, R.C. Simultaneous determination of clarithromycin and 14(R)-hydroxyclarithromycin in plasma and urine using high-performance liquid chromatography with electrochemical detection. *J. Chromatogr. B Biomed. Sci. Appl.* **1991**, *571*, 199–208. [CrossRef]
17. Hedenmo, M.; Eriksson, B.-M. Liquid chromatographic determination of the macrolide antibiotics roxithromycin and clarithromycin in plasma by automated solid-phase extraction and electrochemical detection. *J. Chromatogr. A* **1995**, *692*, 161–166. [CrossRef]
18. Choi, S.J.; Kim, S.B.; Lee, H.S.H.-Y.Y.; Na, D.H.; Yoon, Y.S.; Lee, S.S.; Kim, J.H.; Lee, K.C.; Lee, H.S.H.-Y.Y. Column-switching high-performance liquid chromatographic determination of clarithromycin in human plasma with electrochemical detection. *Talanta* **2001**, *54*, 377–382. [CrossRef]
19. Kees, F.; Spangler, S.; Wellenhofer, M. Determination of macrolides in biological matrices by high-performance liquid chromatography with electrochemical detection. *J. Chromatogr. A* **1998**, *812*, 287–293. [CrossRef]

20. Wibawa, J.I.; Shaw, P.; Barrett, D. Quantification of clarithromycin, its 14-hydroxy and decladinose metabolites in rat plasma, gastric juice and gastric tissue using high-performance liquid chromatography with electrochemical detection. *J. Chromatogr. B* **2003**, *783*, 359–366. [CrossRef]
21. Foroutan, S.M.; Zarghi, A.; Shafaati, A.; Madadian, B.; Abolfathi, F. Rapid high performance liquid chromatographic method for determination of clarithromycin in human plasma using amperometric detection: Application in pharmacokinetic and bioequivalence studies. *Iran. J. Pharm. Res.* **2013**, *12*, 65–69. [PubMed]
22. Leonard, S.; Ferraro, M.; Adams, E.; Hoogmartens, J.; Schepdael, A. Van Application of liquid chromatography/ion trap mass spectrometry to the characterization of the related substances of clarithromycin. *Rapid Commun. Mass Spectrom.* **2006**, *20*, 3101–3110. [CrossRef] [PubMed]
23. Calza, P.; Medana, C.; Padovano, E.; Giancotti, V.; Baiocchi, C. Identification of the unknown transformation products derived from clarithromycin and carbamazepine using liquid chromatography/high-resolution mass spectrometry. *Rapid Commun. Mass Spectrom.* **2012**, *26*, 1687–1704. [CrossRef] [PubMed]
24. Ogoko, E.C.; Odoemelam, S.A.; Ita, B.I.; Eddy, N.O. Adsorption and inhibitive properties of clarithromycin for the corrosion of Zn in 0.01 to 0.05 M H_2SO_4. *Port. Electrochim. Acta* **2009**, *27*, 713–724. [CrossRef]
25. Pappa-Louisi, A.; Papageorgiou, A.; Zitrou, A.; Sotiropoulos, S.; Georgarakis, E.; Zougrou, F. Study on the electrochemical detection of the macrolide antibiotics clarithromycin and roxithromycin in reversed-phase high-performance liquid chromatography. *J. Chromatogr. B Biomed. Sci. Appl.* **2001**, *755*, 57–64. [CrossRef]
26. Sahu, P.K.; Ramisetti, N.R.; Cecchi, T.; Swain, S.; Patro, C.S.; Panda, J. An overview of experimental designs in HPLC method development and validation. *J. Pharm. Biomed. Anal.* **2018**, *147*, 590–611. [CrossRef]
27. Vander Heyden, Y.; Nijhuis, A.; Smeyers-Verbeke, J.; Vandeginste, B.G.; Massart, D. Guidance for robustness/ruggedness tests in method validation. *J. Pharm. Biomed. Anal.* **2001**, *24*, 723–753. [CrossRef]
28. Elkhoudary, M.M.; Salam, R.A.A.; Hadad, G.M. Robustness Testing in HPLC Analysis of clarithromycin, norfloxacin, doxycycline, tinidazole and omeprazole in pharmaceutical dosage forms using experimental design. *Curr. Pharm. Anal.* **2014**, *10*, 58–70. [CrossRef]
29. Dejaegher, B.; Vander Heyden, Y. Experimental designs and their recent advances in set-up, data interpretation, and analytical applications. *J. Pharm. Biomed. Anal.* **2011**, *56*, 141–158. [CrossRef]
30. Lewis, G.A.; Mathieu, D.; Phan-Tan-Luu, R. (Eds.) *Pharmaceutical Experimental Design*, 1st ed.; CRC Press: Boca Raton, FL, USA, 1998.
31. Dejaegher, B.; Vander Heyden, Y. The use of experimental design in separation science. *Acta Chromatogr.* **2009**, *21*, 161–201. [CrossRef]
32. Massart, D.L.; Vandeginste, B.G.; Buydens, L.M.C.; Lewi, P.J.; Smeyers-Verbeke, J.; De Jong, S. *Handbook of Chemometrics and Qualimetrics*; Elsevier: New York, NY, USA, 1997.
33. Bansal, S.; DeStefano, A. Key elements of bioanalytical method validation for small molecules. *AAPS J.* **2007**, *9*, E109–E114. [CrossRef] [PubMed]
34. General Chapter <621> Chromatography. In *United States Pharmacopeia 40 National Formulary 35 (USP 40–NF 35)*; United States Pharmacopeial: Rockville, MD, USA, 2017; pp. 508–520.
35. ICH Q2 (R1) Harmonised Tripatite Guidline. Validation of Analytical Procedures, Texts and Methodology. Available online: https://www.ich.org/fileadmin/Public_Web_Site/ICH_Products/Guidelines/Quality/Q2_R1/Step4/Q2_R1__Guideline.pdf (accessed on 25 July 2019).
36. Shabir, G.A.; John Lough, W.; Arain, S.A.; Bradshaw, T.K. Evaluation and Application of Best Practice in Analytical Method Validation. *J. Liq. Chromatogr. Relat. Technol.* **2007**, *30*, 311–333. [CrossRef]
37. LoBrutto, R.; Patel, T. Method Validation. HPLC for Pharmaceutical Scientists. In *Method Validation. HPLC for Pharmaceutical Scientists*; John Wiley & Sons, Inc.: Hoboken, NJ, USA, 2006; pp. 455–502.
38. Dolan, J. Method Adjustment the USP Way. Available online: http://www.chromatographyonline.com/method-adjustment-usp-way (accessed on 13 August 2019).
39. Blessy, M.; Patel, R.D.; Prajapati, P.N.; Agrawal, Y.K. Development of forced degradation and stability indicating studies of drugs-A review. *J. Pharm. Anal.* **2014**, *4*, 159–165. [CrossRef]
40. Dong, M.W. *Modern HPLC for Practicing Scientists*, 1st ed.; Wiley Interscience: Hoboken, NJ, USA, 2006.
41. Khamanga, S.M.; Walker, R.B. The use of experimental design in the development of an HPLC–ECD method for the analysis of captopril. *Talanta* **2011**, *83*, 1037–1049. [CrossRef] [PubMed]
42. Tsuji, K.; Goetz, J.F. High-performance liquid chromatographic determination of erythromycin. *J. Chromatogr.* **1978**, *147*, 359–367. [CrossRef]

43. Brisaert, M.; Heylen, M.; Plaizier-Vercammen, J. Investigation on the chemical stability of erythromycin in solutions using an optimization system. *Pharm. World Sci.* **1996**, *18*, 182–186. [CrossRef] [PubMed]
44. Kirkland, J.J.; Henderson, J.W.; DeStefano, J.J.; van Straten, M.A.; Claessens, H.A. Stability of silica-based, endcapped columns with pH 7 and 11 mobile phases for reversed-phase high-performance liquid chromatography. *J. Chromatogr. A* **1997**, *762*, 97–112. [CrossRef]
45. Makoni, P.A.; Khamanga, S.M.; Wa Kasongo, K.; Walker, R.B. The use of experimental design for the development and validation of an HPLC-ECD method for the quantitation of efavirenz. *Pharmazie* **2018**, *73*, 570–578.
46. Snyder, L.R.; Kirkland, J.J.; Glajch, J.L. *Practical HPLC Method Development*; Wiley: Hoboken, NJ, USA, 1997.
47. Zhang, S.; Huang, X.; Yao, N.; Horváth, C. Preparation of monodisperse porous polymethacrylate microspheres and their application in the capillary electrochromatography of macrolide antibiotics. *J. Chromatogr. A* **2002**, *948*, 193–201. [CrossRef]
48. Snyder, L.R.; Kirkland, J.J. *Introduction to Modern Liquid Chromatography*, 2nd ed.; John Wiley: New York, NY, USA, 1979.
49. Fauzee, A.F.B.; Khamanga, S.M.; Walker, R.B. The impact of manufacturing variables on in vitro release of clobetasol 17-propionate from pilot scale cream formulations. *Drug Dev. Ind. Pharm.* **2014**, *40*, 1683–1692. [CrossRef]
50. Davey, P.G. The pharmacokinetics of clarithromycin and its 14-OH metabolite. *J. Hosp. Infect.* **1991**, *19*, 29–37. [CrossRef]
51. Erah, P.; Goddard, A.F.; Barrett, D.A.; Shaw, P.N.; Spiller, R.C. The stability of amoxycillin, clarithromycin and metronidazole in gastric juice: Relevance to the treatment of Helicobacter pylori infection. *J. Antimicrob. Chemother.* **1997**, *39*, 5–12. [CrossRef] [PubMed]
52. USP Monographs: Clarithromycin Tablets. Available online: http://ftp.uspbpep.com/v29240/usp29nf24s0_m17995.html (accessed on 13 August 2019).
53. USP Monographs: Clarithromycin for Oral Suspension. Available online: http://ftp.uspbpep.com/v29240/usp29nf24s0_m17993.html (accessed on 13 August 2019).

Saudi Pharmaceutical Journal 28 (2020) 308–315

Contents lists available at ScienceDirect

Saudi Pharmaceutical Journal

journal homepage: www.sciencedirect.com

Original article

The use of quantitative analysis and Hansen solubility parameter predictions for the selection of excipients for lipid nanocarriers to be loaded with water soluble and insoluble compounds

Pedzisai A. Makoni, Janeeta Ranchhod, Kasongo WaKasongo [1], Sandile M. Khamanga, Roderick B. Walker *

Division of Pharmaceutics, Faculty of Pharmacy, Rhodes University, 6140 Grahamstown, South Africa

ARTICLE INFO

Article history:
Received 5 November 2019
Accepted 26 January 2020
Available online 31 January 2020

Keywords:
Hansen solubility parameter
Lipid nanoparticles and nanocarriers
Solubility
Clarithromycin
Efavirenz
Minocycline hydrochloride
Mometasone furoate
Didanosine

ABSTRACT

The aim of these studies was to determine the miscibility of different API with lipid excipients to predict drug loading and encapsulation properties for the production of solid lipid nanoparticles and nanostructured lipid carriers. Five API exhibiting different physicochemical characteristics, *viz*., clarithromycin, efavirenz, minocycline hydrochloride, mometasone furoate, and didanosine were used and six solid lipids in addition to four liquid lipids were investigated. Determination of solid and liquid lipids with the best solubilization potential for each API were performed using a traditional shake-flask method and/or a modification thereof. Hansen solubility parameters of the API and different solid and liquid lipids were estimated from their chemical structure using Hiroshi Yamamoto's molecular breaking method of Hansen Solubility Parameters in Practice software. Experimental results were in close agreement with solubility parameter predictions for systems with $\Delta\delta T < 4.0$ MPa$^{1/2}$. A combination of Hansen solubility parameters with experimental drug-lipid miscibility tests can be successfully applied to predict lipids with the best solubilizing potential for different API prior to manufacture of solid lipid nanoparticles and nanostructured lipid carriers.

1. Introduction

Solid lipid nanoparticles (SLN) and nanostructured lipid carriers (NLC) are two major types of lipid-based nanocarriers developed to overcome the limitations of other colloidal carriers, such as emulsions, liposomes and polymeric nanoparticles (Naseri et al., 2015). Some of these limitations include limited stability when stored over extended periods, poor batch-to-batch reproducibility, low drug loading capacity (LC) and failure to manipulate biological membrane barriers to achieve sufficient API delivery for therapeutic activity (Beija et al., 2012; Riehemann et al., 2009). The encapsulation of drug molecules in nanoparticles shields them from the effect of efflux transporters and the small particle size facilitates uptake of drugs across biological membranes (Ahmad et al., 2018b). SLN and NLC are nanovectors manufactured using solid lipids or a combination of solid and liquid lipids, respectively (Mehnert and Mader, 2002; Riehemann et al., 2009). SLN are usually used as aqueous dispersions and are produced using a solid lipid, an API and surfactant(s) which impart stability to the system (Mehnert and Mader, 2002). NLC differ from SLN only from an excipients point of view, in that binary mixtures of solid and liquid lipids are used for formulation (Uner, 2006). In addition to excellent physical stability, SLN and NLC have an ability to exhibit complex functions, such as controlled delivery of API across different biological membrane barriers and consequently targeting organs leading to adhesion and improved cellular uptake (Ahmad et al., 2018b; Naseri et al., 2015; Riehemann et al., 2009).

The manufacture of SLN or NLC formulations involves melting a solid lipid or a binary mixture of solid and liquid lipid, followed by re-dispersion of the molten lipids as submicron-size droplets in an aqueous medium containing surfactant(s) (Uner, 2006). Acute and/or chronic toxicity during *in vivo* use has been associated with carriers of traditional colloidal systems, including polymeric-based systems (Müller et al., 2002). Thus, a prerequisite for manufacture of SLN and NLC is that only pharmaceutical grade excipients that are generally regarded as safe (GRAS) are used for production

* Corresponding author.
E-mail address: r.b.walker@ru.ac.za (R.B. Walker).
[1] Current address: Pharmaceutical Affairs, Aspen Pharmacare, Woodmead, Sandton 2196, South Africa.

Peer review under responsibility of King Saud University.

Production and hosting by Elsevier

https://doi.org/10.1016/j.jsps.2020.01.010
1319-0164/

(Muchow et al., 2008; Müller et al., 2002; Wissing et al., 2004). Mehnert and Mader (2002), in addition to Souto and Müller (2007), have reported broad lists of lipids and surfactants that can and have been used for the manufacture of SLN and NLC.

An important aspect to be considered prior to the development and optimization of SLN/NLC is the solubility of the API in the lipid (s) to be used. The usefulness of SLN and/or NLC as API carrier systems is usually dependent on LC and encapsulation efficiency (EE) of the nanocarriers for that particular API (Souto and Muller, 2011). Consequently a major factor affecting the LC and EE of SLN and/or NLC for an API is the solubility of that API in molten lipid (Hou et al., 2003; Müller et al., 2000; Wissing et al., 2004). Thus an adequate LC and EE can only be achieved if the solubility of an API in the molten lipid is relatively high (Hou et al., 2003; Müller et al., 2000; Wissing et al., 2004). Consequently it is imperative to evaluate the solubility of the API in different solid and liquid lipids, in order to select a solid and/or liquid lipid combination with the best solubilizing potential for that API.

Screening of solubility of API in lipids for production of SLN and NLC has been performed using the traditional shake flask method in order to determine equilibrium solubility (Baka et al., 2008; Cirri et al., 2018; Kasongo et al., 2011; Son et al., 2019). Modification of the shake flask method have also been used in the case of some poorly lipid soluble API (Joshi and Patravale, 2008, 2006). In addition, the selection of oil excipients for the production of nanoemulsions has been done two-fold through investigating API solubilty in a variety of oils using the shake flask method followed by comparative stability studies of produced nanoemulsions using four oils which demonstrated the highest API solubility (Ahmad et al., 2018a). Determination of the solubilization potential of different lipids is established using high performance liquid chromatography (HPLC) analysis, UV spectrophotometry and/or visual inspection (Ahmad et al., 2018a; Joshi and Patravale, 2008, 2006; Kasongo et al., 2011; Parveen et al., 2011). The shake-flask technique is a simple procedure but is time-consuming, costly and requires performing a number of laboratory experiments. Moreover, there is no accepted or standard approach when using this method (Box et al., 2006) and published solubility study data reveal large differences in the experimental conditions used, in particular stirring/shake times, sample preparation and separation techniques prior to analysis. Furthermore the solubility of ten compounds with different physicochemical profiles in ten lipid excipients was unsuccessful in elucidating a clear link between the physicochemical properties of API investigated and solubility in the excipients (Thi et al., 2009). Solubilization of API in lipids is complex and is comprised of different kinetic and thermodynamic factors that include parameters such as interfacial tension, molecular volume, crystal structure, hydrophilicity, surface charge and/or charge density as well as the physical and chemical environment of the reaction media (Shah and Agrawal, 2013; Steven Abbott, 2015). Recent advances in computational technologies have facilitated the development of more powerful *in silico* simulation and modelling approaches in which molecular structure, physiochemical properties and specific solute-solvent interactions may be taken into account (Kasimova et al., 2012; Persson et al., 2013; Rane et al., 2008).

The Hildebrand solubility parameter (δ) is a numerical value that indicates the relative solvency behavior of a specific solvent and is represented by Eq. (1) (Martin et al., 1980). The parameter expresses the square root of the cohesive energy density (CED) of the components holding the substances together. It is derived from the CED of the solvent, which in turn is derived from the heat of vaporization (Martin et al., 1980; Shah and Agrawal, 2013).

$$\delta = (\mathrm{CED})^{1/2} = (\Delta \mathrm{Ev}/\mathrm{Vm})^{1/2} \quad (1)$$

where ΔEv is the molar energy of vaporization and Vm is the molar volume of the solvent.

The Hildebrand approach works well for low molecular weight non polar solvents but fails to adequately describe the solubility behavior when polar and hydrogen bonding solvents are introduced. Consequently, Steven Abbott (2015) developed an approach to solubility parameters that takes into account the two latter mentioned forces. Hansen solubility parameters (HSP) have been applied to select API carriers using a combination of the theoretical solubility parameters and experimentally determined partition coefficients (Hossin et al., 2016).

The HSP divides the total solubility parameter (δT) into individual parts arising from dispersion forces (δD), permanent dipole–permanent dipole forces (δP), and hydrogen bonding (δH) (Steven Abbott, 2015) and can be estimated using Equation (2).

$$\delta \mathrm{T}^2 = \delta \mathrm{D}^2 + \delta \mathrm{P}^2 + \delta \mathrm{H}^2 \quad (2)$$

The use of theoretical solubility parameter prediction based on the molecular structure of compounds provides an early, rapid screening approach for the selection of lipid candidates without the need for lengthy experimental procedures to generate data (Hansen and Smith, 2004; Stefanis and Panayiotou, 2008; Steven Abbott, 2015). According to the HSP, the best miscibility of an API and an excipient is predictable when intermolecular forces., *viz* dispersion, polar, and hydrogen bonding forces between the molecules of the solute and solvent are of similar strength (Medarević et al., 2019; Shah and Agrawal, 2013; Steven Abbott, 2015). The difference in the solubility parameters between an API and an excipient can be used to estimate their compatibility and thus miscibility (Long et al., 2006). The HSP has therefore been used to describe numerous physical properties of materials in addition to predicting the miscibility and compatibility of API and excipients (Forster et al., 2001; Long et al., 2006; Rowe, 1988).

This study reports the validity of the HSP approach in screening lipid excipients for use in SLN and NLC production. Apparent solubility studies were performed with five (5) API with different physicochemical properties and the data generated by different researchers in our research group was used to evaluate and augment theoretical calculations based on the HSP. Minocycline hydrochloride (MNH), mometasone furoate (MF), efavirenz (EFV), didanosine (DDN) and clarithromycin (CLA) were evaluated to establish their miscibility and compatibility with different lipids in an attempt to identify and select the lipids with the best solubilization potential for the different API. The selection of lipids used in the studies was based on the similarity of application and availability. EFV, MF and CLA have low aqueous solubility and high intestinal permeability and are classified as a Biopharmaceutical Classification System (BCS) Class II compounds (Kristin et al., 2017; Madgulkar et al., 2019; Taneja et al., 2016). MNH and DDN exhibit high aqueous solubility and low intestinal permeability and are classified as BCS Class III compounds (Papich and Martinez, 2015; Pretorius and Bouic, 2009). The molecular structure of each API are depicted in Fig. 1.

2. Materials and methods

2.1. Materials

MNH and DDN were donated by Aspen Pharmacare (Port Elizabeth, Eastern Cape, South Africa). MF was purchased from Symbiotec Pharmalab Limited (Rau, Indore, India) and EFV was donated by Adcock Ingram® Limited (Johannesburg, Gauteng, South Africa). CLA was purchased from Skyrun Industrial Co. Limited (Taizhou, China). Gelucire® 48/16 (polyethylene glycol monostearate), Compritol® 888 (glyceryl behenate), Precirol® ATO 5

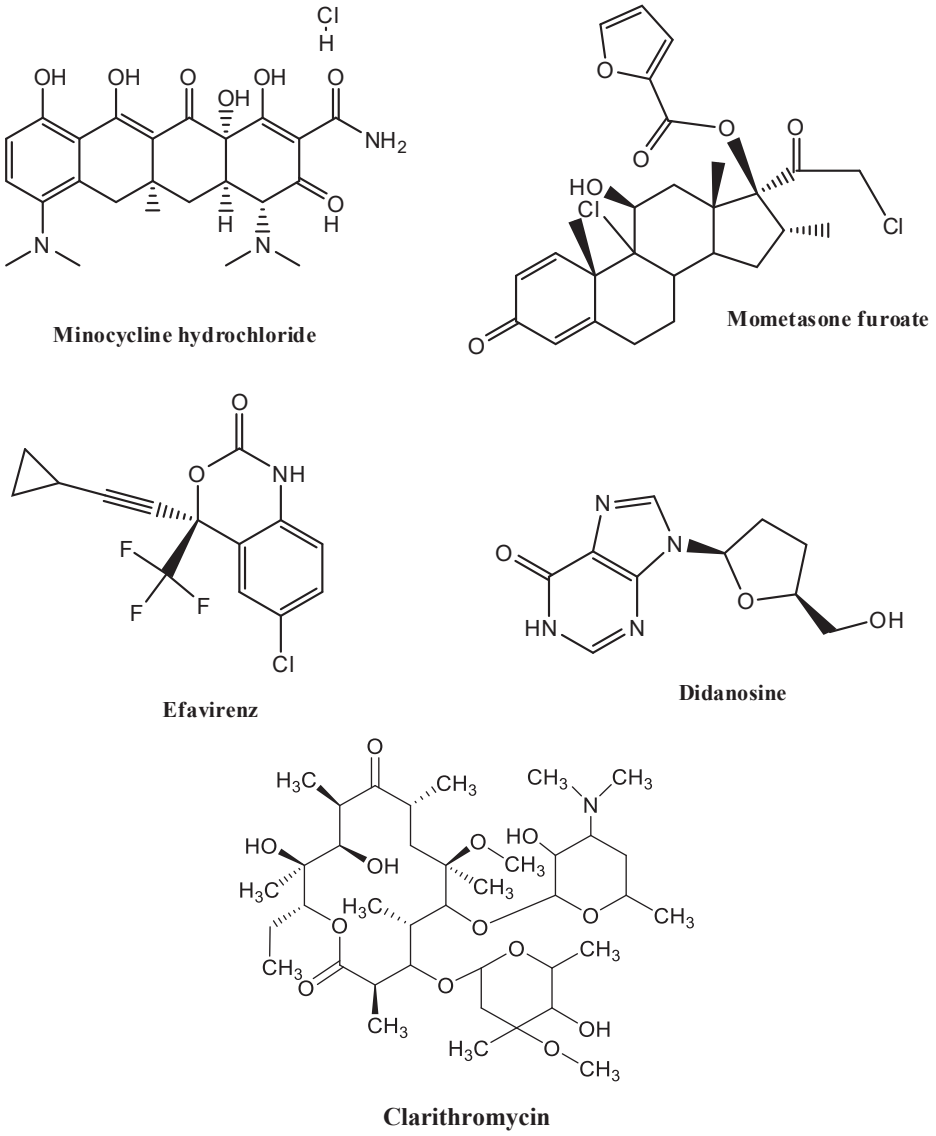

Fig. 1. Chemical structures of MNH, MF, EFV, DDN and CLA.

(glyceryl distearate), Geleol™ (glyceryl monostearate) and cetyl palmitate were donated by Gattefossé SAS (Gattefossé SAS, Saint-Priest Cedex, France). Stearic acid was purchased from Sigma Aldrich Chemical Co. (Milwaukee, WI, USA). Transcutol® HP (diethylene glycol monoethyl ether), Labrafac® PG (propylene glycol dicaprylate), Lauroglycol® FCC (propylene glycol monolaurate) and Capryol™ 90 (propylene glycol caprylate) were donated by Gattefossé SAS (Gattefossé SAS, Saint-Priest Cedex, France). MeOH and ACN (Romil®) was purchased from Microsep® (Port Elizabeth, Eastern Cape, South Africa). Potassium dihydrogen phosphate and sodium hydroxide pellets were purchased from Merck® Chemicals (Midrand, Gauteng, South Africa). HPLC-grade water was prepared using a Milli-RO® 15 water purification system (Millipore Co., Bedford, MA, USA) that consisted of a Super-C® carbon cartridge, two Ion-X® ion exchange cartridges and an Organex-Q® cartridge. The water was filtered through a 0.22 μm Millipak® 40 stack filter (Millipore Co., Bedford, MA, USA) prior to use. HPLC-water was also prepared using a Milli Q Plus (Millipore Co, Schwalbach, Germany). All reagents and solvents were of analytical grade and used without further purification.

2.2. Solubility studies

2.2.1. Selection of solid lipids

The solubility of API in different solid lipids was determined by either dissolving increasing amounts of individual API in a fixed amount of molten lipid or dissolving fixed amounts of API by addition of increasing amounts of solid lipid whilst heating and shaking the mixtures. Evaluation of the melt was performed visually (Joshi and Patravale, 2006; Kasongo et al., 2011). Required amounts of API and/or solid lipid were accurately weighed using a Model PA 2102 Ohaus® top-loading analytical balance (Ohaus® Corp. Pine Brook, NJ USA) and transferred into individual test tubes (Pyrex® Laboratory Glassware, England). The samples heated at 85 °C for an hour using a LABOTEC® shaking water bath (Laboratory Thermal Equipment, Greenfield NR. Oldham) set at 100 rpm.

An excess amount of API (MNH and EFV) was added to molten solid lipid individually and the melt evaluated visually. Following solution, additional aliquots of API were added until saturation was observed and no additional API dissolved in the molten lipid after shaking for 24 h at 85 °C. In order to study the solubility of

Table 1
Solubility of EFV and MNH in solid lipid excipients.

EFV		MNH	
Lipid (1.0 g)	Solubility (g)	Lipid (2.0 g)	Solubility (g)
Compritol® 888 ATO	0.25	Compritol® 888 ATO	0.0125
Precirol® ATO 5	0.30	Precirol® ATO 5	0.0075
Gelucire® 48/16	0.40	Gelucire® 48/16	0.0175
Cetyl palmitate	0.05	Cetyl palmitate	<0.0025
Stearic acid	0.10	Stearic acid	–
Geleol™	5.50	Geleol™	0.0300

-Solubility studies not performed.

DDN, MF and CLA in solid lipids, 50 mg of the individual API was weighed and placed into a test tube and solid lipid was added in 1.0 g aliquots after which the test tube was exposed to a temperature of 85 °C at 100 rpm using a LABOTEC® shaking water bath (Laboratory Thermal Equipment, Greenfield NR. Oldham). The amount of lipid required to solubilize the API in the molten state was estimated at the point that no further solid API could be solubilized by the molten lipid after shaking at 100 rpm at 85 °C for 24 h.

2.2.2. Selection of liquid lipids

The solubility of EFV, CLA and MF in different liquid lipids was determined by dissolving increasing amounts of the API in a fixed amount of molten lipid and evaluation of the melt visually as described in Section 2.2.1.

The saturation solubility of DDN in different liquid lipids was determined after shaking a liquid lipid containing an excess of DDN at 200 rpm for 24 h at 85 °C using a Model 4230 Innova refrigerated incubator shaker (New Brunswick Scientific). The oil–DDI mixtures were centrifuged using a Model 22 R Heraeus Biofuge centrifuge (Thermo Electron LED GmbH, Langenselbold, Germany) at 17 000 rpm for 30 min in order to separate DDI from the oil. The supernatant was filtered through a 0.45 μm hydrophilic Sartorius® membrane filter (Sartorius AG, Goettingen, Germany). The filtrate was diluted with MeOH and analyzed using a validated reversed-phase (RP)-HPLC method (Kasongo et al., 2011). The saturation solubility of MNH was determined by dispersing 10 mg MNH in 2.0 g of molten lipid to which 2 mL of hot distilled water was added. The mixture was shaken for 30 min at 85 °C using a LABOTEC® shaking water bath (Laboratory Thermal Equipment, Greenfield NR. Oldham) set at a speed of 100 rpm. The oil-MNH mixture was separated by centrifugation using a Model HN-SII IEC centrifuge (Damon, Needham HTS, MA, USA) at 1500 rpm for 10 min prior to analysis using a validated HPLC method (Ranchhod, 2017).

2.3. Solubility parameter calculations

The Hansen solubility parameter of the API and different solid and liquid lipids were calculated using the chemical structure and applying Hiroshi Yamamoto's molecular breaking method (Y-MB) using version 5.2.02 Hansen Solubility Parameters in Practice (HSPiP) software (Hansen Solubility, Hørsholm, Denmark). The chemical structures of the API and lipids were transformed by ChemDraw Ultra version 10.0 (CambridgeSoft corporation, Cambridge, MA, USA) to their simplified molecular input line entry syntax (SMILES) notation which was then used to calculate the solubility parameters *in situ* using Equation (2). The units of these solubility parameters are reported as $(Joules/cm^3)^{½}$ or, equivalently, $MPa^{½}$ (Steven Abbott, 2015).

3. Results and discussion

3.1. Selection of lipid excipients

The results of the solubility studies of the API in different solid lipids are depicted in Tables 1 and 2.

The results of the solubility studies of the API in liquid lipids are depicted in Tables 3 and 4.

The data listed in Tables 1–2 reveal that Geleol™ was the solid lipid with the best solubilizing potential for EFV, MNH and MF.

Table 4
Solubility of MNH and DDN in liquid lipid excipients.

MNH		DDN	
Liquid Lipid	Solubility (g)	Liquid Lipid	Solubility (g)
Labrafac® PG	0.0117 ± 0.001	Labrafac® PG	0.014 ± 0.00035
Transcutol® HP	0.3624 ± 0.017	Transcutol® HP	0.267 ± 0.0160
Capryol™ 90	0.0097 ± 0.003	Capryol™ 90	0.079 ± 0.00038
Lauroglycol® FCC	0.0043 ± 0.001	Lauroglycol® FCC	0.022 ± 0.00029

Table 2
Solubility of MF, DDN and CLA in solid lipid excipients.

MF (0.005 g)		DDN (0.01 g)		CLA (0.01 g)	
Lipid	Amount(g)	Lipid	Amount(g)	Lipid	Amount(g)
Compritol® 888 ATO	–	Compritol® 888 ATO	3.0	Compritol® 888 ATO	–
Precirol® ATO 5	–	Precirol® ATO 5	4.0	Precirol® ATO 5	–
Gelucire® 48/16	7.0	Gelucire® 48/16	–	Gelucire® 48/16	–
Cetyl palmitate	–	Cetyl palmitate	–	Cetyl palmitate	–
Stearic acid	–	Stearic acid	–	Stearic acid	3.0
Geleol™	6.0	Geleol™	–	Geleol™	–

-Complete solubilization of API not achieved as lipid(s) with best solubilization potential for the API had been identified.

Table 3
Solubility of EFV, MF and CLA in liquid lipid excipients.

EFV		MF		CLA	
Liquid Lipid	Amount (g)	Solid Lipid	Amount (g)	Solid Lipid	Amount (g)
Labrafac® PG	1.50	Labrafac® PG	<0.05	Labrafac® PG	<0.10
Transcutol® HP	4.50	Transcutol® HP	0.10	Transcutol® HP	0.20
Capryol™ 90	2.10	Capryol™ 90	<0.05	Capryol™ 90	<0.10
Lauroglycol® FCC	1.50	Lauroglycol® FCC	<0.05	Lauroglycol ® FCC	<0.10

Geleol™ has the highest δP (4.2 $MPa^{1/2}$) value of the solid lipids investigated (Table 5) due to the presence of two hydroxyl groups of the glycerin and the shortest alkyl chain of solid lipids investigated (Fig. 2). The presence of oxygen and hydroxyl functional groups increases the polarity and hydrogen bonding possibilities of the compound thus possibly contributing to the increased solubility of EFV, MNH and MF in Geleol™. In addition, the presence of mono- and diglycerides in lipid matrices has been shown to promote solubilization of API (Müller et al., 2000). DDN showed greatest solubility in Compritol® 888 while CLA showed greatest solubility in stearic acid. Compritol® 888 and stearic acid also possess oxygen and hydroxyl functional groups thus aiding molecular interactions leading to API solubilization in these lipids. However, there is no clear link between the physicochemical properties of the each API, the BCS classification and their ability to be solubilized in lipid excipients tested.

Table 5
Solubility parameters of solid and liquid lipids.

Solid Lipid	δD	δP	δH	δT
Compritol® 888 ATO	16.5	1	1.2	16.6
Precirol® ATO 5	16.2	2.4	7.6	18
Gelucire® 48/16	15.9	4	8.3	18.4
Cetyl palmitate	16	1.4	1.8	16.1
Geleol™	16.2	4.2	10.3	19.7
Stearic acid	16.2	2.8	5.2	17.2
Liquid Lipid	**δD**	**δP**	**δH**	**δT**
Lauroglycol ®FCC	16.3	4.2	8.7	18.9
Labrafac® PG	16.2	3.2	4.2	17.1
Transcutol® HP	16.3	7.4	12	21.6
Capryol™ 90	16.4	5.1	8.7	19.3

The data reported in Tables 3 and 4 reveal that all API were highly soluble in Transcutol® HP, which is a combination of diethylene glycol monoethyl ethers (Gattefosse, n.d.). Transcutol® HP has the highest δP and δH values (Table 5) due to the presence of two ester and a hydroxyl functional group in addition to possessing the shortest alkyl chain of all liquid lipids examined (Fig. 3).

3.2. Solubility parameter calculations

The results of the solubility parameter estimation for the API and lipids tested and exhibiting the best solubilizing potential using HSPiP software are listed in Table 6. Although the difference between solubility parameters of API and polymer should be small, if components are miscible, it is difficult to establish a threshold for the ΔδT value below which components are considered to be mis-

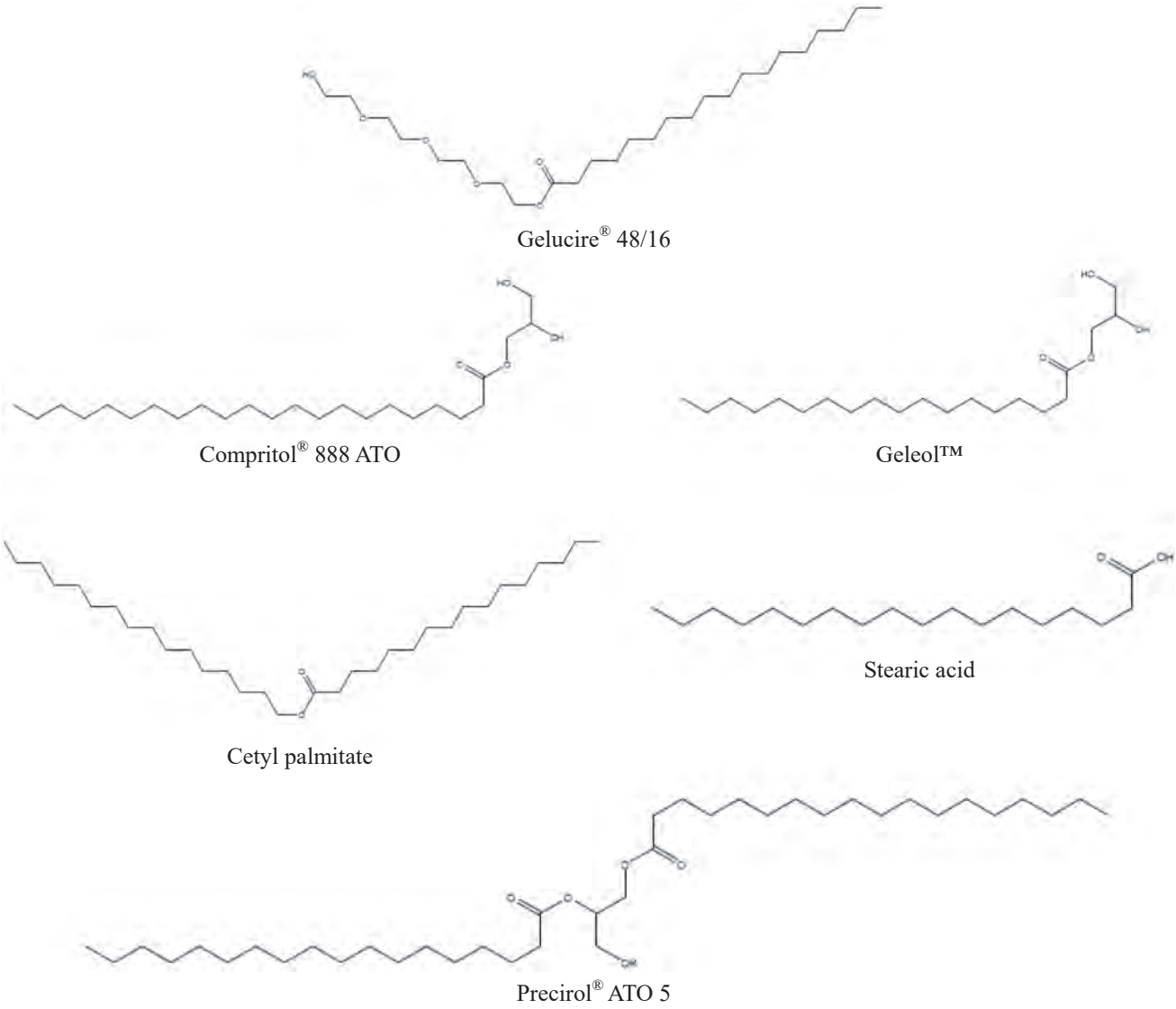

Fig. 2. Chemical structures of solid lipids tested.

Transcutol® HP

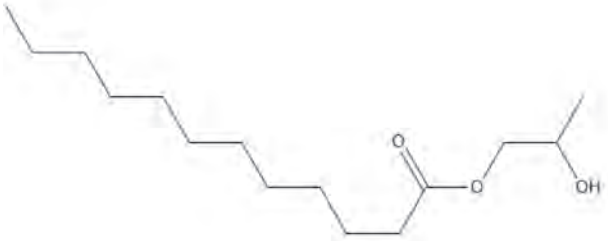

Lauroglycol ®FCC

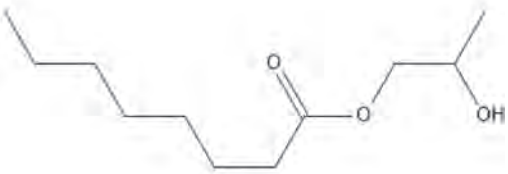

Capryol™ 90

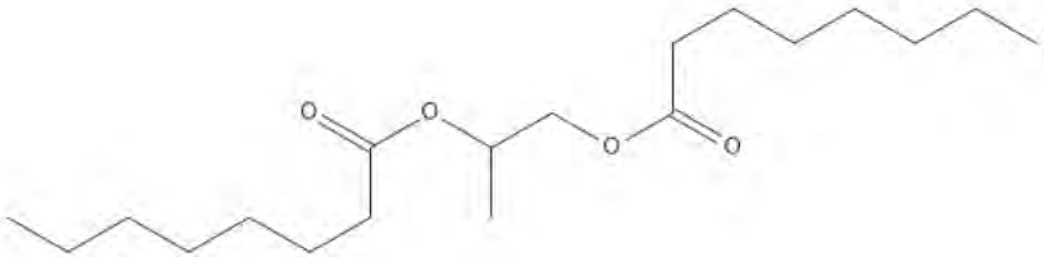

Labrafac® PG

Fig. 3. Chemical structures of liquid lipids.

Table 6
Solubility parameters of API and lipidic excipients.

API- Lipid System	δD ($MPa^{½}$)	δP ($MPa^{½}$)	δH ($MPa^{½}$)	δT ($MPa^{½}$)	ΔδT ($MPa^{1/2}$)	Group*
EFV	18.4	8.9	5.6	21.1		
Geleol™	16.2	4.2	10.3	19.7	1.4	1
Transcutol® HP	16.3	7.4	12	21.6	0.5	1
MN**	20.1	15.1	13.6	28.6		
HCL	20	0.1	19.8	28.1		
MNH Average				28.35		
Geleol™	16.2	4.2	10.3	19.7	8.65	2
Transcutol® HP	16.3	7.4	12	21.6	6.75	2
MF	19.6	9.4	3.6	22.1		
Geleol™	16.2	4.2	10.3	19.7	2.4	1
Transcutol® HP	16.3	7.4	12	21.6	0.5	1
DDN	19	12.4	9.4	24.6		
Compritol® 888 ATO	16.5	1	1.2	16.6	8	2
Transcutol® HP	16.3	7.4	12	21.6	3	1
CLA	17.7	4.1	4.4	18.6		
	16.2	4.5	7.6	18.5		
CLA Average				18.55		
Stearic acid	16.2	2.8	5.2	17.2	1.35	Ng***
Transcutol® HP	16.3	7.4	12	21.6	3.05	Ng***

* Group 1 lipids with best solubilization potential based on ΔδT. Group 2 lipids likely to be miscible with API and require experimental confirmation.
** MN = Minocycline.
*** Not grouped.

cible. Greenhalgh et al. (1999) proposed limits for ΔδT which indicate components are likely be miscible if ΔδT < 7.0 $MPa^{1/2}$, while ΔδT > 10.0 $MPa^{1/2}$, suggests the likelihood of components being immiscible. However Forster et al. (2001) suggested more stringent limits which predict materialization of a solid solution if ΔδT < 2.0 $MPa^{1/2}$, while immiscibility is anticipated for systems with ΔδT > 10.0 $MPa^{1/2}$. API-polymer systems with a ΔδT between 5.0 and 10.0 $MPa^{1/2}$ are likely to ensure an unreliable conclusion as to whether the system would be miscible or immiscible. Our studies confirm alignment of API-lipid miscibility studies of systems having ΔδT < 4.0 $MPa^{1/2}$ (Group 1) as summarized in Table 6. For API-lipid systems with a ΔδT > 4.0 $MPa^{1/2}$ (Group 2), HSPiP was unable to predict the lipid with the best solubilization potential for the API and results for these are based solely on experimental studies. This conclusion is based on a ΔδT of 4.9 $MPa^{1/2}$ for the DDN-Geleol™ system prediction which failed to align with experi-

mental findings that suggested Compritol® 888 ATO was the solid lipid with best solubilization potential for DDN with a $\Delta\delta T$ of 8.0 $MPa^{1/2}$ for this API-lipid system. In addition, Y-MB fails to provide HSP values for molecules with more than 120 atoms, other than H atoms, such as CLA. Consequently, the recommendation is to split the molecule (into two parts) while finding an appropriate functionality at the splitting point. The Y-MB of each structure is then calculated and a conclusion as to how the combined molecule is likely to behave then elucidated (Steven Abbott, 2015). This procedure resulted in inconsistent findings between HSP and experimental procedures for the solubility predictions for CLA in the lipids investigated thus preventing grouping of the system.

4. Conclusions

Evaluation of API-lipid miscibility and solubility is integral to the rational design, formulation and manufacture of lipid nanocarrier technologies. The selection of lipids for production with a specific API can be based on differences between calculated total solubility parameters of API and lipid without having to conduct lengthy and tedious laboratory experiments. When the difference between API and lipid total solubility parameters is <4.0 $MPa^{1/2}$, the best solubilization of API is likely to result from that specific lipid, when compared to other lipids. When the difference between API and lipid total solubility parameters is >4.0 $MPa^{1/2}$ HSP predictions alone cannot be used to identify the lipid with the best solubilizing potential for that API. Confirmation with experimental studies is required in addition to an understanding of the physicochemical properties of the API and lipid. Furthermore the molecular weight of the API and/or lipid was found to have limitations when predicting miscibility using HSP alone, as molecules with more than 120 atoms other than H atoms require splitting prior to using Y-MB, resulting in inaccurate predictions. Further studies using a larger sample size of model API are required to determine if the proposed model of solubility parameter use for lipid screening in SLN and NLC manufacture is applicable to different BCS class API and other lipids.

Declaration of Competing Interest

The authors report no conflicts of interest. The authors alone are responsible for the content and writing of this article.

Acknowledgements

This research was funded by the Rhodes University Research Committee.

References

Ahmad, N., Ahmad, R., Alam, M.A., Ahmad, F.J., Amir, M., 2018a. Impact of ultrasonication techniques on the preparation of novel Amiloride-nanoemulsion used for intranasal delivery in the treatment of epilepsy. Artif. Cells, Nanomed., Biotechnol. 46, S192–S207. https://doi.org/10.1080/21691401.2018.1489826.

Ahmad, N., Alam, M.A., Ahmad, R., Umar, S., Jalees Ahmad, F., 2018b. Improvement of oral efficacy of Irinotecan through biodegradable polymeric nanoparticles through in vitro and in vivo investigations. J. Microencapsul. 35, 327–343. https://doi.org/10.1080/02652048.2018.1485755.

Baka, E., Comer, J.E.A., Takács-Novák, K., 2008. Study of equilibrium solubility measurement by saturation shake-flask method using hydrochlorothiazide as model compound. J. Pharm. Biomed. Anal. 46, 335–341. https://doi.org/10.1016/J.JPBA.2007.10.030.

Beija, M., Salvayre, R., Lauth-de Viguerie, N., Marty, J.-D., 2012. Colloidal systems for drug delivery: from design to therapy. Trends Biotechnol. 30, 485–496. https://doi.org/10.1016/J.TIBTECH.2012.04.008.

Box, K.J., Völgyi, G., Baka, E., Stuart, M., Takács-Novák, K., Comer, J.E.A., 2006. Equilibrium versus kinetic measurements of aqueous solubility, and the ability of compounds to supersaturate in solution—a validation study. J. Pharm. Sci. 95, 1298–1307. https://doi.org/10.1002/JPS.20613.

Cirri, M., Maestrini, L., Maestrelli, F., Mennini, N., Mura, P., Ghelardini, C., Di Cesare Mannelli, L., 2018. Design, characterization and in vivo evaluation of nanostructured lipid carriers (NLC) as a new drug delivery system for hydrochlorothiazide oral administration in pediatric therapy. Drug Deliv. 25, 1910–1921. https://doi.org/10.1080/10717544.2018.1529209.

Forster, A., Hempenstall, J., Tucker, I., Rades, T., 2001. Selection of excipients for melt extrusion with two poorly water-soluble drugs by solubility parameter calculation and thermal analysis. Int. J. Pharm. 226, 147–161. https://doi.org/10.1016/S0378-5173(01)00801-8.

Gattefosse, n.d. Gattefosse-Personal care ingredients and pharmaceutical excipients <https://www.gattefosse.com/> (accessed 20 January 2020)

Greenhalgh, D.J., Williams, A.C., Timmins, P., York, P., 1999. Solubility parameters as predictors of miscibility in solid dispersions. J. Pharm. Sci. 88, 1182–1190. https://doi.org/10.1021/JS9900856.

Hansen, C.M., Smith, A.L., 2004. Using Hansen solubility parameters to correlate solubility of C60 fullerene in organic solvents and in polymers. Carbon N. Y. 42, 1591–1597. https://doi.org/10.1016/J.CARBON.2004.02.011.

Hossin, B., Rizi, K., Murdan, S., 2016. Application of Hansen Solubility Parameters to predict drug–nail interactions, which can assist the design of nail medicines. Eur. J. Pharm. Biopharm. 102, 32–40. https://doi.org/10.1016/J.EJPB.2016.02.009.

Hou, D., Xie, C., Huang, K., Zhu, C., 2003. The production and characteristics of solid lipid nanoparticles (SLNs). Biomaterials 24, 1781–1785. https://doi.org/10.1016/s0142-9612(02)00578-1.

Joshi, M., Patravale, V., 2008. Nanostructured lipid carrier (NLC) based gel of celecoxib. Int. J. Pharm. 346, 124–132. https://doi.org/10.1016/J.IJPHARM.2007.05.060.

Joshi, M., Patravale, V., 2006. Formulation and Evaluation of Nanostructured Lipid Carrier (NLC)–based Gel of Valdecoxib. Drug Dev. Ind. Pharm. 32, 911–918. https://doi.org/10.1080/03639040600814676.

Kasimova, A.O., Pavan, G.M., Danani, A., Mondon, K., Cristiani, A., Scapozza, L., Gurny, R., Möller, M., 2012. Validation of a novel molecular dynamics simulation approach for lipophilic drug incorporation into polymer micelles. J. Phys. Chem. B 116, 4338–4345. https://doi.org/10.1021/jp2104819.

Kasongo, K.W., Pardeike, J., Muller, R.H., Walker, R.B., 2011. Selection and Characterization of Suitable Lipid Excipients for use in the Manufacture of Didanosine-Loaded Solid Lipid Nanoparticles and Nanostructured Lipid Carriers. https://doi.org/10.1002/jps.22711.

Kristin, F., René, H., Boontida, M., Buraphacheep, J.V., Maximilian, A., Johanna, M., Peter, L., 2017. Dissolution and dissolution/permeation experiments for predicting systemic exposure following oral administration of the BCS class II drug clarithromycin. Eur. J. Pharm. Sci. 101, 211–219. https://doi.org/10.1016/j.ejps.2017.02.003.

Long, C., Zhang, L., Qian, Y., 2006. Preparation and crystal modification of ibuprofen-loaded solid lipid microparticles. Chin. J. Chem. Eng. 14, 518–525. https://doi.org/10.1016/S1004-9541(06)60107-9.

Madgulkar, A.R., Padalkar, R.R., Amale, S.K., 2019. Preformulation studies of intranasal solid lipid nanoparticles of mometasone furoate. J. Drug Deliv. Ther. 9, 526–528. https://doi.org/10.22270/jddt.v9i4.3100.

Martin, A., Newburger, J., Adjei, A., 1980. Extended hildebrand solubility approach: solubility of theophylline in polar binary solvents. J. Pharm. Sci. 69, 487–491. https://doi.org/10.1002/jps.2600690503.

Medarević, D., Djuriš, J., Barmpalexis, P., Kachrimanis, K., Ibrić, S., 2019. Analytical and computational methods for the estimation of drug-polymer solubility and miscibility in solid dispersions development. Pharmaceutics 11, 372. https://doi.org/10.3390/pharmaceutics11080372.

Mehnert, W., Mader, K., 2002. Solid lipid nanoparticles production, characterization and applications. Adv. Drug Deliv. Rev. 47, 165–196. https://doi.org/10.1016/s0169-409x(01)00105-3.

Muchow, M., Maincent, P., Müller, R.H., 2008. Lipid Nanoparticles with a Solid Matrix (SLN®, NLC®, LDC®) for Oral Drug Delivery. Drug Dev. Ind. Pharm. 34, 1394–1405. https://doi.org/10.1080/03639040802130061.

Müller, R.H., Mäder, K., Gohla, S., 2000. Solid lipid nanoparticles (SLN) for controlled drug delivery- a review of the state of the art. Eur. J. Pharm. Biopharm. 50, 161–177. https://doi.org/10.1080/026520499289185.

Müller, R.H., Radtke, M., Wissing, S.A., 2002. Nanostructured lipid matrices for improved microencapsulation of drugs. Int. J. Pharm. 242, 121–128. https://doi.org/10.1016/S0378-5173(02)00180-1.

Naseri, N., Valizadeh, H., Zakeri-Milani, P., 2015. Solid lipid nanoparticles and nanostructured lipid carriers: structure, preparation and application. Adv. Pharm. Bull. 5, 305–313. https://doi.org/10.15171/apb.2015.043.

Papich, M.G., Martinez, M.N., 2015. Applying Biopharmaceutical Classification System (BCS) criteria to predict oral absorption of drugs in dogs: challenges and pitfalls. AAPS J. 17, 948–964. https://doi.org/10.1208/s12248-015-9743-7.

Parveen, R., Baboota, S., Ali, J., Ahuja, A., Vasudev, S.S., Ahmad, S., 2011. Oil based nanocarrier for improved oral delivery of silymarin: in vitro and in vivo studies. Int. J. Pharm. 413, 245–253. https://doi.org/10.1016/j.ijpharm.2011.04.041.

Persson, L.C., Porter, C.J.H., Charman, W.N., Bergström, C.A.S., 2013. Computational prediction of drug solubility in lipid based formulation excipients. Pharm. Res. 30, 3225–3237. https://doi.org/10.1007/s11095-013-1083-7.

Pretorius, E., Bouic, P.J.D., 2009. Permeation of four oral drugs through human intestinal mucosa. AAPS PharmSciTech 10, 270–275. https://doi.org/10.1208/s12249-009-9207-4.

Ranchhod, J., 2017. Formulation, Development and Evaluation of Lipid Nanocarriers for Minocycline Hydrochloride. Rhodes University.

Rane, S.S., Cao, Y., Anderson, B.D., 2008. Quantitative solubility relationships and the effect of water uptake in triglyceride/monoglyceride microemulsions. Pharm. Res. 25, 1158–1174. https://doi.org/10.1007/s11095-007-9500-4.

Riehemann, K., Schneider, S.W., Luger, T.A., Godin, B., Ferrari, M., Fuchs, H., 2009. Nanomedicine-challenge and perspectives. Angew. Chem. Int. Ed. 48, 872–897. https://doi.org/10.1002/anie.200802585.

Rowe, R.C., 1988. Adhesion of film coatings to tablet surfaces —a theoretical approach based on solubility parameters. Int. J. Pharm. 41, 219–222. https://doi.org/10.1016/0378-5173(88)90195-0.

Shah, M., Agrawal, Y., 2013. High throughput screening: an *in silico* solubility parameter approach for lipids and solvents in SLN preparations. Pharm. Dev. Technol. 18, 582–590. https://doi.org/10.3109/10837450.2011.635150.

Son, G.-H., Na, Y.-G., Huh, H.W., Wang, M., Kim, M.-K., Han, M.-G., Byeon, J.-J., Lee, H.-K., Cho, C.-W., 2019. Systemic design and evaluation of ticagrelor-loaded nanostructured lipid carriers for enhancing bioavailability and antiplatelet activity. Pharmaceutics 11, 222. https://doi.org/10.3390/pharmaceutics11050222.

Souto, E.B., Müller, R., 2007. Lipid nanoparticles (SLN and NLC) for drug delivery. In: Domb, A., Tabata, M., Kumar, R., Farber, S. (Eds.), Nanoparticles for Pharmaceutical Applications. American Scientific Publishers, pp. 103–122.

Souto, E.B., Muller, R.H., 2011. Solid lipid nanoparticles and nanostructured lipid carriers-lipid nanoparticles for medicals and pharmaceuticals. Encycl. Nanosci. Nanotechnol. 23, 313–328.

Stefanis, E., Panayiotou, C., 2008. Prediction of Hansen solubility parameters with a new group-contribution method. Int. J. Thermophys. 29, 568–585. https://doi.org/10.1007/s10765-008-0415-z.

Steven Abbott, C.M.H. and H.Y., 2015. Hansen Solubility Parameters in Practice, 5th ed, Hansen-Solubility.com.

Taneja, S., Shilpi, S., Khatri, K., 2016. Formulation and optimization of efavirenz nanosuspensions using the precipitation-ultrasonication technique for solubility enhancement. Artif. Cells, Nanomedicine Biotechnol. 44, 978–984. https://doi.org/10.3109/21691401.2015.1008505.

Thi, T., Speybroeck, M., Barillaro, V., Martens, J., Annaert, P., Augustijns, P., Humbeck, J., Vermant, J., Mooter, Gv, 2009. Formulate-ability of ten compounds with different physicochemical profiles in SMEDDS. Eur. J. Pharm. Sci. 38, 479–488. https://doi.org/10.1016/J.EJPS.2009.09.012.

Uner, M., 2006. Preparation, characterization and physico-chemical properties of solid lipid nanoparticles (SLN) and nanostructured lipid carriers (NLC): their benefits as colloidal drug carrier systems. Pharmazie 61, 375–386.

Wissing, S.A., Kayser, O., Müller, R.H., 2004. Solid lipid nanoparticles for parenteral drug delivery. Adv. Drug Deliv. Rev. 56, 1257–1272. https://doi.org/10.1016/j.addr.2003.12.002.

Journal of Drug Delivery Science and Technology xxx (xxxx) xxx

Contents lists available at ScienceDirect

Journal of Drug Delivery Science and Technology

journal homepage: www.elsevier.com/locate/jddst

Research paper

Muco-adhesive clarithromycin-loaded nanostructured lipid carriers for ocular delivery: Formulation, characterization, cytotoxicity and stability

Pedzisai A. Makoni, Sandile M. Khamanga, Roderick B. Walker *

Division of Pharmaceutics, Faculty of Pharmacy, Rhodes University, Makhanda, 6140, South Africa

ARTICLE INFO

Keywords:
Clarithromycin
Nanostructured lipid carriers
Muco-adhesive
Design of experiments
Cytotoxicity
Stability

ABSTRACT

Topical ophthalmic formulations are the preferred approach to treat the anterior segment of the eye as it is a non-invasive therapeutic approach. The ocular bioavailability of drugs is generally limited, due to the presence of impervious anatomical barriers and low residence time and contact with the target tissue. Optimization of clarithromycin-loaded nanostructured lipid carriers using Design of Experiments was undertaken. Manufacture of nanostructured lipid carriers was achieved using hot emulsification ultrasonication. Formulation and process parameters were successfully identified following screening and subsequently optimized using Tween® 20, as a stabilizer. Muco-adhesive properties that could potentially increase ocular residence time, *in vitro* clarithromycin release and cytotoxicity against HeLa cells were evaluated. Short term stability studies of the optimized lipidic formulations was assessed at 4 °C and 22 °C. The optimized formulation exhibited muco-adhesive properties under stationary conditions assessed using Laser Doppler Anemometry, sustained release of API over 24 h under *in vitro* conditions. *In vitro* cytotoxicity studies revealed that the NLC were less cytotoxic to HeLa cells in comparison to pure API. The results suggest that the optimized carriers may have the potential to enhance precorneal retention, increase ocular availability and permit dose reduction or permit use of a longer dosing frequency.

1. Introduction

Non-tuberculous causing *mycobacteria* are environmental pathogens that have gained recognition as a significant cause of different human diseases. *Mycobacterium fortuitum and Mycobacterium chelonae* are among these *mycobacteria* and are a leading cause of infectious keratitis [1,2]. Development of ocular non-tuberculous mycobacterial (NTM) keratitis has been primarily attributed to penetration trauma of the corneal epithelium. Steroid use has been shown to suppress granulomatous inflammation facilitating the growth of non-tuberculous mycobacteria in the eye [2,3]. Outbreaks of NTM keratitis following laser-assisted *in situ* keratomileusis (LASIK) has been reported in Brazil, USA and Japan. These outbreaks are due to improper sterilization of surgical fluids and instruments leading to the introduction of pathogens to the corneal stroma during surgical procedures [4–6]. NTM is a common pathogen causing post-LASIK keratitis (47%) [7]. The causative agents of infectious keratitis vary by region and the incidence of infections ranges between 0.0063% and 0.71% with higher rates observed in developing countries [2,8].

Clarithromycin (CLA) is a macrolide antibiotic which is a structural analogue of erythromycin A [9]. CLA is mainly used in combination for the treatment of *Mycobacterium avium* complex and *Helicobacter pylori* [10]. Nie et al. [11], reported that CLA exhibited inhibition activity against > 275 non-tuberculosis mycobacterium clinical isolates. A comparative study in which the activity of four macrolides, *viz.* azithromycin, erythromycin, CLA and roxithromycin against *Mycobacterium fortuitum* and *Mycobacterium chelonae* was investigated revealed that CLA demonstrated remarkable potency against these strains [1]. The treatment of NTM keratitis with topical CLA has been successful [12] however, toxic reactions, intolerance and patient discomfort due to frequent instillation of topical solutions of CLA have been reported [13]. Commercially available CLA dosage forms for ocular use are non-existent and the *in vivo* efficacy of CLA for the treatment of NTM keratitis has, to date, been determined by reconstitution and use of lyophilized parenteral formulations administered *via* the ocular route [12,14,15].

The eye is an intricate organ of unique anatomy and physiology. Efficient protective mechanisms of the eye, such as the blinking reflex, lachrymal secretion and nasolacrimal drainage make it difficult to achieve the target concentration at the treatment site. Furthermore, the

* Corresponding author.
E-mail address: r.b.walker@ru.ac.za (R.B. Walker).

https://doi.org/10.1016/j.jddst.2020.102171
Received 25 August 2020; Received in revised form 12 October 2020; Accepted 17 October 2020
Available online 22 October 2020

anatomy and safeguard barrier of the cornea impede rapid absorption of active pharmaceutical ingredients (API) into the organ [16–18]. A number of ocular diseases are treated using either topical or systemically delivered medicines [18,19]. Ease of administration and affordability have made topical application of ocular medicinal products a preferred method for treatment of disorders which affect the anterior segment of the eye. Anatomical and physiological barriers hinder drugs from reaching the posterior segment of the eye, specifically the choroid and retina [19,20]. As much as topical instillation of eye-drops is non-invasive and widely preferred for treating diseases affecting the anterior segment of the eye, elimination of drops, irrespective of the instilled volume, occurs rapidly, usually within five to 6 min following administration, therefore, only a small amount (1–3%) of the instilled drop reaches intraocular tissues. In order to maintain minimum inhibitory anti-bacterial concentrations, ocular formulations need to be dosed frequently often resulting in poor patient adherence [16,19,21]. It is difficult to deliver and sustain sufficient concentrations of API in the precorneal region and to enhance the amount of active substance reaching target tissues. In order to exert an effective local effect, the residence time of the compound in the tear film should be increased. Furthermore, the use of once-a-day administered ocular formulations may improve patient adherence. Consequently, numerous ophthalmic dosage forms such as viscous solutions, suspensions, emulsions, ointments, aqueous gels, and polymeric inserts have been evaluated in an attempt to increase the bioavailability of API delivered *via* the ophthalmic route, by prolonging the contact time between the formulation and the corneal/conjunctival epithelium [17,21].

Micro- and nanoparticle-based delivery systems, formulated using excipients with multifunctional surface groups, have been developed with the intention of attempting to increase the retention and contact time of API on ocular surfaces. The excipients used and systems developed possess bio-adhesive polymer chains, functional groups and/or surface charges that interact with the mucin layer on ocular surfaces and prolong interaction of the formulation with the corneal surface [22]. Furthermore encapsulation of API into nanoparticles has been shown to protect the compound from enzymatic degradation, thereby permitting the use of lower amounts to achieve a therapeutic effect whilst avoiding adverse events [23]. Nanoparticles are colloidal carriers of 10–1000 nm in dimension and have gained attention for ocular drug delivery with numerous researchers attempting to develop nanoparticles for delivery of API to both anterior and posterior ocular tissue(s) [24–29]. API molecules loaded into lipid nanoparticles have the ability to cross the corneal epithelium effectively, due to the lipophilic properties of these carriers [30]. Lipid-based nanocarriers have properties similar to films of tears. Following instillation, the continuous phase is able to enhance the aqueous layer of the film and moisten the cornea. As oil droplets disrupt, encapsulated API is released allowing the oil phase to merge and enhance the natural lipid layer in the ocular region, reducing fluid loss by evaporation. In addition, the use of generally regarded as safe (GRAS) lipids for the production of the nanocarriers exhibits excellent ocular biocompatibility [31]. The biocompatibility of lipids used for nano-encapsulation is an important approach for enhancing the bioavailability of encapsulated API and provides protection against natural and processing effects. This in turn improves dosing outcomes, due to the controlled delivery of API, administration of low doses and improved shelf-life of encapsulated moieties, ultimately reducing the potential emergence of side effects [32]. To date, state of the art lipidic formulations of CLA have been formulated as solid lipid nanoparticles (SLN) in an attempt to improve the antibacterial activity of the encapsulated API against *Staphylococcus aureus* [33,34].

Many polysaccharides exhibit muco-adhesive properties at comparatively low viscosity, making them suitable for prolonging the contact time of ocular technologies, thereby allowing for reduced dosing frequencies and ultimately enhancement of patient adherence. The ocular disposition, pharmacokinetics, efficacy and safety of nanoparticle-formulations for ophthalmic drug use has been documented [35] revealing that the products were well tolerated, with enhanced corneal and aqueous humor concentrations observed, when compared to commercially available eyes drops, and also displayed improved ocular bioavailability and therapeutic efficacy [35]. Polyethylene glycol (PEG), chitosan and hyaluronic acid have been investigated as precorneal residence time enhancers in nanoparticle products [35] and the muco-adhesive properties of chitosan is well documented, with a variety of mechanisms of activity such as formation of hydrogen bonds with mucin and electrostatic interaction between positively charged amines and negatively charged sialic acid residues of mucin, postulated. However, the limited solubility of chitosan, under physiological conditions, is a major drawback for the successful translation of use into clinical practice with researchers harnessing the chemical reactivity of the polymer to overcome this challenge [36]. PEG coating of nanoparticles has been found to enhance the transport of nanomaterials across the ocular epithelium through imparting muco-penetrative properties to the experimental technology [37]. The objectives of these studies included optimization of PEG coated CLA-loaded NLC, investigation of the muco-adhesive, *in vitro* release and biocompatibility properties of test formulations to identify compositions that exhibited the potential to increase ocular residence time. In addition, short term stability studies of the optimized NLC formulation was assessed by measuring the critical quality attributes (CQA) over 28 days storage at 22 °C and 4 °C.

2. Materials and methods

2.1. Materials

CLA was purchased from Skyrun Industrial Co. Limited (Taizhou, China). Stearic acid, polyethylene glycol (PEG) 6000, Tween® 20 (polysorbate 20) and type II mucin from porcine stomach were purchased from Sigma Aldrich Chemical Co. (Milwaukee, WI, USA). Transcutol® HP (diethylene glycol monoethyl ether) was donated by Gattefossé SAS (Gattefossé SAS, Saint-Priest Cedex, France). Glycerine was purchased from Barrs Pharmaceutical Industries (Ndabeni, Cape Town, South Africa). HPLC-grade water was produced using a RephiLe® Direct-Pure UP ultrapure RO water system (Microsep®, Johannesburg, South Africa). All excipients used have GRAS status and are non-toxic and non-irritant [38]. All chemicals were used as received without further purification.

2.2. CLA-excipient compatibility and selection of lipids

Prior to the development and optimization of CLA-loaded lipid nanocarriers, an investigation into the solubility of the molecule in the potential lipids must be undertaken. To reduce the amount of lipid required and maximize nanocarrier product quality, it is necessary to select lipid excipients that exhibit the highest loading capacity (LC) and encapsulation efficiency (EE) for an API [39]. The solid lipid, stearic acid (SA) and the liquid lipid, Transcutol® HP (THP) were selected to manufacture NLC as previously reported [40]. SA and THP were mixed in ratios of 50:50 to 95:5 (SA: THP % *w/w*) and melted at 85 °C which is higher than the melting point of SA [40], in order to identify the best composition for a binary mixture of the lipids to manufacture NLC containing CLA. Binary mixtures exhibiting melting points >40 °C [41,42] and were miscible were considered suitable for use. The miscibility of the two lipids was established by differential scanning calorimetry (DSC) using a Model DSC-6000 PerkinElmer differential scanning calorimeter (PerkinElmer® Ltd, Connecticut, USA) and visual assessment. The use of DSC to assess the miscibility of SA and THP was based on the fact that a depression in melting point of the SA would be observed, following incorporation of THP into the lamellar structure of the solid lipid [42]. Visual assessment, to establish the presence of liquid lipid droplets on filter paper used was considered a clear indication of poor miscibility of the lipids and any binary mixture in which droplet formation was observed was considered unsuitable for use and not

investigated further.

Formulation of NLC dispersions requires the use of one or more emulsifying agents, solid and liquid lipids and water to ensure stability of the delivery system. The selection of a suitable surfactant is based on the intended purpose of the formulation. The primary objective of these studies was to develop muco-adhesive NLC for ophthalmic use. Therefore, it was vital that the surfactant or combination of surfactants used exhibit high ocular tolerability. Tween® 20 and Brij® 35 have been found to be the most effective in increasing corneal permeability [43]. The cytotoxicity of surfactants to corneal epithelial cells of rabbits revealed that nonionic surfactants are the least cytotoxic [44] therefore, Tween® 20 was selected for the formulation development studies of CLA-loaded NLC based on cost and availability.

When formulating new or re-formulating existing products, it is important to use data relating to physical and chemical interactions between the API and excipients used which may precipitate changes in the chemical nature, stability, solubility, absorption and therapeutic response of that API [45]. Fourier-transform infrared spectroscopy (FT-IR) was used to investigate potential physical interactions between the lipids and CLA using a PerkinElmer® Precisely FT-IR spectrophotometer Spectrum 100 (PerkinElmer® Pty Ltd, Beaconsfield, England). A ternary mixture of CLA, solid and liquid lipids was analyzed prior to and following exposure to a temperature of 85 °C for 1 h, so as to mimic the manufacturing process of the nanocarriers, in order to establish the effects thereof.

2.3. Manufacture of clarithromycin-loaded NLC

CLA-loaded NLC were prepared by hot emulsification ultrasonication (HEUS) [46,47]. Briefly, the lipid phase containing CLA was heated to approximately 85 °C. An aqueous phase of Tween® 20 with or without PEG 6000 was heated to the same temperature prior to dispersion in the molten lipid phase using a Model T 18 Ultra-Turrax® BS2 homogenizer (Janke & Kunkel GmbH and Co KG, Staufen, Germany) at 6000 rpm for 1 min to produce a pre-emulsion. The resultant pre-emulsion was subjected to ultrasound using a Sonoplus® HD 4200 probe sonicator (Bandelin, Berlin, Germany) fitted with a titanium flat tip (Bandelin, Berlin, Germany) at a predetermined amplitude for a set time. The nano-emulsion formed was filled and sealed into 100 mL siliconized glass vials (Lasec®, Port Elizabeth, South Africa) and cooled to room temperature (22 °C) to permit recrystallization and formation of CLA-loaded NLC *in situ*. All batches produced were characterized 24 h after manufacture.

2.4. Particle size (PS), polydispersity index (PDI) and Zeta Potential (ZP)

The mean PS and PDI of NLC were measured using a Model Nano-ZS Zetasizer (Malvern Instruments Ltd, Worcestershire, UK) with the instrument set to PCS mode. Approximately 30 µL of an aqueous dispersion of NLC was diluted with 10 mL HPLC-grade water prior to analysis. The sample was placed into a 10 × 10 × 45 mm polystyrene cell and all measurements were performed in replicate ($n = 10$) at 25 °C using a standard 4 mW laser set at 633 nm at a scattering angle of 90°. The analysis of PC data was achieved using Mie theory with the real and imaginary refractive indices set at 1.456 and 0.01, respectively.

For the measurement of ZP, the Nano-ZS Zetasizer (Malvern Instruments Ltd, Worcestershire, UK) was set in the Laser Doppler Anemometry (LDA) mode at a wavelength of 633 nm. The sample was prepared as described for PS and PDI analysis and placed into folded capillary cells. All measurements ($n = 10$) were performed at an applied field strength of 20 V/cm and the Helmholtz-Smoluchowsky equation [48] was used, *in situ*, to calculate the ZP of each sample.

2.5. Encapsulation efficiency (EE) and loading capacity (LC)

The % LC and % EE of CLA in the NLC was investigated using a validated RP-HPLC-ECD method [49] following filtration of an aqueous dispersion using Centrisart® filter tubes (Sartorius AG, Goettingen, Germany). The filter tubes were fitted with a filter membrane of molecular cut-off of 200 kDa at the base of the sample recovery chamber. Approximately 2.5 mL of the aqueous dispersion of NLC was placed into the outer chamber of the tube after which the sample recovery chamber was fitted. The unit was centrifuged at 2500 rpm for 20 min using a Model HN–SII IEC centrifuge (Damon, Needham HTS, MA, USA) prior to the amount of CLA in the aqueous filtrate being quantified using a validated RP-HPLC [49]. The LC and EE of CLA in the formulations was calculated using Equations (1) and (2) [49].

$$LC = \frac{W_a - W_s}{W_a - W_s + W_L} \times 100\% \quad (1)$$

$$EE = \frac{W_a - W_s}{W_a} \times 100\% \quad (2)$$

where,

W_a = weight of CLA added to formulation
W_s = weight of CLA in supernatant after centrifugation
W_L = weight of lipid added to the formulation

2.6. Screening and optimization of CLA-Loaded NLC

2.6.1. Screening of formulation parameters using box behnken design (BBD)

Design of Experiments (DoE) specifically a BBD was used to investigate the impact of five input variables on the production of CLA-loaded NLC. The variables tested were lipid, Tween® 20, PEG 6000, amplitude and sonication time. The number of experimental runs for the BBD was established using Version 12 Design Expert® statistical software (Stat-Ease Inc., Minneapolis, MN, USA). The concentration range and level including composition for the input variables are listed in Table 1.

HEUS was used to produce the NLC (Section 2.3). In total, forty-six (46) formulations with an intended 10% *w/w* CLA loading in relation to lipid content, were manufactured in batch sizes of 100 mL. When analyzing the formulations in terms of the CQA *viz.*, PS, ZP, PDI, EE and LC, it was observed that some formulations had formed a gel-like structure following storage for 24 h and were therefore not subject to further analysis. BBD has been reported to be insensitive to outliers and missing data [50,51] nevertheless, the experiments were continued in an attempt to evaluate the target product attributes, as envisaged. Numerical optimization was used in an attempt to optimize the formulations however, the predicted formulation was manufactured and a creamed gel-like structure formed after 24 h storage. Consequently, the experimental data generated using the BBD were used to identify a formulation with values that corresponded to the target CQA *viz.* a PS in the nano-range, PDI <0.5, ZP ≥ ± 30 mV, and EE > 80%. The formulation composition identified was then used for a subsequent

Table 1
Input variable and experimental design (BBD) values.

Variable		Level		
Input		−1	0	+1
Lipids	% *w/w*	1	3	5
Tween® 20	% *w/w*	1	3	5
Sonication time	min	10	20	30
Amplitude	%	10	55	100
PEG 6000	% *w/w*	0	1	2
Output		**Constraint**		
EE		Maximize		
LC	%	Maximize		
ZP	% mV	Minimize		
PS	Nm	Minimize		
PDI		Minimize		

optimization process of the manufacturing parameters *viz.,* sonication time and amplitude. ZP values of ±30 mV are targeted to ensure NLC stabilized through electrostatic repulsion are produced, so as to prevent aggregation [52]. Stable nanocarriers for which the ZP was <30 mV have been manufactured using Tween® 80 [53]. Polysorbate surfactants provide stability through both electrostatic and steric hindrance mechanisms mitigating the need for a ZP of ±30 mV to ensure stability [53,54].

2.6.2. Optimization of manufacturing parameters using central composite design (CCD)

Following the identification of the most ideal formulation composition based on the CQA monitored, process optimization in relation to manufacturing parameters was undertaken in an attempt to increase the EE, further reduce the PS and PDI while producing a stable formulation. Sonication time and amplitude of sound waves have been identified as important parameters when fabricating nanoparticles of small size using ultrasonication [52]. An increase in time and sonication amplitude results in a decrease in particle size [55]. However, high sonication amplitudes have also been shown to produce lipid nanoparticles of increased size, due to the formation of aggregates [52,55,56]. Consequently, the effect of sonication time and the amplitude of ultrasound on the CQA of the NLC was investigated. The number of experimental runs using CCD was established using version 12 Design Expert® statistical software (Stat-Ease Inc., Minneapolis, MN, USA) and the input variables and ranges tested are listed in Table 2.

2.7. pH and osmolarity

The human eye can tolerate formulations with an osmolality of between 250 and 450 mOsm/kg and a pH of 3.5–10.5 [57,58]. The osmolarity of the optimized CLA-loaded NLC formulations was adjusted to a physiological value with glycerin and was then determined by freezing point depression using a calibrated Gonotec Osmomat 3000 osmometer (Gonotec, Berlin, Germany). The pH of the nanocarrier suspensions was monitored at 22 °C using a calibrated Model GLP 20+ Basic pH-meter (Crison Instruments, Barcelona, Spain).

2.8. Muco-adhesion

Nanoparticles with a negative ZP exhibit reduced ocular residence times since interactions between the nanocarriers and mucin, a negatively charged glycoprotein, are unlikely to occur [52]. Consequently, the incorporation of PEG into the NLC formulation was investigated, to establish if muco-adhesive properties had been imparted to the test technology. ZP measurements are a common approach used for the investigation of muco-adhesive properties of biopolymers [59–62].

The muco-adhesive properties of the NLC was evaluated by monitoring changes in ZP following incubation of the NLC, with mucin [63] following preparation of a 0.1% *w/w* stock dispersion of mucin in HPLC-grade water. The dispersion was stirred for 30 min at 500 rpm using a hotplate stirrer (VWR®,Batavia, IL, USA) prior to filtration through a 0.45 μm Millipore® Millex-HV Hydrophilic PVDF filter membrane (Millipore® Co., Bedford, MA, USA). A 60 μL aliquot of the NLC dispersion was injected into 20 mL filtered mucin dispersion and the mixture stirred at 200 rpm for 6 h at 32 °C, to simulate the temperature of the ocular surface, using a digital hotplate stirrer (VWR®, Batavia, IL, USA) in a glass cylinder [64]. The ZP of the mixtures was measured at 0, 30, 60, 120, 240 and 360 min and the data analyzed as described in Section 2.4. Aqueous dispersions of filtered mucin and NLC were also monitored and analyzed over the 6-h period as controls. Confirmation of PEG coating on the nanocarriers was determined using DSC with a Model DSC-6000 PerkinElmer differential scanning calorimeter (PerkinElmer® Ltd, Connecticut, USA).

Table 2
Variables and experimental design values for CCD.

Variable		Level			
Input		-α	−1	1	+α
Sonication time	Min	5.86	10	30	34.14
Amplitude	%	12.57	25	85	97.43
Output		Constraints			
EE	%	maximize			
LC	%	maximize			
ZP	MV	minimize			
PS	Nm	minimize			
PDI		minimize			

2.9. In vitro release and kinetic modelling

In vitro release of CLA from the optimized NLC dispersion after adjustment with glycerin was investigated using the dialysis bag method. One milliliter of the nano-suspension was transferred into a closed dialysis bag (MWCO 14000 Da, Sigma Aldrich Chemical Co., Milwaukee, WI, USA) and placed into 70 mL borosilicate vials. The dissolution medium containing 20 mL HPLC-grade water (pH = 7.20) was maintained at 32 °C, to simulate the temperature of the ocular surface, and stirred using a shaking water bath using a LABOTEC® shaking water bath (Laboratory Thermal Equipment, Greenfield NR. Oldham) at 80 rpm. Sink conditions were maintained by replacing 1.0 mL of fresh dissolution medium at predetermined time intervals. The studies were performed in triplicate (n = 3) for 24 h. The amount of CLA in the receptor medium was determined using RP-HPLC [49].

The *in vitro* release data for optimized CLA-loaded NLC was fitted to first-order, Higuchi, Korsemeyer–Peppas, Hixson-Crowell and Baker-Lonsdale models using DDSolver, an add-in program for Microsoft Excel [65]. The model that best fitted the data was selected based on the adjusted coefficient of determination (Rsqr_adj), Akaike Information Criterion (AIC) and Model Selection Criterion (MSC), which are the most popular evaluation criteria in the field of dissolution [65]. The highest Rsqr_adj and MSC values and the lowest AIC values were used to determine the model that best fit the observed release [33,65].

2.10. Cytotoxicity assay

Many authors have demonstrated that the organ and species of origin of cells used in cytotoxicity assays have a strong correlation to the results observed in such studies [66,67]. As a general rule, it is crucial to select an appropriate cell line for a study based on the expected target organ *in vivo* and application of the carrier system used [68,69]. Nevertheless in a study to assess the cytotoxicity of bio-active silica nanoparticles in 19 different cell lines representing all major organ types, the results revealed reduced toxicity in all cell types investigated, thereby implying the influence of the cell line characteristics on the final toxicity response observed was minimal [70]. Consequently, in an attempt to assess the biocompatibility of CLA-NLA for potential use in humans, a human cell line viz., human cervix adenocarcinoma cells, available in our institution was selected for evaluating potential cytotoxicity of the test technology.

HeLa (human cervix adenocarcinoma cells) (Cellonex) were cultured in Dulbecco's Modified Eagle Medium (DMEM) – (Lonza) supplemented with 10% fetal calf serum and antibiotics (penicillin/streptomycin/amphotericin B) at 37 °C in a 5% CO_2 incubator. HeLa cells were plated in 96-well plates at a cell density of 1 × 104 cells per well in 150 μL culture medium and grown overnight. A single concentration of 50 μg/mL of the test compounds were incubated with the cells for an additional 48 h, and cell viability in the wells assessed by adding 20 μL of 0.54 mM resazurin in phosphate buffered saline (PBS) for an additional 2–4 h. The relative amount of cells surviving drug treatment were determined by reading resorufin fluorescence readings (excitation 560 nm, emission 590 nm) in a SpectraMax® M3 plate reader (Molecular Devices San Jose, CA, USA). Fluorescence readings obtained for the individual wells were

converted to % cell viability relative to the average readings obtained from untreated control wells (HeLa cells without test compounds), after subtracting background readings obtained from wells without cells.

2.11. Statistical analysis

Statistical analysis was performed using version 12 Design Expert® statistical software (Stat-Ease Inc., Minneapolis, MN, USA). The significance of relevant factors was calculated using Fisher's statistical test for Analysis of Variance (ANOVA) and models considered statistically significant when a p value < 0.05 was observed at a 95% level of confidence. Three-dimensional (3-D) surface plots were used to identify the process parameters which resulted in the manufacture of CLA-loaded NLC that exhibited the desired CQA.

2.12. Stability studies

The short term stability testing protocol strategy for the optimized CLA-loaded NLC formulation was conducted based on existing global stability guidelines [71]. For these studies, CLA-loaded NLC were packed into 50 g clear glass ointment jars and tightly sealed prior to being stored at room temperature (22 °C) and in the refrigerator (4 °C). Formulations tested at each pull time were discarded and not returned to the storage area. PS, PDI, ZP, EE, pH and osmolarity were evaluated weekly for 28 days in triplicate (n = 3).

3. Results and discussion

3.1. CLA-excipient compatibility and selection of lipids

The influence of THP inclusion on the melting point and peak onset of SA in terms of liquid lipid content is depicted in Fig. 1 and a summary of the melting events observed for the binary mixtures tested are summarized in Table 3.

The data plotted in Fig. 1 and summarized in Table 3 reveal that all binary mixtures tested, produced mixtures for which the melting point was >40 °C. However, the onset melting point and enthalpy for the melting of SA appears to decrease gradually with an increase in the amount of THP included in the mixture up to 20% *w/w*. The gradual depression in onset of melting of SA when up to 20% *w/w* THP is added, suggests that the two lipids are miscible when THP is used in amounts between 5 and 20% *w/w* in the mixtures. The lack of miscibility was confirmed by the presence of THP droplets on filter paper when the amounts of THP used, was >20% *w/w* providing further evidence that THP and SA are poorly miscible when mixed at these concentrations. The results suggest that a liquid lipid content of ≤20% *w/w* would be ideal and that concentrations >20% *w/w* are likely to result in the production of immiscible mixtures of these lipids. Consequently, a 20% *w/w* Transcutol® HP and 80% *w/w* SA binary mixture was considered the most suitable composition for the formulation and manufacture of CLA-loaded NLC.

Table 3
DSC events for binary mixtures of stearic acid and Transcutol® HP following exposure to 85 °C for 1 h.

Ratio SA:THP	Thermal event	Melting point °C	Onset °C	Enthalpy J/g
95:5	Endothermic	61.02	58.85	134.15
90:10	Endothermic	60.50	58.45	125.23
85:15	Endothermic	59.84	56.77	120.57
80:20	Endothermic	59.08	56.19	75.45
75:25	Endothermic	51.08	48.37	29.54
70:30	Endothermic	50.11	46.35	33.47
60:40	Endothermic	49.17	45.74	32.45
50:50	Endothermic	45.48	44.13	47.59

The FT-IR spectra generated for CLA and SA prior to exposure to heat and that of a 1:1:1 ternary mixture of CLA, SA and THP following exposure to 85 °C for 1 h are depicted in Fig. 2. Evaluation of the FT-IR spectrum for the ternary mixture reveals the presence of peaks (circled in red) that are the same as those observed for SA alone, confirming that neither THP nor CLA appears to interact with the crystalline structure of SA. However, the presence of a peak representing molecular vibrations for CLA (green) is most likely the result of CLA not being completely included in a molecular dispersion in the ternary mixture.

3.2. Manufacture of clarithromycin-loaded NLC using DoE

3.2.1. Formulation screening parameters from box behnken design (BBD)

The BBD design matrix for the responses of formulations that did not form a gel-like structure and were analyzed after 24 h is summarized in

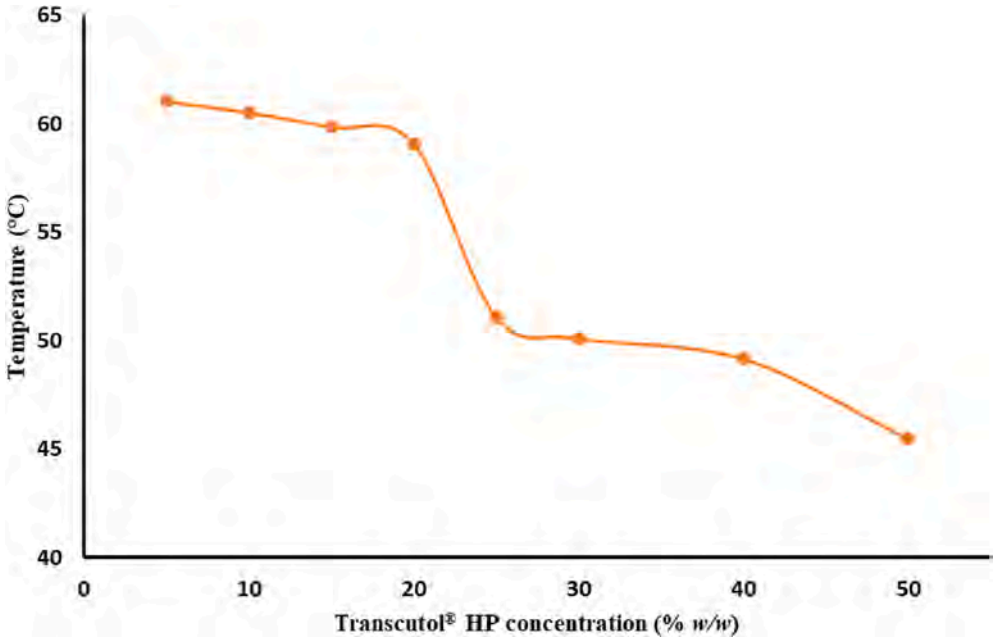

Fig. 1. Impact of Transcutol® HP concentration on the melting point and peak onset for stearic acid.

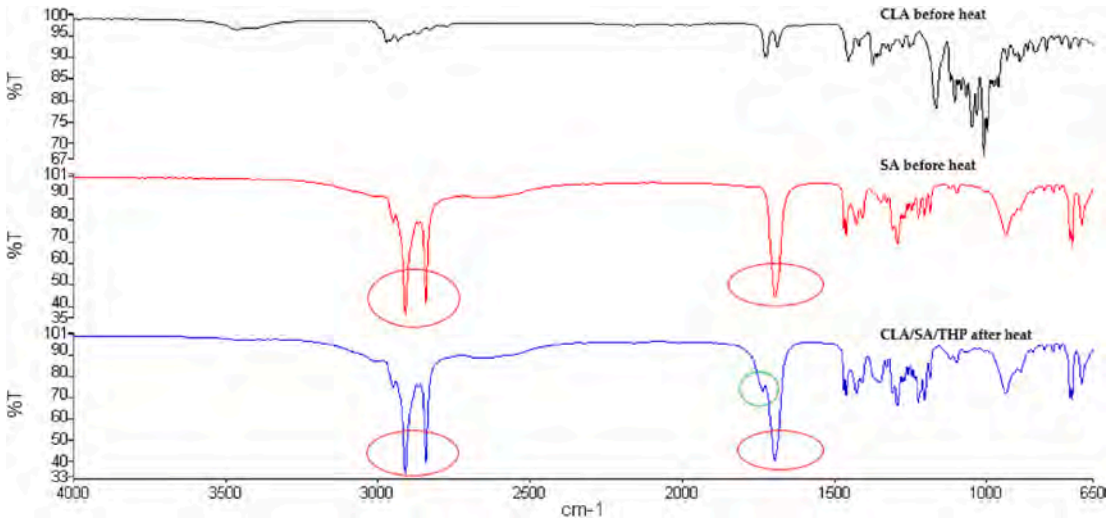

Fig. 2. FT-IR spectra of CLA and SA prior to exposure to heat and for a 1:1:1 ternary mixture of CLA, SA and THP following exposure to 85 °C for 1 h.

Table 4
Responses observed for stable NLC formulations following BBD experiments.

Run	Input Variables					Responses (CQA)				
	Lipid	Tween® 20	Amplitude	Time	PEG400	EE	LC	ZP	PS	PDI
	% w/w	% w/w	%	min	% w/w	%	%	mV	nm	
1	5	3	55	20	2	76.67	7.12	−25.4	7095	0.716
6	3	1	55	20	2	76.06	7.07	−15.9	6196	0.963
7	3	1	100	20	1	78.7	7.3	−17	1568	0.846
9	3	3	55	30	2	67.83	6.35	−28	8306	0.762
10	3	1	55	20	0	82.13	7.59	−17.9	4053	0.721
11	1	3	100	20	1	58.99	5.57	−18.6	2483	0.866
12	5	3	55	10	1	79.47	7.36	−24.1	6864	0.614
13	3	3	10	20	0	79.85	7.4	−21.2	8184	0.877
16	1	3	10	20	1	65.9	6.18	−16.9	10770	0.785
17	3	1	55	30	1	65.61	6.16	−16.3	4084	0.893
20	1	5	55	20	1	36.97	3.57	−26.2	2607	0.887
22	1	3	55	30	1	38.25	3.68	−17	13390	0.743
23	1	1	55	20	1	26.86	2.62	−20.9	14180	0.577
26	5	3	10	20	1	55.78	5.28	−25.3	6869	0.807
29	1	3	55	10	1	32.68	3.16	−20.3	35380	0.793
33	3	1	55	10	1	70.57	6.59	−17.3	2494	0.901
37	1	3	55	20	2	30.56	2.97	−23.7	5800	0.803
41	1	3	55	20	0	38.51	3.71	−33.3	23910	0.878
43	3	3	55	10	0	66.49	6.23	−21.9	15710	0.738
*44	5	1	55	20	1	86.53	7.96	−20.3	499.8	0.456
45	3	1	10	20	1	75.02	6.98	−15.7	6130	0.738

Table 4.

The data listed in Table 4 reveal that the formulation produced as run 44* (F 44) was the only formulation that met the desired CQA for EE, ZP, PS and PDI. Consequently, batch F 44 was further optimized with respect to process parameters in an attempt to assess the robustness of the formulation composition, to changes in process conditions.

3.2.2. *Optimization of process parameters using a central composite design (CCD)*

The input variables used to optimize the manufacture of CLA-loaded NLC using CCD in addition to the observed responses are summarized in Table 5.

The manufacturing parameters used for the production of CLA-loaded NLC were optimized using a CCD. The data generated was analyzed using version 12 Design Expert® statistical software (Stat-Ease Inc., Minneapolis, MN, USA). Fisher's test for Analysis of Variance (ANOVA) was used to determine the significance of any difference(s) between the factors investigated, with the error term set at $p = 0.05$. The overall design summary revealed that three linear and two quadratic mathematical models described the two independent factors. Significant model variables were identified during optimization and the best combination of factors yielding the target CQA, elucidated.

The overall contribution of model factors used to produce nanoparticles with the target EE, LC, ZP, PS and PDI were statistically significant and the models be used to navigate the design space. ANOVA analysis revealed that the significant model term for the linear models for EE, LC and ZP was amplitude of sonication ($p < 0.05$). The significant model term(s) for the quadratic models, PS and PDI established at $p < 0.05$ were amplitude of sonication and the quadratic effect of amplitude. The 3D response surface plots for these data are depicted in Fig. 3 (A-E). The 3D surface plots are used to facilitate the examination of effect(s) of experimental factors on the responses monitored. These graphical representations illustrate the responses to different experimental values and facilitate identification of major interactions between variables. When using 3-D plots, one variable must be set at an arbitrary and fixed value and the response surface plotted using the other two additional variables displayed on the X and Y-axes. The response surface generated is therefore a function of the selected value for the constant variable and

Table 5
Responses observed for CCD experiments during optimization of process conditions for NLC manufacture.

Run	Input Variables		Responses (CQA)				
	Sonication time	Amplitude	EE	LC	ZP	PS	PDI
	Min	%	%	%	mV	nm	
1	10	85	87.1	8	−18.5	661	0.668
2	30	25	88.1	8.1	−17.6	1008	0.948
3	10	25	88.1	8.1	−18.6	1130	0.886
4	20	55	88	8.1	−19.1	477.8	0.545
5	20	55	86.4	8	−21.8	511.3	0.487
[a]6	20	13	–	–	–	–	–
7	34.14	55	87.9	8	−26.1	477.2	0.531
8	20	55	87.8	8	−21.8	483.1	0.592
9	30	85	84.9	7.8	−25.6	495	0.555
10	6.15	55	87.1	8	−21.7	434.4	0.476
11	20	55	88.6	8.1	−23.8	424.6	0.454
12	20	97	84.3	7.8	−29.1	419.4	0.392
13	20	55	86.5	8	−21.4	441.0	0.479

[a] Formulation that was deemed unstable after 24 h storage.

will differ depending on the actual value used [72].

3.2.2.1. Encapsulation efficiency (EE) and loading capacity (LC). LC is an essential parameter to monitor when establishing whether a novel carrier system is suitable for use and has an impact on the long term stability of systems in that the API remains entrapped in the carrier [73]. The optimization process for NLC must therefore include an investigation of the LC and EE [74]. The lipid core should shield the payload and minimize degradation whilst ensuring a high EE and long term retention in the lipid matrix [75]. The 3-D response surface plots (Fig. 3A and B) depict an inverse relationship between amplitude of sonication and the CQA monitored. Application of higher amplitudes during sonication on previously formed lipid carriers resulted in expulsion of entrapped API into the aqueous dispersion medium, resulting in a reduction in EE and LC [55,76]. Consequently, high amplitudes are likely to lead to CLA-NLC with a reduced payload, thereby exposing CLA to possible hydrolytic degradation, which in turn requires the use of large amounts of the compound to produce a therapeutic effect, which may lead to adverse events.

3.2.2.2. Zeta Potential (ZP). The ZP for all formulations tested, ranged between −17.6 and −29.8 mV. The 3-D response surface plot revealing the effect of amplitude of sonication on ZP (Fig. 3**C**) reveals that stable formulations exhibiting relatively high negative ZP values were produced at relatively high sonication amplitudes. Adsorption of non-ionic surfactant steric stabilizers, decreases the ZP in colloidal systems resulting in strong repulsive forces between particles thereby preventing aggregation [55,73]. An increase in amplitude is likely to generate increased temperatures during manufacture, which in turn result in a reduction in adsorption and/or degradation of surfactant [46] and an increase in ZP. However, the ZP is primarily affected by the type and concentration of lipids and surfactants used and not the method of manufacture [77] and this factor will have to be monitored during long-term stability studies of CLA-loaded NLC intended for ophthalmic use.

3.2.2.3. Particle size (PS) and polydispersity index (PDI). The mean PS of CLA-loaded NLC ranged between 419.4 and 1130 nm. The particle size of the NLC produced can be considered suitable for instillation into the eye, since the human eye can tolerate particles of up to 10 μm in diameter [78]. The PDI provides an indication of the width of the size distribution of particles and completely monodisperse systems generally have a PDI of 0, which increases to 0.500 for systems with a relatively broad particle size distribution [79,80]. The PDI for all formulations tested, ranged between 0.392 and 0.948. The 3-D response surface plots depicting the impact of amplitude of sonication on PS and PDI (Fig. 3**E** and **F**) reveal an increase in PS and PDI when lower amplitudes are applied to the process. It has been suggested that low processing temperatures lead to the formation of nanoparticles of large particle size [81]. High amplitudes of sonication lead to an increase in ultrasonic wave energy and temperature, which in turn increases the shear cavitation force with an ultimate breakdown of the oil droplets into nanometric sized droplets [52]. Consequently, a compromise in terms of amplitude application and the target PS and PDI must be reached to ensure the production of stable formulations.

3.2.3. Formulation optimization

Numerical optimization was undertaken using Design Expert® software with the aim of identifying and selecting the optimum manufacturing parameters that would ensure the production of stable NLC formulations of CLA. Numerical optimization locates a point at which the desirability function for a system is maximized, while the characteristics of the target can be modified by adjusting the importance of that target [82]. The instrumental parameters resulting in the highest desirability *viz.* a sonication time of 26.33 min and amplitude of 59.7%, were used to manufacture the optimized NLC formulation, which was then characterized in terms of the target CQA. The responses generated for the optimized CLA-loaded NLC are summarized in Table 6 and include the experimental and predicted responses, with the corresponding percent prediction error for the relevant parameters. The size distribution curve depicted in Fig. 4 shows a Gausian distribution peak with peak intensity between 400 and 500 nm, correlating to the observed experimental value and PDI of <0.5.

The low magnitude of the calculated percent prediction error indicates the robustness of the mathematical model used. The predictive errors of ZP and PS are $>10\%$ implying that the model may have poor predictive ability for these responses. However, the NLC produced carriers were considered stable and fell in the nanometer size range. The high predictive ability of DoE has been demonstrated suggesting the efficiency of DoE as a tool, for process optimization when developing pharmaceutical dosage forms [83].

3.3. pH and osmolarity

The pH of the optimized CLA-loaded NLC formulation was 7.73 ± 0.01 which suggests it would be tolerated when administered to the human eye [57]. The osmolarity was adjusted to 250–450 mOsm/kg with glycerine to ensure the formulation fell within the physiological range to make it compatible for ophthalmic administration [58]. The final pH and osmolarity of the optimized CLA-loaded NLC formulation was 7.76 ± 0.01 and 316 ± 2 mOsm/Kg. It was established that the CQA of the NLC did not change following the addition of glycerine to the dispersion and the values for EE, ZP, PS and PDI were 88.62 ± 0.23%, −20.5 ± 4.82 mV, 461.9 ± 40.16 nm and 0.523 ± 0.104, respectively. These are comparable to the EE, ZP, PS and PDI of 89.75 ± 0.19%, −20.4 ± 5.21 mV, 489.1 ± 41.62 nm and 0.486 ± 0.097, prior to adjustment. The ultimate impact of inclusion of glycerine into these formulations would need to be monitored during long-term stability studies.

3.4. Muco-adhesion

The interaction of NLC with mucin was investigated in addition to the use of PEG in the formulation. The adsorption of PEG to the surfaces of NLC due to its hydrophilic nature, was intended to promote a muco-adhesive interaction with mucin which in turn would suggest an interaction with the ocular surface and result in enhanced precorneal retention and a possible increase in ocular availability permitting dose reduction and use of a longer dosing frequency.

Muco-adhesion can occur by different mechanisms *viz.* electrostatic, adsorption, wetting, and diffusion that allow for polymer chains and

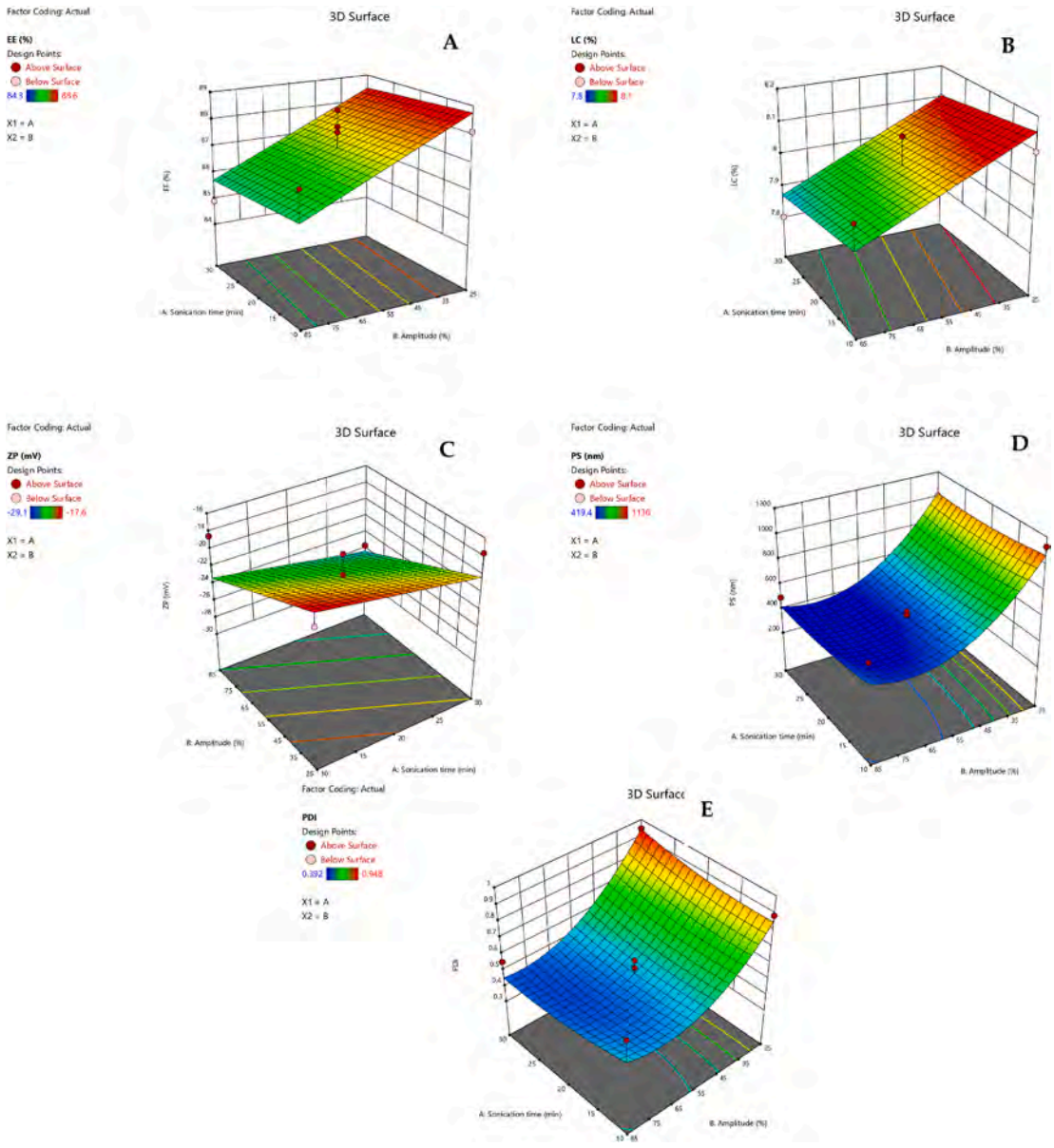

Fig. 3. The 3-D surface plots portraying the effect of the sonication time and amplitude on encapsulation efficiency (A), loading capacity (B), Zeta potential (C), particle size (D) and polydispersity index (E).

Table 6
Comparison of predicted and observed outputs for the optimized formulation.

Response	Experimental value	Predicted value	% prediction error
EE %	89.75 ± 0.19	86.93	3.14
LC %	8.24 ± 0.68	7.98	3.16
ZP mV	−20.4 ± 5.21	−23.19	−13.68
PS nm	489.1 ± 41.62	419.4	14.25
PDI	0.486 ± 0.097	0.493	−1.44

mucin to inter-penetrate and entangle to form interactive bonds [84,85]. Sequentially, the polymer swells during wetting, forms non-covalent bonds at the mucus-polymer interface *via* electrostatic interaction and adsorption and then the polymer and mucin interpenetrate and entangle to form bonds [84]. A decrease in the magnitude of ZP for NLC following incubation with mucin was observed (Fig. 5) suggesting that the NLC with surface adsorbed/coated PEG would likely exhibit enhanced muco-adhesion capabilities. The DSC thermograms depicted in Fig. 6 reveal the presence of melting endotherms consistent with those of PEG in the thermogram of lyophilized NLC. This is further evidence suggesting that the hydrophilic polymer is adsorbed and coated around the nanocarriers, and is not molecularly dispersed within the core of the NLC.

The adsorption interaction is the most likely mechanism of muco-adhesion for the NLC produced in these studies, as these are negatively charged particles that would be unlikely to exhibit electrostatic interactions with the negatively charged mucin. However, it should be noted that demonstration of muco-adhesive properties of nanoparticles should be evaluated using multiple approaches in which particle diffusion, attachment and aggregation are monitored in order to accurately classify a system as being muco-penetrative or muco-adhesive [86].

3.5. *In vitro release and kinetic modelling*

The *in vitro* release profile of CLA from the optimized NLC formulation is depicted in Fig. 7.

The *in vitro* release data show that the cumulative amount of CLA released from the NLC over a 24-h period was 56.13 ± 0.23%. A mass

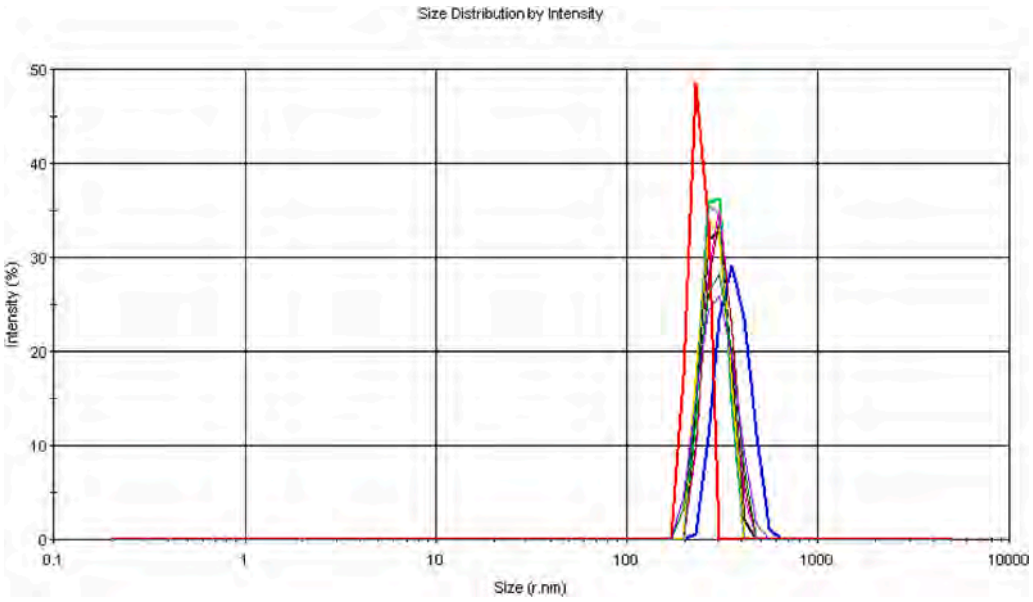

Fig. 4. Particle size distribution by intensity for optimized CLA-NLC ($n = 10$).

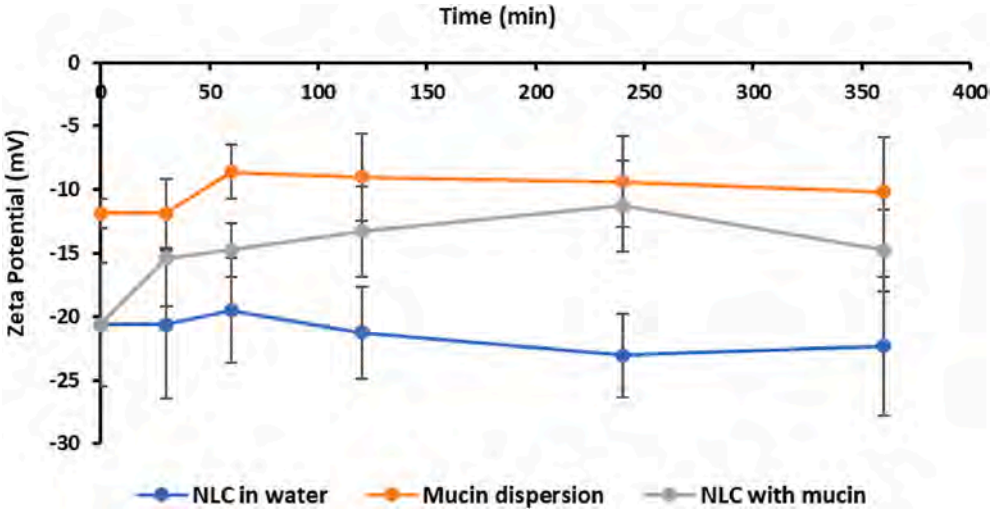

Fig. 5. Estimation of the Zeta Potential for NLC incubated in a 0.1% *m/v* aqueous dispersion of mucin ($n = 10$).

balance of the harvested lipidic formulations from the dialysis tubing yielded an amount of 41.38 ± 0.02% showing a controlled and sustained release of CLA from the nanoparticles. Drug release from nanoparticles have been shown to be affected by factors such as intrinsic solubility of the API, movement of API across depleted layers of the formulation, composition of lipid matrix and diffusion from interfacial barriers like dialysis membrane [34]. Consequently, kinetic modelling of the release profile was undertaken using DDSolver in order to ascertain the factors that influence API release of the formulated lipid carriers.

Fig. 8 depicts the release kinetics obtained from DDSolver with Table 7 showing the corresponding criteria used in evaluation of release. The highest R^2, R^2 adjusted and MSC values and the lowest AIC values were used in evaluating First-order, Higuchi, Korsmeyer-Peppas, Hixson- Crowell and Baker-Lonsdale models [65].

Table 7 shows that the highest R^2 adjusted and MSC values and the lowest AIC for the investigated models was obtained for the Baker-Lonsdale model. The Baker-Lonsdale model describes a controlled release mechanism of the API from spherical shaped lipid matrices, involving diffusion and degradation as factors affecting release and is derived from the Higuchi model [87].

3.6. Cytotoxicity

The effect of encapsulating CLA into NLC and the biocompatibility of the lipids used in the production process was investigated. None of the investigated samples produced a significant (reduced viability of HeLa cells to below 50%) cytotoxic effect at a concentration of 50 μg/mL. CLA-NLC exhibited improved cell viability when compared to that observed for the API alone, which may be due to the shielding effect of the encapsulating lipids, showing the protective technology of theses nanocarriers. In addition, PEG is assumed to form a protective hydrophilic layer on the surface of the nanoparticles thus opposing interaction and ultimate uptake by HeLa cells [88,89]. Furthermore, the high % viability of HeLa cells after exposure to blank NLC confirms that the lipids used in these studies are of GRAS status. The summary of the *in vitro* cytotoxicity is depicted in Fig. 9.

3.7. Stability studies

Table 8 shows the PS, PDI, EE, ZP, pH and osmolarity of NLC generated following storage at 4 °C and 22 °C for 28 days. The

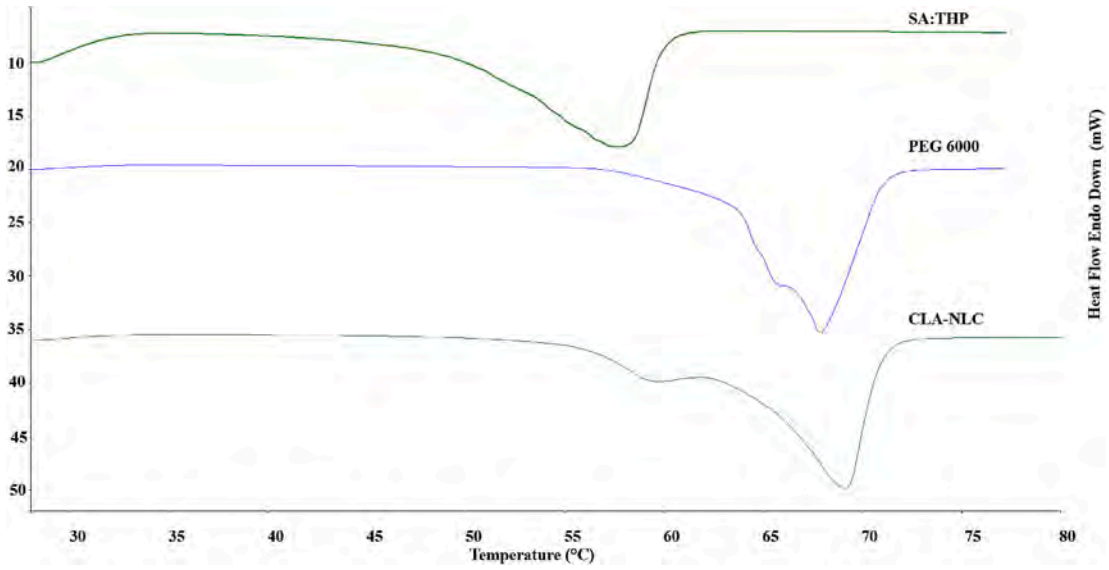

Fig. 6. DSC thermograms of an 80:20 binary mixture of SA and THP, PEG 6000 and lyophilized CLA-NLC.

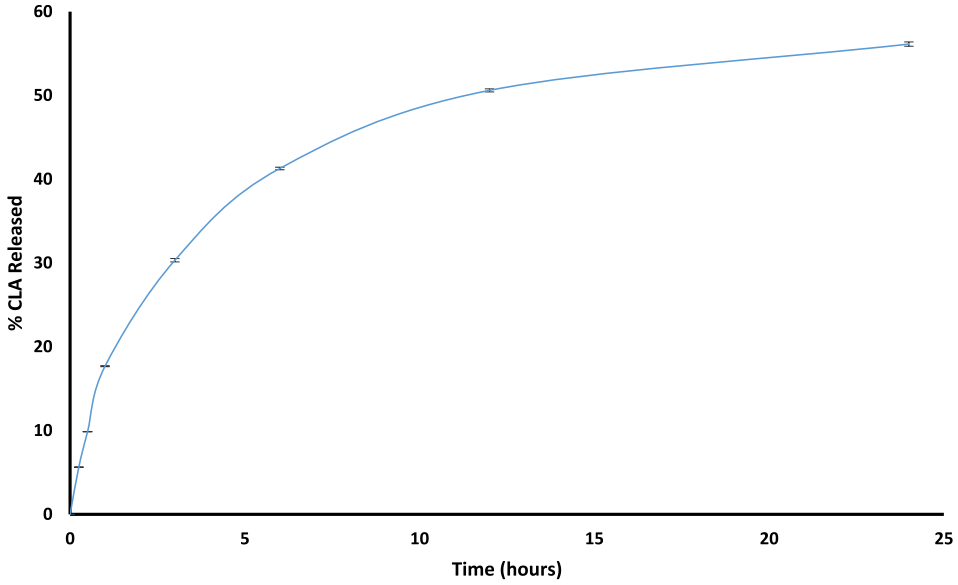

Fig. 7. *In vitro* release profile of CLA from the optimized NLC formulation ($n = 3$).

corresponding graphical representations of PS, PDI, EE and ZP are provided as supplementary material.

Stability studies showed a fairly constant PS and PDI for NLC stored at 4 °C in comparison to formulations stored at 22 °C which showed an increase in both PS and PDI. Higher temperatures have been shown to increase the kinetic energy of particles which in turn leads to collisions between particles and thus particle size increase from particle agglomeration [53]. The PS for NLC stored at 4 °C remained within the nanometer range during the incubation period with those stored at 22 °C increasing to approximately 1.8 μm. However, these formulations can be considered suitable for ocular use as the human eye can tolerate particles of up to 10 μm in diameter [78].

An unexpected loss in API of up to 14.42% occurred at 4 °C in comparison to 5.14% for NLC stored at 22 °C after storage for 28 days. Heiati et al. [90] explained API leakage from SLN stored at 4 °C to be a consequence of temporary non-homogeneity in phospholipid bilayers coating the nanoparticles when stored at these conditions. Consequently, DSC was carried out on lyophilized NLC after storage at 4 °C and 22 °C so as to ascertain the reason behind the observed anomaly. The resultant thermograms are depicted in Fig. 10.

The generated thermogram of the NLC formulations stored at 4 °C shows a change in the polymorphic form of PEG 6000 that was used to coat and impart muco-adhesive properties to the nanoparticles. PEG has been shown to have a depolarizing effect which alters the partition of hydrophobic molecules between the interior and the exterior of lipid bilayers [91].

The ZP for CLA-NLC generally indicate good physical stability of the nanoparticles (≥ -30 mV) at days 14 and 28 following storage at 4 °C and 22 °C. However, although the ZP values for the formulations were lower than −30 mV between day 0 and day 7 and at day 21, the stability of the nanoparticles could be inferred since the polysorbate surfactant provides stability through both electrostatic and steric hindrance mechanisms. The ZP values for the formulations were relatively higher after storage for 28 days in comparison to when assessed 24 h after manufacture. Furthermore, the increase in the negative charge on the surface of the particles did not seem to enhance the stability to the

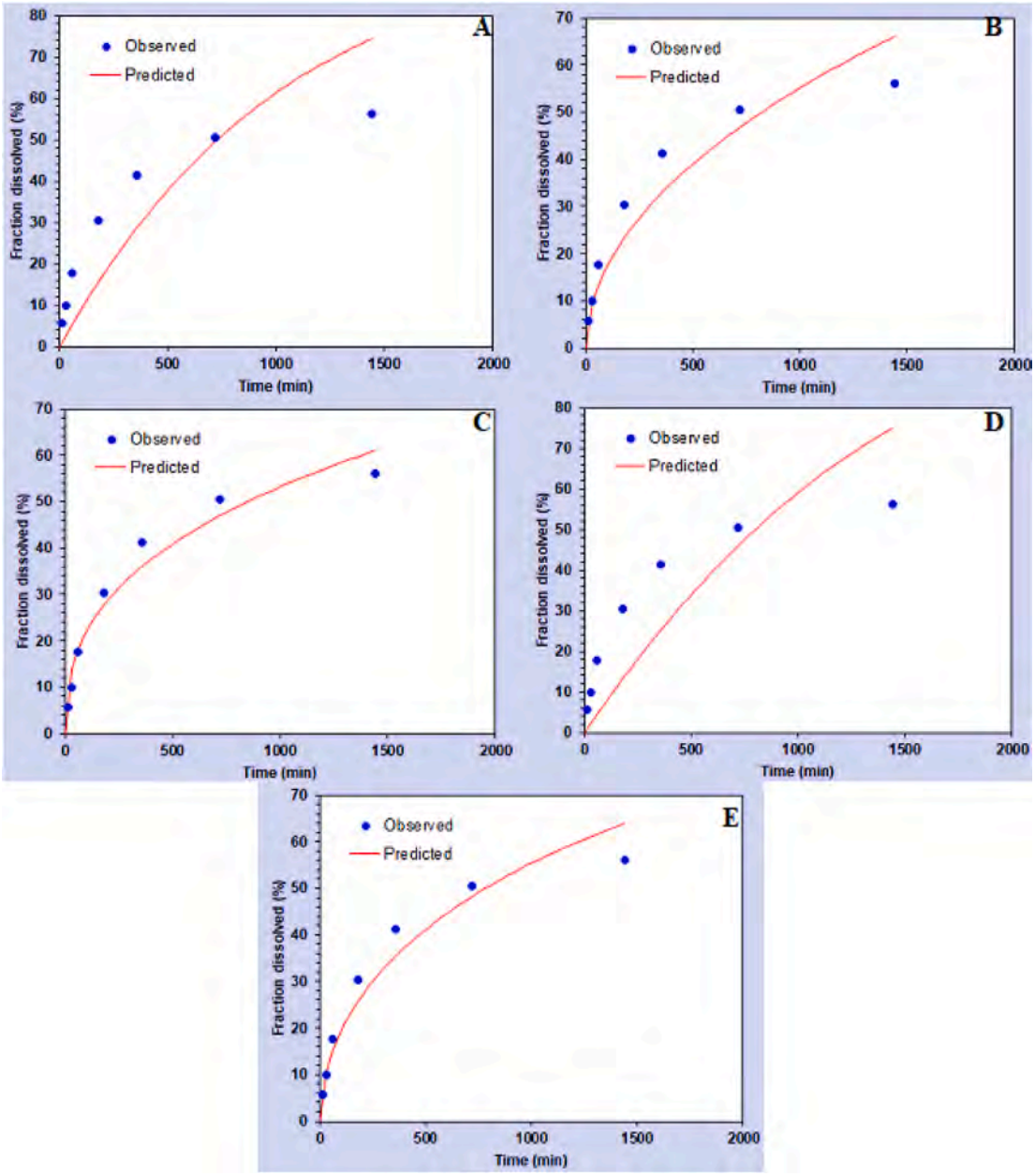

Fig. 8. Release kinetics of CLA-NLC automatically generated from DDSolver.

Table 7
Release kinetic modelling and code evaluation criteria results for NLC.

Model and Equation	Code Evaluation Criteria		
	Rsqr_adj	AIC	MSC
First order (A) $F = 100^{a}[1\text{-}Exp(-k1^{a}t)]$	0.6142	49.7717	0.6667
Higuchi (B) $F = kH^{a}t\hat{}0.5$	0.8954	40.6333	1.9722
Korsmeyer-Peppas (C) $F = kKP^{a}t\hat{}n$	0.9416	37.2827	2.4509
Hixson-Crowell (D) $F = 100^{a}[1\text{-}(1\text{-}kHC^{a}t)\hat{}3]$	0.5067	51.4924	0.4209
Baker-Lonsdale (E) $3/2^{a}[1\text{-}(1\text{-}F/100)\hat{}(2/3)]\text{-}F/100 = kBL^{a}t$	0.9442[a]	36.2357[a]	2.6004[a]

[a] Shows selected evaluation criteria.

formulations since particle growth was observed especially at storage conditions of 22 °C. It is possible that the observed increase and decrease in the negative potential was unrelated to the presence of the surfactant but rather to an increase in the amount of the basic CLA molecule, either in its ionized or unionized form, on the surface of the particles correlating to the reduced EE over time. No agglomeration of formulations was observed following storage for 28 days corresponding to failure to attain the agglomeration threshold range of −20 to −11 mV [53] in these studies.

The pH and osmalirity values of the NLC formulations stored at 4 °C and 22 °C for 28 days were within 3.5–10.5 and 250–450 mOsm/kg, respectively which is tolerable to the human eye [57,58].

4. Conclusions

CLA-loaded lipid carriers for potential use as an ocular delivery technology have been successfully manufactured and characterized in these studies. The results suggest that the optimized NLC have the

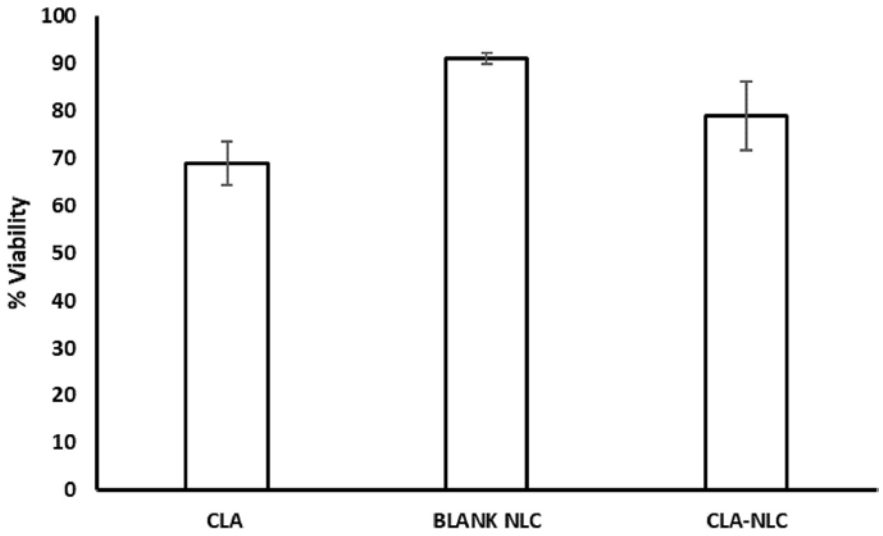

Fig. 9. Cytotoxicity assay of CLA, blank-NLC and CLA-NLC ($n = 3$).

Table 8
Critical Quality Attributes monitored for CLA-NLC stored at 4 °C and 22 °C for 28 days.

Time (days)	Storage Conditions	PS (nm)	PDI	EE (%)	ZP (mV)	pH	Osmolarity (mOsm/kg)
0	4 °C	461.9 ± 40.16	0.523 ± 0.104	88.62 ± 0.23	−20.5 ± 4.82	7.75 ± 0.01	314 ± 2
	22 °C	461.9 ± 40.16	0.523 ± 0.104	88.62 ± 0.23	−20.5 ± 4.82	7.76 ± 0.01	314 ± 2
7	4 °C	581.6 ± 84.47	0.504 ± 0.129	83.18 ± 0.55	−27.4 ± 5.46	7.58 ± 0.02	316 ± 1
	22 °C	624.5 ± 81.5	0.613 ± 0.218	86.5 ± 0.01	−14.7 ± 2.10	7.65 ± 0.01	312 ± 2
14	4 °C	466 ± 32.8	0.331 ± 0.126	NP	−31.5 ± 2.01	7.30 ± 0.01	313 ± 2
	22 °C	1148 ± 60.4	0.919 ± 0.118	NP	−23.1 ± 5.38	7.53 ± 0.01	310 ± 2
21	4 °C	478.9 ± 10.8	0.462 ± 0.119	78.11 ± 0.13	−19.3 ± 4.17	7.35 ± 0.01	318 ± 1
	22 °C	973.9 ± 34.8	0.910 ± 0.137	84.6 ± 0.11	−23.4 ± 6.20	7.47 ± 0.01	314 ± 2
28	4 °C	578.1 ± 21	0.452 ± 0.179	74.2 ± 0.14	−32.2 ± 3.90	7.42 ± 0.01	317 ± 1
	22 °C	1754 ± 100	0.890 ± 0.103	83.48 ± 0.08	−33.7 ± 4.14	7.24 ± 0.02	316 ± 2

NP=Not performed.

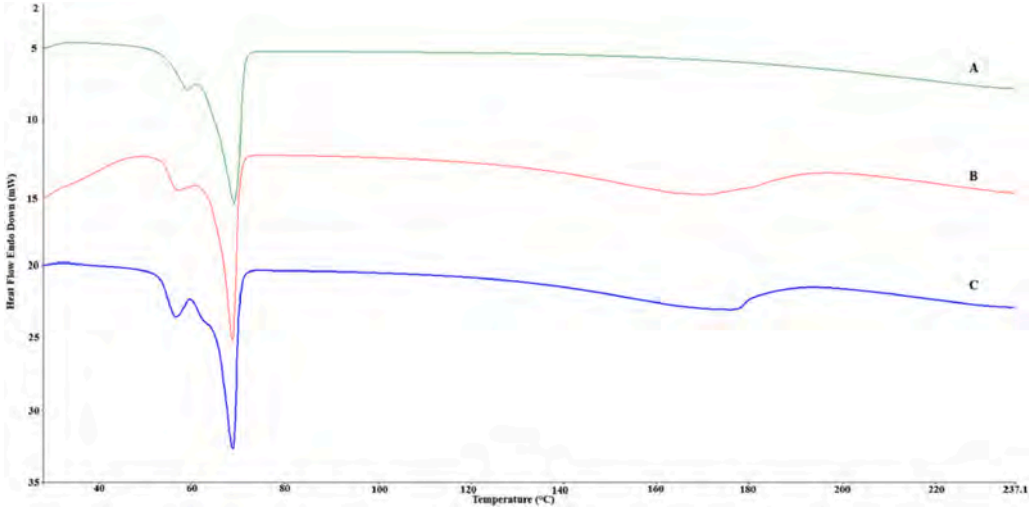

Fig. 10. DSC thermograms of lyophilized CLA-NLC 24 h after production (A) and storage for 28 days at 22 °C (B) and 4 °C (C).

potential to enhance precorneal retention and increase ocular availability, which in turn may be useful to reduce the dose and dosing frequency when administering CLA.

Although stability studies revealed reduced encapsulation efficiency over time at 4 °C and 22 °C, increased particle size into the μm range at 22 °C, the formulations were still deemed appropriate for ocular use, as they were <10 μm in size. The CLA-NLC produced in these studies provide a useful foundation for the delivery of antibiotics to the eye and need further evaluation to establish whether they would be effective when used to treat ocular infections through sensitivity testing and microbiological investigation. In this way the impact of use of this formulation on CLA efficacy against *Mycobacterium fortuitum and Mycobacterium chelonae* could be assessed. In addition, further studies using cell lines from ocular organs would be necessary to fully evaluate

the biocompatibility of the formulation in addition to facilitating an accurate prediction of correlation, *in vivo*.

Author contributions

Conceptualization, P.A.M. and R.B·W.; methodology, P.A.M.; formal analysis, P.A.M.; investigation, P.A.M.; resources, R.B·W.; data curation, P.A.M. and R.B·W.; writing—original draft preparation, P.A.M.; writing—review and editing, R.B.W. and S.M.M.K.; supervision, R.B.W. and S.M.M.K. All authors have read and agreed to the published version of the manuscript.

Declaration of competing interest

The authors declare that they have no known competing financial interests or personal relationships that could have appeared to influence the work reported in this paper.

Acknowledgements

The authors acknowledge financial support from Rhodes University (PAM, SMK and RBW).

Appendix A. Supplementary data

Supplementary data to this article can be found online at https://doi.org/10.1016/j.jddst.2020.102171.

References

[1] B.A. Brown, R.J. Wallace, G.O. Onyi, V. De Rosas, R.J. Wallace, Activities of four macrolides, including clarithromycin, against Mycobacterium fortuitum, Mycobacterium chelonae, and M. Chelonae-like organisms, Antimicrob. Agents Chemother. 36 (1992) 180–184.

[2] H.S. Chu, F.R. Hu, Non-tuberculous mycobacterial keratitis, Clin. Microbiol. Infect. 19 (3) (2013) 221–226, https://doi.org/10.1111/1469-0691.12094.

[3] F.R. Hu, W.J. Huang, S.F. Huang, Clinicopathologic study of satellite lesions in nontuberculous mycobacterial keratitis, Jpn. J. Ophthalmol. 42 (1998) 115–118, https://doi.org/10.1016/S0021-5155(97)00117-2.

[4] N.S. Chandra, M.F. Torres, K.L. Winthrop, D.A. Bruckner, D.G. Heidemann, H. M. Calvet, M. Yakrus, B.J. Mondino, G.N. Holland, Cluster of Mycobacterium chelonae keratitis cases following laser in-situ keratomileusis, Am. J. Ophthalmol. 132 (2001) 819–830, https://doi.org/10.1016/S0002-9394(01)01267-3.

[5] D. Freitas, L. Alvarenga, J. Sampaio, M. Mannis, E. Sato, L. Sousa, L. Vieira, M. C. Yu, M.C. Martins, A. Hoffling-Lima, R. Belfort, An outbreak of Mycobacterium chelonae infection after LASIK, Ophthalmology 110 (2003) 276–285, https://doi.org/10.1016/S0161-6420(02)01643-3.

[6] T. Yamaguchi, H. Bissen-Miyajima, Y. Hori-Komai, Y. Matsumoto, N. Ebihara, H. Takahashi, K. Tsubota, J. Shimazaki, Infectious keratitis outbreak after laser in situ keratomileusis at a single laser center in Japan, J. Cataract Refract. Surg. 37 (2011) 894–900, https://doi.org/10.1016/j.jcrs.2010.11.034.

[7] M.A. Chang, S. Jain, D.T. Azar, Infections following laser in situ keratomileusis: an Integration of the published literature, Surv. Ophthalmol. 49 (3) (2004) 269–280, https://doi.org/10.1016/j.survophthal.2004.02.007.

[8] P.A. Thomas, P. Geraldine, Infectious keratitis, Curr. Opin. Infect. Dis. 20 (2007) 129–141, https://doi.org/10.1097/QCO.0b013e328017f878.

[9] K.A. Rodvold, Clinical pharmacokinetics of clarithromycin, Clin. Pharmacokinet. 37 (5) (1999) 385–398, https://doi.org/10.2165/00003088-199937050-00003.

[10] D. Rossiter, University of Cape Town Division of Clinical Pharmacology, in: South African Medicines Formulary, twelfth ed., Health and Medical Pub. Group, Claremont South Africa, 2016.

[11] W. Nie, H. Duan, H. Huang, Y. Lu, N. Chu, Species identification and clarithromycin susceptibility testing of 278 clinical nontuberculosis mycobacteria isolates, BioMed Res. Int. (2015) 2015, https://doi.org/10.1155/2015/506598.

[12] R.S. Moorthy, S. Valluri, N.A. Rao, Nontuberculous mycobacterial ocular and adnexal infections, Surv. Ophthalmol. 57 (3) (2012) 202–235, https://doi.org/10.1016/j.survophthal.2011.10.006.

[13] J.G. Ford, A.J.W. Huang, S.C. Pflugfelder, E.C. Alfonso, R.K. Forster, D. Miller, Nontuberculous mycobacterial keratitis in South Florida, Ophthalmology 105 (1998) 1652–1658, https://doi.org/10.1016/S0161-6420(98)99034-0.

[14] R.H. Gross, G.N. Holland, S.J. Elias, R. Tuz, Corneal pharmacokinetics of topical clarithromycin, Investig. Ophthalmol. Vis. Sci. 36 (1995) 965–968.

[15] C.J. Helm, G.N. Holland, R. Lin, O.G.W. Berlin, D.A. Bruckner, Comparison of topical antibiotics for treating Mycobacterium fortuitum keratitis in an animal model, Am. J. Ophthalmol. 116 (1993) 700–707, https://doi.org/10.1016/S0002-9394(14)73469-5.

[16] J. Hao, X. Wang, Y. Bi, Y. Teng, J. Wang, F. Li, Q. Li, J. Zhang, F. Guo, J. Liu, Fabrication of a composite system combining solid lipid nanoparticles and thermosensitive hydrogel for challenging ophthalmic drug delivery, Colloids Surf. B Biointerfaces 114 (2014) 111–120, https://doi.org/10.1016/j.colsurfb.2013.09.059.

[17] A. Ludwig, The use of mucoadhesive polymers in ocular drug delivery, Adv. Drug Deliv. Rev. 57 (2005) 1595–1639, https://doi.org/10.1016/J.ADDR.2005.07.005.

[18] A. Patel, Ocular drug delivery systems: an overview, World J. Pharmacol. 2 (2013) 47, https://doi.org/10.5497/wjp.v2.i2.47.

[19] R. Gaudana, J. Jwala, S.H.S. Boddu, A.K. Mitra, Recent perspectives in ocular drug delivery, Pharm. Res. (N. Y.) 26 (5) (2009) 1197–1216, https://doi.org/10.1007/s11095-008-9694-0.

[20] V.H.L. Lee, J.R. Robinson, Topical ocular drug delivery: recent developments and future challenges, J. Ocul. Pharmacol. 2 (1986) 67–108, https://doi.org/10.1089/jop.1986.2.67.

[21] N. Kuno, S. Fujii, Recent advances in ocular drug delivery systems, Polymers 3 (2011) 193–221, https://doi.org/10.3390/polym3010193.

[22] D.R. Janagam, L. Wu, T.L. Lowe, Nanoparticles for drug delivery to the anterior segment of the eye, Adv. Drug Deliv. Rev. 122 (2017) 31–64, https://doi.org/10.1016/j.addr.2017.04.001.

[23] C. Jumelle, S. Gholizadeh, N. Annabi, R. Dana, Advances and limitations of drug delivery systems formulated as eye drops, J. Contr. Release 321 (2020) 1–22, https://doi.org/10.1016/j.jconrel.2020.01.057.

[24] S.M. Agnihotri, P.R. Vavia, Diclofenac-loaded biopolymeric nanosuspensions for ophthalmic application, Nanomed. Nanotechnol. Biol. Med. 5 (2009) 90–95, https://doi.org/10.1016/j.nano.2008.07.003.

[25] P. Bhagav, H. Upadhyay, S. Chandran, Brimonidine tartrate-eudragit long-acting nanoparticles: formulation, optimization, in vitro and in vivo evaluation, AAPS PharmSciTech 12 (2011) 1087–1101, https://doi.org/10.1208/s12249-011-9675-1.

[26] H. Gupta, M. Aqil, R.K. Khar, A. Ali, A. Bhatnagar, G. Mittal, Sparfloxacin-loaded PLGA nanoparticles for sustained ocular drug delivery, Nanomed. Nanotechnol. Biol. Med. 6 (2010) 324–333, https://doi.org/10.1016/j.nano.2009.10.004.

[27] H.K. Ibrahim, I.S. El-Leithy, A.A. Makky, Mucoadhesive nanoparticles as carrier systems for prolonged ocular delivery of gatifloxacin/prednisolone bitherapy, Mol. Pharm. 7 (2010) 576–585, https://doi.org/10.1021/mp900279c.

[28] R.C. Nagarwal, R. Kumar, J.K. Pandit, Chitosan coated sodium alginate-chitosan nanoparticles loaded with 5-FU for ocular delivery: in vitro characterization and in vivo study in rabbit eye, Eur. J. Pharmaceut. Sci. 47 (2012) 678–685, https://doi.org/10.1016/j.ejps.2012.08.008.

[29] K.L. Nair, S. Vidyanand, J. James, G.S.V. Kumar, Pilocarpine-loaded poly(DL-lactic-co-glycolic acid) nanoparticles as potential candidates for controlled drug delivery with enhanced ocular pharmacological response, J. Appl. Polym. Sci. 124 (2012) 2030–2036, https://doi.org/10.1002/app.35229.

[30] A. Seyfoddin, J. Shaw, R. Al-Kassas, Solid lipid nanoparticles for ocular drug delivery, Drug Deliv. 17 (2010) 467–489, https://doi.org/10.3109/10717544.2010.483257.

[31] L. Gan, J. Wang, M. Jiang, H. Bartlett, D. Ouyang, F. Eperjesi, J. Liu, Y. Gan, Recent advances in topical ophthalmic drug delivery with lipid-based nanocarriers, Drug Discov. Today 18 (5–6) (2013) 290–297, https://doi.org/10.1016/j.drudis.2012.10.005.

[32] B.A. Witika, P.A. Makoni, S.K. Matafwali, B. Chabalenge, C. Mwila, A.C. Kalungia, C.I. Nkanga, A.M. Bapolisi, R.B. Walker, Biocompatibility of biomaterials for nanoencapsulation: current approaches, Nanomaterials 10 (2020) 1649, https://doi.org/10.3390/nano10091649.

[33] A.A. Öztürk, A. Aygül, B. Şenel, Influence of glyceryl behenate, tripalmitin and stearic acid on the properties of clarithromycin incorporated solid lipid nanoparticles (SLNs): formulation, characterization, antibacterial activity and cytotoxicity, J. Drug Deliv. Sci. Technol. 54 (2019) 101240, https://doi.org/10.1016/j.jddst.2019.101240.

[34] M. Sharma, N. Gupta, S. Gupta, Implications of designing clarithromycin loaded solid lipid nanoparticles on their pharmacokinetics, antibacterial activity and safety, RSC Adv. 6 (2016) 76621–76631, https://doi.org/10.1039/c6ra12841f.

[35] H.-Z. Bu, H. Gukasyan, L. Goulet, X.-J. Lou, C. Xiang, T. Koudriakova, Ocular disposition, pharmacokinetics, efficacy and safety of nanoparticle-formulated ophthalmic drugs, Curr. Drug Metabol. 8 (2007) 91–107, https://doi.org/10.2174/138920007779815977.

[36] A. Kumar, P.K. Naik, D. Pradhan, G. Ghosh, G. Rath, Mucoadhesive formulations: innovations, merits, drawbacks and future outlook, Pharmaceut. Dev. Technol. 1–43 (2020), https://doi.org/10.1080/10837450.2020.1753771.

[37] A.M. De Campos, A. Sánchez, R. Gref, P. Calvo, M.J. Alonso, The effect of a PEG versus a chitosan coating on the interaction of drug colloidal carriers with the ocular mucosa, Eur. J. Pharmaceut. Sci. 20 (2003) 73–81, https://doi.org/10.1016/S0928-0987(03)00178-7.

[38] R. Rowe, P. Sheskey, M. Quinn, Handbook of Pharmaceutical Excipients, sixth ed., The Pharmaceutical Press, London, 2009.

[39] N.P. Aditya, S. Ko, Solid lipid nanoparticles (SLNs): delivery vehicles for food bioactives, RSC Adv. 5 (2015) 30902–30911, https://doi.org/10.1039/c4ra17127f.

[40] P.A. Makoni, J. Ranchhod, K. WaKasongo, S.M. Khamanga, R.B. Walker, The use of quantitative analysis and Hansen solubility parameter predictions for the selection of excipients for lipid nanocarriers to be loaded with water soluble and insoluble compounds, Saudi Pharmaceut. J. 28 (2020) 305–315, https://doi.org/10.1016/j.jsps.2020.01.010.

[41] M. Joshi, V. Patravale, Formulation and evaluation of nanostructured lipid carrier (NLC)–based gel of valdecoxib, Drug Dev. Ind. Pharm. 32 (2006) 911–918, https://doi.org/10.1080/03639040600814676.
[42] K.W. Kasongo, J. Pardeike, R.H. Muller, R.B. Walker, Selection and characterization of suitable lipid excipients for use in the manufacture of didanosine-loaded solid lipid nanoparticles and nanostructured lipid carriers, J. Pharmacol. Sci. 100 (2011) 5185–5196, https://doi.org/10.1002/jps.22711.
[43] T. Hua, X. Zhang, B. Tang, C. Chang, G. Liu, L. Feng, Y. Yu, D. Zhang, J. Hou, Tween-20 transiently changes the surface morphology of PK-15 cells and improves PCV2 infection, BMC Vet. Res. 14 (2018), https://doi.org/10.1186/s12917-018-1457-5.
[44] R.K. Sahoo, N. Biswas, A. Guha, N. Sahoo, K. Kuotsu, Nonionic Surfactant Vesicles in Ocular Delivery: Innovative Approaches and Perspectives, 2014, https://doi.org/10.1155/2014/263604.
[45] P. Mura, M.T. Faucci, A. Manderioli, S. Furlanetto, S. Pinzauti, Thermal analysis as a screening technique in preformulation studies of picotamide solid dosage forms, Drug Dev. Ind. Pharm. 24 (1998) 747–756, https://doi.org/10.3109/03639049809082722.
[46] B. Abismaïl, J.P. Canselier, A.M. Wilhelm, H. Delmas, C. Gourdon, Emulsification by ultrasound: drop size distribution and stability, Ultrason. Sonochem. 6 (1999) 75–83, https://doi.org/10.1016/S1350-4177(98)00027-3.
[47] A.C. Taylor, Advances in nanoparticle reinforcement in structural adhesives, in: Advances in Structural Adhesive Bonding, Elsevier Inc., 2010, pp. 151–182, https://doi.org/10.1533/9781845698058.1.151.
[48] A. Sze, D. Erickson, L. Ren, D. Li, Zeta-potential measurement using the Smoluchowski equation and the slope of the current-time relationship in electroosmotic flow, J. Colloid Interface Sci. 261 (2003) 402–410, https://doi.org/10.1016/S0021-9797(03)00142-5.
[49] P.A. Makoni, M.T.R. Chikukwa, S.M. Khamanga, R.B. Walker, Stability indicating HPLC-ECD method for the analysis of clarithromycin in pharmaceutical dosage forms: method scaling versus Re-validation, Sci. Pharm. 87 (2019) 31, https://doi.org/10.3390/scipharm87040031.
[50] I. Stat-Ease, Handbook for Experimenters A Conscise Collection of Handy Tips to Help You Set up and Analyze Your Designed Experiments, 2014. Minneapolis.
[51] D.C. Whittinghill, A note on the robustness of Box-Behnken designs to the unavailability of data, Metrika 48 (1998) 49–52, https://doi.org/10.1007/PL00003971.
[52] S. Cunha, C.P. Costa, J.A. Loureiro, J. Alves, A.F. Peixoto, B. Forbes, J.M.S. Sousa Lobo, A.C. Silva, Double optimization of rivastigmine-loaded nanostructured lipid carriers (NLC) for nose-to-brain delivery using the quality by design (QbD) approach: formulation variables and instrumental parameters, Pharmaceutics 12 (2020) 599, https://doi.org/10.3390/pharmaceutics12070599.
[53] P.A. Makoni, K.W. Kasongo, R.B. Walker, Short term stability testing of efavirenz-loaded solid lipid nanoparticle (SLN) and nanostructured lipid carrier (NLC) dispersions, Pharmaceutics 11 (2019) 397, https://doi.org/10.3390/PHARMACEUTICS11080397.
[54] J.Y. Fang, C.L. Fang, C.H. Liu, Y.H. Su, Lipid nanoparticles as vehicles for topical psoralen delivery: solid lipid nanoparticles (SLN) versus nanostructured lipid carriers (NLC), Eur. J. Pharm. Biopharm. 70 (2008) 633–640, https://doi.org/10.1016/j.ejpb.2008.05.008.
[55] B. Shah, D. Khunt, H. Bhatt, M. Misra, H. Padh, Application of quality by design approach for intranasal delivery of rivastigmine loaded solid lipid nanoparticles: effect on formulation and characterization parameters, Eur. J. Pharmaceut. Sci. 78 (2015) 54–66, https://doi.org/10.1016/j.ejps.2015.07.002.
[56] T. Alam, S. Khan, B. Gaba, M.F. Haider, S. Baboota, J. Ali, Adaptation of quality by design-based development of isradipine nanostructured–lipid carrier and its evaluation for in vitro gut permeation and in vivo solubilization fate, J. Pharmacol. Sci. 107 (2018) 2914–2926, https://doi.org/10.1016/j.xphs.2018.07.021.
[57] J.F. Charlton, K.P. Dalla, A. Kniska, Storage of extemporaneously prepared ophthalmic antimicrobial solutions, Am J Heal. Pharm 55 (1998).
[58] R. Mazet, L. Choisnard, D. Levilly, D. Wouessidjewe, A. Gèze, Investigation of combined cyclodextrin and hydrogel formulation for ocular delivery of dexamethasone acetate by means of experimental designs, Pharmaceutics 10 (2018) 249, https://doi.org/10.3390/pharmaceutics10040249.
[59] N.A. Fefelova, Z.S. Nurkeeva, G.A. Mun, V.V. Khutoryanskiy, Mucoadhesive interactions of amphiphilic cationic copolymers based on [2-(methacryloyloxy) ethyl]trimethylammonium chloride, Int. J. Pharm. 339 (2007) 25–32, https://doi.org/10.1016/j.ijpharm.2007.02.019.
[60] A.C. Mendes, J.S. Moreno, M. Hanif, T.E.L. Douglas, M. Chen, I.S. Chronakis, Morphological, mechanical and mucoadhesive properties of electrospun chitosan/phospholipid hybrid nanofibers, Int. J. Mol. Sci. 19 (2018), https://doi.org/10.3390/ijms19082266.
[61] N. Nikogeorgos, P. Efler, A.B. Kayitmazer, S. Lee, "Bio-glues" to enhance slipperiness of mucins: improved lubricity and wear resistance of porcine gastric mucin (PGM) layers assisted by mucoadhesion with chitosan, Soft Matter 11 (2015) 489–498, https://doi.org/10.1039/c4sm02021a.
[62] H. Takeuchi, J. Thongborisute, Y. Matsui, H. Sugihara, H. Yamamoto, Y. Kawashima, Novel mucoadhesion tests for polymers and polymer-coated particles to design optimal mucoadhesive drug delivery systems, Adv. Drug Deliv. Rev. 57 (11) (2005) 1583–1594, https://doi.org/10.1016/j.addr.2005.07.008.
[63] R.S. Bhatta, H. Chandasana, Y.S. Chhonker, C. Rathi, D. Kumar, K. Mitra, P. K. Shukla, Mucoadhesive nanoparticles for prolonged ocular delivery of natamycin: in vitro and pharmacokinetics studies, Int. J. Pharm. 432 (2012) 105–112, https://doi.org/10.1016/j.ijpharm.2012.04.060.
[64] E. Terreni, P. Chetoni, S. Tampucci, S. Burgalassi, A. Al-kinani, R. Alany, D. Monti, Assembling surfactants-mucoadhesive polymer nanomicelles (ASMP-Nano) for ocular delivery of cyclosporine-A, Pharmaceutics 12 (2020) 253, https://doi.org/10.3390/pharmaceutics12030253.
[65] Y. Zhang, M. Huo, J. Zhou, A. Zou, W. Li, C. Yao, S. Xie, DDSolver: an add-in program for modeling and comparison of drug dissolution profiles, AAPS J. 12 (2010) 263–271, https://doi.org/10.1208/s12248-010-9185-1.
[66] R. Foldbjerg, J. Wang, C. Beer, K. Thorsen, D.S. Sutherland, H. Autrup, Biological effects induced by BSA-stabilized silica nanoparticles in mammalian cell lines, Chem. Biol. Interact. 204 (2013) 28–38, https://doi.org/10.1016/j.cbi.2013.04.007.
[67] D.R. Nogueira, M. Carmen Morán, M. Mitjans, V. Martínez, L. Pérez, M. Pilar Vinardell, New cationic nanovesicular systems containing lysine-based surfactants for topical administration: toxicity assessment using representative skin cell lines, Eur. J. Pharm. Biopharm. 83 (2013) 33–43, https://doi.org/10.1016/j.ejpb.2012.09.007.
[68] I. Bácskay, D. Nemes, F. Fenyvesi, J. Váradi, G. Vasvári, P. Fehér, M. Vecsernyés, Z. Ujhelyi, Role of cytotoxicity experiments in pharmaceutical development, InTech, Cytotoxicity, 2018, https://doi.org/10.5772/intechopen.72539.
[69] D. Nogueira, M. Mitjans, C. Rolim, M. Vinardell, Mechanisms underlying cytotoxicity induced by engineered nanomaterials: a review of in vitro studies, Nanomaterials 4 (2014) 454–484, https://doi.org/10.3390/nano4020454.
[70] S.W. Ha, J.A. Sikorski, M.N. Weitzmann, G.R. Beck, Bio-active engineered 50nm silica nanoparticles with bone anabolic activity: therapeutic index, effective concentration, and cytotoxicity profile in vitro, Toxicol. Vitro 28 (2014) 354–364, https://doi.org/10.1016/j.tiv.2013.12.001.
[71] B.R. Matthews, G.M. Wall, Stability storage and testing of ophthalmic products for global registration, Drug Dev. Ind. Pharm. 26 (2000) 1227–1237, https://doi.org/10.1081/DDC-100102304.
[72] A.A. Ahmad, B.H. Hameed, A.L. Ahmad, Removal of disperse dye from aqueous solution using waste-derived activated carbon: optimization study, J. Hazard Mater. 170 (2009) 612–619, https://doi.org/10.1016/j.jhazmat.2009.05.021.
[73] R.H. Müller, K. Mäder, S. Gohla, Solid lipid nanoparticles (SLN) for controlled drug delivery- a review of the state of the art, Eur. J. Pharm. Biopharm. 50 (2000) 161–177, https://doi.org/10.1080/026520499289185.
[74] E.B. Souto, R.H. Muller, Solid lipid nanoparticles and nanostructured lipid carriers-lipid nanoparticles for medicals and pharmaceuticals, Encycl. Nanosci. Nanotechnol. 23 (2011) 313–328.
[75] S.A. Wissing, O. Kayser, R.H. Müller, Solid lipid nanoparticles for parenteral drug delivery, Adv. Drug Deliv. Rev. 56 (2004) 1257–1272, https://doi.org/10.1016/j.addr.2003.12.002.
[76] W. Mehnert, K. Mäder, Solid lipid nanoparticles: production, characterization and applications, Adv. Drug Deliv. Rev. 64 (2012) 83–101, https://doi.org/10.1016/j.addr.2012.09.021.
[77] A. Siddiqui, A. Alayoubi, Y. El-Malah, S. Nazzal, Modeling the effect of sonication parameters on size and dispersion temperature of solid lipid nanoparticles (SLNs) by response surface methodology (RSM), Pharmaceut. Dev. Technol. 19 (2014) 342–346, https://doi.org/10.3109/10837450.2013.784336.
[78] E. Gonzalez-Mira, M.A. Egea, M.L. Garcia, E.B. Souto, Design and ocular tolerance of flurbiprofen loaded ultrasound-engineered NLC, Colloids Surf. B Biointerfaces 81 (2010) 412–421, https://doi.org/10.1016/j.colsurfb.2010.07.029.
[79] B. Heurtault, P. Saulnier, B. Pech, J.-E. Proust, J.-P. Benoit, Physico-chemical stability of colloidal lipid particles, Biomaterials 24 (2003) 4283–4300.
[80] A. Radomskasoukharev, Stability of lipid excipients in solid lipid nanoparticles☆, Adv. Drug Deliv. Rev. 59 (2007) 411–418, https://doi.org/10.1016/j.addr.2007.04.004.
[81] M. Uner, Preparation, characterization and physico-chemical properties of solid lipid nanoparticles (SLN) and nanostructured lipid carriers (NLC): their benefits as colloidal drug carrier systems, Pharmazie 61 (2006) 375–386.
[82] A. Nath, P.K. Chattopadhyay, Optimization of oven toasting for improving crispness and other quality attributes of ready to eat potato-soy snack using response surface methodology, J. Food Eng. 80 (2007) 1282–1292, https://doi.org/10.1016/J.JFOODENG.2006.09.023.
[83] A.F.B. Fauzee, S.M. Khamanga, R.B. Walker, The impact of manufacturing variables on in vitro release of clobetasol 17-propionate from pilot scale cream formulations, Drug Dev. Ind. Pharm. 40 (2014) 1683–1692, https://doi.org/10.3109/03639045.2013.842579.
[84] N. Dubashynskaya, D. Poshina, S. Raik, A. Urtti, Y.A. Skorik, Polysaccharides in ocular drug delivery, Pharmaceutics 12 (22) (2020) 1–30, https://doi.org/10.3390/pharmaceutics12010022.
[85] S. Rossi, B. Vigani, M.C. Bonferoni, G. Sandri, C. Caramella, F. Ferrari, Rheological analysis and mucoadhesion: a 30 year-old and still active combination, J. Pharmaceut. Biomed. Anal. 156 (2018) 232–238, https://doi.org/10.1016/j.jpba.2018.04.041.
[86] R. Machado Cruz, M.J. Santos-Martinez, L. Tajber, Impact of polyethylene glycol polymers on the physicochemical properties and mucoadhesivity of itraconazole nanoparticles, Eur. J. Pharm. Biopharm. 144 (2019) 57–67, https://doi.org/10.1016/j.ejpb.2019.09.004.
[87] S. Scioli Montoto, M.L. Sbaraglini, A. Talevi, M. Couyoupetrou, M. Di Ianni, G. O. Pesce, V.A. Alvarez, L.E. Bruno-Blanch, G.R. Castro, M.E. Ruiz, G.A. Islan, Carbamazepine-loaded solid lipid nanoparticles and nanostructured lipid carriers: physicochemical characterization and in vitro/in vivo evaluation, Colloids Surf. B Biointerfaces 167 (2018) 73–81, https://doi.org/10.1016/j.colsurfb.2018.03.052.
[88] B. Romberg, W.E. Hennink, G. Storm, Sheddable coatings for long-circulating nanoparticles, Pharm. Res. (N. Y.) 25 (1) (2008) 55–71, https://doi.org/10.1007/s11095-007-9348-7.

[89] B.A. Witika, V.J. Smith, R.B. Walker, Quality by design optimization of cold sonochemical synthesis of zidovudine-lamivudine nanosuspensions, Pharmaceutics 12 (2020) 367, https://doi.org/10.3390/pharmaceutics12040367.
[90] H. Heiati, R. Tawashi, N.C. Phillips, Drug retention and stability of solid lipid nanoparticles containing azidothymidine palmitate after autoclaving, storage and lyophilization, J. Microencapsul. 15 (1998) 173–184, https://doi.org/10.3109/02652049809006847.
[91] L.T. Boni, T.P. Stewart, S.W. Hui, Alterations in phospholipid polymorphism by polyethylene glycol, J. Membr. Biol. 80 (1984) 91–104, https://doi.org/10.1007/BF01868693.